Universidad de Deusto

Contributions to fractional-order modelling and control of dynamic systems: A theoretical and practical approach

Tesis doctoral presentada por Juan José Gude Prego
dentro del Programa de Doctorado de
Ingeniería para la Sociedad de la Información y Desarrollo Sostenible

Dirigida por Dr. Pablo García Bringas

Universidad de Deusto

Contributions to fractional-order modelling and control of dynamic systems: A theoretical and practical approach

Tesis doctoral presentada por Juan José Gude Prego
dentro del Programa de Doctorado de
Ingeniería para la Sociedad de la Información y Desarrollo Sostenible

Dirigida por Dr. Pablo García Bringas

El doctorando | El director

Bilbao, febrero de 2023

Contributions to fractional-order modelling and control of dynamic systems:
A theoretical and practical approach

Author: Juan José Gude Prego
Advisor: Pablo García Bringas

Text printed in Bilbao
First edition, february 2023

A Elisabet, Ander y Mikel.

A mis aitas, que son el mejor ejemplo a seguir.

Resumen

Los enormes avances tecnológicos han marcado una nueva etapa en el campo del control de procesos en la industria de procesos. En las tres últimas décadas se ha producido un notable desarrollo en el uso del cálculo fraccionario, que generaliza los operadores diferenciales e integrales a órdenes no enteros, para la modelización y el control.

La gran ventaja que ofrece el cálculo de orden fraccionario aplicado a la modelización de sistemas dinámicos reside en su capacidad para proporcionar métodos más precisos de modelización e identificación de fenómenos del mundo real. A su vez, el control de orden fraccionario puede considerarse una herramienta emergente en el campo del control de procesos, siendo la principal razón de su éxito la robustez intrínseca que ofrece con un mayor grado de libertad para el diseño.

Es evidente que el cálculo fraccionario también plantea desventajas. Entre ellas, la implementación de los operadores de orden fraccionario es más complicada que la de los de orden entero, lo que ha dado lugar a numerosas investigaciones, aún en curso, para encontrar implementaciones sencillas y fiables. Aunque se ha demostrado que los modelos y controles de orden fraccionario son tecnológicamente superiores, su adopción industrial aún no está generalizada, siendo la razón principal los problemas de implementación antes mencionados.

La presente tesis está dedicada a la investigación en identificación y control de sistemas dinámicos basada en el cálculo de orden fraccionario. Está dividida en dos partes:

La Parte I de esta tesis está dedicada al desarrollo de procedimientos de identificación de modelos de orden fraccionario basados en la curva de reacción del proceso. Para que dichos procedimientos tengan impacto en la industria de procesos, deben ser sencillos de entender y de aplicar para ingenieros y operadores de planta. Por ello, se ha puesto especial énfasis en la simplicidad de los mismos.

En esta parte, se proporcionan algunos ejemplos numéricos para mostrar la sencillez y eficacia del procedimiento propuesto. Se han obtenido buenos resultados en comparación con otros métodos de identificación de modelos de orden entero y fraccionario bien conocidos, especialmente cuando se hace énfasis en la simplicidad.

La Parte II de esta tesis proporciona los recursos necesarios para la implementación práctica de los procedimientos de identificación desarrollados en la Parte I, así como de los algoritmos de control de orden fraccionario. Más concretamente, se presenta la conceptualización de una novedosa arquitectura hardware de control orientada a la implementación práctica de algoritmos de identificación y control de orden fraccionario en diferentes tecnologías de control.

A continuación, se muestran los resultados obtenidos aplicando los algoritmos de identificación propuestos sobre un prototipo de laboratorio de un proceso térmico e implementado sobre la arquitectura hardware descrita. Por último, también se evalúa la efectividad y aplicabilidad de la arquitectura hardware de control mediante la implementación práctica de algoritmos de control PID de orden entero y fraccionario en dos plataformas hardware de tiempo real, es decir, en una plataforma hardware basada en microprocesador y en otra basada en FPGA, respectivamente.

En consecuencia, la arquitectura hardware de control propuesta contribuye, por un lado, a la implementación práctica de algoritmos de identificación y control de sistemas de orden fraccionario en plataformas hardware en tiempo real y, por otro, ayuda a salvar la brecha existente entre las simulaciones de modelos y controles fraccionarios basadas en software y las soluciones hardware en tiempo real. Esto permitiría la mejora de muchos sistemas actuales sin necesidad de una gran inversión en equipos y la aplicación de técnicas de identificación y control de orden fraccionario a un núcleo de sistemas más amplio del que se aborda en el panorama actual.

Abstract

Enormous technological advances have marked a new stage in the field of process control in the process industry. Last three decades have witnessed a remarkable development in the use of fractional calculus, which generalizes differential and integral operators to non-integer orders, for modeling and control.

The great advantage of fractional-order calculus applied to the modeling of dynamic systems lies in its ability to provide more accurate methods for modeling and identifying real-world phenomena. At the same time, fractional-order control can be considered as an emerging tool in the field of process control, being the main reason for its success the intrinsic robustness it offers with a higher degree of freedom for design.

It is clear that fractional calculus also presents disadvantages. Among them, the implementation of fractional-order operators is more complicated than that of integer-order operators, which has led to numerous investigations, still ongoing, to find simple and reliable implementations. Although fractional-order models and controls have been shown to be technologically superior, their industrial adoption is not yet widespread, being the main reason the aforementioned implementation problems.

The present thesis is devoted to research on identification and control of dynamic systems based on fractional-order calculus. It is divided into the following two parts:

Part I of this thesis is devoted to the development of fractional-order model identification procedures based on the process reaction curve. For such procedures to have a significant impact on the process industry, they must be simple to understand and to apply for engineers and plant operators. Therefore, special emphasis has been placed on their simplicity.
In this part, some numerical examples are provided to show the simplicity and effectiveness of the proposed procedure. Good results have been obtained in comparison with other well-known integer and fractional order model identification methods, especially when simplicity is emphasized.

Part II of this thesis provides the necessary resources for the practical implementation of the identification procedures developed in Part I, as well as of the fractional-order control algorithms. More specifically, the conceptualization of a novel hardware control architecture aimed to the practical implementation of fractional-order identification and control algorithms in different control technologies is presented.

Then, the results obtained by applying the proposed identification algorithms on a thermal-based laboratory prototype and implemented on the described hardware architecture are shown. Finally, the effectiveness and applicability of the control hardware architecture is also evaluated through the practical implementation of integer- and fractional-order PID control algorithms on two real-time hardware platforms, i.e., on a microprocessor-based hardware platform and on an FPGA-based hardware platform, respectively.

Consequently, the proposed control hardware architecture contributes, on the one hand, to the practical implementation of fractional-order system identification and control algorithms on real-time targets and, on the other hand, helps to bridge the gap between software-based fractional modelling and control simulations and real-time hardware solutions. This could provide the improvement of many current systems without the need for a large hardware investment and the application of fractional-order identification and control techniques to a broader range of industrial systems.

Agradecimientos

En primer lugar, quiero agradecer a Elisabet, Ander y Mikel, que son mi motivación principal, por todo el tiempo que esta tesis les ha quitado. Esto no habría sido posible sin todo el apoyo y ánimo que me han dado.

En segundo lugar, quiero agradecer a mi director de tesis, Pablo García Bringas, quien ha sabido darme la confianza y la motivación necesaria. Su apoyo, consejo y guía han hecho posible que todo el trabajo de estos años haya llegado a buen puerto.

Merece un reconocimiento muy especial Evaristo Kahoraho, con quien he aprendido tanto.

No me puedo olvidar de mis compañeros del área de Electrónica y Automática y mis compañeros de la Universidad de Deusto, con quienes comparto mi día a día.

Eskerrik asko!

Table of contents

List of figures

List of Tables

Acronyms

3D	Three dimensions
AI	Analog input
AMIGO	Aproximated MIGO
AO	Anolog output
ARM	Advanced RISC Machine
BIBO	Bounded-input bounded-output
CFE	Continuous fraction expansion
DAQ	Data acquisition
DC	Direct current
Deusto FabLab	Deusto Digital Fabrication Laboratory
Deusto HES	Deusto Heater Experimental Setup
DIO	Digital input/output
DPPDT	Dual-Pole Plus Dead-time
FIFO	First-in first-out
F-MIGO	Fractional-MIGO
FOTF toolbox	Fractional-order Transfer Function toolbox
FFOPDT	Fractional First-order Plus Dead-time
FOPDT	First-order Plus Dead-time
FO-PI	Fractional-order proportional integral
FO-PID	Fractional-order proportional integral derivative
FPGA	Field programmable gate array

FSOPDT	Fractional Second-order Plus Dead-time
GUI	Graphical user interface
HFE	Heat Flow Experiment
HMI	Human-machine interface
I2C	Inter-integrated circuit
IDC	Insulation displacement connector
IEC	International Electrotechnical Commission
I/O	Input-output
LabVIEW	Laboratory Virtual Instrument Engineering Workbench
LCD	Liquid crystal display
LED	Light emitting diode
MAE	Mean absolute error
MATLAB	MATrix LABoratory
MIGO	M_S constrained integral gain optimization
MSE	Mean Squared Error
PAC	Programmable automation controller
PC	Personal computer
PI	Proportional integral
PID	Proportional integral and derivative
PLC	Programmable logic controller
PMSM	Permanent magnet synchronous motor
PSE	Power series expansion
PWM	Pulse-width modulation
RISC	Reduced instruction set computer
RPPDT	Repeated pole Plus Dead-time
RT	Real time
SCADA	Supervisory control and data acquisition

SISO	Single-input single-output.
SoC	System on chip
SOPDT	Second-order Plus Dead-time
SPI	Serial peripheral interface
UART	Universal asynchronous receiver-transmitter
USB	Universal serial bus

'I just take the train from platform nine and
three-quarters at eleven o'clock,' he read.
His aunt and uncle stared.
'Platform what?'
'Nine and three-quarters.'
'Don't talk rubbish', said Uncle Vernon,
'there is no platform nine and three-quarters'.

J. K. Rowling (1965 – …)
Harry Potter and the Philosopher's Stone, 6

CHAPTER

1

Introduction

DURING the last 300 years, fractional-order calculus has been moderately active in the literature (Chen, Petras and Xue 2009). More specifically, the mathematical theory on that subject is well established; see, e.g., (Ortigueira 2011), (Podlubny 1999a), and (Petráš 2011a), and provides additional modelling and control possibilities (Padula and Visioli 2014).

In the last three decades, there has been remarkable development in the use of fractional calculus in various fields, such as process modelling and control. It is now an important tool for the international industrial and scientific communities. In fact, the development of fractional calculus has enabled a large industrial and academic effort focused on the transition from conventional modelling and control to those described by fractional-order differential equations (Tepljakov 2017). Another relevant monograph that covers the design and implementation of different types of fractional-order controllers is (Monje, Chen, et al. 2010).

In particular, fractional calculus has found applications in complex mathematical and physical problems (Hilfer 2000) and (Oldham and Spanier 2006). As a sample, heat conduction through a semi-infinite solid (Gabano and Poinot 2011) (Gabano, Poinot and Kanoun 2011) and bioengineering applications reported in (Ionescu, et al. 2017) are particular examples of fractional systems.

Moreover, since fractional calculus is a generalization of conventional calculus, fractional models are generally expected to provide a more accurate description of the system dynamics than those based on classical differential equations (Monje, Chen, et al. 2010).

In this regard, control of industrial processes and, in particular, the application of fractional process models and fractional-order PID controllers (Podlubny 1999b), are of significant interest.

The use of fractional models and controllers is expected to lead to a significant overall improvement of industrial control loop quality thus providing an increase in the control system precision, performance and energy efficiency (Chen, Petras and Xue 2009).

The present thesis is devoted to the investigation of identification and control of dynamical systems based on fractional-order calculus with process control applications.

In particular, in Part I of this dissertation, different procedures for identifying fractional-order models based on the process reaction curve are proposed and discussed. In order for these identification procedures to have an impact on the process industry, they need to be simple to understand and to apply. Therefore, emphasis has been focused on their simplicity. Part II of this dissertation provides the required resources for the practical application of the identification procedures developed in Part I. Consequently, this part supports, on the one hand, the practical implementation of identification and control algorithms for fractional-order systems on real-time targets and, on the other hand, bridges the gap between software-based simulations of fractional systems and controllers and real-time hardware solutions.

Finally, experiments with laboratory prototypes and real industrial equipment are carried out and the results obtained are analyzed.

The remainder of this chapter is structured as follows: Section 1.1 explains the context and the motivation behind this research; Section 1.2 formulates the hypothesis, the goals to achieve, and the scope of the work; Section 1.3 describes the methodology to achieve these goals; Section 1.4 enumerates the contributions of this dissertation; and Section 1.5 presents a scheme of the dissertation.

1.1. Context and motivation

Enormous technological advances have marked a new stage in the field of process control in the process industries. Due to the remarkable development in the use of fractional calculus in various fields, such as process control and modelling, which has occurred in the last three decades, it can now be considered as an important tool for the international industrial and scientific communities (Monje, Chen, et al. 2010), (Padula and Visioli 2014), (Podlubny 1999a).

Therefore, fractional calculus contributes to alleviate the limitations of conventional differential equations. This results in ubiquitous phenomena, such as the fractional behaviour reported in (Sabatier 2021), being taken into account, leading to more accurate models of dynamical systems (Tepljakov 2017) and more efficient control systems (Monje, Chen, et al. 2010). Indeed, the development of fractional calculus has enabled a large industrial and academic effort focused on the transition from conventional modelling and control to those described by fractional-order differential equations (Tepljakov, Alagoz, et al. 2021).

Contemporary industrial control systems have considerable complexity (Yu 2006), (Rojas, Arrieta and Vilanova 2021), so such systems are likely to exhibit such fractional behaviour (Monje, Chen, et al. 2010). Furthermore, fractional-order dynamics have been observed in the time-domain responses of relatively simple systems, see, e.g., (Yuan, et al. 2022) and (Sabatier 2021).

Hence, the application of fractional-order identification and control methods to real industrial control problems is expected to have a positive impact on industrial processes in terms of improved performance, efficiency and cost reduction.

Therefore, it is interesting to study process control with respect to fractional dynamics. If a process exhibits such dynamics, the model-based control design procedure can be carried out using the corresponding tools. This gives rise to the problem of fractional model identification, which is related to several issues (Tepljakov 2017):

- The selection of an efficient simple-structure fractional-order model.
- The choice of an efficient simulation method for the identified fractional-order model.
- The election of the model parameters to be identified and the limitation of the number of parameters to improve the conditioning of the corresponding optimization problem.
- To ensure the practical usefulness of the model obtained, methods for its validation against experimental data should be implemented.
- The choice of an appropriate optimization algorithm to estimate the model parameters.

Once a valid model of a process has been established, the design of the model-based control can proceed.

Furthermore, it is known that fractional dynamics are best compensated by fractional-order controllers. However, tuning is more complicated compared to conventional controllers, in addition to their well-known implementation issues (Chen, Petras and Xue 2009), (Petráš 2011b), (Caponetto, et al. 2010).

Due to the additional tuning flexibility, fractional-order PID controllers are typically capable to outperform their conventional counterparts, since more design specifications can be met. Therefore, the development of a general method for tuning FOPID controllers is highly desirable (Monje, Chen, et al. 2010).

As mentioned above, the use of fractional models and controllers in industrial applications is of particular importance. Literature review studies show that about 90% of industrial control loops are of the PI/PID type (Åström and Hägglund 2006), (Vilanova and Visioli 2012); furthermore, it was found that about 80% of these existing control loops are poorly tuned (O'Dwyer 2009).

Since fractional-order PID controllers offer more tuning freedom and stabilization capabilities, industrial integration of these controllers is expected to be of considerable benefit. Therefore, some specific lines of research that can be proposed are as follows:

- To study fractional-order process models and provide means for the application of automatic controller tuning.
- To investigate the design of new fractional controllers that offer superior performance to conventional controllers.
- To study methods of implementing fractional-order systems and controls in industrial hardware devices.
- To develop a hardware controller prototype based on the developed controller design and synthesis methods.

Figure 1.1 illustrates the aforementioned concepts around which this dissertation revolves, namely fractional-order modelling and control and their practical implementation on industrial hardware devices. More specifically, the intersection of the three major concepts, which is intersection 1 in this figure, represents the approach covered in this dissertation, while the remaining three intersections comprise the various domains that compose this dissertation. Intersection 2 represents the methods for identifying fractional-order models oriented to control system design. Intersection 3 represents the implementation on industrial hardware devices of the identification methods discussed above. Intersection 4 deals with the implementation of the control algorithms on industrial hardware devices.

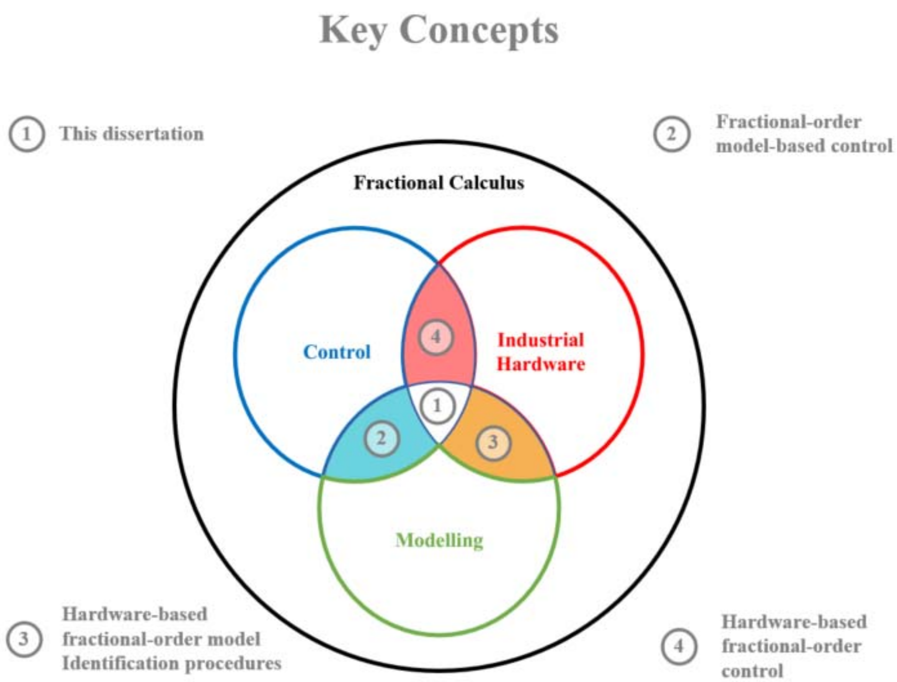

Figure 1.1. Venn diagram associating all the key concepts included in this dissertation as well as the intersection between them.

The primary objective of this dissertation is to make significant contributions to the research field of modelling and control of fractional-order systems and to promote their introduction and more widespread use in the industrial field by contributing to bridge the gap between theoretical research in fractional-order models and controls and their practical application in the process industry.

The use of fractional calculus in modelling and control-oriented applications is also the main motivation for the work presented in this dissertation. The author strongly believes that the use of generalized fractional models in system theory is a natural progression towards more accurate modelling and the development of more efficient control systems, as this thesis aims to prove. Therefore, it is expected that the use of fractional models and controllers will become standard practice in the coming years.

1.2. Hypothesis, Objectives and Scope

Based on the reviewed current State of the Art in fractional-order modelling and control approaches and their implementation on hardware equipment, the hypothesis of the present dissertation is:

Hypothesis: It is possible to conceive and implement a novel architecture, integrating various hardware technologies, that enables a straightforward and simple implementation of newly developed algorithms for identification and control of fractional-order systems, contributing to overcome the implementation issues of such systems on real-time targets and promoting their use at industrial level.

Hence, this dissertation sets the following goal in order to validate the aforementioned hypothesis:

Goal: Design and implement a novel control hardware architecture that enables implementation in various real-time hardware technologies of:
(i) New fractional-order model identification procedures, which are characterized by their effectiveness and simplicity,
(ii) Fractional-order control algorithms,
and that contributes to overcoming their implementation issues on such real-time targets, generally used in industry.

This general goal can be achieved by addressing the following more specific and measurable objectives:

- O1: To study the current State of the Art on approaches to fractional calculus-based identification and control methods and their implementation on hardware devices.
- O2: To develop procedures for the identification of simple-structure fractional-order models from time-domain information taken from the process reaction curve, according to an approach that simplifies their implementation on hardware devices.
- O3: To design and build a laboratory prototype with industrial characteristics, which enables the integration of industrial control hardware providing the appropriate characteristics for the application of fractional-order identification and control algorithms.
- O4: To conceive and implement an architecture integrating hardware and software resources that optimally provides access to various real-time targets.
- O5: To implement procedures for the identification and control of fractional-order systems on real-time targets and to identify an evaluation methodology for such procedures.

This hypothesis and objectives determine the activities that have been carried out in this research with a view to their validation.

1.3. Research methodology

In order to achieve the statement and derived objectives presented in Section 1.2 above, the following strategy has been defined:

1. Exploratory phase. Exploring the literature related to the research field in order to build a solid theoretical basis on which to support the rest of the research process. Although this literature review task is presented as an initial step in the research work, it is a continuous and incremental process that needs to be carried out throughout the entire research process.
2. Definition of the scope and validation scenario. After the first stage of reviewing the State of the Art and on the basis of the existing knowledge, the scope, context and motivation of this work are defined. Then, the scenario in which the project will be developed will be defined in accordance with the objectives set and knowing the limitations and advantages of the research proposal. Defining a solid initial framework is fundamental to guide future research towards the analysis that forms its basis.

3. Specification, design and development of the solution. At this stage, the previous knowledge will be used to determine the solution that better fits the identified requirements. Based on those requirements, the solution that is considered to achieve the best results is designed and developed, including the inputs obtained in the previous stages and the possible iterations of this research process.
4. Evaluation of the solution. After the design and development phase, the implemented solution is evaluated. This evaluation requires assessing specified requirements and verifying its validity and applicability in real environments and contexts.
5. Final conclusions, dissemination and writing of the PhD dissertation. The final task of the research process will focus on the analysis of the obtained results, the derived conclusions and the contributions of this process. It is expected that those conclusions and contributions will be innovative and of considerable significance, and that they will contribute to both academic and industrial fields when disseminated. Finally, the research work will be completed and improved with the development of this dissertation and its subsequent presentation and defence.

Figure 1.2 illustrates this research methodology, specifying the different phases and tasks involved and the iterative process followed to refine the initial conceptualization of the implemented solutions.

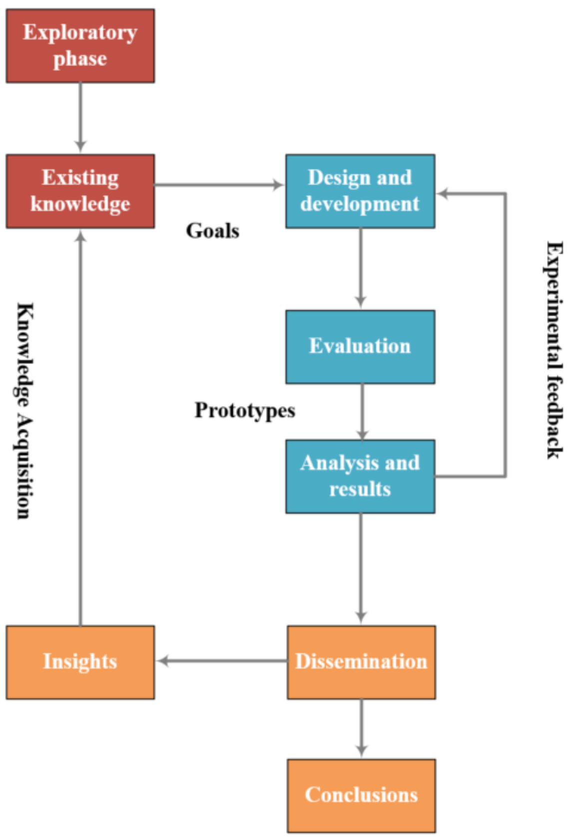

Figure 1.2. Schematic representation of the research methodology followed in this dissertation.

1.4. Main contributions

This section summarizes the main contributions of this dissertation. Although the focus of a dissertation are its scientific contributions, several significant technical ones have also been achieved, and are included here. Table 1.1 outlines the contributions, indicates their focus, and lists which objective they are related to, and in which chapters they are described.

Contribution		Focus	Objective	Chapter
Scientific	SC1	State of the Art	O1	Chapter 2
	SC2	Modelling	O2	Chapter 4
	SC3	Modelling	O2	Chapter 5
	SC4	Modelling	O2	Chapter 6
	SC5	Software/Hardware implementation	O4	Chapter 7
	SC6	Modelling Control Software/Hardware implementation	O5	Chapter 8 Chapter 9
Technical	TC1	Modelling Control Software/Hardware implementation	O3	Chapter 7 Chapter 8 Chapter 9
	TC2	Software/Hardware implementation	O4	Chapter 8 Chapter 9

Table 1.1. Summary of scientific and technical contributions.

1.4.1. Main scientific contributions

- SC1: A survey of current methods for identifying fractional-order models, a review of the different laboratory prototypes used to verify fractional-order identification and control methods, and an analysis of the implementation issues of fractional-order systems on real-time hardware targets.

  The related State of the Art is reviewed in Chapter 2.

- SC2: A fractional-order model identification method based on fitting three symmetrical points on the process reaction curve.

The development of the identification procedure for a set of symmetrical points, the derivation of their analytical equations, and the application to some numerical examples to verify the effectiveness of this procedure are discussed in Chapter 4.

- SC3: A method that improves the accuracy of the identified model obtained with the identification procedure for a set of symmetrical points by maintaining the symmetry of the extreme points and moving the central point.

The development of the proposed identification procedure, the derivation of their analytical equations, new insights on the selection of the central point x_2 in the context of the considered identification procedure, and the application to some numerical examples to verify the effectiveness of this procedure are discussed in Chapter 5.

- SC4: Validation of the general fractional order model identification procedure considering both symmetrical and asymmetrical sets of points on the process reaction curve.

In Chapter 6, the general identification procedure is developed, the procedure is validated for symmetrical and asymmetrical sets of points, and some numerical examples are provided to show the simplicity and effectiveness of the proposed procedure.

Very good results are obtained in comparison with other well-known identification methods, especially when simplicity is emphasized. The effect of the location of the three points on the accuracy of the identified fractional order model is also discussed. Finally, some comments and reflections about practical issues related to industrial practice are offered.

- SC5: Conceptualization and implementation of a novel control hardware architecture aimed to the practical implementation of identification and control algorithms for fractional-order systems using different available hardware technologies.

The proposed control hardware architecture has been implemented by combining the hardware components available on the myRIO platform using the most advanced LabVIEW programming techniques, which provide the capability of implementing PC-based control applications with embedded applications on microprocessor- and FPGA-based real-time targets. A detailed description of the hardware architecture as well as the hardware and software features are detailed in Chapter 7.

- SC6: Verification of the effectiveness and applicability of the proposed control hardware architecture for the practical implementation of fractional-order identification and control algorithms.

Chapters 8 and 9 provide detailed results of implementing different fractional-order identification and control algorithms on real-time hardware targets. In addition, the practical issues related to the implementation of such algorithms on different hardware platforms are studied in detail.

1.4.2. Main technical contributions

- TC1: Design and construction of a temperature-based experimental prototype, which has been used to demonstrate the effectiveness and applicability of the control hardware architecture proposed in this dissertation.

Chapter 7 and the first part of Chapter 8 describe in detail the temperature-based laboratory prototype and its main characteristics. More specifically, the temperature process, which involves thermal conduction, exhibits fractional behaviour in the different configurations. Also noteworthy is its nonlinear behaviour and the possibility to choose multiple operating points with different dynamic characteristics. All these features make this laboratory prototype suitable for the application of all the aspects related to the modelling and implementation of integer- and fractional-order model identification methods discussed in this thesis.

- TC2: The LabVIEW-based programming developed in this thesis, which includes the implementation of the fractional-order differential and integral operators and enables the hardware control architecture for the implementation of fractional-order system identification and control algorithms using the different hardware technologies available.

Part II of this thesis, comprising Chapters 7 to 9, details the control hardware architecture and the LabVIEW-based applications that have been implemented to operate the laboratory prototype and implement the aforementioned identification and control algorithms.

1.5. Thesis outline

The thesis is structured in ten chapters. Each chapter begins with a summary of the research problems discussed therein. Relevant examples are provided where appropriate, including those involving several chapters to illustrate developing ideas. Each chapter of the dissertation ends with a section of concluding remarks about the theoretical and practical results presented in the corresponding chapter. In what follows, a summary of each chapter is provided.

In the current one, Chapter 1, this dissertation is introduced, including the context and motivation, the hypothesis, objectives and contributions, as well as the research methodology followed to achieve them.

Chapter 2 presents an analysis of the State-of-the-Art in those concepts that constitute the theoretical basis of this dissertation. Those are categorised into: (i) fractional-order model identification methods, (ii) fractional-order control algorithms, (iii) industrial control hardware or real-time devices that allow implementing the mentioned identification and control methods in an industrial environment or in a real process.

Chapter 3 introduces the reader to the basic concepts and algorithms used in the dissertation. This chapter includes an introduction to the tools of fractional calculus, the definitions and properties of fractional operators, and the tools related to the modelling and analysis of dynamical systems.

The thesis is then divided into two parts:

Part I of this dissertation is devoted to developing fractional-order model identification procedures based on the process reaction curve.

In this part of the dissertation:

Chapter 4 presents a general FFOPDT model identification procedure based on fitting three arbitrary points (x_1-x_2-x_3%) on the process reaction curve. Such a procedure is particularized for the case where the three points on the reaction curve are symmetrically placed (x-50-(100–x)%).

Chapter 5 explores the potential improvement of the accuracy for the identified fractional-order model by moving the central point x_2 on the process reaction curve, while maintaining the symmetry of the extreme points with respect to the center of the total range.

Chapter 6 validates the general identification procedure presented in Chapter 4 by considering both symmetrical and asymmetrical set of points on the process reaction curve. The effect of the location of the three points on the acuraccy of the identified fractional-order model is also discussed.

Part II of this dissertation provides the required resources for the practical implementation of the identification procedures developed in Part I.

In this part of the dissertation:

Chapter 7 presents the conceptualization of a novel control hardware architecture aimed to the practical implementation of fractional-order identification and control algorithms.

Chapter 8 shows the results obtained by applying the identification algorithms presented in Part I of this dissertation on a temperature-based experimental setup and implemented using the hardware architecture described in Chapter 7.

Chapter 9 evaluates the effectiveness and applicability of the control hardware architecture presented in Chapter 7 through the practical implementation of integer- and fractional-order PID control algorithms on two real-time targets, i.e., on microprocessor- and FPGA-based hardware.

Finally, Chapter 10 summarizes the main findings and conclusions of this dissertation and outlines the future research lines related to it.

Figure 1.3 schematizes the structure of the dissertation, as indicated above.

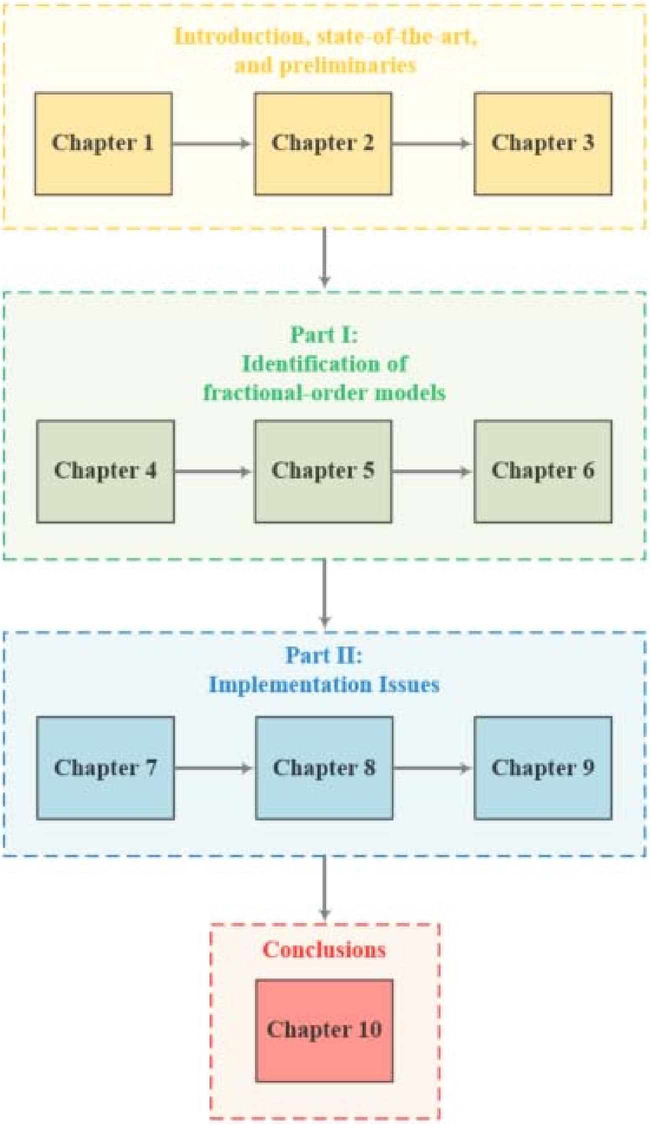

Figure 1.3. Schematic representation of the dissertation structure.

If we knew what it was we were doing, it would not be called research, would it?

Albert Einstein (1879 – †1955)

CHAPTER 2

Related work

THE wide scope of this dissertation makes it necessary to introduce concepts from several research fields in order to provide the required background for the sake of understanding the rest of the work. For this reason, this chapter will present a compilation of the existing literature that, in one way or another, addresses similar aspects around which this dissertation revolves.

Following the Venn diagram shown in Figure 1.1, this section will be articulated around three main concepts within the fractional calculus framework: (i) model identification methods, with special attention to those works characterized by seeking a trade-off between their effectiveness and computational cost; (ii) fractional-order control algorithms, as a tool to improve the control system performance; and (iii) industrial control hardware or real-time devices that allow implementing the mentioned identification and control methods in an industrial environment or in a real process.

Therefore, Section 2.1 of this chapter presents a brief introduction to developments in fractional calculus. Then, Section 2.2 presents the main advances in fractional-order model identification methods based on process reaction curve and Section 2.3 discusses industrial hardware and laboratory prototypes used in the literature to implement fractional-order models and controls. Finally, Section 2.4 summarises the chapter.

2.1. Introduction

The birth of noninteger- or fractional-order systems can be traced back to 1695 when Leibnitz and L'Hospital communicated with each other regarding the possibility of a derivative to assume a noninteger/fractional value, e.g. 1/2. In their correspondence Leibnitz used for the first time, the notation $d^{1/2}y$ in 1697 (B. Ross 1975).

However, the first work that formally considers a fractional-order derivative was written more than a hundred years later by Lacroix in 1819, (Lacroix 1819), (B. Ross 1975). The book is devoted to differential and integral calculus, but the author also addressed the problem of the fractional-order derivative. In that proposition, the fractional-order derivative has been described by using the Legendre's Gamma function. At the same time, fractional calculus was considered by Abel in 1823, where it was delivered in a mechanical problem related to the isochrone curve (Abel 1881). In that article, Abel proposed a fractional-order integration formula known as the Riemann-Liouville fractional integral and fractional-order differentiation known as the Caputo fractional derivative (Abel 1881). However, upon Abel's death his contribution remained in the shadow of other contributions. As can be read in reference (Podlubny, Magin and Trymorush 2017), the reason for this was the limited accessibility of the article. Abel's first and second works have been translated and published for a broader audience in 1881 and 1839, respectively (Abel 1881).

Somewhat later, works on the fractional calculus problem were provided by Liouville. He proposed the first widely known formal definitions of the fractional-order integrator. In particular, he provided two definitions for the fractional-order derivative and integrator. The second definition is similar to the Riemann-Liouville definition used today. Already as a student, Bernhard Riemann had explored the continuation investigation under the fractional-order derivative. In particular, Riemann proposed his definition of the fractional-order integrator. Nevertheless, Liouville's and Riemann's definitions were different, both from each other and from the Lacroix proposition. To solve this, the above mentioned discrepancies led to several works including Cauchy's integral formula. The first results were proposed by Sonin in 1869 and then extended by Letnikov in 1872. Ultimately, the problem was solved by Laurent, where the current Riemann-Liouville definition was proposed. Under mild conditions, the proposed generalized definition is equivalent to the Riemann, Liouville, and Lacroix propositions. Other work by Letnikov published and the results of another German mathematician Grünwald, have also led to an alternative definition of the fractional-order derivative, called the Grünwald-Letnikov definition.

The foundations of fractional calculus, including the currently explored definitions of fractional-order operators in terms of the Riemann-Liouville, Caputo, and Grünwald-Letnikov definitions, were proposed in the late 19th century. It should be noted that fractional calculus has been investigated with interest by scientists right from its birth. Numerous well-recognized engineers and mathematicians have contributed with their research on the field of fractional calculus, to mention Laplace, Riemann, Laurent, Heavyside or later Riesz (B. Ross 1977).

There are several more comprehensive and interesting historical studies in the area of fractional calculus, which are presented in the following references (Lützen 1990), (Podlubny, Magin and Trymorush 2017), (B. Ross 1977), (B. Ross 1975).

In addition, the seminal work summarizing the achievements in the fractional calculus area is the book (Oldham and Spanier 1974), which was first published in 1974. Since then, an increasing attention and interest in applied fractional calculus in science and technology can be observed. In particular, one can observe the extensive applications in this field during the last decade of the 20th century.

This fact can also be observed in Figure 2.1, which presents the number of publications indexed in the Web of Science Core Collection, that have been published in particular years with the phrase "fractional-order" or "noninteger-order" in their titles, keywords or abstracts (Kulczycki, Korbicz and Kacprzyk 2022).

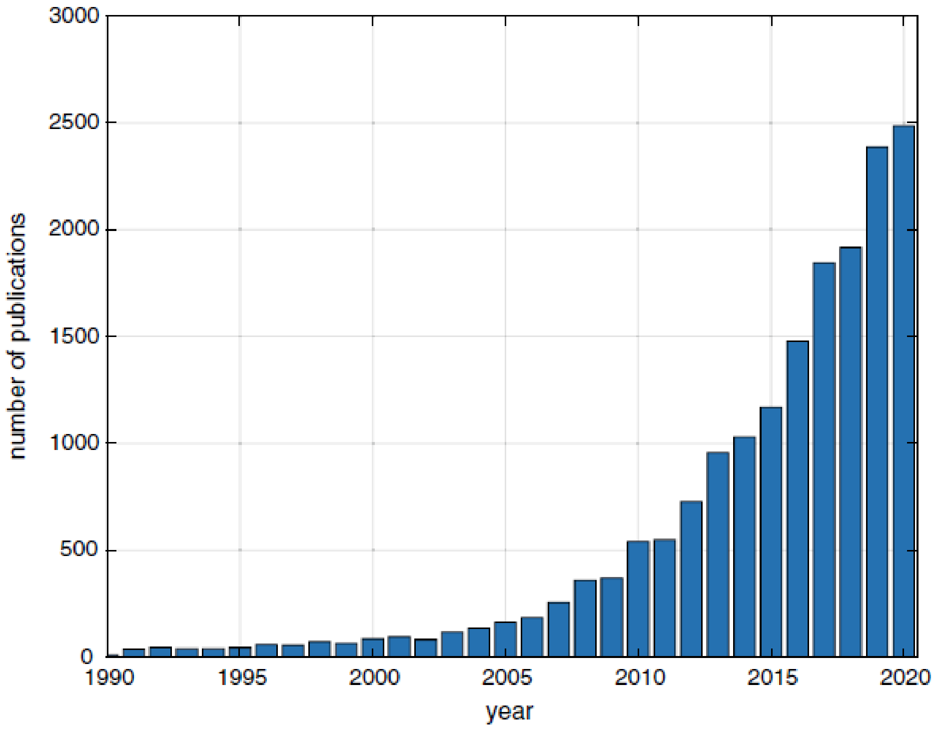

Figure 2.1. Number of publications indexed in Web of Sciences in the fractional-order area in particular years (Kulczycki, Korbicz and Kacprzyk 2022).

Fractional-order systems have been successfully applied in several areas of science and engineering. This can be observed from Figure 2.2, where the main areas of published papers are presented.

More specifically in Figure 2.2, it can be seen that the topic of fractional-order systems covers most of science and engineering, including various areas of physics and mathematics, control, electrical, mechanics, optics, telecommunication, medicine, and many other areas.

It is noteworthy that in 2020, papers considering fractional-order systems represented some 1.5% to 1.6 % of all papers in the sections of "Automation control systems" and "Mathematics-applied" included in the Web of Science system (Kulczycki, Korbicz and Kacprzyk 2022).

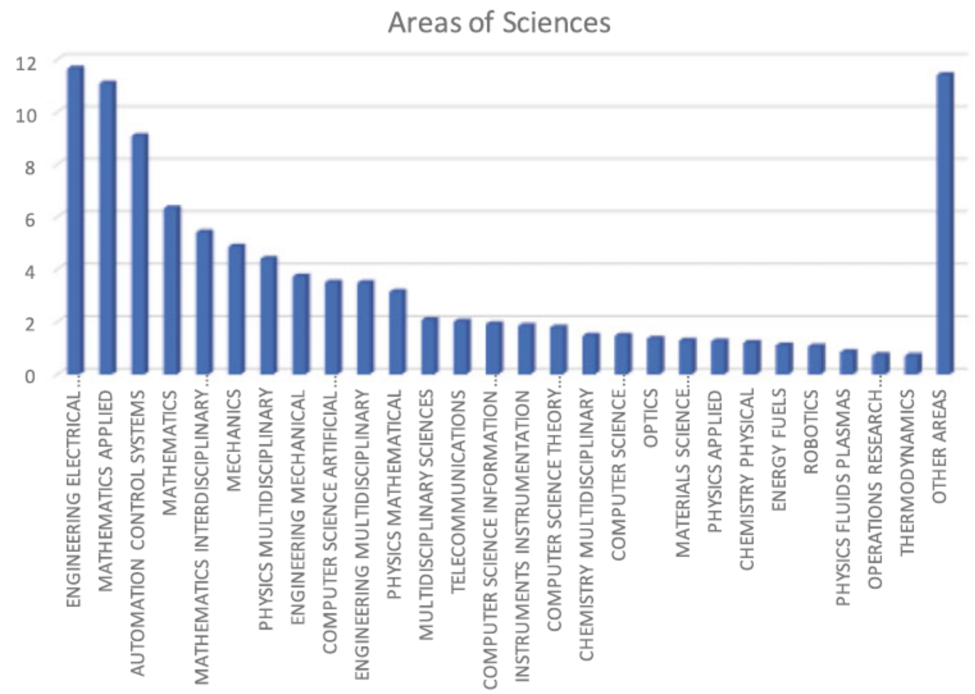

Figura 2.2. Fractional calculus applied in several areas of sciences and engineering (Kulczycki, Korbicz and Kacprzyk 2022).

2.2. Model identification methods

Although it might be possible to obtain a model of the process analytically –physical model–, it is more frequent that the dynamic information of the process is obtained through experimental tests –empirical model– from the process reaction curve, the critical gain and the period of oscillations of the control system at the limit of stability, or by feedback with a relay (Liu, Wang and Huang 2013).

From the controller point of view, the controlled process includes the process itself, the final controlling element, and the measuring instrument. In control studies and for the design and tuning of the controller in a feedback control loop, it is necessary to have information about the dynamic behaviour of the controlled process, usually in the form of a reduced-order mathematical model (Franklin, Powell and Emami-Naeini 2019). The controlled process model provides the dynamic information between the controller and the measuring instrument output signals. This model should be simple but, at the same time, it should provide reliable information about the controlled process behaviour at the operating point. This information usually includes: the gain, time constant(s), and apparent dead-time of the controlled process.

In spite of all the considerable advances in process control over the past several decades, it is common knowledge that PID controllers are widely and successfully used in industrial control applications, having become an industrial standard for process control, see (Åström and Hägglund 2006). It is acknowledged by the academic and industrial community that the most widely used controlled process models for this control algorithm are the first-order, dual-pole, and second-order plus dead-time (FOPDT, DPPDT, SOPDT) ones, however in some cases these models cannot represent the process dynamics with the required accuracy. This was already suggested in e.g. (Åström and Hägglund 2004), where it is indicated that it is necessary to have better information about the process to obtain optimal PID tuning rules for lag-dominated processes.

Practical experience shows that controller tuning can be generally accomplished with very little information about the plant from the point of view of standard design techniques. Experimental process model identification using an open-loop step-test is widely covered in the technical literature. See, e.g., the identification procedures described in (Huang and Jeng 2005), (Visioli 2006), (Tan, et al. 1999), and (Liu and Gao 2012).

Some papers also reported identification algorithms based on fitting several representative points in the process transient response to a step change (Rangaiah and Krishnaswamy 1996), (Huang, Lee and Chen 2001), (Alfaro 2006). In the technical literature there are several two- or three-point identification methods for FOPDT, DPPDT, and SOPDT models based on information taken from the reaction curve.

In the case of two-point procedures, the following methods and times can be considered: (Ho, Hang and Cao 1995) (35-85%), (Smith 1972) (28.3-63.2%), or (Vitecková, Vitecek and Smutny 2000) (33-70%).

In the case of three-point methods, the following references and corresponding times can be considered: (Jahanmiri and Fallahi 1997) (2-70-90%) and (5-70-90%), Stark in (Mollenkamp 1984) (15-45-75%), and (Rangaiah and Krishnaswamy 1994) (14-55-91%).

The 123c identification method (Alfaro 2006) uses the times sets (25-75%) for FOPDT and DPPDT, and (25-50-75%) for SOPDT models, respectively. This method has been recently extended in (Alfaro and Vilanova 2021) for the identification of RPPDT model.

In the previously mentioned references, the location of such points is diverse: in some cases, no explanation is given for the selection, in others significant points closely related to model parameters are selected. In some methods, see e.g. (Alfaro 2006), these points are not arbitrarily fixed, but have been selected in order to optimize the identified model parameters. It is obvious that the accuracy of the identified model depends on the selection of these points on the process reaction curve, as will be discussed later.

Over the last decades, the emergence of fractional calculus has made possible a great deal of academic and industrial effort focused on obtaining methods for more accurate modelling and identification of real-world phenomena, see for example (Ionescu, et al. 2017), (Narang, Sirish and Chen 2011), (Gabano, Poinot and Kanoun 2011). There is a wide variety of fractional-order modelling techniques based on the process reaction curve in the technical literature, being the most common approach the one based on nonlinear optimization, see for example (Guevara, et al. 2015), (Malek, Luo and Chen 2013), (Alagoz, et al. 2019), (Ahmed 2015). In these methods the fractional-order model parameters are generally obtained by minimizing the error between the process reaction curve and the fractional-order model step response. These techniques require a higher computational effort compared to existing analytical methods, whose main characteristic is the simplicity of their application. However, there are not many analytical techniques for modelling fractional-order processes based on the process reaction curve. In (Tavakoli-Kakhki, Haeri and Tavazoei 2010) some strategies have been proposed in order to determine the parameters of a FFOPDT model by making use of the step response data. It combines numerical computation and graphical estimation. This reference can be considered as a pioneering work in the fractional-order case. Integral-based estimating methods are proposed in (Tavakoli-Kakhki and Tavazoei 2014) and (Tavakoli-Kakhki, Tavazoei and Mesbahi 2013), which are robust against the presence of measurement noise. These last two methods can be considered as an extension of the area methods existing in the classical case (Åström and Hägglund 2006).

Even though fractional model has been proven technologically superior, industrial adoption for fractional approach requires more analysis (Tepljakov, Alagoz, et al. 2021).

In addition, recent surveys have outlined fractional-order PID controllers as an emerging tool in the field of process control with the major reason for its success being the intrinsic robustness they offer at a higher degree of freedom to operate and tune the parameters, see (Tepljakov, Alagoz, et al. 2018), (Birs, et al. 2019), (Dastjerdi, Vinagre, et al. 2019), and (Shah and Agashe 2016). In some of the existing methodologies of designing fractional-order PID controllers, a simple model of the process is utilized to tune the parameters of the intended controller (Monje, Vinagre and Feliu, et al. 2008), (Luo, et al. 2010), (Li, Luo and Chen 2010), (Tavakoli-Kakhki and Haeri 2011), (Gude and Kahoraho 2009c), and (Gude and Kahoraho 2010b).

According to all the above, obtaining a simple-structure fractional-order model for a process is of great importance and would be very useful in practically designing integer- and fractional-order control systems. Since the physical interpretation of a process step response is straightforward and identification algorithms for integer-order models based on fitting several representative points on the process reaction curve are easy to apply, it can be considered natural to extend such methods for the fractional-order case.

2.3. Laboratory equipment and control hardware

Enormous advances in technology have marked a new stage in the field of process control in the process industries, causing the need for universities and educational institutions to continually update themselves (Rossiter, et al. 2018). Alongside technological advances, laboratory equipment plays a significant role in control engineering research and education. The lack of adequate equipment to bring students closer to the reality in industry is one of the main problems encountered by a Faculty of Engineering in the practical education in the field of control engineering (Gude and Kahoraho 2010a). Due to this situation, there is a gap between the technical-practical and the theoretical education of the university graduates, which increases the deep-rooted distrust that companies have in academia because generally the practical training in these institutions does not meet industrial demands (Sánchez-Peña, Quevedo and Puig 2007).

The past three decades have witnessed remarkable development in the use of fractional calculus in various fields, such as process control and modelling. It is now an important tool for the international industrial and scientific communities. In fact, the development of fractional calculus has enabled a major industrial and academic effort centered on the transition from conventional modelling and control to those described by fractional-order differential equations (Tepljakov 2017). Another relevant monograph is (Monje, Chen, et al. 2010), which covers the design and implementation of different kinds of fractional-order controllers.

In particular, in these last two references, experimental equipment and practical experience play an important role in demonstrating the usefulness and applicability of fractional calculus in the areas of modelling and control. However, there are not many process rigs that clearly and comprehensibly illustrate the advantages of fractional systems and their control and are therefore suitable for fractional-order modelling and control. As a review of such platforms, the following references can be found in the literature:

Malti and co-workers developed an aluminum heat transfer platform in (Victor, et al. 2013) to investigate parameter and order estimation of fractional-order models. A similar platform has recently been presented in (Thomson and Padula 2022) to introduce fractional systems and fractional calculus as an effective tool for the study of both fractional-order modelling and control. Sierociuk and co-workers developed a metal beam with Peltier elements with a heating-cooling experimental platform in (Sierociuk, et al. 2013,) to study heat transfer in heterogeneous media. Macias and Sierociuk studied fractional-order PID control on the same platform in (Macias and Sierociuk 2012). Malek et al. used the Quanser-based heat flow experimental (HFE) platform to explore the modelling and control of fractional-order heat processes in (Malek, Luo and Chen 2013).

The identification and control algorithms are implemented on a PC and the process is accessed through a data acquisition card. Reference (Li, Zhao and Chen 2014) presents a low-cost hardware platform based on a Peltier cell for the modelling and control of multi-input multi-output (MIMO) fractional-order dynamic systems. In (Radici, et al. 2019) the same platform is used as a single-input single-output (SISO) system to introduce students to fractional systems, and to demonstrate that such systems can be very effective in the modelling task. In both cases, an Arduino-type microcontroller is used as the control hardware.

From the above references, one can see that most of them use experimental platforms related to temperature or heat transfer to deal with fractional-order processes. However, the hardware used is generally not emphasized, but taken as ancillary.

Furthermore, it has also been shown that fractional calculus in the design of control systems results in controllers that are more efficient in comparison with tradition-al integer-order controllers (Tepljakov 2017). However, the use of fractional-order control algorithms in industry is currently low, despite the fact that the fractional-order PID controller, as a generalization of the standard PID controller, provides significant benefits over the integer-order controller. Although the fractional-order PID controller was introduced in 1999, see (Podlubny 1999b), and since then there has been considerable development in design methods, tuning methods, and available software tools (Shah and Agashe 2016), the well-known implementation issues have contributed to the difficulties in conveying the advantages of fractional-order controllers in industry (Tepljakov, Alagoz, et al. 2018).

Therefore, considering the above, there is a need for laboratory equipment for training and researching in applied fractional calculus in order to bridge the gap existing between theoretical fractional-order identification and control algorithms and their practical implementation in a control hardware device. Training in implementation and tuning methods for fractional-order controllers is of major interest for making them more convenient and attractive for industry, thus facilitating their transition from state-of-the-art to state-of-use, see (Chevalier, et al. 2019). To the author's knowledge, there is currently no work in the literature on hardware architectures such as the one presented in this paper.

2.4. Summary and conclusions

Throughout this chapter, the State of the Art of fractional-order model identification methods and control and their implementation on industrial hardware and equipments has been analyzed. For that, a compilation of works that deal with the concepts around which this dissertation revolves has been presented. To begin with, the main concerns and barriers detected in the literature that affect model identification methods have been addressed. In particular, the focus has been set on methods based on the open-loop step-test experiment. This is followed by a discussion of the laboratory equipment and hardware technologies used in industry to implement fractional order systems.

From the analysis of the State of the Art, it can be concluded that:

- Over the last decades, the emergence of fractional calculus has made possible a great deal of academic and industrial effort focused on obtaining methods for more accurate modelling and identification of real-world phenomena.
- It is well-known that obtaining a simple-structure fractional-order model for a process has significant relevance and is very useful in practice for the design of both integer-order and fractional-order control systems.
- Industry requires methods for identification of fractional-order models.
- For these identification procedures to have an impact on the process industry, they must be simple to understand by engineers and practitioners and to implement in industrial control hardware devices.
- Laboratory equipment is required that exhibits fractional behaviour and allows testing of methods of identification and control of fractional order systems.
- Implementation issues for fractional-order systems in hardware devices need to be solved.

All men by nature desire to know.

Aristotle (384 BC – †322 BC)
Methaphysics

CHAPTER

3

Theoretical background and preliminaries

THE following chapter introduces the reader to core concepts and algorithms used in the thesis. The chapter begins with an introduction to fractional calculus tools, including fractional operator definitions and properties. Next, tools related to modeling and analysis of dynamic systems are discussed. Finally, a brief overview about time-domain analysis of fractional-order models is given.

3.1. Mathematical basis

In this section, some basic concepts and elementary definitions in fractional calculus are provided. Elementary ideas from fractional calculus can be found in many books, such as (Podlubny 1999a) and (Das 2010).

Fractional calculus is a generalization of integration and differentiation to non-integer fundamental operator ${}_aD_t^\alpha$. The continuous integro-differential operator is defined as:

$$
{}_aD_t^\alpha = \begin{cases} \dfrac{d^\alpha}{dt^\alpha}, & \alpha > 0 \\ 1, & \alpha = 0 \\ \displaystyle\int_a^t (d\tau)^\alpha, & \alpha < 0 \end{cases} \tag{3.1}
$$

where a and t are bounds of the operation and $\alpha \in \mathbb{R}$.

There are several different definitions of fractional operators, see (Podlubny 1999a). For the readers' convenience, the most common used definitions are briefly listed below.

Riemann-Liouville definition

One of the most used definition of the fractional integration is the Riemann-Liouville definition.

The fractional integral of order α for function $f(t)$ is defined as:

$$ {}_0I_t^\alpha f(t) \equiv {}_0D_t^{-\alpha} f(t) = \frac{1}{\Gamma(\alpha)} \int_0^t (t-\tau)^{\alpha-1} f(\tau) d\tau \tag{3.2}$$

where $t \geq 0$, $\alpha \in \mathbb{R}^+$, and $\Gamma(\cdot)$ is the Gamma function, (Podlubny 1999a).

The α-th order Riemann-Liouville definition of fractional derivative of the given function f(t) is defined as:

$$ {}_0D_t^\alpha f(t) = \frac{1}{\Gamma(m-\alpha)} \frac{d^m}{dt^m} \int_0^t (t-\tau)^{m-\alpha-1} f(\tau) d\tau \tag{3.3}$$

where $m-1<\alpha<m$, $m \in \mathbb{Z}^+$. In definitions (3.2) and (3.3), the subscripts 0 and t are the limits of operation and known as the terminals of fractional integration and differentiation, respectively.

Caputo definition

The Caputo definition of fractional-order differentiation takes the integer-order differentiation of the function first and then take the fractional-order integration:

$$ {}_0D_t^\alpha f(t) = \frac{1}{\Gamma(1-\alpha)} \int_0^t \frac{f'(\tau)}{(t-\tau)^\alpha} d\tau \tag{3.4}$$

Under this definition, D and ${}_0D_t^{-(1-\alpha)}$ do not commute because the initial value needs to be considered:

$$ {}_0D_t^\alpha f(t) = {}_0D_t^{-(1-\alpha)} f(t)[Df(t)] + \frac{f(0^+)t^{-\alpha}}{\Gamma(1-\alpha)} \tag{3.5}$$

Grünwald-Letnikov definition

The Grünwald-Letnikov definition defines the fractional integration and differentiations in a unified way:

$$ {}_0D_t^{\alpha}f(t) = \lim_{h\to 0}\frac{1}{h^{\alpha}}\sum_{j=0}^{[(t-a)/h]}(-1)^j\binom{\alpha}{j}f(t-jh) \tag{3.6}$$

where [·] means the integer part, and h is the step size.

Properties

Fractional-order differentiation has the following properties (Monje, Chen, et al. 2010), (Podlubny 1999a):

1. If $f(t)$ is an analytic function, then the fractional-order differentiation ${}_0D_t^{\alpha}f(t)$ is also analytic with respect to t.
2. If $\alpha = n$ and $n \in \mathbb{Z}^+$, then the operator ${}_0D_t^{\alpha}$ can be understood as the usual operator d^n/dt^n.
3. Operator of order $\alpha = 0$ is the identity operator: ${}_0D_t^{\alpha}f(t) = f(t)$.
4. Fractional-order differentiation is linear; if a, b are constants, then

$$ {}_0D_t^{\alpha}[af(t) + bg(t)] = a \cdot {}_0D_t^{\alpha}f(t) + b \cdot {}_0D_t^{\alpha}g(t) \tag{3.7}$$

5. For the fractional-order operators with $\mathrm{Real}(\alpha) > 0$, $\mathrm{Real}(\beta) > 0$, and under reasonable constraints on the function $f(t)$ it holds the additive law of exponents:

$$ {}_0D_t^{\alpha}\left[{}_0D_t^{\beta}f(t)\right] = {}_0D_t^{\beta}[{}_0D_t^{\alpha}f(t)] = {}_0D_t^{\alpha+\beta}f(t) \tag{3.8}$$

6. The fractional-order derivative commutes with integer-order derivative

$$ \frac{d^n}{dt^n}[{}_aD_t^{\alpha}f(t)] = {}_aD_t^{\alpha}\left(\frac{d^nf(t)}{dt^n}\right) = {}_aD_t^{\alpha+n}f(t) \tag{3.9}$$

under the condition $t = a$ we have $f^{(k)}(a) = 0$, $(k = 0, 1, 2, \ldots, n-1)$.

Laplace transform

The Laplace integral transform in an essential tool in dynamic systems and control engineering. A function $F(s)$ of the complex variable s is called the Laplace transform of the original function $f(t)$ and defined as:

$$ F(s) = L\{f(t)\} = \int_0^{\infty} e^{-st}f(t)dt \tag{3.10}$$

The original function $f(t)$ can be recovered from the Laplace transform $F(s)$ by applying the reverse Laplace transform defined as:

$$f(t) = L^{-1}\{F(s)\} = \frac{1}{j2\pi}\int_{c-j\infty}^{c+j\infty} e^{st}F(s)ds \tag{3.11}$$

where c is greater than the real part of all the poles of function $F(s)$ (Monje, Chen, et al. 2010).

In what follows, for the sake of simplicity, ${}_0D_t^{-\alpha}$ is denoted by $D^{-\alpha}$ and ${}_0D_t^{\alpha}$ by D^{α}. The Laplace transform of the Riemann-Liouville based fractional derivative is:

$$L\{D^{\alpha}f(t)\} = s^{\alpha}L\{f(t)\} - \sum_{k=0}^{m-1} s^k\, D^{\alpha-k-1}f(0) \tag{3.12}$$

where $m - 1 < \alpha < m$. For zero initial conditions, (3.12) is reduced to:

$$L\{D^{\alpha}f(t)\} = s^{\alpha}L\{f(t)\} \tag{3.13}$$

The reader interested in further study of fractional calculus can refer to (Podlubny 1999a) for fractional calculus in general, (Tepljakov 2017) for aspects related to fractional-order identification and control, and (Monje, Chen, et al. 2010) for fractional-order control.

3.2. Fractional-order models

A general fractional-order continuous-time dynamic system can be described by a fractional differential equation of the following form (Monje, Chen, et al. 2010):

$$\begin{aligned} &a_nD^{\alpha_n}y(t) + a_{n-1}D^{\alpha_{n-1}}y(t) + \cdots a_0D^{\alpha_0}y(t) = \\ &\quad = b_mD^{\beta_m}u(t) + b_{m-1}D^{\beta_{m-1}}u(t) + \cdots + b_0D^{\beta_0}u(t) \end{aligned} \tag{3.14}$$

where a_k $(k = 0, \ldots, n)$ and b_k $(k = 0, \ldots, m)$ are constants, and α_k $(k = 0, \ldots, n)$, β_k $(k = 0, \ldots, m)$ are arbitrary real or rational numbers and without loss of generality they can be arranged as $\alpha_n > \alpha_{n-1} > \cdots > \alpha_0$, and $\beta_m > \beta_{m-1} > \cdots > \beta_0$.

In particular case, the system is said to be of commensurate order when in (3.14) there is a real number q, which it is called the commensurate order, as the greatest common divisor of α_k $(k = 1, \ldots, n)$ and β_k $(k = 1, \ldots, m)$ such that $\alpha_k, \beta_k = kq$, $q \in \mathbb{R}^+$. Therefore, the incommensurate order system (3.14) can then be rewritten in commensurate form as follows:

$$\sum_{k=0}^{n} a_kD^{kq}y(t) = \sum_{k=0}^{m} b_kD^{kq}u(t) \tag{3.15}$$

If in the fractional-order differential equation (3.15) the order is $q = 1/r$, $r \in \mathbb{Z}^+$, the system will be of rational order.

The diagram with linear time-invariant (LTI) system classification is depicted in Figure 3.1.

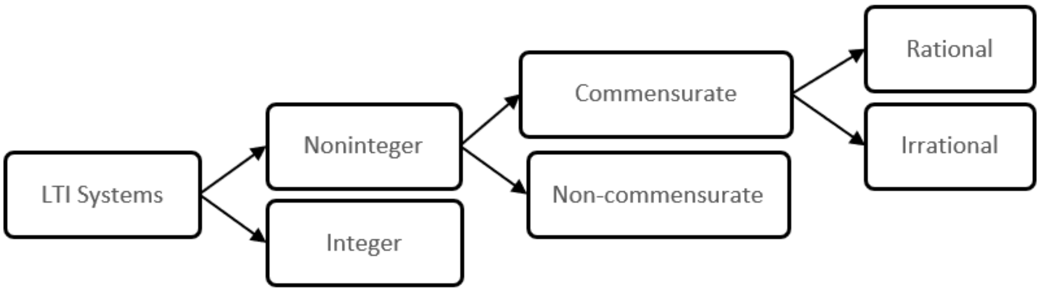

Figure 3.1. Classification of LTI systems.

Applying the Laplace transform to (3.14) with zero initial conditions, the corresponding fractional-order transfer function of incommensurate real orders has the following form (Podlubny 1999a):

$$G(s) = \frac{Q(s^{\beta_k})}{P(s^{\alpha_k})} = \frac{b_m s^{\beta_m} + b_{m-1} s^{\beta_{m-1}} + \cdots + b_0 s^{\beta_0}}{a_n s^{\alpha_n} + a_{n-1} s^{\alpha_{n-1}} + \cdots + a_1 s^{\alpha_1} + a_0 s^{\alpha_0}} \tag{3.16}$$

where $P(s^{\alpha_k})$ and $Q(s^{\beta_k})$ have no common zeros, and the commensurate transfer function is:

$$G(s) = \frac{Q(s^q)}{P(s^q)} = \frac{\sum_{k=0}^{m} b_k s^{kq}}{\sum_{k=0}^{n} a_k s^{kq}} \tag{3.17}$$

The number of fractional poles in (3.16) can be considered as the pseudo-order of the fractional-order system. In the case of fractional-order system with commensurate order q, it is possible to take $\sigma = s^q$ and consider the following continuous-time pseudo-rational transfer function:

$$H(\lambda) = \frac{\sum_{k=0}^{m} b_k \sigma^k}{\sum_{k=0}^{n} a_k \sigma^k} \tag{3.18}$$

3.2.1. Process models

In the context of this dissertation, where process control problems are dealt with, the fractional-order transfer function representation of a process model consists of the expression (3.16) and an input-delay term. The general form is as follows:

$$G(s) = \frac{b_m s^{\beta_m} + b_{m-1} s^{\beta_{m-1}} + \cdots + b_0 s^{\beta_0}}{a_n s^{\alpha_n} + a_{n-1} s^{\alpha_{n-1}} + \cdots + a_1 s^{\alpha_1} + a_0 s^{\alpha_0}} e^{-Ls} \tag{3.19}$$

where it is usual to take $\beta_0 = \alpha_0 = 0$ so that the static gain of the system is given by $K = b_0/a_0$, and $L \in \mathbb{R}^+$.

The particular case where $\{b_m = b_{m-1} = \ldots = b_1 = 0;\ a_n = a_{n-1} = \ldots = a_2 = 0;\ a_1 = T;\ a_0 = 1;\ b_0 = K;\ \beta_0 = 0;\ \alpha_1 = \alpha;\ \alpha_0 = 0\}$ leads to the following fractional-order differential equation:

$$T \cdot D^{\alpha}y(t) + y(t) = K \cdot u(t - L) \tag{3.20}$$

where K is the process gain, $T > 0$ is the time constant, $L \geq 0$ is the apparent dead-time, and α is the fractional order of the model. The initial conditions are generally taken as zero to obtain the standard FFOPDT transfer function model:

$$P(s) = \frac{Ke^{-Ls}}{1 + Ts^{\alpha}} \tag{3.21}$$

The following set of parameters:

$$\theta_P = \{K, T, L, \alpha\} \tag{3.22}$$

represents the FFOPDT model parameters, which will be identified in this thesis using information taken from the process reaction curve.

The standard FOPDT model:

$$P(s) = \frac{Ke^{-Ls}}{1 + Ts} \tag{3.23}$$

can be considered as a particular case of the FFOPDT model (3.21) with $\alpha = 1$.

The step response of the considered fractional-order model (3.21) can conveniently describe both monotonic or non-monotonic behaviours depending on the fractional order α. The step responses of FFOPDT models for increasing values of α, from $\alpha = 0.2$ to 1.8, are shown in Figure 3.2 for illustrative purposes. The step response of the considered system for $\alpha = 1$ is represented in dashed line.

The FOPDT model (3.23) has been broadly used in practice to capture the essential dynamic response of industrial processes for the purpose of control design; see, e.g., (Åström and Hägglund 2006). In this dissertation, the set of parameters (3.22) characterize the dynamic behaviour of the considered controlled process. The FFOPDT model (3.21) can be considered as a generalization of the classical FOPDT and the relevance of this generalization has great implications in both the identification of dynamic processes as well as in the controller parameter design of dynamic feedback loops (Muresan and Ionescu 2020).

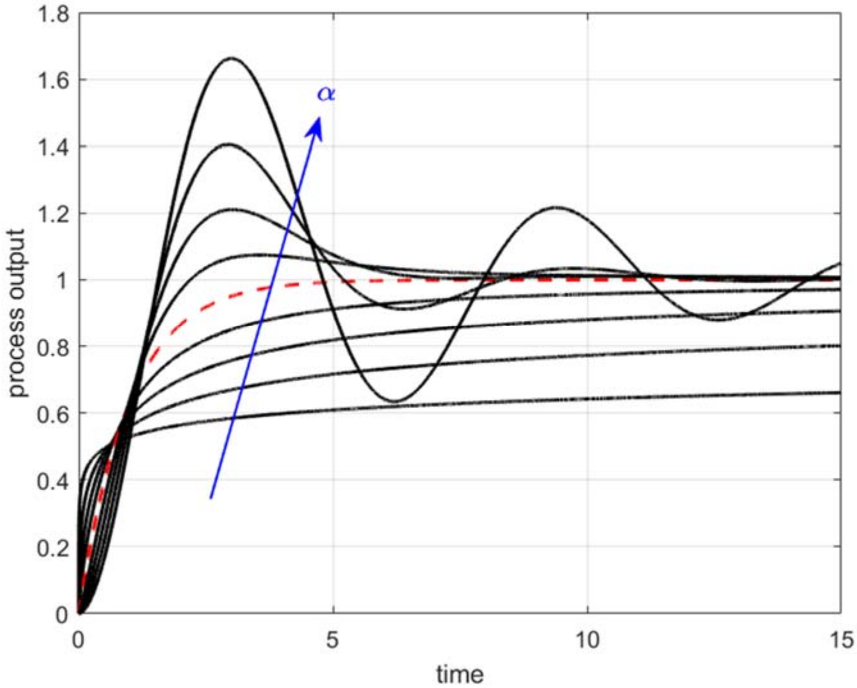

Figure 3.2. Step responses of the considered fractional-order system with $\alpha \in [0.2, 1.8]$. The step response for $\alpha = 1$ is in red dashed line.

It is also useful to consider a few parameters to characterize process dynamics. T_{ar} is the average residence time, which can be defined in the context of a fractional-order model as:

$$T_{ar} \doteq \frac{\int_0^\infty tg(t)dt}{\int_0^\infty g(t)dt} = L + T^{1/\alpha} \tag{3.24}$$

where g(t) is the impulse response of the system. The average residence time is essentially a rough measure of how long it takes the input to have a significant influence on the output.

In the same context, the normalized dead-time τ, which has the property $0 \leq \tau \leq 1$, can also be extended for a FFOPDT model as:

$$\tau \doteq \frac{L}{T_{ar}} = \frac{L}{L + T^{1/\alpha}} \tag{3.25}$$

This parameter can be used to characterize the difficulty of controlling a process. Roughly speaking, processes with small τ are easy to control, and the difficulty in controlling the system increases as τ increases. For the particular case $\alpha = 1$, T_{ar} and τ parameters correspond to their standard definition for a FOPDT model (Åström and Hägglund 2006).

Although the step response of the considered fractional model can conveniently describe both monotonic or non-monotonic behaviours depending on the fractional order α, this identification procedure is only applied to process having an S-shaped step response, since systems with essentially monotone step responses are very common in process control (Åström and Hägglund 2006). Furthermore, it is suggested in (Åström and Hägglund 2004) that the class of processes where PID is suitable can be characterized as having essentially monotone step responses. One way to characterize such processes is to introduce the monotonicity index:

$$\alpha_m \doteq \frac{\int_0^\infty g(t)dt}{\int_0^\infty |g(t)|dt} \tag{3.26}$$

where g(t) is the impulse response of the system. Systems with $\alpha_m = 1$ have monotone step responses, and systems with $\alpha_m > 0.8$ are considered essentially monotone.

Figure 3.3 shows the normalized step responses of the FFOPDT model (3.21) for different values of the fractional order α and different values of the normalized dead-time τ. Notice that all curves intersect at one-point $t = T_{ar}$ because of the normalization.

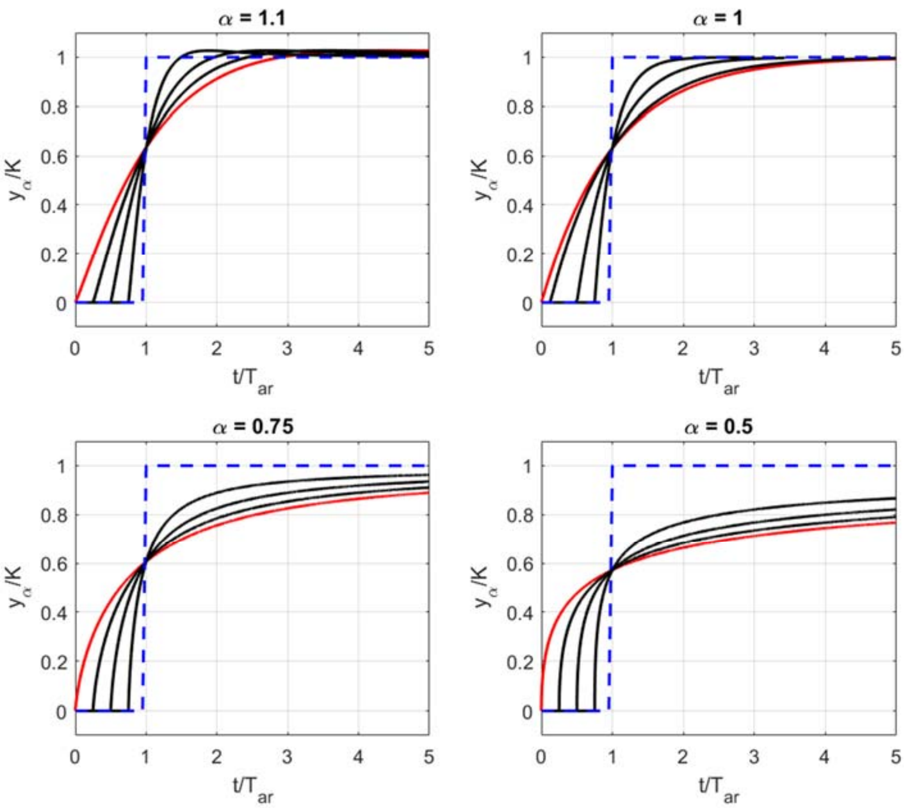

Figure 3.3. Normalized step responses y_α/K of the FFOPDT model (3.21) for different values of the fractional order α and different values of the normalized dead-time τ. The normalized dead-times are $\tau = 0$ (red), 0.25, 0.5, 0.75, and 1 (blue). Notice that time is normalized with respect to the average residence time T_{ar}.

3.2.2. Stability analysis

In this subsection, the stability of a fractional-order system given by (3.15) is considered.

It has been proven that the commensurate system G(s) brought in (3.17) is BIBO stable if all the roots of polynomial equation $P(x) = 0$ in which $x = s^q$ are positioned out of the sector $|\arg(x)| \leq q\pi/2$ (Monje, Chen, et al. 2010).

Stability regions of a fractional-order system are shown in Figure 3.4.

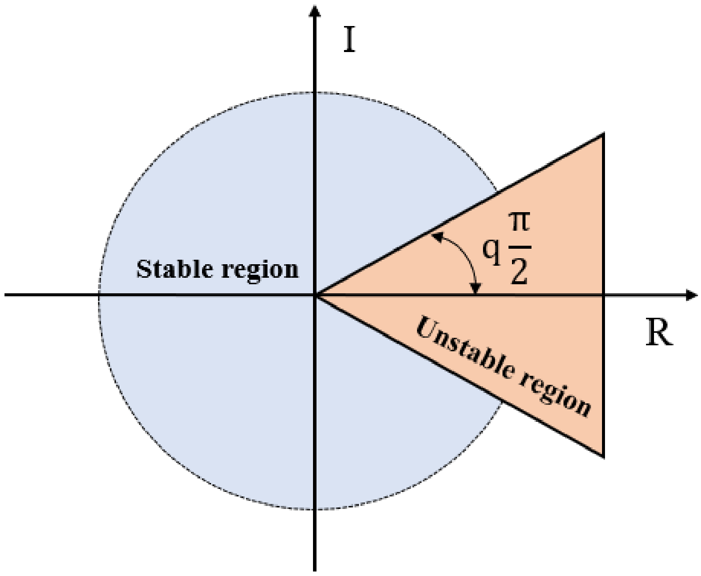

Figure 3.4. LTI fractional-order system stability requion for $0 < q \leq 1$.

3.2.3. Time-domain analysis

Regarding the analysis in the time domain, considering $n > m$, the function (3.16) becomes a proper rational function in the complex variable s^α and if it is supposed that roots of $P(x) = 0$ are distinct, the partial fraction expansion of transfer function (3.16) can be written in the following general form:

$$G(s^\alpha) = \sum_{i=1}^{n} \frac{r_i}{s^\alpha + \lambda_i} \tag{3.27}$$

where λ_i, $i = 1, \ldots, n$ are the roots of $P(x) = 0$, and r_i, $i = 1, \ldots, n$ are the corresponding residues.

Taking inverse Laplace transform from (3.27) results in the impulse response of $G(s^{\alpha})$ which is given in (Podlubny 1999a).

$$h(t) = L^{-1}\left\{\sum_{i=1}^{n} \frac{r_i}{s^{\alpha} + \lambda_i}\right\} = \sum_{i=1}^{n} r_i t^{\alpha-1} E_{\alpha,\alpha}(-\lambda_i t^{\alpha}) \tag{3.28}$$

where $E_{\alpha,\alpha}(z)$ denotes the so called two-parameter Mittag-Leffler function, which for an arbitrary value z is defined as:

$$E_{\alpha,\beta}(z) = \sum_{r=0}^{\infty} \frac{z^r}{\Gamma(\alpha r + \beta)} \tag{3.29}$$

Integrating the right-hand side of (3.28), the following step response of the transfer function $G(s^{\alpha})$ is obtained:

$$g(t) = \sum_{i=1}^{n} r_i \frac{E_{\alpha,1}(-\lambda_i t^{\alpha}) - 1}{\lambda_i} \tag{3.30}$$

Each component of the step response g(t) in (3.30) converges to its final value in a similar way as function $t^{-\alpha}$ does, as has been shown in (Tavakoli-Kakhki and Haeri 2011).

Another approach involves numerical computation of fractional-order derivatives which is carried out by means of a revised Grünwald-Letnikov definition (3.6) rewritten as

$${}_aD_t^{\alpha} f(t) = \lim_{h\to 0} \frac{1}{h^{\alpha}} \sum_{j=0}^{\left[\frac{t-a}{h}\right]} \omega_j^{(\alpha)} f(t - jh) \tag{3.31}$$

where h is the computation step-size and $\omega_j^{(\alpha)} = (-1)^j \binom{\alpha}{j}$ can be evaluated recursively from

$$\omega_0^{(\alpha)} = 1, \qquad \omega_j^{(\alpha)} = \left(1 - \frac{\alpha + 1}{j}\right) \omega_{j-1}^{(\alpha)}, \qquad j = 1, 2, \dots \tag{3.32}$$

To obtain a numerical solution for the equation in (3.14) the signal $\hat{u}(t)$ should be obtained first, using the algorithm in (3.31), where

$$\hat{u}(t) = b_m D^{\beta_m} u(t) + b_{m-1} D^{\beta_{m-1}} u(t) + \cdots + b_0 D^{\beta_0} u(t) \tag{3.33}$$

The time response of the system can then be obtained using the following equation:

$$y(t)=\frac{1}{\sum_{i=0}^{n}\frac{a_i}{h^{\alpha_i}}}\left[\hat{u}(t)-\sum_{i=0}^{n}\frac{a_i}{h^{\alpha_i}}\sum_{j=1}^{\left[\frac{t-a}{h}\right]}\omega_j^{(\alpha)}y(t-jh)\right] \tag{3.34}$$

The presented method is a fixed step method. The accuracy of simulation therefore may depend on the step size, see (Monje, Chen, et al. 2010).

If the system (3.19) has an input-output delay L, the resulting delayed response $y_d(t)$ with $y_d(0) = 0$ is obtained such that

$$y_d(t)=\begin{cases} y(t-L), & t>L \\ 0, & \text{otherwise} \end{cases} \tag{3.35}$$

Science will never be able to discover all the secrets of nature, because science is made by people and people are part of it.

J. Juan Rosales García (1967 – …)
Ecuaciones diferenciales ordinarias

PART I

Identification of fractional-order models

It is well-known that obtaining a fractional-order model for a process is of significant relevance and is very useful in practice for the design of both integer- and fractional-order control systems.

Since the physical interpretation of the step response of a process is straightforward and algorithms for identifying integer-order models based on fitting several representative points of the process reaction curve are easy to apply, it may be considered natural to extend such methods to the fractional-order case.

Part I of this dissertation is devoted to developing fractional-order model identification procedures based on the process reaction curve.

In order for such identification procedures to have an impact in the process industry, they need to be simple to understand and to apply. Therefore, emphasis has been placed on the simplicity of the procedures.

In this part of the dissertation:

Chapter 4 presents a general FFOPDT model identification procedure based on fitting three arbitrary points (x_1-x_2-x_3%) on the process reaction curve. Such a procedure is particularized for the case where the three points on the reaction curve are symmetrically placed (x-50-(100–x)%).

Chapter 5 explores the potential improvement of the accuracy for the identified fractional-order model by moving the central point x_2 on the process reaction curve, while maintaining the symmetry of the extreme points with respect to the center of the total range.

Chapter 6 validates the general identification procedure presented in Chapter 4 by considering both symmetrical and asymmetrical set of points on the process reaction curve. The effect of the location of the three points on the acuraccy of the identified fractional-order model is also discussed.

Symmetry is what we see at a glance; based on the fact that there is no reason for any difference...

Blaise Pascal (1623 – †1662)
Pensées

CHAPTER

4

Fractional-order model identification method: the symmetrical case

A general procedure for identifying an FFOPDT model is presented in this chapter. This procedure is based on fitting three arbitrary points on the process reaction curve, where process information is obtained from a simple open-loop test. A simplification of the general identification procedure is also considered, where only points symmetrically located on the reaction curve are selected. The proposed symmetrical procedure has been applied to the following sets of representative points: (5-50-95%), (10-50-90%), (15-50-85%), (20-50-80%), (25-50-75%), and (30-50-70%). Analytical expressions of the corresponding FFOPDT model parameters for these sets of symmetrical points have been obtained.

Some numerical examples are proposed in order to show the effectiveness of this procedure and to get insight into the influence of selection of the set of symmetrical points on the accuracy of the identified model.

4.1. Introduction

Although it might be possible to obtain a model of the process analytically –physical model–, it is more frequent that the dynamic information of the process is obtained through experimental tests –empirical model– from the process reaction curve, the critical gain and the period of oscillations of the control system at the limit of stability, or by feedback with a relay (Liu, Wang and Huang 2013).

From the controller point of view, the controlled process includes the process itself, the final controlling element, and the measuring instrument. In control studies and for the design and tuning of the controller in a feedback control loop, it is necessary to have information about the dynamic behaviour of the controlled process, usually in the form of a reduced-order mathematical model (Franklin, Powell and Emami-Naeini 2019). The controlled process model provides the dynamic information between the controller and the measuring instrument output signals. This model should be simple but, at the same time, it should provide reliable information about the controlled process behaviour at the operating point. This information usually includes: gain, time constant(s), and apparent dead-time of the controlled process.

According to the State of the Art in Chapter 2, obtaining a simple-structure fractional-order model for a process is of significant importance and would be very useful in practically designing integer- and fractional-order control systems. Since the physical interpretation of a process step response is straightforward and identification algorithms for integer-order models based on fitting several representative points on the process reaction curve are easy to apply, it can be considered natural to extend such methods for the fractional-order case. For that purpose, a general identification procedure for FFOPDT models has been conducted in this chapter based on fitting three-points in the transient process response to a step input. In the same framework, a simplification of the general identification procedure is proposed, considering that the points are selected symmetrically on the process reaction curve. Analytical expressions of the corresponding FFOPDT model parameters for several sets of symmetrical points are obtained in order show the applicability of the proposed procedure, and to get insight into the influence of the set of symmetrical points on the accuracy of the identified model.

This chapter is organised as follows. Section 4.2 is devoted to presenting the general method for identifying an FFOPDT model from any three points on the process reaction curve. In Section 4.3, a simplification of the general identification procedure is considered, where the points are selected symmetrically on the process reaction curve. In this section, analytical expressions of the corresponding FFOPDT model parameters are also obtained for several sets of symmetrical points. Section 4.4 illustrates the identification algorithm in order to facilitate the software implementation of the proposed identification method. In Section 4.5, some examples are provided to show the effectiveness and applicability of the proposed procedure in obtaining the parameters of the FFOPDT model in comparison with other integer- and fractional-order identification methods. In addition, this section also illustrates the results of several numerical simulations to find out the influence of the selection of the set of symmetrical points on the accuracy of the identified model. Finally, conclusions and concluding remarks are presented in Section 4.6.

4.2. General identification method

In this section, a general procedure for identifying a fractional-order model is presented. The procedure uses time-domain information and the parameters of the fractional model are obtained by considering three arbitrary points on the process reaction curve.

This section is divided into two parts: In the first part, some fundamentals about system identification are introduced. In the second part, the general FFOPDT model identification procedure is developed.

4.2.1. System identification fundamentals

This thesis will mainly consider the black box modelling approach (Ljung 1999). Strictly speaking, no assumptions are made about the internal physical structure of the system under study.

In this case, the aim of system identification is to derive a dynamical system model based on experimentally collected data.

For a black box model, it is necessary to obtain a relationship between inputs and outputs of the system under external stimuli (input signals or disturbances) in order to determine and predict the behaviour of the system.

A general form of a single-input single-output (SISO) system with disturbances is illustrated in Figure 4.1.

The general system identification procedure is summarized in Figure 4.2. and consists of the following concepts (Pillonetto, et al. 2022):

- X: the experimental conditions under which the experimental data D is generated. Experiment design involves all questions that concern the collection of estimation data, such as selecting which signals to measure, which sampling rate to use, and also the design of the input including possible feedback configurations;
- M: the structure of the model and its parameters θ. A model structure M is a set of parametrized models that describe the relations between the inputs and outputs of the system. The parameters are denoted by θ so a particular model will be denoted by $\mathrm{M}(\theta)$;
- I: the identification method by which the value of a parameter $\hat{\theta}$ in the model structure $\mathrm{M}(\theta)$ is determined from the data D. The goal of the identification is to match the model to the data;
- V: the validation process that builds confidence in the identified model. Model validation is about obtaining a model that, at least for the time being, can be accepted. It amounts to examining and scrutinizing the model to check if it can be used for its purpose.

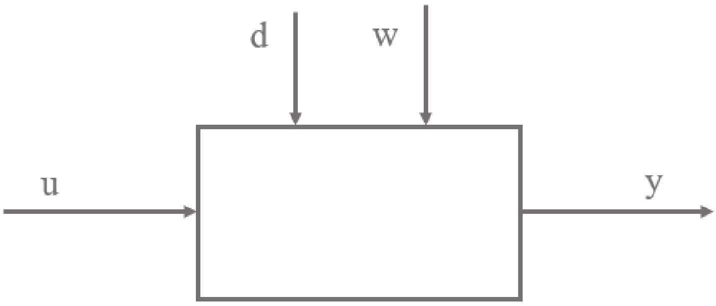

Figure 4.1. A general system with input u, output y, measured disturbance d, and unmeasured disturbance w.

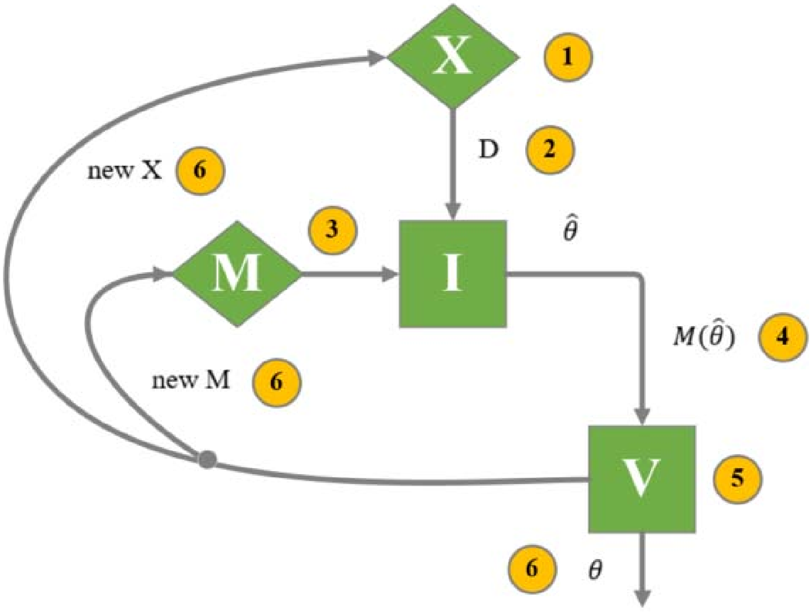

Figure 4.2. Typical system identification procedure.

It is usually an iterative process to arrive at a model that passes the validation test, which involves revisions of the necessary options. This figure also includes the following steps (Tepljakov 2017):

1. Design of experiment. For dynamic systems, it is common to collect transient response data in the time domain by applying a set of predetermined input signals, or the frequency response (magnitude and phase) in the frequency domain (e.g., by frequency sweep).
2. Record the data set of an experiment. The data collected should be as informative and limited as possible.
3. Choose a set of models and/or the model structure and the criterion to be fitted.
4. Calculate the model using an appropriate algorithm.
5. Validate the obtained model. It is advisable to use two different data sets for identification and validation.
6. If the model is satisfactory, use it for the intended purpose. If not, revise modelling/identification strategy and repeat the above steps.

A key step in the identification process is the determination of the amount of contribution of noise and disturbances to the collected data.

In the following, methods for system identification using a fractional-order model based on time-domain experiments will be investigated.

4.2.2. Model identification using the process reaction curve

A general identification procedure for identifying an FFOPDT model from the process reaction curve is presented in this section.

The step response of the fractional-order model under consideration can conveniently describe both monotonic and non-monotonic behaviours depending on the fractional order α, as discussed in Chapter 3.

Although the identification procedure presented below is general and applicable to processes exhibiting overdamped or underdamped behaviour, in this thesis this identification procedure is only applied to processes having an S-shaped step response, since systems with essentially monotonic step responses are very common in process control (Åström and Hägglund 2006). Furthermore, it is suggested in (Åström and Hägglund 2004) that the class of processes where PID is appropriate can be characterised as having essentially monotonic step responses.

In the following, the expressions required to determine the parameters (3.22) of an FFOPDT model (3.21) from the process reaction curve will be developed.

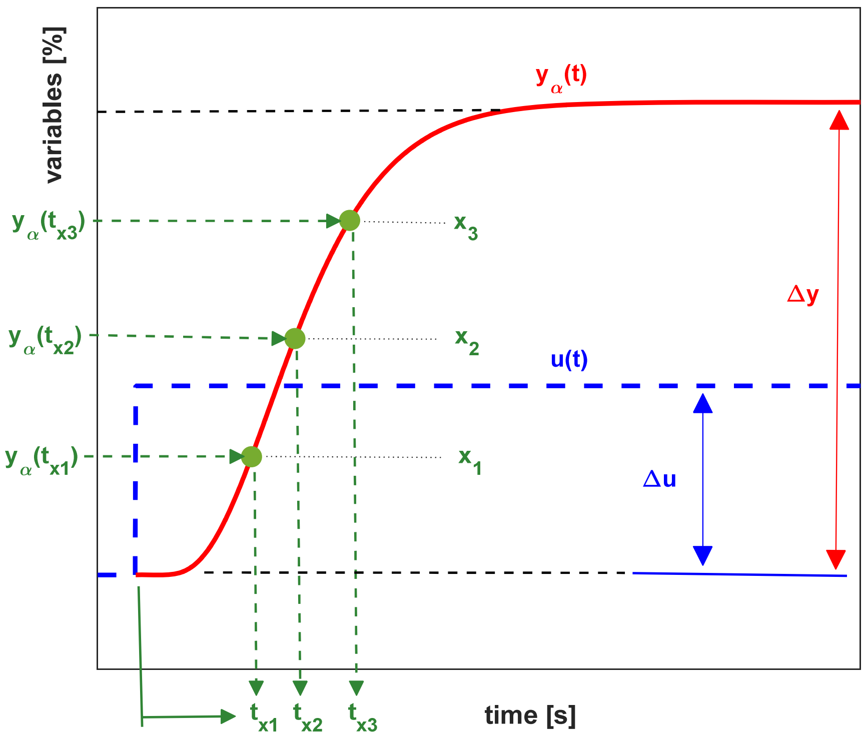

Figure 4.3. Step input signal and arbitrary representative points on the process reaction curve.

A step signal $u(t)$ with amplitude Δu will be considered as input and a signal $y_\alpha(t)$ with an amplitude Δy as response of the system, as shown in Figure 4.3. FFOPDT model (3.21) response to a Δu step input change is:

$$y_\alpha(t) = \begin{cases} 0, & 0 \leq t < L \\ K\left\{1 - E_{\alpha,1}\left[-\frac{1}{T}(t-L)^\alpha\right]\right\}\Delta u, & t \geq L \end{cases} \tag{4.1}$$

where $E_{\alpha,\beta}$ is the two-parameter Mittag-Leffler function defined in (3.29).

From the process reaction curve (4.1), the gain is given by:

$$K = \frac{\Delta y}{\Delta u} \tag{4.2}$$

where Δu is the amplitude of the input signal and Δy is the total process output change, as shown in Figure 4.3.

The process output $y_\alpha(t)$ can be normalized to its final value $\Delta y = K{\cdot}\Delta u$ and using the shifted and normalized time $\tau = \frac{1}{T}(t-L)^\alpha$, equation (4.1) is reduced to the following expression:

$$\tilde{y}_\alpha(\tau) = 1 - E_{\alpha,1}(-\tau), \quad \tau \geq 0 \tag{4.3}$$

If $\tilde{y}_\alpha(\tau)$ is the normalized process output, τ_x is the normalized time required to reach some specific output normalized value $\tilde{y}_\alpha(\tau_x)$ –being between 0 and 1, or 0% and 100% of the process output total change–. The value of τ_x can be easily obtained using (4.3).

Correspondingly, the time t_x required for the process output to reach $x\%$ of the process output total change is:

$$t_x = L + (\tau_x T)^{1/\alpha} \tag{4.4}$$

As the remaining FFOPDT model parameters $\{T, L, \alpha\}$ must be obtained, it is necessary to determine the times $\{t_{x1}, t_{x2}, t_{x3}\}$ to reach three points $\{y_\alpha(t_{x1}), y_\alpha(t_{x2}), y_\alpha(t_{x3})\}$ on the process reaction curve. Considering equation (4.4), the following equations set is defined:

$$\begin{cases} t_{x1} = L + (\tau_{x1}T)^{1/\alpha} \\ t_{x2} = L + (\tau_{x2}T)^{1/\alpha} \\ t_{x3} = L + (\tau_{x3}T)^{1/\alpha} \end{cases} \tag{4.5}$$

The so-called ratio index Δ, see, e.g., (Alfaro and Vilanova 2021), can be adapted to this fractional framework accordingly and can be used to determine the fractional order α:

$$\Delta \doteq \frac{t_{x3} - t_{x1}}{t_{x2} - t_{x1}} = \frac{\tau_{x3}{}^{1/\alpha} - \tau_{x1}{}^{1/\alpha}}{\tau_{x2}{}^{1/\alpha} - \tau_{x1}{}^{1/\alpha}} \tag{4.6}$$

where τ_{x1}, τ_{x2}, and τ_{x3} are normalized times and can be obtained using equation (4.3). Equation (4.6) can be expressed as a function relating the fractional order α and ratio index Δ, $\alpha = f_1(\Delta)$. The time-based parameters $\{T, L\}$ can be solved from (4.5) by considering two points, $\{y_\alpha(t_{x1}), t_{x1})\}$and $\{y_\alpha(t_{x3}), t_{x3})\}$ on the process reaction curve, which equivalent normalized points are $\{\tilde{y}_\alpha(\tau_{x1}), \tau_{x1}\}$ and $\{\tilde{y}_\alpha(\tau_{x3}), \tau_{x3}\}$. Then, the expressions for these parameters are:

$$T = a^\alpha (t_{x3} - t_{x1})^\alpha \tag{4.7}$$

and

$$L = t_{x3} - \tau_{x3}{}^{1/\alpha} T^{1/\alpha} \tag{4.8}$$

where

$$a = \frac{1}{\tau_{x3}{}^{1/\alpha} - \tau_{x1}{}^{1/\alpha}} \tag{4.9}$$

To conclude, the set of equations (4.10) comprises the general expressions for determining the parameters of the FFOPDT model, $\theta_P = \{K, T, L, \alpha\}$, using the times required for the response to reach any three-points on the reaction curve.

$$\begin{cases} K = \dfrac{\Delta y}{\Delta u} \\ \alpha = f_1(\Delta) \\ T = f_2(\alpha)(t_{x3} - t_{x1})^\alpha \\ L = \max\left[t_{x3} - f_3(\alpha) T^{1/\alpha}, 0\right] \end{cases} \tag{4.10}$$

where f_1 depends on Δ, which is defined as a function of the generic three points in (4.6), $f_2(\alpha) = a^\alpha$ and $f_3(\alpha) = \tau_{x3}{}^{1/\alpha}$ are functions that depend on the normalized times τ_{x1} and τ_{x3}, and τ_{x3}, respectively, and a-parameter is defined in (4.9). Notice in (4.10) how the values of T and L have a high dependence on the value of α, which has a significant influence on the shape of the response. This fact emphasizes the importance of determining the value of α parameter accurately, as will be discussed later.

In (4.10), $\alpha > 0$ and $T > 0$ are fulfilled in a natural way, since $\tau_{x1} < \tau_{x2} < \tau_{x3}$ and $t_{x1} < t_{x2} < t_{x3}$. Another condition that must be fulfilled in order to meet $L \geq 0$ is:

$$t_{x3} \geq (\tau_{x3} T)^{1/\alpha} \tag{4.11}$$

4.3. Symmetrical method

In the general development of the identification procedure presented in previous section, it has been assumed that the required three-points on the reaction curve could be any. In this section, a simplification of the general method in which these points can be arbitrarily selected but located symmetrically on the response curve is presented.

Note that, as depicted in Figure 4.4, the central point will be located in the middle of the range and will correspond to the time needed to reach 50% of the process output total change on the reaction curve $y_\alpha(t_{50})$, $t_{x2} = t_{50}$. The remaining points could be located arbitrarily but symmetrically placed with respect to central point. One of the symmetrical points will be denoted x, the other being $100–x$. This means that the times to be determined will now be $t_{x1} = t_x$ and $t_{x3} = t_{100–x}$, where t_x and $t_{100–x}$ denote the time needed to reach $x\%$ and $(100–x)\%$ of the process output total change, respectively, where $0 < x < 50$.

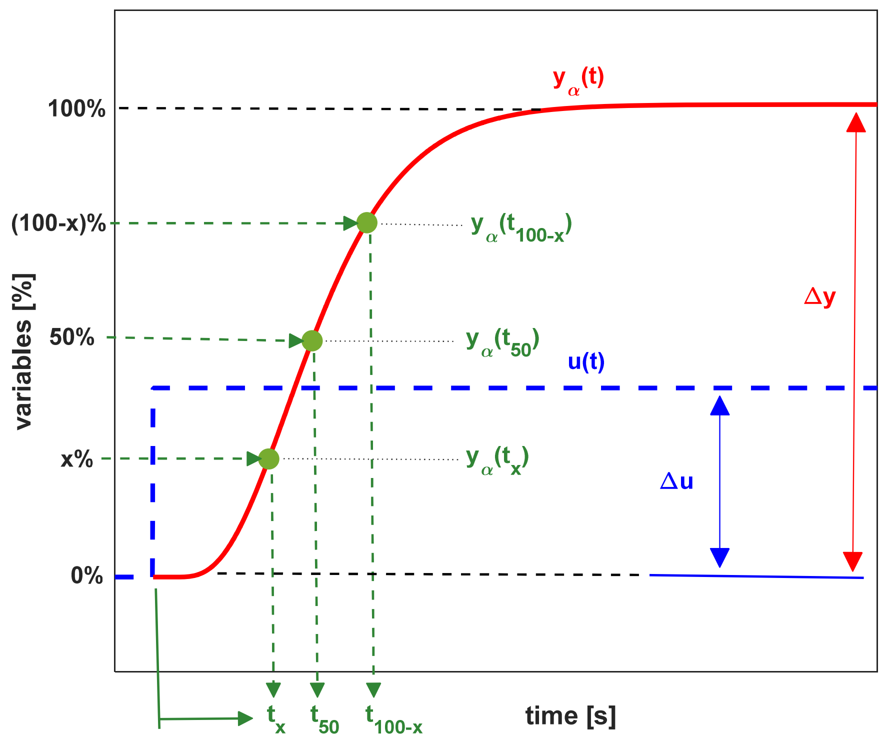

Figure 4.4. Step input signal and symmetrical representative points on the process reaction curve.

Adapting equations (4.10) with these symmetry considerations, the following expressions are obtained:

$$\begin{cases} K = \dfrac{\Delta y}{\Delta u} \\ \alpha = f_1(\Delta) \\ T = f_2(\alpha)[(t_{100-x}) - t_x]^{\alpha} \\ L = \max\left[(t_{100-x}) - f_3(\alpha)T^{1/\alpha}, 0\right] \end{cases} \tag{4.12}$$

where f_1 is the function that relates fractional order α with the times ratio Δ.

Additionally, Δ is defined as a function of the symmetrical three-points as:

$$\Delta \doteq \frac{(t_{100-x}) - t_x}{t_{50} - t_x} = \frac{(\tau_{100-x})^{1/\alpha} - (\tau_x)^{1/\alpha}}{(\tau_{50})^{1/\alpha} - (\tau_x)^{1/\alpha}} \tag{4.13}$$

and depends on the normalized times τ_x, τ_{50}, and τ_{100-x}.

The remaining functions f_2 and f_3 have the following expressions: $f_2(\alpha) = a^{\alpha}$, where

$$a = \frac{1}{(\tau_{100-x})^{1/\alpha} - (\tau_x)^{1/\alpha}} \tag{4.14}$$

and $f_3(\alpha) = (\tau_{100-x})^{1/\alpha}$. They are functions that depend on the normalized times τ_x and τ_{100-x}, and τ_{100-x}, respectively.

In this chapter, the following sets of symmetrical points will be considered: (5-50-95%), (10-50-90%), (15-50-85%), (20-50-80%), (25-50-75%), and (30-50-70%), which correspond to the following values of $x = 5, 10, 15, 20, 25, 30$, respectively. The objective is to get insight into the influence of the selection of representative points on the accuracy of the obtained fractional-order model, as has been mentioned previously. Tables 4.1 – 4.6 contain the values of the normalized times τ_x, τ_{50}, and τ_{100-x}, for values of $x = 5, 10, 15, 20, 25$, and 30, respectively. Hereafter, considering values of the corresponding normalized times, data sets $\{\Delta, \alpha\}$, $\{\alpha, a^{\alpha}\}$, and $\{\alpha, (\tau_{100-x})^{1/\alpha}\}$ are obtained for each one of the considered sets of symmetrical points. From these data, the analytical expressions for $f_1(\Delta)$, $f_2(\alpha)$, and $f_3(\alpha)$ are estimated using curve fitting. Finally, fractional-order model parameters $\{T, L, \alpha\}$ can be determined from expressions (4.12) and experimental values t_x, t_{50}, and t_{100-x} collected from the reaction curve.

α	τ_5 [s]	τ_{50} [s]	τ_{95} [s]
0.50	0.0021	0.5916	126.3400
0.55	0.0040	0.5990	69.3350
0.60	0.0060	0.6058	41.4000
0.65	0.0090	0.6150	26.3090
0.70	0.0130	0.6231	17.5400
0.75	0.0172	0.6340	12.1030
0.80	0.0225	0.6435	8.6100
0.85	0.0286	0.6560	6.2560
0.90	0.0355	0.6670	4.6920
0.95	0.0430	0.6810	3.6640
1.00	0.0513	0.6932	2.9980
1.05	0.0603	0.7080	2.5600
1.10	0.0699	0.7220	2.2633

Table 4.1. Numeric values of normalized times τ_5, τ_{50}, and τ_{95} for different values of α.

α	τ_{10} [s]	τ_{50} [s]	τ_{90} [s]
0.50	0.0093	0.5916	30.8550
0.55	0.0142	0.5990	19.7430
0.60	0.0203	0.6058	13.4810
0.65	0.0276	0.6150	9.6760
0.70	0.0359	0.6231	7.2250
0.75	0.0453	0.6340	5.5750
0.80	0.0558	0.6435	4.4280
0.85	0.0670	0.6560	3.6140
0.90	0.0791	0.6670	3.0310
0.95	0.0919	0.6810	2.6100
1.00	0.1059	0.6932	2.3040
1.05	0.1195	0.7080	2.0810
1.10	0.1350	0.7220	1.9150

Table 4.2. Numeric values of normalized times τ_{10}, τ_{50}, and τ_{90} for different values of α.

α	τ_{15} [s]	τ_{50} [s]	τ_{85} [s]
0.50	0.0229	0.5916	13.2100
0.55	0.0321	0.5990	9.3140
0.60	0.0428	0.6058	6.9304
0.65	0.0546	0.6150	5.3770
0.70	0.0677	0.6231	4.3117
0.75	0.0817	0.6340	3.5590
0.80	0.0966	0.6435	3.0097
0.85	0.1122	0.6560	2.6050
0.90	0.1285	0.6670	2.3004
0.95	0.1452	0.6810	2.0730
1.00	0.1626	0.6932	1.8973
1.05	0.1802	0.7080	1.7660
1.10	0.1984	0.7220	1.6626

Table 4.3. Numeric values of normalized times τ_{15}, τ_{50}, and τ_{85} for different values of α.

α	τ_{20} [s]	τ_{50} [s]	τ_{80} [s]
0.50	0.0450	0.5916	7.0390
0.55	0.0588	0.5990	5.3510
0.60	0.0750	0.6058	4.2490
0.65	0.0907	0.6150	3.4920
0.70	0.1082	0.6231	2.9493
0.75	0.1261	0.6340	2.5520
0.80	0.1448	0.6435	2.2526
0.85	0.1639	0.6560	2.0260
0.90	0.1834	0.6670	1.8501
0.95	0.2031	0.6810	1.7160
1.00	0.2232	0.6932	1.6096
1.05	0.2434	0.7080	1.5290
1.10	0.2639	0.7220	1.4642

Table 4.4. Numeric values of normalized times τ_{20}, τ_{50}, and τ_{80} for different values of α.

α	τ_{25} [s]	τ_{50} [s]	τ_{75} [s]
0.50	0.0780	0.5916	4.2100
0.55	0.0965	0.5990	3.4020
0.60	0.1170	0.6058	2.8480
0.65	0.1370	0.6150	2.4510
0.70	0.1590	0.6231	2.1580
0.75	0.1793	0.6340	1.9370
0.80	0.2021	0.6435	1.7662
0.85	0.2224	0.6560	1.6350
0.90	0.2450	0.6670	1.5310
0.95	0.2659	0.6810	1.4510
1.00	0.2880	0.6932	1.3870
1.05	0.3095	0.7080	1.3380
1.10	0.3314	0.7220	1.3000

Table 4.5. Numeric values of normalized times τ_{25}, τ_{50}, and τ_{75} for different values of α.

α	τ_{30} [s]	τ_{50} [s]	τ_{70} [s]
0.50	0.1242	0.5916	2.6917
0.55	0.1478	0.5990	2.2940
0.60	0.1716	0.6058	2.0079
0.65	0.1952	0.6150	1.7980
0.70	0.2188	0.6231	1.6376
0.75	0.2422	0.6340	1.5160
0.80	0.2655	0.6435	1.4191
0.85	0.2884	0.6560	1.3450
0.90	0.3114	0.6670	1.2854
0.95	0.3341	0.6810	1.2410
1.00	0.3567	0.6932	1.2041
1.05	0.3792	0.7080	1.1780
1.10	0.4016	0.7220	1.1568

Table 4.6. Numeric values of normalized times τ_{30}, τ_{50}, and τ_{70} for different values of α.

Δ values for different values of α, $0.5 \leq \alpha \leq 1.1$, have been obtained in Figure 4.5, according to expression (4.13) and using the normalized times τ_x, τ_{50}, and τ_{100-x}, for x = 5, 10, 15, 20, 25, and 30, obtained from Tables 4.1 – 4.6. Note that Δ index represents the ratio between the time difference in reaching from x to $(100–x)\%$ and from x to 50% of the process output total change, as indicated in (4.13).

The data set $\{\Delta, \alpha\}$ allows establishing a relationship between α and Δ in the form of an analytic function, $\alpha = f_1(\Delta)$.

Figure 4.5 shows the data sets $\{\Delta, \alpha\}$ obtained from equation (4.13) for different values of α, where $0.5 \le \alpha \le 1.1$, and their corresponding results of least-squares curve-fitting for the different sets of symmetrical points. Note that Δ depends on normalized times $\{\tau_x, \tau_{50}, \text{and } \tau_{100-x}\}$, as indicated in (4.13), and has a significant dependence on α parameter. Data is fitted using the Levenberg–Marquardt least-squares curve-fitting algorithm in all graphs in Figure 4.5, and the following rational function is considered in all cases:

$$f_1(\Delta) = \frac{p_1\Delta^2 + p_2\Delta + p_3}{\Delta^2 + q_1\Delta + q_2} \tag{4.15}$$

where Table 4.7 shows the values of the parameters $\{p_i, q_i\}$ for function $f_1(\Delta)$ and each one of the selected sets of symmetrical points.

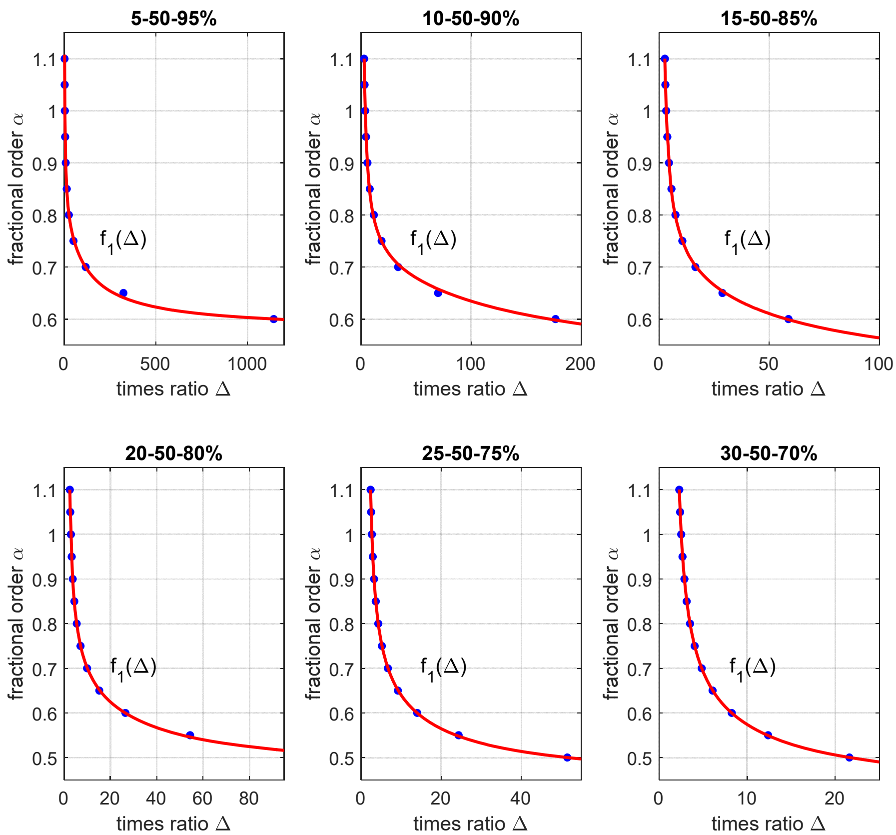

Figure 4.5. Data sets $\{\Delta, \alpha\}$, where Δ is defined in (4.13), $x = 5, 10, 15, 20, 25$, and 30, and results of curve fitting for $f_1(\Delta)$.

It is important to note that for increasing values of x, Δ range becomes shorter. $f_1(\Delta)$ is a non-linear function whose slope is steeper for increasing values of x, indicating that the sensitivity is greater.

5-50-95%	10-50-90%	15-50-85%	20-50-80%	25-50-75%	30-50-70%
$p_1 = 0.5786$	$p_1 = 0.4882$	$p_1 = 0.4767$	$p_1 = 0.4613$	$p_1 = 0.4424$	$p_1 = 0.4174$
$p_2 = 93.2$	$p_2 = 109.6$	$p_2 = 38.15$	$p_2 = 17.04$	$p_2 = 8.106$	$p_2 = 3.942$
$p_3 = 133.9$	$p_3 = 201.7$	$p_3 = 24.63$	$p_3 = -0.0419$	$p_3 = -3.652$	$p_3 = -3.208$
$q_1 = 114.3$	$q_1 = 152.6$	$q_1 = 52.91$	$q_1 = 23.18$	$q_1 = 10.40$	$q_1 = 4.384$
$q_2 = 26.59$	$q_2 = 30.39$	$q_2 = -29.59$	$q_2 = -22.93$	$q_2 = -14.00$	$q_2 = -8.02$

Table 4.7. Parameters $\{p_i, q_i\}$ of the rational function $f_1(\Delta)$ for the different sets of symmetrical points.

Figure 4.6 shows the data sets $\{\alpha, a^\alpha\}$, where a-parameter is obtained from equation (4.14), for different values of α, $0.5 \le \alpha \le 1.1$, and their corresponding results of least-squares curve-fitting for the different sets of symmetrical points. Note that $f_2(\alpha) = a^\alpha$ depends on α and normalized times τ_x and τ_{100-x}.

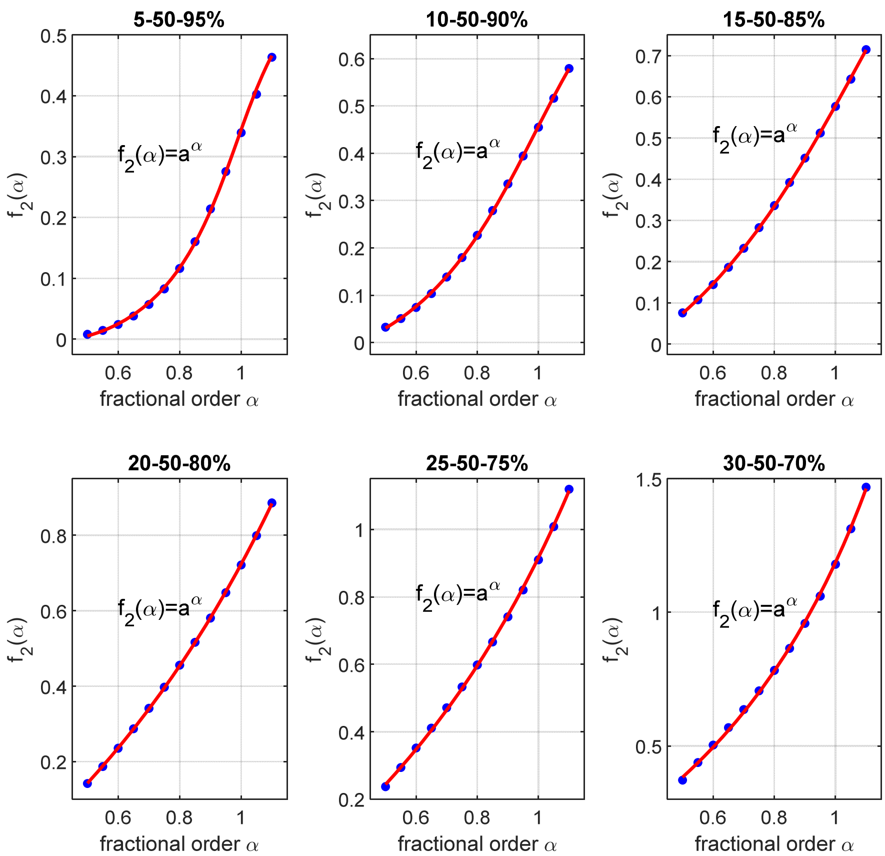

Figure 4.6. Data sets $\{\alpha, a^\alpha\}$, where a is defined in (4.14), $x = 5, 10, 15, 20, 25$, and 30, and results of curve fitting for $f_2(\alpha)$.

In Figure 4.6, it can be seen that the amplitude of f_2 increases for increasing values of x. On the other hand, for decreasing values of x function f_2 presents a more pronounced curvature for small values of α. Data is fitted using the Levenberg–Marquardt least-squares curve fitting algorithm in all graphs in Figure 4.6, and the following rational function is used in all cases:

$$f_2(\alpha) = \frac{p_1\alpha + p_2}{\alpha^2 + q_1\alpha + q_2} \quad (4.16)$$

where the values of the parameters $\{p_i, q_i\}$ for function $f_2(\alpha)$ and each one of the selected sets of symmetrical points are shown in Table 4.8.

5-50-95%	10-50-90%	15-50-85%	20-50-80%	25-50-75%	30-50-70%
$p_1 = 0.06589$	$p_1 = 0.2417$	$p_1 = 0.9406$	$p_1 = 9746$	$p_1 = 1.715 \cdot 10^4$	$p_1 = 3.691 \cdot 10^4$
$p_2 = -0.03054$	$p_2 = -0.0986$	$p_2 = -0.3488$	$p_2 = -3199$	$p_2 = -3675$	$p_2 = -426.5$
$q_1 = -2.23$	$q_1 = -2.338$	$q_1 = -2.722$	$q_1 = -5405$	$q_1 = -1.074 \cdot 10^4$	$q_1 = -3.276 \cdot 10^4$
$q_2 = 1.333$	$q_2 = 1.651$	$q_2 = 2.745$	$q_2 = 1.445 \cdot 10^4$	$q_2 = 2.544 \cdot 10^4$	$q_2 = 6.349 \cdot 10^4$

Table 4.8. Parameters $\{p_i, q_i\}$ of the rational function $f_2(\alpha)$ for the different sets of symmetrical points.

Figure 4.7 shows data sets $\{\alpha, (\tau_{100-x})^{1/\alpha}\}$ and their corresponding results of least-squares curve-fitting for the different sets of symmetrical points. Note that $f_3(\alpha) = (\tau_{100-x})^{1/\alpha}$ depends on α and normalized time τ_{100-x}. The range of amplitudes in f_3 is reduced for increasing values of x, as can be shown in Figure 4.7.

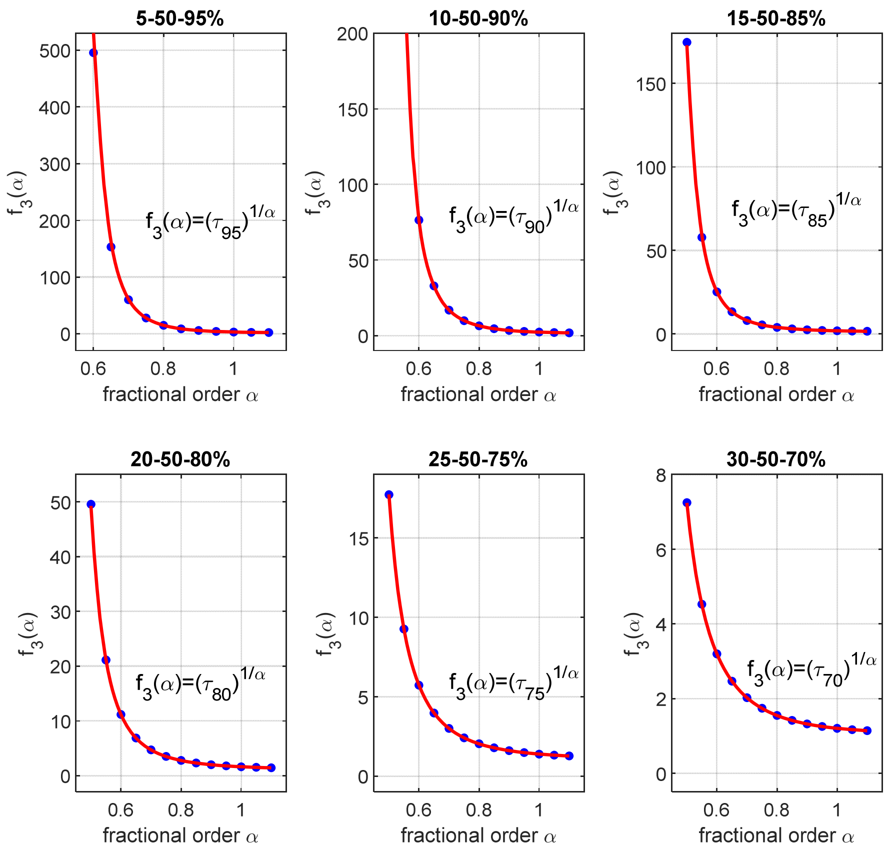

Figure 4.7. Data sets $\{\alpha, (\tau_{100-x})^{1/\alpha}\}$ where $x = 5, 10, 15, 20, 25,$ and 30, and curve fitting for $f_3(\alpha)$.

Data is fitted using the Levenberg–Marquardt least-squares curve-fitting algorithm in all graphs in Figure 4.7, and the following rational function is used for all cases:

$$f_3(\alpha) = \frac{p_1\alpha^2 + p_2\alpha + p_3}{\alpha^2 + q_1\alpha + q_2} \tag{4.17}$$

where the values of the parameters $\{p_i, q_i\}$ for function $f_3(\alpha)$ and each one of the selected sets of symmetrical points are shown in Table 4.9.

5-50-95%	10-50-90%	15-50-85%	20-50-80%	25-50-75%	30-50-70%
$p_1 = 5.492$	$p_1 = 3.351$	$p_1 = 1.7$	$p_1 = 1.302$	$p_1 = 1.243$	$p_1 = 1.315$
$p_2 = -11.05$	$p_2 = -6.134$	$p_2 = -2.584$	$p_2 = -1.629$	$p_2 = -1.368$	$p_2 = -1.306$
$p_3 = 6.092$	$p_3 = 3.36$	$p_3 = 1.42$	$p_3 = 0.846$	$p_3 = 0.666$	$p_3 = 0.6238$
$q_1 = -1.154$	$q_1 = -0.9959$	$q_1 = -0.9406$	$q_1 = -0.8693$	$q_1 = -0.7536$	$q_1 = -0.5318$
$q_2 = 0.3351$	$q_2 = 0.2491$	$q_2 = 0.2235$	$q_2 = 0.1919$	$q_2 = 0.1433$	$q_2 = 0.05728$

Table 4.9. Parameters $\{p_i, q_i\}$ of the rational function $f_3(\alpha)$ for the different sets of symmetrical points.

It is important to emphasize that estimated values of α, T, and L obtained from expressions (4.12) depend on functions $f_1(\Delta)$, $f_2(\alpha)$, and $f_3(\alpha)$. Thus, these functions play a significant role in the process identification procedure as the features of normalized step responses (4.3) can be well characterized due to their contribution.

Note that, for any different choice of times set $\{t_{x1}\ t_{x2}, t_{x3}\}$ to reach three points $\{y_\alpha(t_{x1}), y_\alpha(t_{x2}), y_\alpha(t_{x3})\}$ on the process reaction curve, the accuracy of the identification results only depends upon the fitting precision. In this context, an accurate determination of α-value is of primary importance since, subsequently, functions f_2 and f_3 –and therefore T and L– depend on the estimated value of α.

In the curve-fitting process, it has been found that, in general, functions $f_1(\Delta)$, $f_2(\alpha)$, and $f_3(\alpha)$ for low values of x require more parameters than those with higher x values to be able to fit the data with the rational function. Although some of the data sets could have been adjusted with fewer parameters, for each function $f_1(\Delta)$, $f_2(\alpha)$, and $f_3(\alpha)$ the same expressions with the same number of parameters have been used for curve fitting, respectively. In this manner, comparison of estimated values of α, T, and L, which directly depend on functions f_1, f_2, and f_3 for different sets of symmetrical points can be made in the same conditions. In this section, it has been verified that rational expressions used fit well data sets in Figures 4.5, 4.6, and 4.7.

Remark 1: Expressions (4.15) – (4.17), with parameters in Tables 4.7 – 4.9, for functions f_1, f_2, and f_3 have been obtained for $0.5 \leq \alpha \leq 1.1$. This range includes the dynamics for the majority of the representative processes encountered in process control, which can be characterized as having essentially monotone step responses, see for example the test batch considered in (Åström and Hägglund 2004). For values of α outside this range, the considered curve-fittings are not valid. A significant fact observed is that the step response of an FFOPDT system for α values less than 0.5 becomes extremely slow, as can be seen in Figure 3.2. Note that values of the normalized time τ_{100-x} increase as α decreases, especially in a very significative way for small values of x.

Although the step response of an FFOPDT model is overdamped only for α values between 0 and 1, the value 1.1 has also been included since it has been observed in numerous experiments that for some processes, generally lag-dominated, with high-order integer-order transfer functions, values of α are slightly greater than 1. In this way, a better fit of the transient response of the model is obtained in relation to the process reaction curve. Specifically, the behaviour of the step response for a FFOPDT system when $\alpha = 1.1$ can be observed in Figure 3.3.

4.4. Algorithm for determining FFOPDT model parameters

To facilitate software implementation of the proposed identification method, it is convenient to develop an algorithm.

In this method, the variation in input signal Δu and process output Δy, and times necessary to reach $x\%$ (t_x), 50% (t_{50}), and $(100-x)\%$ (t_{100-x}) of the process output total change on the reaction curve must be collected in order to determine FFOPDT model parameters $\theta_P = \{K, T, L, \alpha\}$.

Chapter 8 will present the corresponding algorithm and show the results of applying the algorithm, when implemented on a microprocessor-based hardware, to an experimental temperature setup.

4.5. Results and discussion

In this section, the proposed identification method for FFOPDT models was tested for several sets of symmetrical points on the reaction curve and compared with other identification methods for integer- and fractional-order models.

4.5.1. Materials and methods

The following process models were selected in order to show the effectiveness of the proposed procedure in finding an approximated four-parameter model (3.21) and to get insight into the influence of the selected set of symmetrical points on the accuracy of the identified model.

$$P_{1,i}(s) = \frac{K_1}{(1 + T_1 s^{\lambda_i})^2} e^{-L_1 s} \tag{4.18}$$

$$P_2(s) = \frac{K_2}{(1 + T_2 s^{\lambda_2})^n} \tag{4.19}$$

On the one hand, processes $P_{1,i}$ are used to compare the proposed identification procedure for several symmetrical points with some two- and three-point identification methods for FOPDT, DPPDT, and SOPDT models, and to get insight into the influence of the location of symmetrical points on the accuracy of the fractional-order identified model.

On the other hand, process P_2 is used to compare the model performance of the method proposed in this chapter with other integer- and fractional-order methods.

A step-change input signal was applied to these processes in order to register the process reaction curve. The output responses of the processes were then used to calculate the parameters of the corresponding models. Note that the sample period used in all the experiments was set to $T_S = 10$ ms.

Given the experimental data from an identification test, it is necessary to verify the effectiveness of the model structure adopted for fitting and the accuracy of the corresponding model parameters. A number of fitting objective functions and model validation methods using a step excitation signal for system identification have been presented in the literature (Liu and Gao 2012).

Without loss of generality, the following time-domain fitting criterion was used to evaluate the performance of the model identification:

$$S(\bar{\theta}) = \frac{1}{N_s} \sum_{k=1}^{N_s} [e(kT_s, \bar{\theta})]^2 = \frac{1}{N_s} \sum_{k=1}^{N_s} [y(kT_s) - y_m(kT_s, \bar{\theta})]^2 \tag{4.20}$$

where $\bar{\theta}$ is the vector of process model parameters, $e(kT_s, \bar{\theta})$ is the open-loop step response difference between the actual process and the identified process model output signal, $y(kT_s)$ and $y_m(kT_s, \bar{\theta})$, respectively, T_S is the sampling period, and $N_S T_S$ is the time length of the dynamic (transient) response. Although in the context of a step response test, $N_S T_S$ may be taken as the settling time that is usually defined as the time to move into an error band of 2% or 5% with respect to the final steady-state output deviation in response to a step change, the upper limit of the time interval is the instant in which the response has reached its final value.

This time-domain criterion is the Mean Squared Error (MSE) and gives a measure of the average of the squares of errors. How accurately a model reproduces the process reaction curve is evaluated with this index.

In this context, a relative performance index is more important than their absolute values since the goodness of an identification method with respect to another can be quantified.

In this chapter, the following relative performance index is used:

$$S_{x,y}(\bar{\theta}_x, \bar{\theta}_y) = \frac{S_x(\bar{\theta}_x)}{S_y(\bar{\theta}_y)} \tag{4.21}$$

where $S_x(\bar{\theta}_x)$ and $S_y(\bar{\theta}_y)$ are the MSE values (4.20) and $\bar{\theta}_x$ and $\bar{\theta}_y$ are the vectors of process model parameters for x and y models, respectively.

The simulation of these illustrative examples has been implemented using MATLAB and FOTF (Fractional Order Transfer Function) toolbox. FOTF is a control toolbox for fractional order systems developed by Xue et al. (Chen, Petras and Xue 2009) which extends many MATLAB built-in functions to deal with fractional-order models. The reference text for the FOTF toolbox is (Xue 2017), where the author explains thoroughly all the commands and applications.

4.5.2. Example 1

The FFOPDT process model (4.18), where $K_1 = 1$, $T_1 = 1$ s, $L_1 = 0.1$ s, and $\lambda_i = 0.60, 0.65, \ldots, 1.00$, is considered in this example. Model (4.18) is a fractional second-order process with dead-time (FSOPDT) to provide some modelling error or deviation from FFOPDT dynamics, which is the model structure selected in the proposed identification method.

The procedure that has been followed with this example is as follows:

1. Nine process plants $P_{1,i}$, where $i = 1, \ldots, 9$, and $\lambda_i = 0.60, 0.65, \ldots, 1.00$, are considered.
2. The FFOPDT model parameters $\bar{\theta}_{ij}$ for each process $P_{1,i}$ are obtained using the proposed identification method for each of the sets of points. $\bar{\theta}_{ij}$ is expressed as follows:

$$\bar{\theta}_{ij} = \{K_{ij}, T_{ij}, L_{ij}, \alpha_{ij}\} \tag{4.22}$$

where $i = 1, \ldots, 9$ represents the value of λ_i process parameter, as indicated in Table 4.10, and $j = 1, \ldots, 6$ represents the identification method employed, as indicated in Table 4.11. In short, a set of 54 process model parameters is obtained.

3. The step responses for each of the 54 models are obtained, and their respective values of the model performance index $S(\bar{\theta}_{ij})$ are determined.

i	λ_i	T_S [s]	N_S	N_ST_S [s]
1	0.60	0.01	58278	582.77
2	0.65	0.01	29312	293.12
3	0.70	0.01	15816	158.15
4	0.75	0.01	8960	89.59
5	0.80	0.01	5224	52.23
6	0.85	0.01	3067	30.66
7	0.90	0.01	1760	17.60
8	0.95	0.01	965	9.64
9	1.00	0.01	594	5.93

Table 4.10. Set of process fractional orders, sampling periods, number of samples, and time length used in FFOPDT step responses for processes $P_{1,i}$ (i = 1, …, 9).

j	Method #	Set of points
1	1	(5-50-95%)
2	2	(10-50-90%)
3	3	(15-50-85%)
4	4	(20-50-80%)
5	5	(25-50-75%)
6	6	(30-50-70%)

Table 4.11. Set of symmetrical points used for FFOPDT model identification.

This batch of processes is used, on the one hand, to validate the proposed identification method for the different sets of symmetrical points and, on the other hand, to get insight into the influence of the selection of representative points on the accuracy of the obtained fractional-order model.

Note that Table 4.10 contains sampling period, number of samples, and time length that have been considered in step responses for each of the processes. Table 4.11 lists the set of points considered for the identification of the FFOPDT models. Figure 4.8 illustrates the values of the model performance index $S(\bar{\theta}_{ij})$ that have been obtained with the proposed procedure for each process (i = 1, ..., 9) and using the different methods (j = 1, ..., 6).

Note that the values $S(\bar{\theta}_{ij})$ in Figure 4.8 decrease substantially when move from method #6 to #1. This behavior occurs for all the processes considered, except for those where λ_i is close to 1, that is, when the process approaches to one of integer-order. This behaviour has already been observed in the technical literature. The 123c method (Alfaro 2006) uses time sets (25-75%) to identify FOPDT and DPPDT models, and (25-50-75%) for SOPDT models. In (Alfaro and Vilanova 2021) points (25-50-75%) are proposed to identify RPPDT models. In these two papers, these points have not been chosen arbitrarily, but rather those that optimize the identified model parameters have been selected, i.e. FOPDT, DPPDT, SOPDT, and RPPDT models, respectively. In Figure 4.8, the lowest value of $S(\bar{\theta}_{ij})$ for $P_{1,9}$, which is an integer-order model, corresponds to method #5 (25-50-75%).

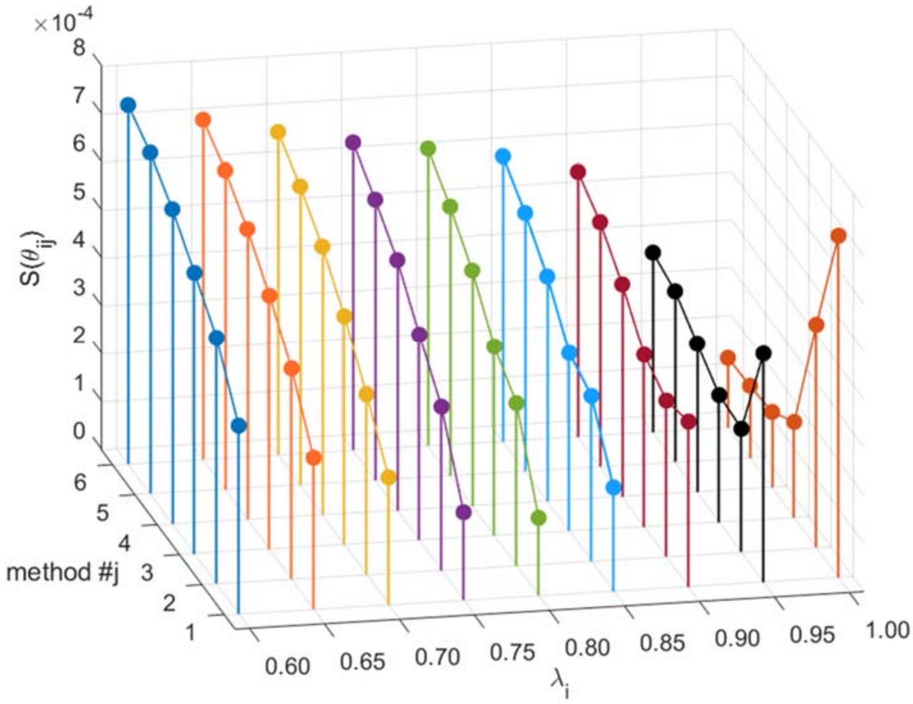

Figure 4.8. Model performance index values $S(\bar{\theta}_{ij})$ for the 54 FFOPDT models with parameters $\bar{\theta}_{ij}$, obtained for each process $P_{1,i}$ ($i = 1, \ldots, 9$) using methods #j ($j = 1, \ldots, 6$).

This figure also shows that the proposed identification method gives good fit between the corresponding identified models and the actual process reaction curves. This is confirmed by the low values in time-domain model performance indices $S(\bar{\theta}_{ij})$ for all processes $P_{1,i}$.

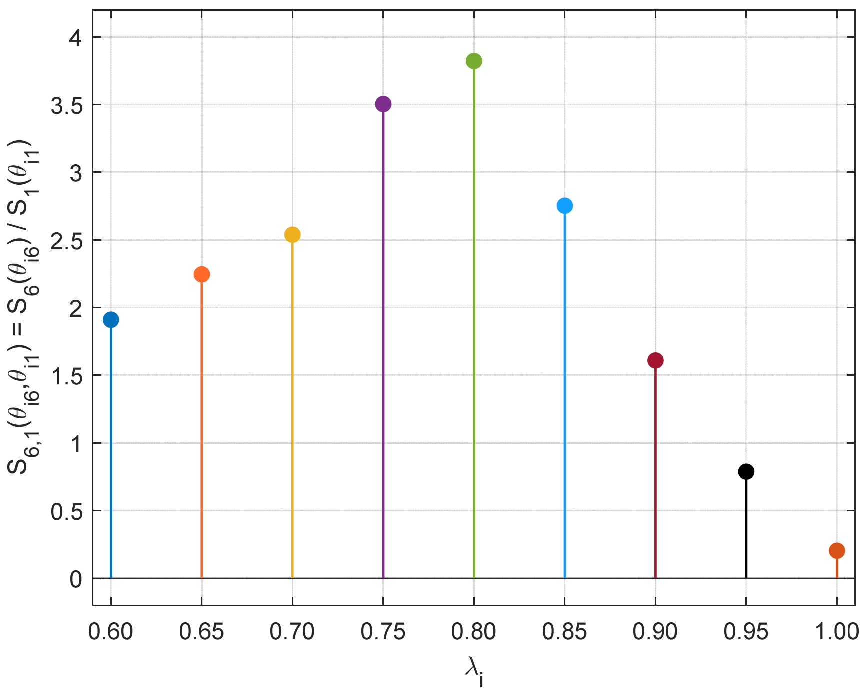

Figure 4.9. Relative performance index values $S_{6,1}(\bar{\theta}_{i6}, \bar{\theta}_{i1})$ for each value of λ_i ($i = 1, \ldots, 9$), which represent the ratio between model performance indices obtained with method #6 and #1.

From the results obtained in Figure 4.8, it can be observed that method #1 is the one that provides the best results and, therefore, the set of points (5-50-95%) is the one that is recommended to be selected when using this symmetrical identification procedure. In this regard, relative performance indices between method #6 ($j = 6$), and method #1 ($j = 1$), $S_{6,1}(\bar{\theta}_{i6}, \bar{\theta}_{i1})$, for $i = 1, \ldots, 9$, are represented in Figure 4.9, where it can be noticed that method #1 is approximately 2.0, 2.25, 2.5, 3.5, 4.0, 2.75, and 1.5 times better in terms of S than the one obtained with method #6, for $i = 1, \ldots, 7$, respectively.

The case $\lambda_5 = 0.8$ for process $P_{1,5}$ is considered among processes $P_{1,i}$. The process reaction curve for this model is shown in Figure 4.10. From this data, the following information is summarized in Table 4.12.

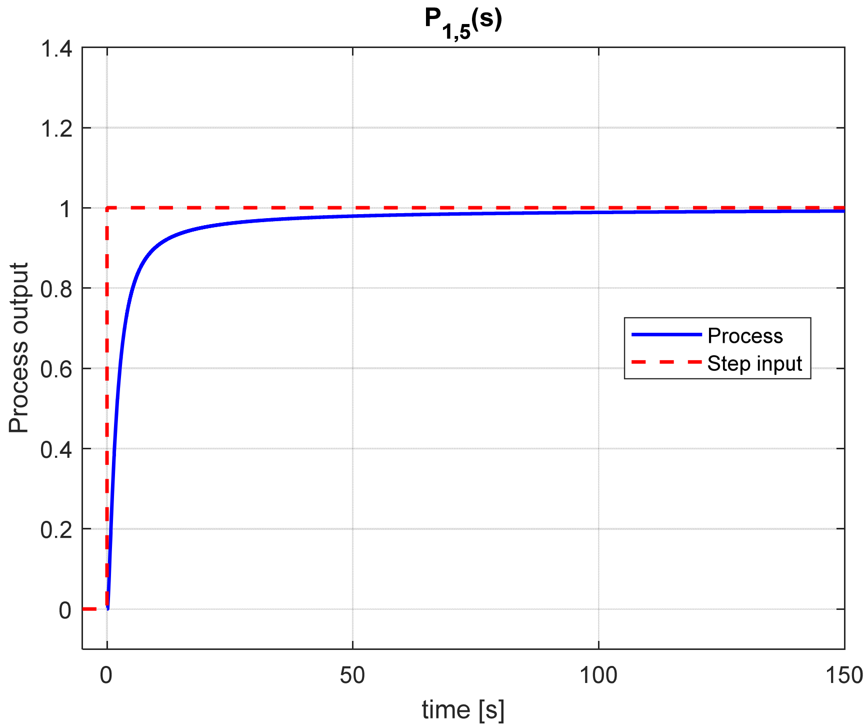

Figure 4.10. Step-input signal and process reaction curve for process $P_{1,5}$.

Method #1: 5-50-95%	Method #2: 10-50-90%	Method #3: 15-50-85%	Method #4: 20-50-80%	Method #5: 25-50-75%	Method #6: 30-50-70%
		$\Delta u = 1$			
		$\Delta y = 1$			
$t_5 = 0.3310$ s	$t_{10} = 0.4890$ s	$t_{15} = 0.6410$ s	$t_{20} = 0.7940$ s	$t_{25} = 0.9540$ s	$t_{30} = 1.1250$ s
		$t_{50} = 1.9900$ s			
$t_{95} = 19.123$ s	$t_{90} = 9.7230$ s	$t_{85} = 6.7390$ s	$t_{80} = 5.2090$ s	$t_{75} = 4.2430$ s	$t_{70} = 3.5600$ s

Table 4.12. Process information for fractional-order model identification of process $P_{1,5}$.

Considering data from Table 4.12, the following FFOPDT process parameters $\bar{\theta}_{i5} = \{K_{i5}, T_{i5}, L_{i5}, \alpha_{i5}\}$, where i = 1, …, 6, have been obtained in Table 4.13 for each one of the proposed sets of symmetrical points in Table 4.11.

Method #1: 5-50-95%	**Method #2: 10-50-90%**	**Method #3: 15-50-85%**	**Method #4: 20-50-80%**	**Method #5: 25-50-75%**	**Method #6: 30-50-70%**
$K_1 = 1.0000$	$K_2 = 1.0000$	$K_3 = 1.0000$	$K_4 = 1.0000$	$K_5 = 1.0000$	$K_6 = 1.0000$
$T_1 = 2.3318$ s	$T_2 = 2.3011$ s	$T_3 = 2.2834$ s	$T_4 = 2.2688$ s	$T_5 = 2.2666$ s	$T_6 = 2.2418$ s
$L_1 = 0.3742$ s	$L_2 = 0.4724$ s	$L_3 = 0.4041$ s	$L_4 = 0.4057$ s	$L_5 = 0.3901$ s	$L_6 = 0.4175$ s
$\alpha_1 = 0.8719$	$\alpha_2 = 0.8882$	$\alpha_3 = 0.8992$	$\alpha_4 = 0.9067$	$\alpha_5 = 0.9122$	$\alpha_6 = 0.9143$

Table 4.13. FFOPDT model parameters for the considered sets of representative points (5-50-95%), (10-50-90%), (15-50-85%), (20-50-80%), (25-50-75%), and (30-50-70%), respectively.

The proposed identification method will be compared with various two- and three-point identification methods for FOPDT, DPPDT, and SOPDT models based on information also obtained from the reaction curve.

In the case of two-point methods, (Alfaro 2006) and (Vitecková, Vitecek and Smutny 2000), both for FOPDT and DPPDT models are used.

Table 4.14 contains the parameters of the FOPDT model identified using the two-point identification methods proposed by Alfaro and by Vitecková, respectively. Table 4.15 shows the parameters of the DPPDT model obtained using the same methods.

In the case of three-point methods, (Jahanmiri and Fallahi 1997) and Stark in (Mollenkamp 1984) for SOPDT model are considered.

Table 4.16 contains the parameters of the SOPDT model obtained using the three-point identification methods proposed by Jahanmiri and Fallahi, and by Stark, respectively.

Method #7: Alfaro 1 25-75%	**Method #8: Vitecková 1 33-70%**
$K_7 = 1.0000$	$K_8 = 1.0000$
$T_7 = 2.9936$ s	$T_8 = 2.8959$ s
$L_7 = 0.0923$ s	$L_8 = 0.0757$ s

Table 4.14. FOPDT model parameters obtained using Alfaro's and Vitecková's two-point methods, respectively.

Method #9: Alfaro 2 25-75%	**Method #10: Vitecková 2 33-70%**
$K_9 = 1.0000$	$K_{10} = 1.0000$
$T_9 = 1.8997$ s	$T_{10} = 1.8468$ s
$L_9 = 0$ s	$L_{10} = 0$ s

Table 4.15. DPPDT model parameters obtained using Alfaro's and Vitecková's two-point methods, respectively.

Method #11: Stark 15-45-75%	Method #12: Jahanmiri-Fallahi 1 2-70-90%	Method #13: Jahanmiri-Fallahi 2 5-70-90%
K_{11} = 1.0000	K_{12} = 1.0000	K_{13} = 1.0000
T_{11a} = 2.8764 s	T_{12a} = 3.9984 s	T_{13a} = 4.0453 s
T_{11b} = 0.3714 s	T_{12b} = 0.0362 s	T_{13b} = 0.0362 s
L_{11} = 0 s	L_{12} = 0.2220 s	L_{13} = 0.3310 s

Table 4.16. SOPDT model parameters obtained using Stark's and Jahanmiri and Fallahi's three-point methods, respectively.

Figures 4.11 – 4.14 compare the process reaction curve with the step responses of the FFOPDT models obtained with the proposed method for different sets of symmetrical points and those of the FOPDT, DPPDT, and SOPDT models proposed by Alfaro, Vitecková, Stark, and Jahanmiri and Fallahi, respectively.

The step responses have been grouped in graphs based on the similarity in the points on the reaction curve that have been used in each of the identification methods.

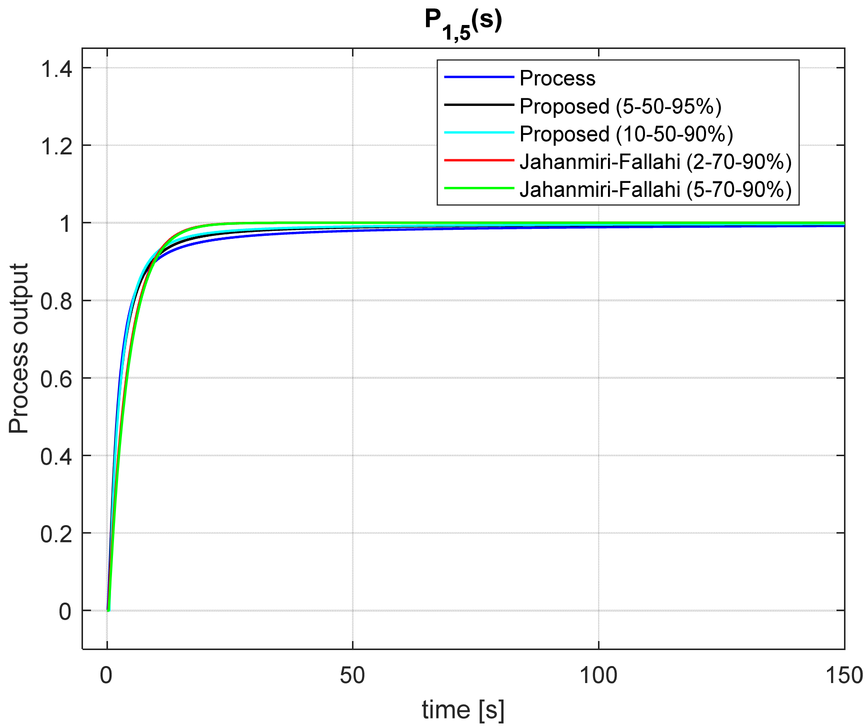

Figure 4.11. Process reaction curve and step responses for FFOPDT model methods #1 and #2 and SOPDT methods #12 and #13, respectively.

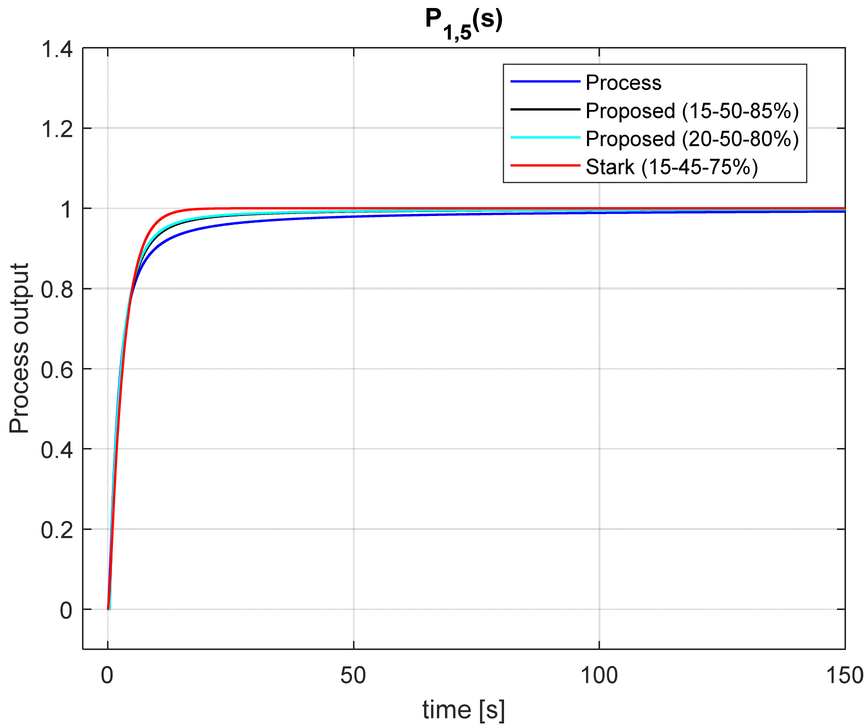

Figure 4.12. Process reaction curve and step responses for FFOPDT model methods #3 and #4 and SOPDT method #11, respectively.

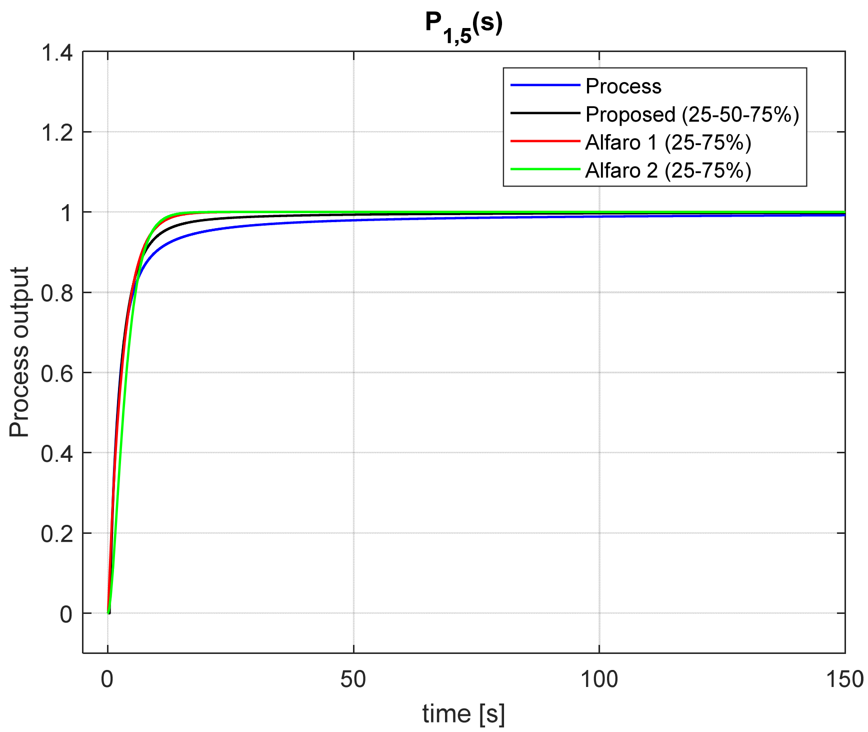

Figure 4.13. Process reaction curve and step responses for FFOPDT model method #5 and FOPDT and DPPDT model methods #7 and #9, respectively.

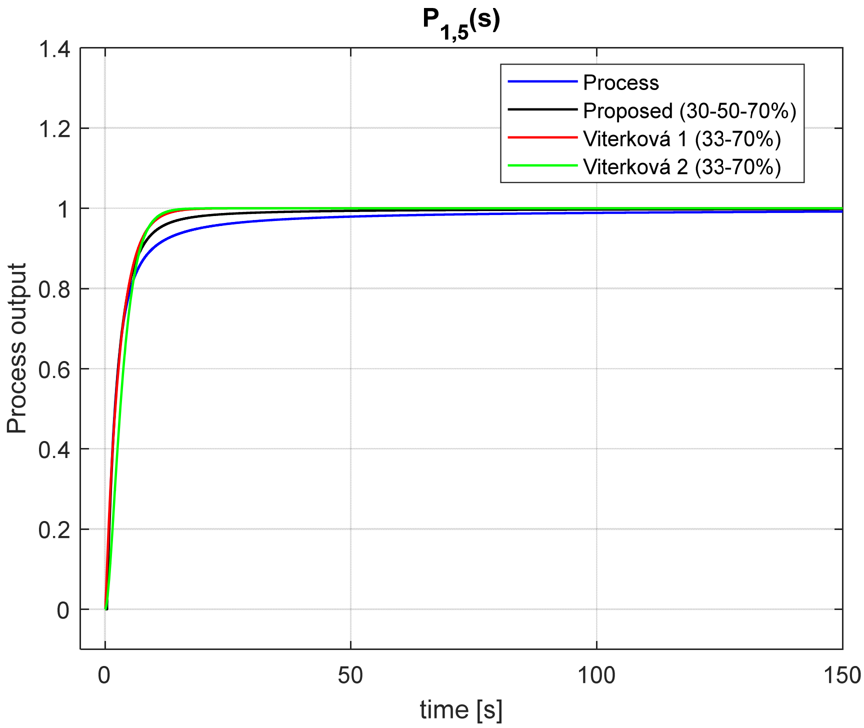

Figure 4.14. Process reaction curve and step responses for FFOPDT model method #6 and FOPDT and DPPDT model methods #8 and #10, respectively.

Table 4.17 shows the values of the time-domain model performance index $S(\bar{\theta})$ for the different identification methods applied to process $P_{1,5}$. The relative performance index values $S_{x,y}(\bar{\theta}_x, \bar{\theta}_y)$, which allow the comparison between different identification methods, are listed in Table 4.18.

Identification Method #	Set of points	Model	S
#1: Proposed	(5-50-95%)	FFOPDT	**$S_1 = 7.78 \cdot 10^{-5}$**
#2: Proposed	(10-50-90%)	FFOPDT	$S_2 = 1.51 \cdot 10^{-4}$
#3: Proposed	(15-50-85%)	FFOPDT	$S_3 = 1.79 \cdot 10^{-4}$
#4: Proposed	(20-50-70%)	FFOPDT	$S_4 = 2.18 \cdot 10^{-4}$
#5: Proposed	(25-50-75%)	FFOPDT	$S_5 = 2.47 \cdot 10^{-4}$
#6: Proposed	(30-50-70%)	FFOPDT	$S_6 = 2.69 \cdot 10^{-4}$
#7: Alfaro 1	(25-75%)	FOPDT	$S_7 = 5.98 \cdot 10^{-4}$
#8: Vitecková 1	(33-70%)	FOPDT	$S_8 = 6.30 \cdot 10^{-4}$
#9: Alfaro 2	(25-75%)	DPPDT	$S_9 = 1.40 \cdot 10^{-3}$
#10: Vitecková 2	(33-70%)	DPPDT	$S_{10} = 1.30 \cdot 10^{-3}$
#11: Stark	(15-45-70%)	SOPDT	$S_{11} = 6.66 \cdot 10^{-4}$
#12: Jahanmiri-Fallahi 1	(2-70-90%)	SOPDT	$S_{12} = 9.25 \cdot 10^{-4}$
#13: Jahanmiri-Fallahi 2	(5-70-90%)	SOPDT	$S_{13} = 1.10 \cdot 10^{-3}$

Table 4.17. Time-domain model performance indices for process $P_{1,5}$.

Figures 4.11 – 4.14 illustrate that the step response of the models identified with the proposed method for the different sets of representative points give a good fit with the process reaction curve, particularly in the interval [x - (100–x)].

For smaller values of x, the interval [x - (100–x)] is larger and, therefore, the step response for these models fits better the process reaction curve, which translates into a lower value in the model performance index S, as can be seen in Table 4.17.

This is mainly due to the fact that the value of the α identified for smaller values of x is closer to its optimal value.

Note that α value of the model has a great influence on the shape of the step response for an FFOPDT model, as can be seen in Figure 3.2.

Regarding two-point methods, Figures 4.13 and 4.14 show step responses of the models obtained by Alfaro's (25-75%) and Vitecková's (33-70%) methods, both for FOPDT and DPPDT, respectively, compared to those of the proposed method for (25-50-75%) and (30-50-70%).

These figures show that Alfaro's and Vitecková's methods fit the reaction curve very well in the ranges (25-75%) and (33-70%), respectively. However, the behaviour of both models outside these ranges deviates from the reaction curve, resulting in a higher S-value.

The value of S for method # 1 is 7.7 and 8.1 times lower than the ones proposed by Alfaro and Vitecková for FOPDT models, respectively. In turn, the value of S for methods # 5 and #6 is 2.4 and 2.3 times lower than methods proposed by Alfaro and Vitecková for FOPDT models, respectively.

Method #1 is 17.8 and 16.7 times better in terms of S than Alfaro's and Vitecková's methods for DPPDT models, respectively. On the other hand, methods #5 and # 6 are 5.6 and 4.8 times better than those of Alfaro and Vitecková for DPPDT models. The responses of DPPDT models for Alfaro and Vitecková have higher values in the model performance index shown in Table 4.17 in comparison with the same methods for FOPDT models.

Regarding three-point methods, Figure 4.11 shows step responses of Jahanmiri-Fallahi's methods (2-70-90%) and (5-70-90%) for a SOPDT model, in comparison with those of the proposed method for (5-50-95%) and (10-50-90%).

The value of S for method #1 is 11.9 and 14.1 times lower than the one for methods #12 and #13, respectively. If both three-point methods are compared with method #2, the latter is 6.1 and 7.2 times better than methods #12 and #13, respectively.

Figure 4.12 shows the step responses of Stark's method (15-45-75%) for a SOPDT model, in comparison with those of the proposed method for (15-50-85%) and (20-50-80%). The value of S for methods # 1 and # 3 is 8.6 and 3.7 times lower than the one for method #11.

There is an improvement in terms of S of 1.9, 2.3, 2.8, 3.2, and 3.4 times for process P_1 in using Method #1 (5-50-95%) with respect to Methods #2, #3, #4, #5, and #6, respectively, as illustrated in Table 4.18.

Compared methods	**$S_{x,y} = S_x/S_y$**
Method #2-Method #1	$S_{2,1} = S_2/S_1 = 1.94$
Method #3-Method #1	$S_{3,1} = S_3/S_1 = 2.30$
Method #4-Method #1	$S_{4,1} = S_4/S_1 = 2.81$
Method #5-Method #1	$S_{5,1} = S_5/S_1 = 3.17$
Method #6-Method #1	$S_{6,1} = S_6/S_1 = 3.45$
Method #7-Method #1	$S_{7,1} = S_7/S_1 = 7.69$
Method #7-Method #5	$S_{7,5} = S_7/S_5 = 2.42$
Method #8-Method #1	$S_{8,1} = S_8/S_1 = 8.10$
Method #8-Method #6	$S_{8,6} = S_8/S_6 = 2.35$
Method #9-Method #1	$S_{9,1} = S_9/S_1 = 17.76$
Method #9-Method #5	$S_{9,5} = S_9/S_5 = 5.60$
Method #10-Method #1	$S_{10,1} = S_{10}/S_1 = 16.75$
Method #10-Method #6	$S_{10,6} = S_{10}/S_6 = 4.85$
Method #11-Method #1	$S_{11,1} = S_{11}/S_1 = 8.57$
Method #11-Method #3	$S_{11,3} = S_{11}/S_3 = 3.72$
Method #12-Method #1	$S_{12,1} = S_{12}/S_1 = 11.89$
Method #12-Method #2	$S_{12,2} = S_{12}/S_2 = 6.12$
Method #13-Method #1	$S_{13,1} = S_{13}/S_1 = 14.07$
Method #13-Method #2	$S_{13,2} = S_{13}/S_2 = 7.25$

Table 4.18. Relative performance index-based comparison between some considered identification methods for process $P_{1,5}$.

4.5.3. Example 2

In this example, the proposed identification method is compared with another identification method for FFOPDT models.

The higher-order lag-dominated fractional-order process model (4.19), where $K_2 = 2$, $T_2 = 1$ s, $\lambda_2 = 0.85$, and $n = 5$, is considered in this example as proposed in (Tavakoli-Kakhki, Haeri and Tavazoei 2010).

The process reaction curve for this model is shown in Figure 4.15. From these data, the process information needed for model identification using the proposed procedure in different sets of times is summarized in Table 4.19.

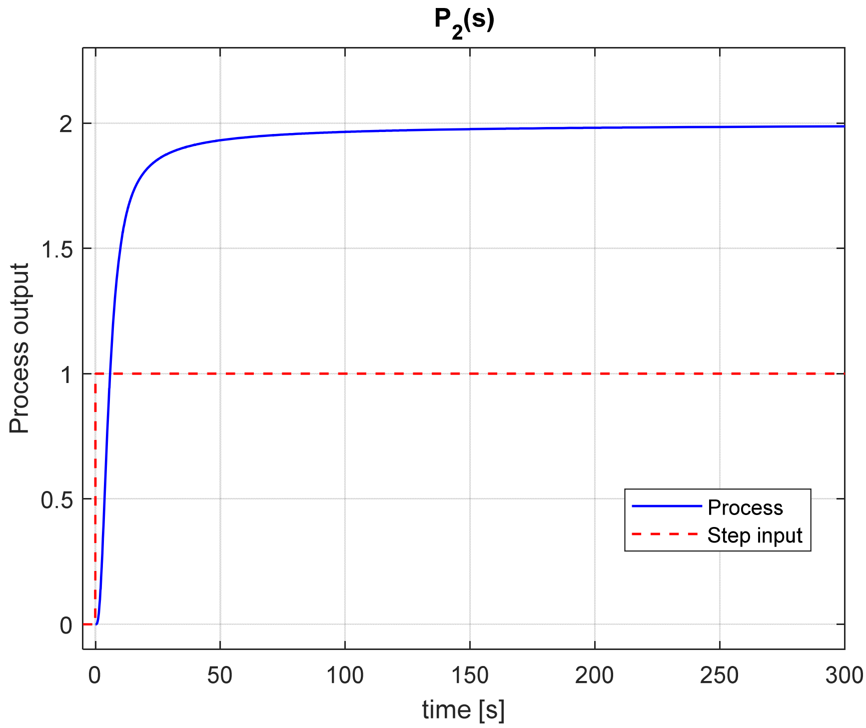

Figure 4.15. Step-input signal and process reaction curve for process P_2.

Method #1: 5-50-95%	**Method #2: 10-50-90%**	**Method #3: 15-50-85%**	**Method #4: 20-50-80%**	**Method #5: 25-50-75%**	**Method #6: 30-50-70%**
$\Delta u = 1$					
$\Delta y = 2$					
$t_5 = 1.7910$ s	$t_{10} = 2.3450$ s	$t_{15} = 2.8000$ s	$t_{20} = 3.2180$ s	$t_{25} = 3.6240$ s	$t_{30} = 4.0320$ s
$t_{50} = 5.9370$ s					
$t_{95} = 34.790$ s	$t_{90} = 19.200$ s	$t_{85} = 14.170$ s	$t_{80} = 11.580$ s	$t_{75} = 9.9300$ s	$t_{70} = 8.7400$ s

Table 4.19. Process information for fractional-order model identification of process P_2.

Considering data from Table 4.19, the following FFOPDT process parameters $\overline{\theta}_i = \{K_i, T_i, L_i, \alpha_i\}$, where $i = 1, \ldots, 6$, have been obtained in Table 4.20 for each one of the proposed sets of representative points on the reaction curve, i.e. (5-50-95%), (10-50-90%), (15-50-85%), (20-50-80%), (25-50-75%), and (30-50-70%), respectively.

Method #1: 5-50-95%	**Method #2: 10-50-90%**	**Method #3: 15-50-85%**	**Method #4: 20-50-80%**	**Method #5: 25-50-75%**	**Method #6: 30-50-70%**
$K_1 = 2.0000$	$K_2 = 2.0000$	$K_3 = 2.0000$	$K_4 = 2.0000$	$K_5 = 2.0000$	$K_6 = 2.0000$
$T_1 = 5.3737$ s	$T_2 = 5.4182$ s	$T_3 = 5.3090$ s	$T_4 = 5.2366$ s	$T_5 = 5.2330$ s	$T_6 = 5.1383$ s
$L_1 = 1.9617$ s	$L_2 = 2.1230$ s	$L_3 = 2.0287$ s	$L_4 = 2.0965$ s	$L_5 = 2.0972$ s	$L_6 = 2.1926$ s
$\alpha_1 = 0.9099$	$\alpha_2 = 0.9397$	$\alpha_3 = 0.9555$	$\alpha_4 = 0.9656$	$\alpha_5 = 0.9741$	$\alpha_6 = 0.9767$

Table 4.20. FFOPDT model parameters for the considered sets of representative points (5-50-95%), (10-50-90%), (15-50-85%), (20-50-80%), (25-50-75%), and (30-50-70%), respectively.

Process (4.19) is approximated by a FFOPDT model following three different strategies proposed in (Tavakoli-Kakhki, Haeri and Tavazoei 2010), where model process parameters $\bar{\theta}_7 - \bar{\theta}_9$ are given in Table 4.21.

Method #7 **Tavakoli-Kakhki 1**	**Method #8** **Tavakoli-Kakhki 2**	**Method #9** **Tavakoli-Kakhki 3**
$K_7 = 2.00$	$K_8 = 2.00$	$K_9 = 2.00$
$T_7 = 5.00$ s	$T_8 = 5.00$ s	$T_9 = 4.48$ s
$L_7 = 1.50$ s	$L_8 = 0.69$ s	$L_9 = 1.50$ s
$\alpha_7 = 0.85$	$\alpha_8 = 0.85$	$\alpha_9 = 0.85$

Table 4.21. FFOPDT model parameters for the different strategies proposed in (Tavakoli-Kakhki, Haeri and Tavazoei 2010).

The process reaction curve and the corresponding step responses of the considered approximated models for (5-50-95%), (10-50-90%), (15-50-85%), (20-50-80%), (25-50-75%), and (30-50-70%), respectively, are compared and illustrated in Figures 4.16 – 4.21. Moreover, the step responses for FFOPDT models proposed in (Tavakoli-Kakhki, Haeri and Tavazoei 2010) for process P_2 in comparison with the process reaction curve are shown in Figure 4.22.

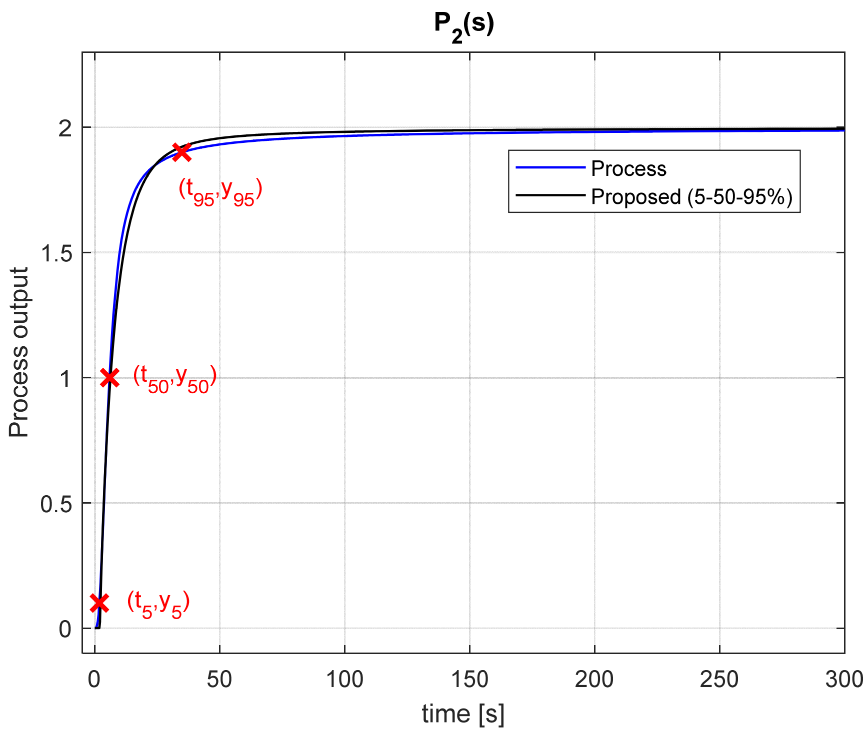

Figure 4.16. Process reaction curve and FFOPDT model method #1 (5-50-95%) step response for process P_2.

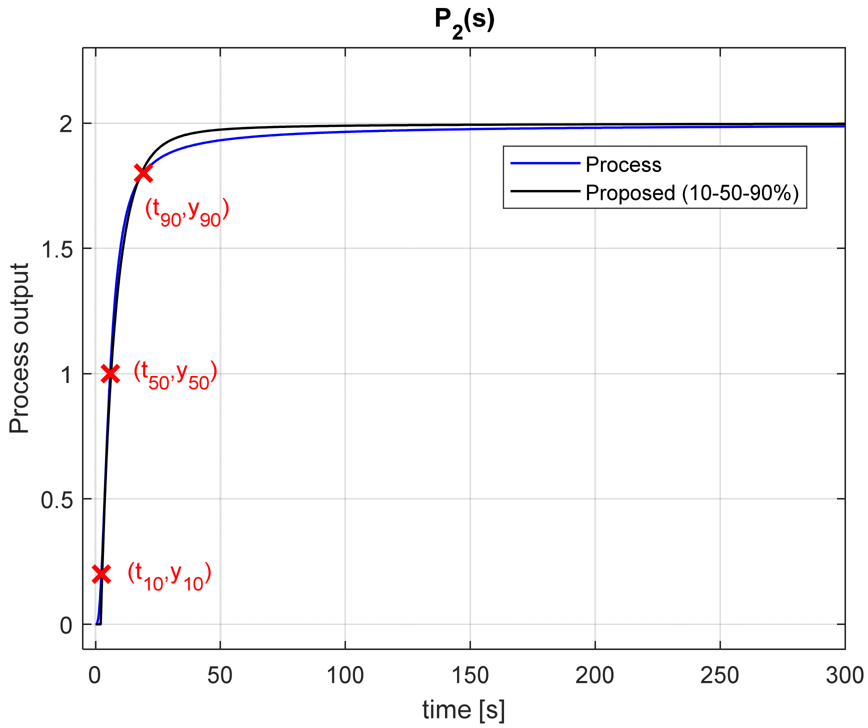

Figure 4.17. Process reaction curve and FFOPDT model method #2 (10-50-90%) step response for process P_2.

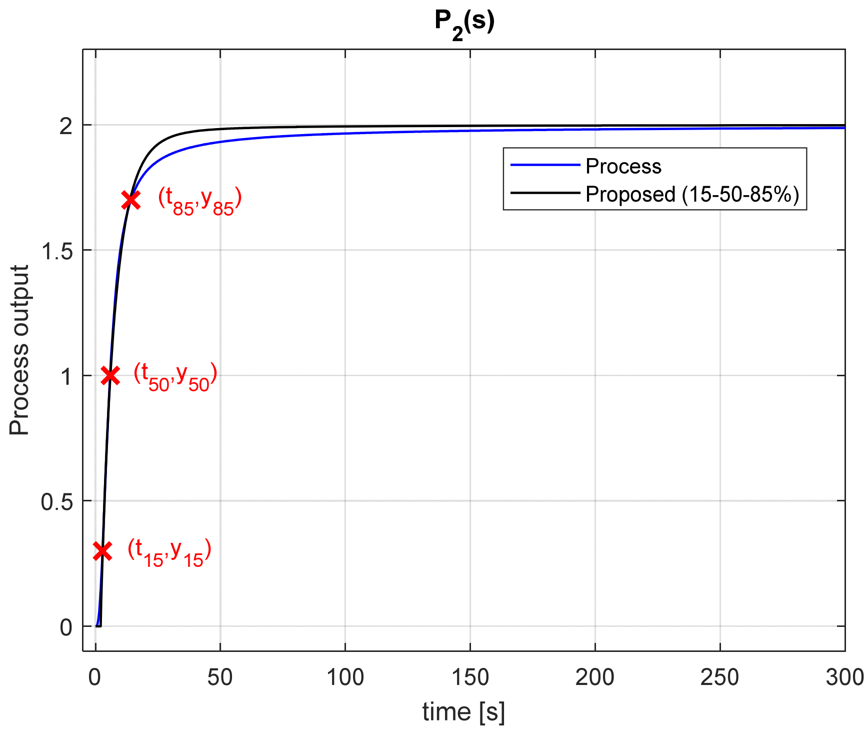

Figure 4.18. Process reaction curve and FFOPDT model method #3 (15-50-85%) step response for process P_2.

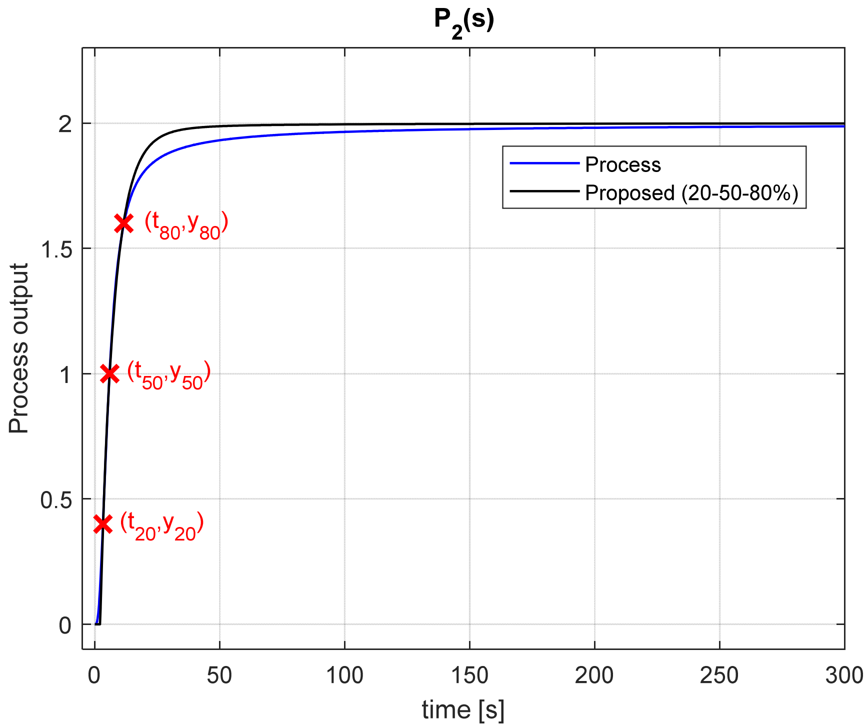

Figure 4.19. Process reaction curve and FFOPDT model method #3 (20-50-80%) step response for process P_2.

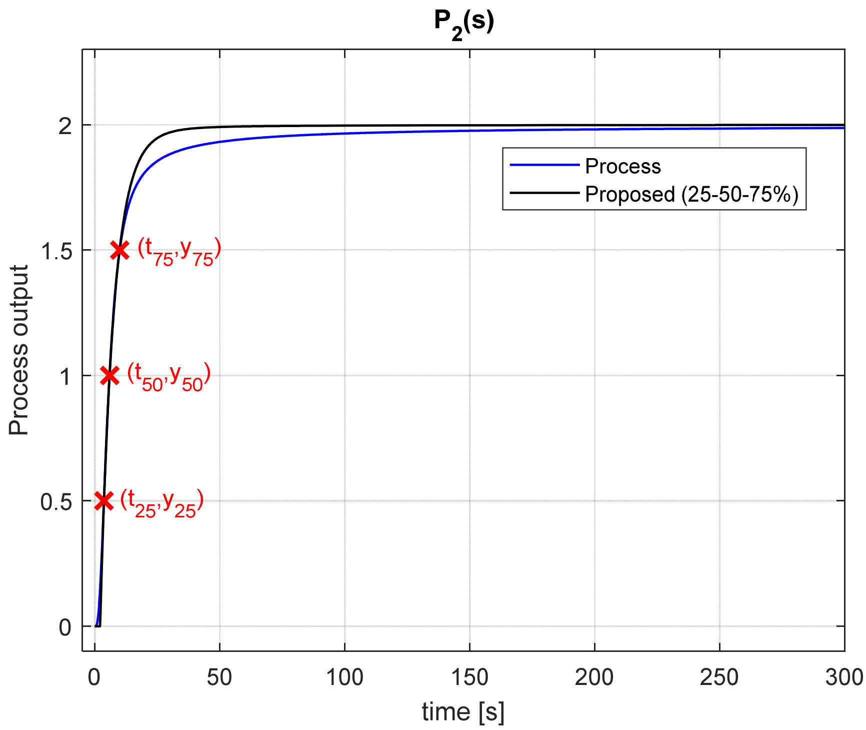

Figure 4.20. Process reaction curve and FFOPDT model method #5 (25-50-75%) step response for process P_2.

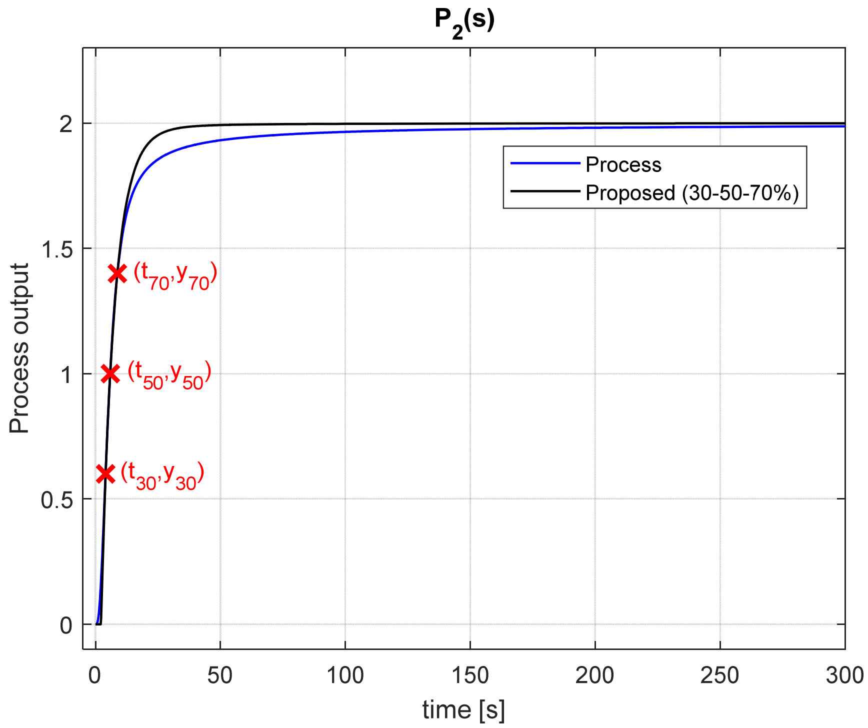

Figure 4.21. Process reaction curve and FFOPDT model method #6 (30-50-70%) step response for process P_2.

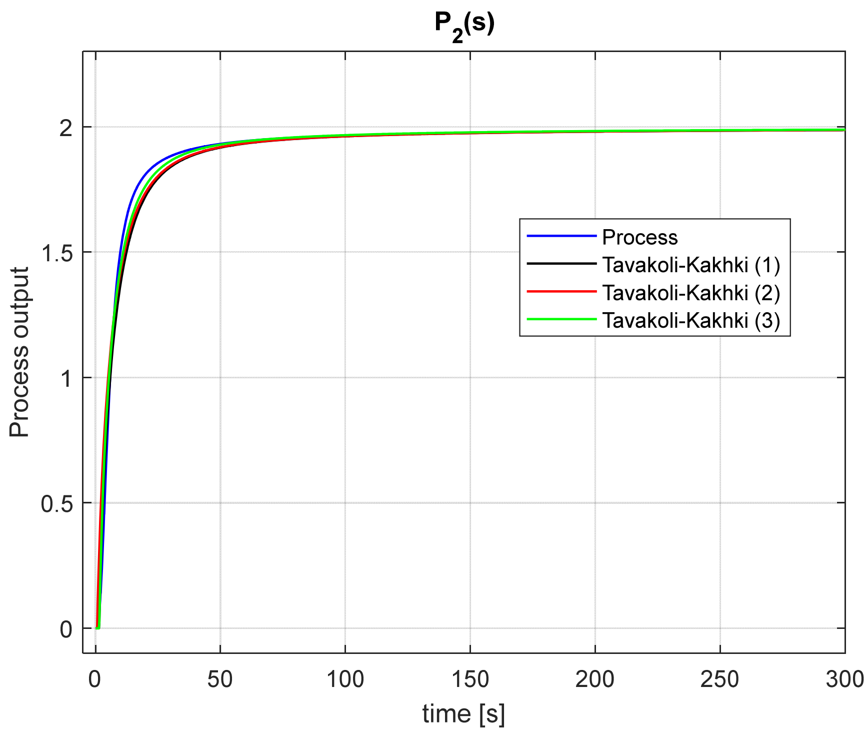

Figure 4.22. Process reaction curve and FFOPDT model methods #7-#9 step responses for process P_2.

Table 4.22 shows the values of the time-domain model performance index $S(\bar{\theta})$ for the different identification methods applied to process P_2. The relative performance index values $S_{x,y}(\bar{\theta}_x, \bar{\theta}_y)$, which show the comparison between different identification methods, are listed in Table 4.23.

Identification Method #	Set of points	Model	S
#1: Proposed	(5-50-95%)	FFOPDT	$S_1 = 5.3\cdot10^{-4}$
#2: Proposed	(10-50-90%)	FFOPDT	$S_2 = 7.4\cdot10^{-4}$
#3: Proposed	(15-50-85%)	FFOPDT	$S_3 = 9.1\cdot10^{-4}$
#4: Proposed	(20-50-70%)	FFOPDT	$S_4 = 1.2\cdot10^{-3}$
#5: Proposed	(25-50-75%)	FFOPDT	$S_5 = 1.4\cdot10^{-3}$
#6: Proposed	(30-50-70%)	FFOPDT	$S_6 = 1.5\cdot10^{-3}$
#7: Tavakoli-Kakhki's method 1	–	FFOPDT	$S_7 = 9.5\cdot10^{-4}$
#8: Tavakoli-Kakhki's method 2	–	FFOPDT	$S_8 = 1.6\cdot10^{-3}$
#9: Tavakoli-Kakhki's method 3	–	FFOPDT	$S_9 = 5.5\cdot10^{-4}$

Table 4.22. Time-domain model performance indices for process P_2.

Compared methods	$S_{xy} = S_x/S_y$
Method #2-Method #1	$S_{21} = S_2/S_1 = 1.40$
Method #3-Method #1	$S_{31} = S_3/S_1 = 1.74$
Method #4-Method #1	$S_{41} = S_4/S_1 = 2.19$
Method #5-Method #1	$S_{51} = S_5/S_1 = 2.57$
Method #6-Method #1	$S_{61} = S_6/S_1 = 2.80$
Method #7-Method #1	$S_{71} = S_7/S_1 = 1.81$
Method #8-Method #1	$S_{81} = S_8/S_1 = 2.97$
Method #9-Method #1	$S_{91} = S_9/S_1 = 1.06$

Table 4.23. Relative performance index-based comparison between some considered fractional-order model identification methods for process P_2.

In this example, a high-order fractional-order lag-dominated process has been used in order to illustrate the applicability and effectivity of the proposed identification procedure for identifying FFOPDT models.

Figures 4.16 – 4.21 show that the proposed method gives good results in the interval [x - (100–x)] for all the considered sets of representative points. Recall that the method tries to place three symmetrical points (x-50-(100–x)%) on the reaction curve. The location of the representative points on the reaction curve is very good for higher values of x, with a slight deviation for x = 5, as can be seen in Figures 4.16 – 4.21.

However, the obtained model fits the reaction curve better for low values of x, since α-value obtained is closer to its optimal value, as have been commented previously. This results in lower values of S for low values of x in the considered sets of representative points, as shown in Table 4.22.

There is an improvement in S of 1.4, 1.7, 2.2, 2.6, and 2.8 times in using Method #1 (5-50-95%) with respect to Methods #2, #3, #4, #5, and #6, respectively, as illustrated in Table 4.23.

Figure 4.22 shows that Tavakoli-Kakhki's methods gives similar results in terms of S to some of the proposed methods and this can be quantified in Table 4.22.

Method #1 is 1.8, 3.0, and 1.1 times better in terms of S than Tavakoli-Kakhki's method #1, #2, and #3, respectively.

Furthermore, the proposed method not only gives better results than the Tavakoli-Kakhki's method in terms of S, but in the author's opinion it is easier to apply.

Remark 2: In the second example, the comparison is restricted to analytical methods for FFOPDT models with a simplicity and computational effort similar to the one proposed in this paper. However, there are not many analytical techniques for modelling fractional-order processes based on the process reaction curve. Therefore, the comparison of the proposed symmetrical method is done with (Tavakoli-Kakhki, Haeri and Tavazoei 2010), which is a well-recognized reference and where three strategies have been proposed in order to determine the parameters of an FFOPDT model by making use of the step response data. It combines numerical computation and graphical estimation.

In Chapter 2, there is a review of fractional-order model identification methods that are based on the process reaction curve, however all of them use optimization to obtain the model parameters. In these cases, the accuracy of the model is improved at the cost of increased computational effort. In the authors' opinion, the comparison of the proposed method with these ones using optimization would not be made under equal conditions.

Remark 3: Since processes are generally nonlinear, the dynamic characteristics of the FFOPDT model –gain, time constant, dead-time and fractional order– will vary when the operating point of the control system changes, due to a modification of the setpoint, or due to the effect of disturbances.

The implicit uncertainty in the nominal model must therefore be taken into consideration.

There are generally two approaches in the technical literature when considering the parametric uncertainty of the plant in an identification method:

The first approach is to consider the uncertainty explicitly in the identification process. This generally makes the identification procedure more complicated.

The second one involves considering possible model uncertainties and variations in the dynamic characteristics of the controlled process in the design of the control system, see, e.g., (Åström and Hägglund 2006) for integer-order controllers and (Monje, Chen, et al. 2010) for the fractional case. A usual way of applying this second approach is to guarantee a certain degree of robustness –relative stability– of the control system designed to ensure its stability in the presence of variations in the process characteristics.

In this chapter, a procedure for the identification of a reduced-order fractional model of the FFOPDT type is presented, where the main use of the identified model is for control purposes. Accordingly, the uncertainty in the parameters of the identified model will be considered in the design of the control system.

In the industrial context, large process industries have hundreds or thousands of control loops. For this reason, simplicity is a fundamental characteristic when identifying a process model for control purposes. Considering this second approach, it is possible to maintain the simplicity of the identification procedure.

4.6. Conclusions

In this chapter, a general procedure to identify an FFOPDT model for industrial processes having S-shaped step responses and based on fitting three arbitrary points on the process reaction curve has been proposed. A simplification of the general identification procedure has also been considered, where only points symmetrically located on the process reaction curve have been selected. The symmetrical method provides an efficient way to obtain the parameters of the model, by requiring to select the optimal location of only one of the points (x), since that the other is immediately established by the requirement of symmetry.

Some numerical examples have been used in order to show the effectiveness and applicability of this procedure for the identification of fractional-order models and to get insight into the influence of selection of the set of symmetrical points on the accuracy of the identified model.

The proposed symmetrical procedure has been applied to the following sets of representative points: (5-50-95%), (10-50-90%), (15-50-85%), (20-50-80%), (25-50-75%), and (30-50-70%). The results of this paper verify that the accuracy of the identified fractional-order model is sensitive to the selection of the set of symmetrical points on the reaction curve and it has been discussed that a more accurate model is obtained for low values of x. New insights about this selection of set of points have been offered in the context of the proposed symmetrical procedure.

This identification procedure gives good results in comparison with other integer- and fractional-order identification methods.

Another aspect to highlight is that the proposed method is analytical, which facilitates its applicability in terms of a lower computational effort compared to complicated identification algorithms generally based on optimization. In the industrial context, large process industries typically have hundreds or thousands of control loops. For this reason, simplicity is of primary interest when identifying a process model for control purposes.

It is the opinion of the author that this type of identification methods, where simplicity is emphasized, will encourage their industrial use and will help in bridging the gap between theoretical research on fractional models and its practical application in the process industry. This expectation is the primary motivation of the present study.

Symmetry, as wide or as narrow as you may define its meaning, is one idea by which man through the ages has tried to comprehend and create order, beauty and perfection.

Herman Weyl (1885 – †1955)
Symmetry

CHAPTER

5

Improving the accuracy of a method for identifying fractional-order models with symmetry considerations

THE previous chapter has presented a general procedure to identify an FFOPDT model. The approach considered there is based on fitting three arbitrary points (x_1-x_2-x_3%) on the process reaction curve. In this general identification procedure, a particular simplification has been considered for the case where the representative points that have been selected are symmetrically located on the process reaction curve, x_1 = x%, x_2 = 50%, and x_3 = (100–x)%. This symmetrical approach is an effective method of estimating the fractional-order model parameters, by only requiring the selection of the optimal location of one of the three points (x) on the process reaction curve, since the others are set immediately by the symmetry requirement.

This chapter explores the possibility of moving the central point x_2 on the process reaction curve, while maintaining the symmetry of the extreme points with respect to the centre of the total range. In this work, results with fractional-order models verify that the accuracy of the estimated model is sensitive to the position of the central point within the symmetrical set of points on the process reaction curve and it has been discussed how a more accurate identified model can be determined.

Finally, new insights into the selection of the central point x_2 have been offered in the context of the considered FFOPDT model identification procedure based on the process reaction curve and symmetrical sets of points. Some reflections about the industrial practice of this identification procedure are also provided.

5.1. Introduction

For a long time, a wide variety of real dynamic processes have been depicted with integer-order models. There is a vast range of identification methods in the technical literature for integer-order models that are based on an open-loop experiment; see, for example, the identification procedures described in (Liu and Gao 2012) and (Huang and Jeng 2005).

More specifically, some references also describe identification algorithms that are based on fitting two or three points on the process reaction curve using FOPDT, DPPDT and SOPDT models.

If the two-point and three-point methods are treated individually, the following methods can be examined in the first group (Alfaro 2006), (Ho, Hang and Cao 1995), (Smith 1972), and (Vitecková, Vitecek and Smutny 2000), while the methods (Jahanmiri and Fallahi 1997), (Mollenkamp 1984), and (Rangaiah and Krishnaswamy 1994) can be considered in the second group. The identification method described in (Alfaro 2006), which is classified as a two-point method for FOPDT and DPPDT models, can also be considered as a three-point method for SOPDT models. Note that the integer-order model identification methods considered above can be divided into those with symmetrical and asymmetrical sets of points respect to the central point of the process reaction curve (50%). In the case of the considered two-point methods, the set of points are asymmetrical with respect to the central point of the reaction curve (50%). The only method with a symmetrical set of points is the 123c identification method proposed by Alfaro in (Alfaro 2006). In the case of the three-point methods considered, references (Jahanmiri and Fallahi 1997) and (Rangaiah and Krishnaswamy 1994) present asymmetrical set of points, while (Alfaro 2006) for the SOPDT models and reference (Mollenkamp 1984) provide sets of points that are symmetrical, although for the latter the central point does not coincide with the central value in the reaction curve.

In recent decades, the advent of fractional calculus and new computational techniques have made possible an increasing evidence that certain dynamic processes can be described more accurately by using fractional-order models; see, e.g., (Dzieliński, Sierociuk and Sarwas 2010), (Tenreiro Machado, Silva, et al. 2010), and (Žecová and Terpák 2015). In fact, fractional calculus has been proven to be an important tool for the scientific and industrial communities (Podlubny 1999a), (Monje, Chen, et al. 2010), being useful and even powerful in many real applications, especially in the field of modelling (Tepljakov 2017).

A broad variety of methods for estimating fractional-order models based on the process reaction curve can be found in the technical literature, with the most common approach in industrial practice being based on nonlinear optimization; see, e.g., (Guevara, et al. 2015), (Malek, Luo and Chen 2013), (Alagoz, et al. 2019), and (Ahmed 2015). These methods generally consist of minimizing the error between the process reaction curve and the step response of the estimated fractional-order model. These techniques require more computational effort in comparison with other existing analytical methods.

However, there are not many procedures involving analytical techniques, which are characterized by simplicity in implementation. Some strategies for estimating the parameters of the FFOPDT model using step-response information have been described in (Tavakoli-Kakhki, Haeri and Tavazoei 2010). In the references (Tavakoli-Kakhki and Tavazoei 2014) and (Tavakoli-Kakhki, Tavazoei and Mesbahi 2013), integral-based estimation methods are proposed, whose main property is their robustness in the presence of measurement noise. More recently, a general procedure for identifying an FFOPDT model has been presented and detailed in Chapter 4. This procedure consists on fitting three arbitrary points (x_1-x_2-x_3%) on the process reaction curve, where the process information is taken from an open-loop step-test experiment. A simplification of the general identification procedure has also been addressed in Chapter 4, particularizing for the case where the points are selected to be symmetrically located on the process reaction curve only (x-50-(100–x)%). This symmetrical method provides an efficient way to obtain the FFOPDT model parameters by requiring the selection of the optimal location of only one of the points (x), since the other is immediately established by the symmetry requirement.

Although it has been demonstrated that this symmetrical identification method gives good results compared to other fractional- and integer-order identification methods, the influence of the selection of the symmetrical set of points on the accuracy of the identified fractional-order model has also been determined. Therefore, this chapter explores whether the location of the symmetrical set of points can improve further the accuracy of the identified fractional-order model.

This paper is organized as follows. Section 5.2 presents an overview of the FFOPDT model identification procedure based on three points of the process reaction curve. In Section 5.3, the problem to be solved in this paper and the methodology employed are stated. Section 5.4 presents the results of some numerical simulations illustrating that the location of the central point (x_2) of the symmetrical set of points (x-x_2-(100–x)%) can significantly improve the accuracy of the identified fractional-order model, while maintaining the simplicity of the procedure. Finally, the conclusions of this work are presented in Section 5.5.

5.2. Overview of FFOPDT model estimation based on the process reaction curve

This section overviews the general procedure for identifying FFOPDT models from process information collected from the process reaction curve.

As indicated in the previous chapter, a step-input open-loop test is applied to the process to be identified. Figure 5.1 illustrates the step-input signal $u(t)$, the process reaction curve $y_\alpha(t)$ and three arbitrary representative points (x_1, x_2 and x_3) on the process reaction curve. Data obtained from the process reaction curve needed for the identification procedure are $\{\Delta y, \Delta u, t_{x1}, t_{x2}, t_{x3}\}$.

In Figure 5.1, Δy is the process output total change, Δu is the step signal amplitude, and set of times $\{t_{x1}, t_{x2}, t_{x3}\}$ are the times required to reach $x_1\%$ ($y_\alpha(t_{x1})$), $x_2\%$ ($y_\alpha(t_{x2})$), and $x_3\%$ ($y_\alpha(t_{x3})$) of the process output total change on the process output $y_\alpha(t)$, respectively.

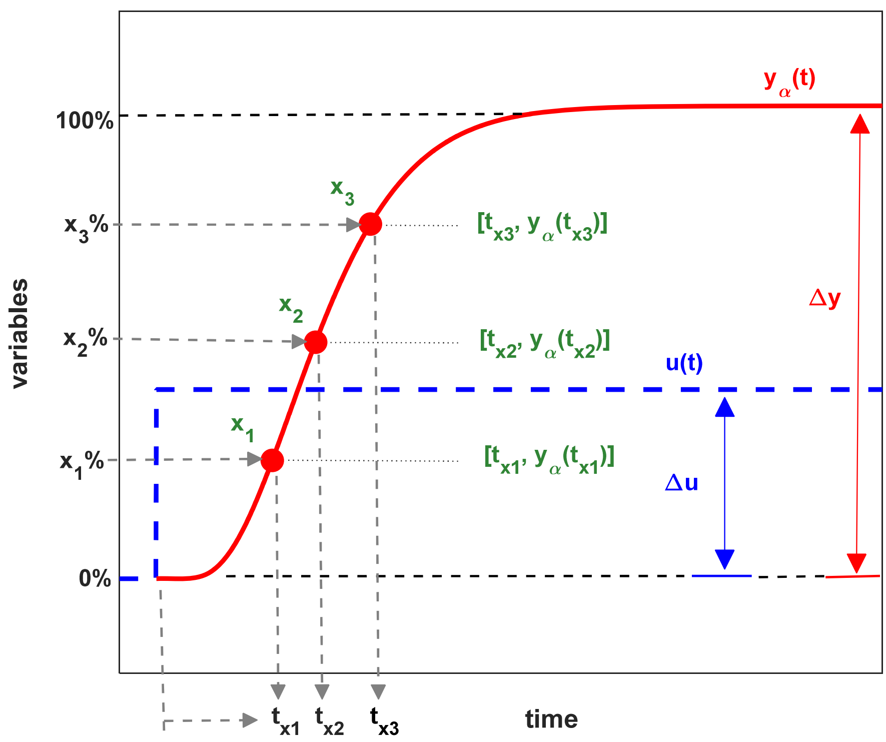

Figure 5.1. Step-input signal $u(t)$, process reaction curve $y_\alpha(t)$, and arbitrary representative points (x_1, x_2, and x_3) on the process reaction curve. Data obtained from the process reaction curve required for the identification procedure are $\{\Delta y, \Delta u, t_{x1}, t_{x2}, t_{x3}\}$.

Accordingly, the general procedure for identifying the FFOPDT model based on three arbitrary points on the process reaction curve is summarized below.

Figure 5.2 illustrates the complete scheme of the general procedure to identify the parameters of an FFOPDT model, $\theta_P = \{K, T, L, \alpha\}$, from three arbitrary points (x_1-x_2-$x_3\%$) on the process reaction curve.

This scheme is divided into two different parts:

Part A is the general procedure to determine rational expressions for functions $f_1(\Delta)$, $f_2(\alpha)$, and $f_3(\alpha)$, as a part of the set of equations (4.10) and which depend on the location of the set of points (x_1-x_2-x_3%). It consists of the following steps, as illustrated in Figure 5.2:

1. The normalized times $\{\tau_{x1}, \tau_{x2}, \tau_{x3}\}$ for the considered three points (x_1, x_2, and x_3) on the process reaction curve are obtained from the normalized process output $\tilde{y}_\alpha(\tau)$ (4.3), for the different values of α, $0.50 \leq \alpha \leq 1.10$.
2. Data sets $\{\Delta, \alpha\}$, $\{\alpha, f_2(\alpha)\}$, and $\{\alpha, f_3(\alpha)\}$ are determined using the values of the corresponding normalized times for the considered set of points (x_1-x_2-x_3%), where $\Delta = \frac{{\tau_{x3}}^{1/\alpha} - {\tau_{x1}}^{1/\alpha}}{{\tau_{x2}}^{1/\alpha} - {\tau_{x1}}^{1/\alpha}}$, $f_2(\alpha) = \left(\frac{1}{{\tau_{x3}}^{1/\alpha} - {\tau_{x1}}^{1/\alpha}}\right)^{\alpha}$, and $f_3(\alpha) = {\tau_{x3}}^{1/\alpha}$.
3. Using a curve-fitting procedure, rational functions are obtained for $f_1(\Delta)$, $f_2(\alpha)$ and $f_3(\alpha)$, respectively.
4. The expressions for the FFOPDT model parameters (4.10) are determined from the rational functions $f_1(\Delta)$, $f_2(\alpha)$, and $f_3(\alpha)$ obtained in the previous step.

Part B illustrates the algorithm for identifying the FFOPDT model from the process reaction curve. It consists of the steps illustrated in Figure 5.2:

1. Data required for the identification procedure are obtained from the process reaction curve $\{\Delta y, \Delta u, t_{x1}, t_{x2}, t_{x3}\}$.
2. The value of the ratio index Δ, $\Delta = (t_{x3} - t_{x1})/(t_{x2} - t_{x1})$, is calculated from the set of times $\{t_{x1}, t_{x2}$, and $t_{x3}\}$.
3. The value of α and the numerical values of f_2 and f_3 are estimated. After that, the FFOPDT model parameters, $\theta_P = \{K, T, L, \alpha\}$, are calculated using the set of equations (4.10) and the experimental data taken from the process reaction curve $\{\Delta y, \Delta u, t_{x1}, t_{x2}, t_{x3}\}$.

For a more detailed information about this identification method based on the process reaction curve, the reader is referred to Chapter 4, where one can find the complete development of the set of equations (4.10), and an analysis of the influence of the symmetrical set of points (x-50-(100–x)%) on the accuracy of the identified model. In Chapter 6, the analysis of the influence of the arbitrary set of points (x_1-x_2-x_3%) on the accuracy of the identified model will be discussed, and some empirical rules for the selection of symmetrical and asymmetrical sets of points will be provided. This chapter also discusses the effectiveness and applicability of this identification method for both symmetrical and asymmetrical sets of points on the process reaction curve.

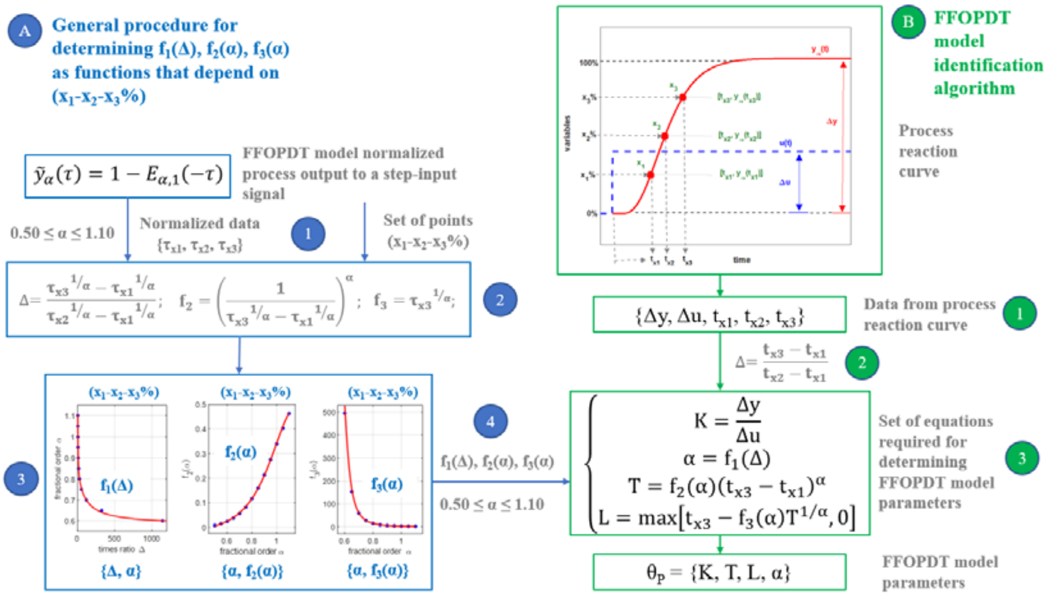

Figure 5.2. Scheme of the complete general procedure for identifying an FFOPDT model considering three arbitrary points (x_1-x_2-x_3%) on the process reaction curve. Note that the scheme is divided into two parts: Part A (blue) represents the procedure to obtain the set of equations for determining FFOPDT model parameters. These equations depend on the set of points (x_1-x_2-x_3%). Part B (green) schematizes the FFOPDT model identification algorithm for estimating model parameters, $\theta_P = \{K, T, L, \alpha\}$, by using the information collected from the process reaction curve. The corresponding steps that constitute each of the two parts of the scheme are also provided in this figure.

5.3. Problem statement

The previous section has summarized the general procedure for FFOPDT model identification based on fitting three arbitrary points (x_1-x_2-x_3%) on the process reaction curve, where the process information is obtained from a simple open-loop test.

Furthermore, the identification procedure discussed in Chapter 4 can be considered as a simplification of the general identification procedure, where only points that are symmetrically located on the process reaction curve are selected. As a result, the central point or centroid will be located in the middle of the output interval, $x_2 = 50\%$ ($t_{x2} = t_{50}$, $y_\alpha(t_{50})$), as can be seen in Figure 5.3. The remaining two points could be located arbitrarily on the process reaction curve, but set symmetrically with respect to the central point ($\Delta x_{32} = \Delta x_{21} = \Delta x$). One of the extreme points will be denoted $x_1 = x$, the other being $x_3 = 100 - x$. In this case, the times to be determined will be $t_{x1} = t_x$, $t_{x2} = t_{50}$, and $t_{x3} = t_{100-x}$, where t_x, t_{50}, and t_{100-x} denote the time required to reach x% ($y_\alpha(t_x)$), 50% ($y_\alpha(t_{50})$), and (100–x)% ($y_\alpha(t_{100-x})$) of the process output total change, respectively, considering the following range $0 < x < 50$.

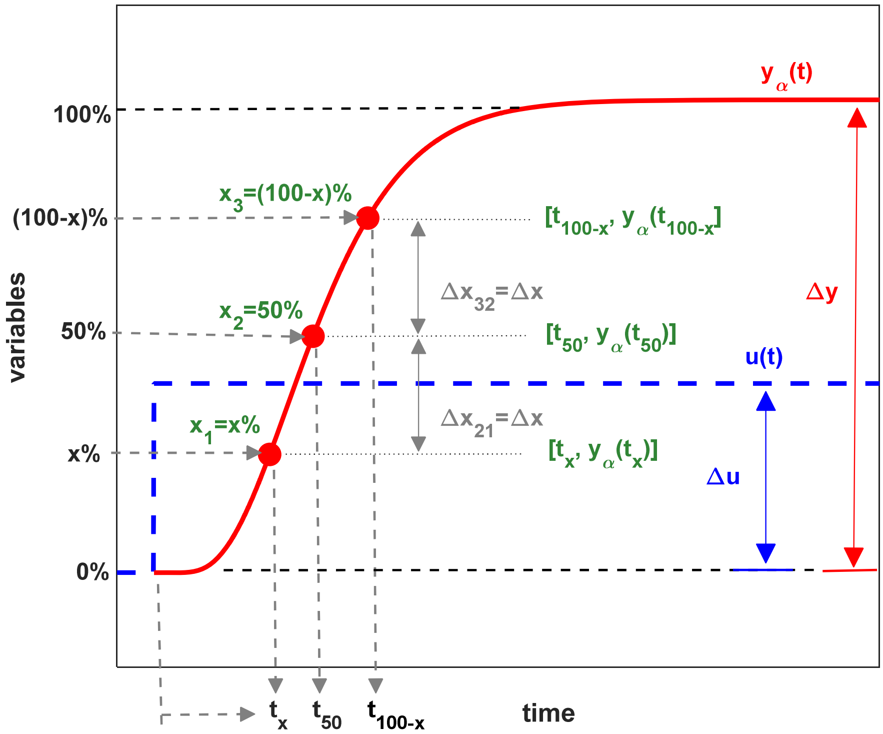

Figure 5.3. Step-input signal $u(t)$, process reaction curve $y_\alpha(t)$, and symmetrical representative points (x_1=x%, x_2=50%, and x_3=(100–x)%) on the process reaction curve. Data obtained from the process reaction curve required for the identification procedure are $\{\Delta y, \Delta u, t_x, t_{50}, t_{100-x}\}$. Note that Δx_{21} and Δx_{32} represent a variation of $(x_2 - x_1)$% and $(x_3 - x_2)$% from the centroid x_2 to the extreme points x_1 and x_3, respectively.

Consequently, this symmetrical identification method provides an efficient way to obtain the FFOPDT model parameters by requiring the selection of the optimal location of only one of the points, $x_1 = x\%$, since the other is immediately set by the symmetry requirement, $x_3 = (100–x)\%$, with respect to the central point $x_2 = 50\%$.

The applicability and effectiveness of this symmetrical procedure for the identification of fractional-order models has been shown and the influence of the selection of the symmetrical set of points on the accuracy of the identified model has been determined using several numerical examples. It has been shown that this identification procedure gives good results compared to other well-known integer- and fractional-order identification methods; see Chapter 4 for a complete reference about these issues.

The results in (Gude and García Bringas 2022) verify that the accuracy of the identified FFOPDT model is sensitive to the position of the central point x_2 within the set of symmetrical points $(x\text{-}x_2\text{-}(100–x)\%)$ on the reaction curve and it has been discussed how a more accurate identified fractional-order model can be obtained.

However, it has been considered in Chapter 4 that the central point x_2 is always located in the middle of the total output change ($x_2 = 50\%$). For this reason, this chapter explores the effect of moving central point or centroid x_2 on the process reaction curve, while maintaining symmetry considerations. Figure 5.4 illustrates that the location of the extreme points exhibits symmetry with respect to the center of the total output range ($\Delta x_{32} = \Delta x_{21} = \Delta x$), while the central point x_2, whose optimal location is the object of study in this work, can be moved along the process reaction curve.

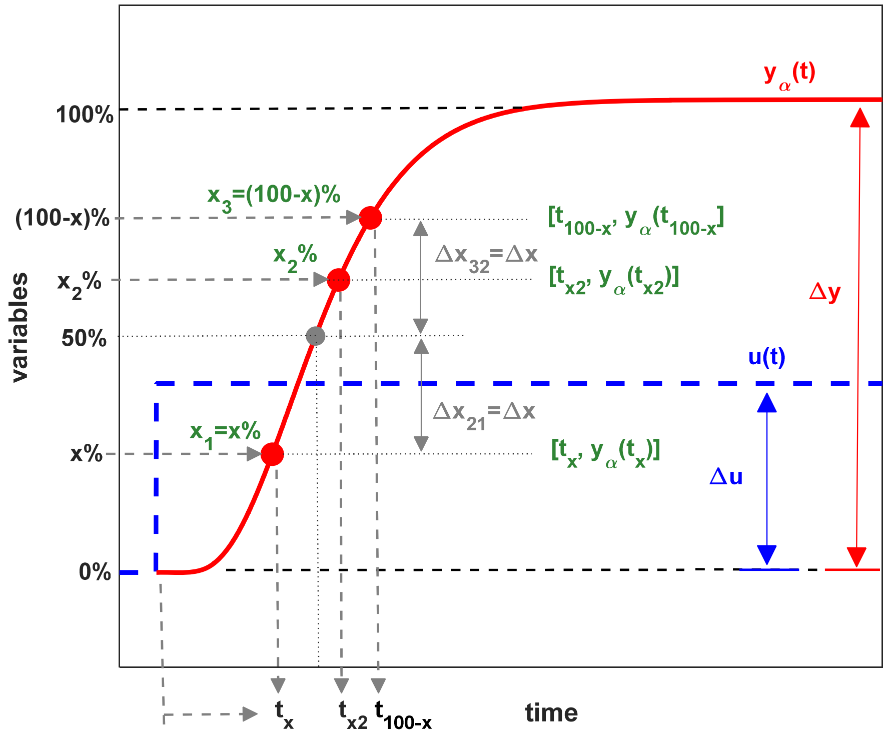

Figure 5.4. Step-input signal $u(t)$, process reaction curve $y_\alpha(t)$, and symmetrical representative points (x_1=x%, x_2, and x_3=(100–x)%) on the process reaction curve. Data obtained from the process reaction curve required for the identification procedure are $\{\Delta y, \Delta u, t_x, t_{x2}, t_{100-x}\}$. Note that Δx_{21} and Δx_{32} represent a variation of $(50 - x_1)\%$ and $(x_3 - 50)\%$ from the centre of the total output range to the extreme points x_1 and x_3, respectively.

The experimental procedure followed to evaluate the effect of the location of x_2 on the accuracy of the identified fractional-order model is as follows:

1. Values of the normalized times $\{\tau_x, \tau_{x2}, \tau_{100-x}\}$ of the three representative points on the process reaction curve are obtained considering $0.50 \le \alpha \le 1.10$. In this chapter, x_2 will be a set of values, $x_2 \in [x_{2,min}, \ldots, x_{2,max}]$, to evaluate the effect of its variation on the accuracy of the identified model.
2. Data sets $\{\Delta, \alpha\}$, $\{\alpha, f_2(\alpha)\}$, and $\{\alpha, f_3(\alpha)\}$ are determined for the considered symmetrical set of points (x-x_2-$(100–x)\%$) by using the values of the corresponding normalized times $\{\tau_x, \tau_{x2}, \tau_{100-x}\}$.

3. The values of the parameters $\{p_i, q_i\}$ in rational functions (5.1) – (5.3) for functions $f_1(\Delta)$, $f_2(\alpha)$, and $f_3(\alpha)$, respectively, are obtained by means of a curve-fitting procedure.

$$f_1(\Delta) = \frac{p_1\Delta^2 + p_2\Delta + p_3}{\Delta^2 + q_1\Delta + q_2} \tag{5.1}$$

$$f_2(\alpha) = \frac{p_1\alpha + p_2}{\alpha^2 + q_1\alpha + q_2} \tag{5.2}$$

$$f_3(\alpha) = \frac{p_1\alpha^2 + p_2\alpha + p_3}{\alpha^2 + q_1\alpha + q_2} \tag{5.3}$$

4. From the rational functions $f_1(\Delta)$, $f_2(\alpha)$, and $f_3(\alpha)$ obtained in the previous step, the expressions for the FFOPDT model parameters (4.10) are completed.
5. Once the numerical values of f_1, f_2, and f_3 are determined, the values of the FFOPDT model parameters, $\theta_P = \{K, T, L, \alpha\}$, are calculated using expressions (4.10) and experimental data collected from the process reaction curve, $\{\Delta y, \Delta u, t_x, t_{x2}, t_{100-x}\}$.
6. Finally, it is required the accuracy of the identified model to be evaluated. The Mean Squared Error (MSE) is used as a time-domain fitting criterion for measuring the performance of the identified model:

$$S(\bar{\theta}) = \frac{1}{N_s}\sum_{k=1}^{N_s}[e(kT_s, \bar{\theta})]^2 = \frac{1}{N_s}\sum_{k=1}^{N_s}[y(kT_s) - y_m(kT_s, \bar{\theta})]^2 \tag{5.4}$$

where T_S is the sampling period, $\bar{\theta}$ is the vector of process model parameters, $e(kT_s, \bar{\theta})$ is the difference between the process reaction curve and the step response of the identified model, $y(kT_s)$ and $y_m(kT_s, \bar{\theta})$, respectively, N_S is the number of collected samples, and $N_S T_S$ is the time length of the dynamic response.

In this context, a relative performance index is also used to quantify the performance of one identification method compared to another. In this chapter, the following relative performance index is used:

$$S_{x,y}(\bar{\theta}_x, \bar{\theta}_y) = \frac{S(\bar{\theta}_x)}{S(\bar{\theta}_y)} \tag{5.5}$$

where $S(\bar{\theta}_x)$ and $S(\bar{\theta}_y)$ are the values of MSE in (5.4) and $\bar{\theta}_x$ and $\bar{\theta}_y$ are the vectors of the process model parameters for the x and y models, respectively.

The experimental procedure explained above is schematized in Figure 5.5.

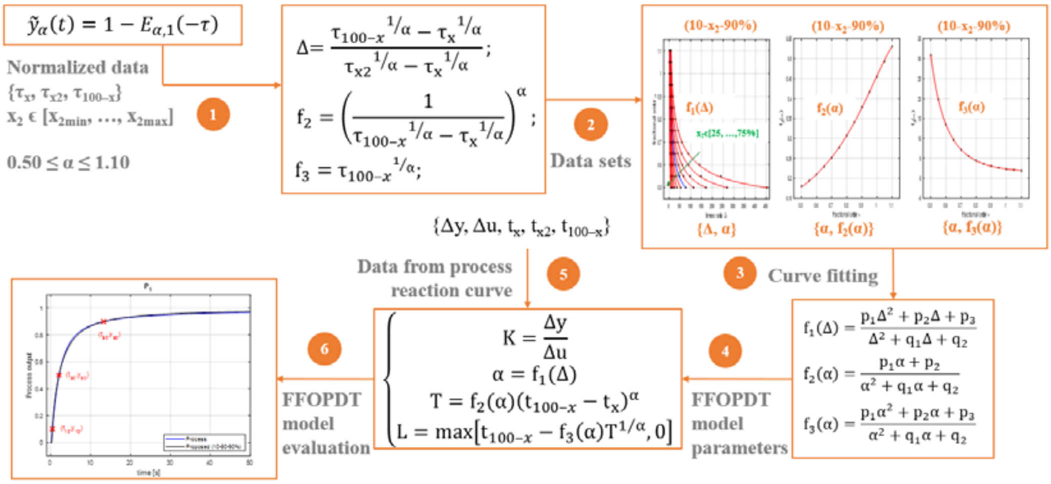

Figure 5.5. Scheme of the experimental procedure followed to evaluate the effect of the location of central point x_2 on the accuracy of the identified fractional-order model.

Data sets $\{\Delta, \alpha\}$, $\{\alpha, f_2(\alpha)\}$, and $\{\alpha, f_3(\alpha)\}$ for $0.50 \le \alpha \le 1.10$, and the results of curve fitting for the symmetrical set of points (x-x2-(100–x)%) are obtained. Figures 5.6 – 5.8 show data sets and the functions $f_1(\Delta)$, $f_2(\alpha)$ and $f_3(\alpha)$ obtained by curve fitting considering the case $x_1 = x = 10\%$, $x_2 = [25, 30, ..., 75\%]$, and $x_3 = 100–x = 90\%$.

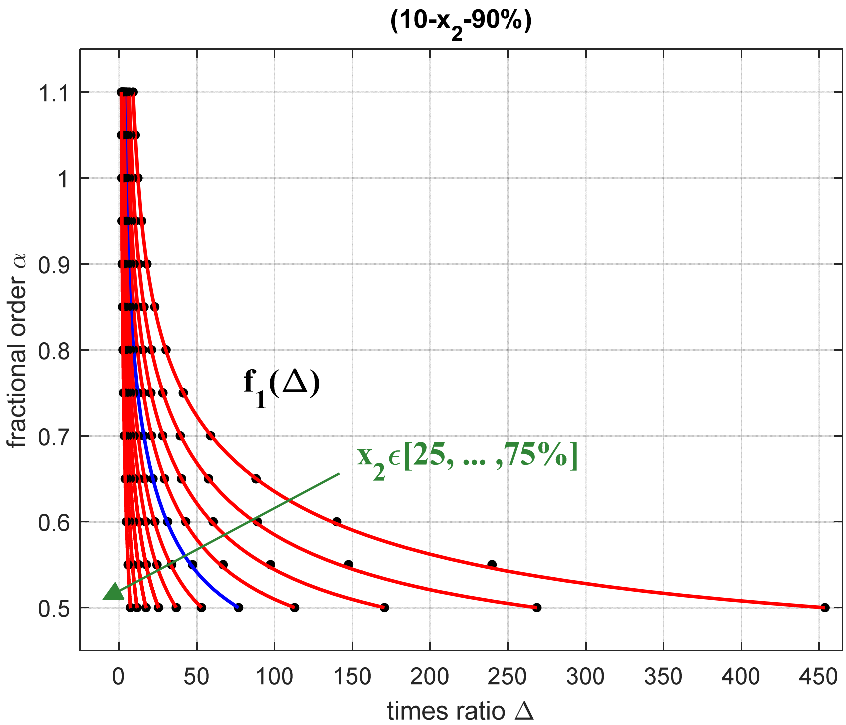

Figure 5.6. Data sets $\{\Delta, \alpha\}$ and results of curve fitting for $f_1(\Delta)$ considering the symmetrical set of points (10-x2-90%). Note that data sets and $f_1(\Delta)$ depend on x_2, where $x_2 \in [25, 30, \dots, 75\%]$. Curve for $x_2 = 50\%$ is represented in blue in this figure.

Note that a family of curves $f_1(\Delta)$ is obtained depending on the value of x_2, while graphs $f_2(\alpha)$ and $f_3(\alpha)$ do not change because they do not depend on the location of x_2.

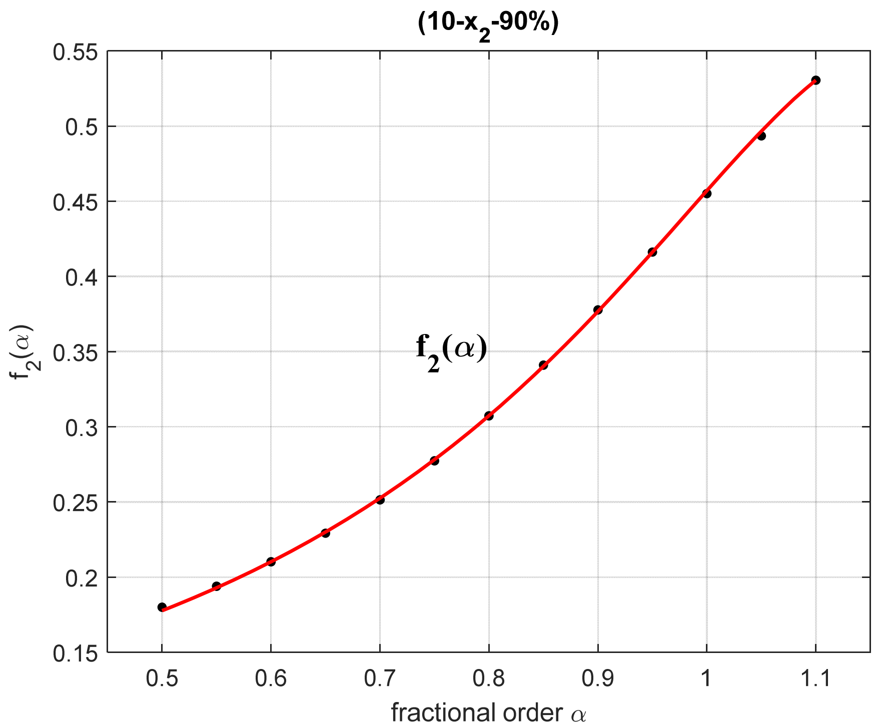

Figure 5.7. Data sets $\{\alpha, f_2(\alpha)\}$ and results of curve fitting for $f_2(\alpha)$ considering the symmetrical set of points (10-x_2-90%). Note that $f_2(\alpha)$ does not depend on x_2.

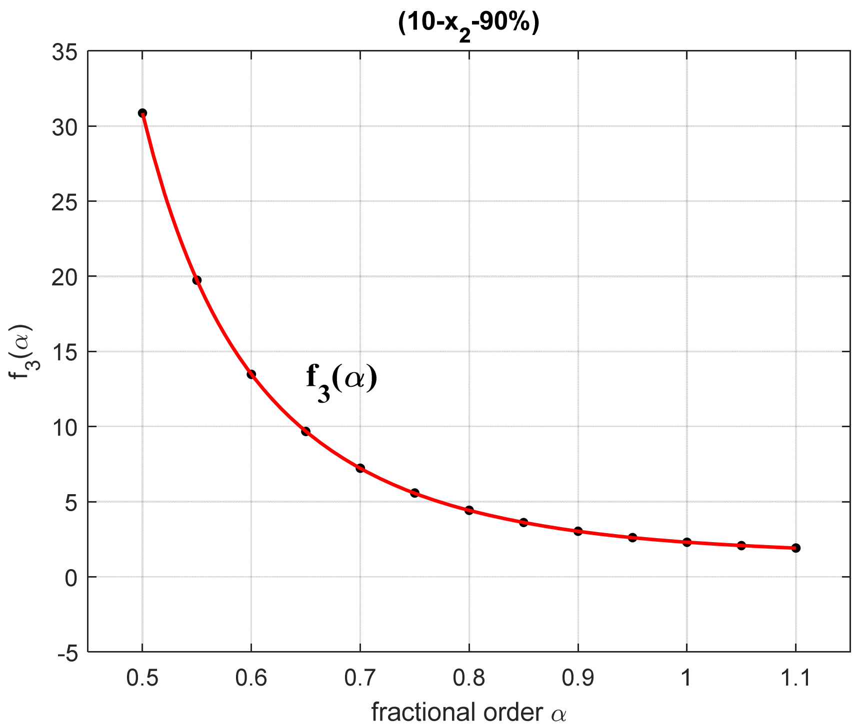

Figure 5.8. Data sets $\{\alpha, f_3(\alpha)\}$ and results of curve fitting for $f_3(\alpha)$ considering the symmetrical set of points (10-x_2-90%). Note that $f_3(\alpha)$ does not depend on x_2.

In this chapter, $x_1 = 10\%$ and $x_3 = 90\%$ are used and symmetry considerations involves that $\Delta x_{32} = \Delta x_{21} = \Delta x = 40\%$ for this case. The selection of these values of x_1 and x_3 has been made taking into account that the accuracy of the identified model is improved for low values of x. More specifically, the influence of the position of the representative symmetrical points on the accuracy of the identified model is explained in detail in Chapter 4. In this regard, it has been demonstrated in Chapter 4 that the step response of the identified model gives a good fit with the process reaction curve for the symmetrical case, particularly in the interval $[x - (100–x)]$.

This identification method exhibits symmetry in the set of points $(x\text{-}x_2\text{-}(100–x)\%)$. Due to this, $x_1 = x$ and $x_3 = 100–x$, and the interval $[x - (100–x)]$ is larger for lower values of x and, thus, the process reaction curve is fitted better by the step response of the identified fractional-order models, which translates into a lower value in the performance index S (5.4).

Figures 5.6 – 5.8 have been obtained by applying the Levenberg-Marquardt least-squares algorithm for fitting data.

The corresponding parameters values $\{p_i, q_i\}$ for functions $f_1(\Delta)$, $f_2(\alpha)$ and $f_3(\alpha)$, and for each value of $x_2 = [25, 30, ..., 75\%]$ are shown in Tables 5.1 – 5.3, respectively.

(10-x_2-90%)	**p_1**	**p_2**	**p_3**	**q_1**	**q_2**
$x_2 = 25\%$	0.4286	85.18	362.5	107.2	13.5
$x_2 = 30\%$	0.4228	52.01	113.2	63.49	−31.62
$x_2 = 35\%$	0.4152	34.91	38.59	41.5	−32.76
$x_2 = 40\%$	0.4063	24.49	11.22	28.26	−26.71
$x_2 = 45\%$	0.3965	17.62	0.7946	19.62	−20.18
$x_2 = 50\%$	0.3854	12.75	−3.517	13.5	−14.93
$x_2 = 55\%$	0.3720	9.265	−4.86	9.156	−10.84
$x_2 = 60\%$	0.3558	6.650	−4.951	5.898	−7.648
$x_2 = 65\%$	0.3351	4.698	−4.393	3.486	−5.172
$x_2 = 70\%$	0.3045	3.333	−3.548	1.841	−3.347
$x_2 = 75\%$	0.2590	2.282	2.712	0.5486	−1.919

Table 5.1. Parameters $\{p_i, q_i\}$ of the rational function $f_1(\Delta)$ for the symmetrical sets of points (10-x_2-90%).

(10-x_2-90%)	**p_1**	**p_2**	**q_1**	**q_2**
$x_2 \in [25, …, 75\%]$	−0.0673	0.1578	−2.501	1.699

Table 5.2. Parameters $\{p_i, q_i\}$ of the rational function $f_2(\alpha)$ for the symmetrical sets of points (10-x_2-90%).

(10-x_2-90%)	**p_1**	**p_2**	**p_3**	**q_1**	**q_2**
$x_2 \in [25, …, 75\%]$	4.066	−7.705	5.055	−0.4136	0.02868

Table 5.3. Parameters $\{p_i, q_i\}$ of the rational function $f_3(\alpha)$ for the symmetrical sets of points (10-x_2-90%).

The set of equations (4.10) can be modified for this particular set of points (10-x_2-90%), as follows:

$$\begin{cases} K = \dfrac{\Delta y}{\Delta u} \\ \alpha = f_1(\Delta) \\ T = f_2(\alpha)(t_{10} - t_{90})^{\alpha} \\ L = \max\left[t_{90} - f_3(\alpha)T^{1/\alpha}, 0\right] \end{cases} \tag{5.6}$$

where $x_1 = x = 10\%$, $x_2 = [25, 30, \ldots, 75\%]$, and $x_3 = (100–x) = 90\%$, and data information collected from the process reaction curve that is needed for identifying the FFOPDT model is $\{\Delta y, \Delta u, t_{10}, t_{x2}, t_{90}\}$.

5.4. Results and discussion

In this section, the FFOPDT model identification procedure for the symmetrical set of points (x-x_2-$(100–x)\%$) summarized in Section 5.2 has been proven for three fractional-order process models.

As mentioned previously in Section 5.3, the following representative points on the process reaction curve have been selected for the considered symmetrical set of points (x-x_2-$(100–x)\%$): $x_1 = x\% = 10\%$, $x_2 \in [25, 30, \ldots, 75\%]$, and $x_3 = (100–x)\% = 90\%$.

One of the main results of this work consists on verifying that an improvement in terms of the accuracy of the identified fractional-order model can be obtained by moving the central point x_2 to another location different from $x_2 = 50\%$.

For this purpose, this section is organized as follows. First, a collection of fractional-order processes is used to gain insight into the effect of the central point location x_2 on the accuracy of the estimated model by considering a fractional order in the range $0.60 \leq \alpha \leq 1.00$. Next, two additional higher-order fractional processes are used to compare the model performance for the x_2 location that maximizes the accuracy of the identified model with the one for the location of $x_2 = 50\%$. The results obtained using the proposed method with both x_2 locations are also compared with other fractional-order models obtained using well-established identification procedures in the technical literature. Finally, a discussion about the obtained results is provided.

The FOTF MATLAB Toolbox, which is a set of built-in functions suitable for dealing with fractional-order systems, has been used in order to perform the simulation results obtained in this section (Xue 2017).

5.4.1. Example 1

The following fractional-order process model is used in this example:

$$P_{1,i}(s) = \frac{K_1}{(1 + T_1 s^{\lambda_i})^2} e^{-L_1 s} \tag{5.7}$$

where $K_1 = 1$, $T_1 = 1$ s, $L_1 = 0.1$ s, and $\lambda_i = 0.60, 0.65, \ldots, 1.00$.

The model used in this example is the one of an FSOPDT, which provides a certain modelling deviation with respect to the FFOPDT model, which is the structure adopted in the identification procedure used in this paper. Indeed, the model (5.7) for the same range of values of λ_i values, $0.60 \leq \lambda_i \leq 1.00$, has been used in Chapter 4, on the one hand, to understand the influence of the location of the symmetrical set of points on the accuracy of the identified FFOPDT model and, on the other hand, as a batch of processes to validate the proposed identification procedure for different symmetrical sets of points.

The objective in this example is to gain insight into the effect of moving the location of the central point x_2 on the accuracy of the estimated FFOPDT model in the context of the fractional-order model identification procedure for a symmetrical set of points on the process reaction curve.

Hereafter, the following experimental procedure has been used in this example:

1. Nine different fractional orders have been considered for the process (5.7). More precisely, Table 5.4 lists the fractional orders λ_i used for the process $P_{1,i}$, where $i = 1, \ldots, 9$, the number of samples N_S, the sampling period T_S, and the time length $N_S T_S$ used in this example.
2. The FFOPDT model parameters $\bar{\theta}_{i,j} = \{K_{i,j}, T_{i,j}, L_{i,j}, \alpha_{i,j}\}$ are obtained for each process $P_{1,i}$ and for each of the sets of points, where $j = 1, \ldots, 11$ represents each of the considered sets of points. Table 5.5 shows the location of the central point x_2 of the symmetrical set of points (10-x_2-90%) considered in the FFOPDT model identification procedure.
3. The response to a step-input signal for the 99 fractional-order models have been determined and their corresponding model performance index values have been determined. Figure 5.9 illustrates the 99 model performance index values multiplied by the number of samples, $S(\bar{\theta}_{i,j}) \cdot N_S$, obtained for each of the different processes $P_{1,i}$ ($i = 1, \ldots, 9$) and using each of the locations of x_2 ($j = 1, \ldots, 11$).

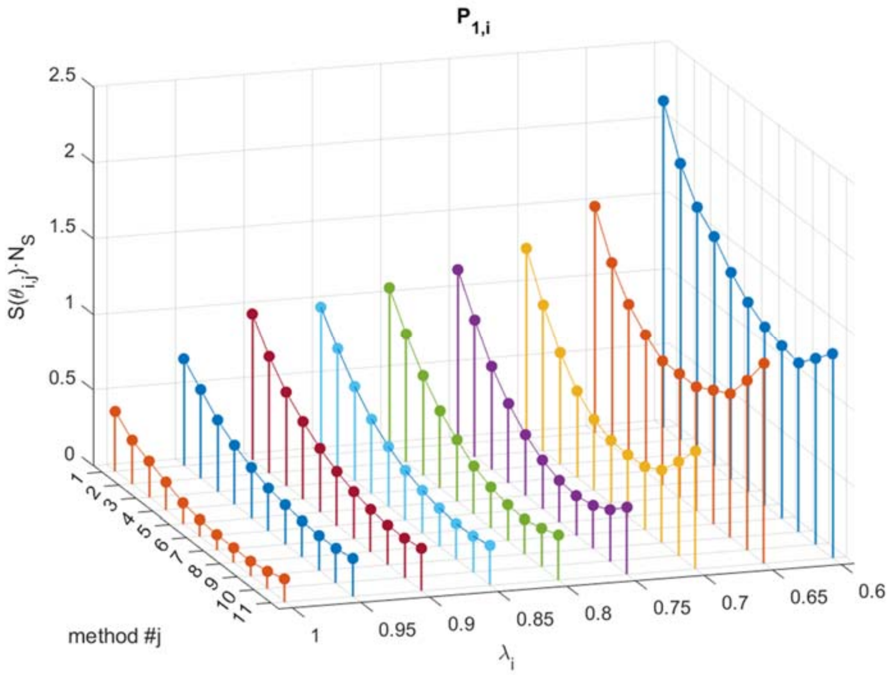

Figure 5.9. Model performance index multiplied by the number of samples, $S(\theta_{i,j})\cdot N_S$, for the 99 FFOPDT models with parameters $\theta_{i,j}$, which have been obtained for each process $P_{1,i}$ ($i = 1, \ldots, 9$) and each x_2 location ($j = 1, \ldots, 11$).

i	λ_i	N_S	T_S [s]	N_ST_S [s]
1	0.60	58040	0.01	580.39
2	0.65	29206	0.01	292.05
3	0.70	15816	0.01	158.15
4	0.75	8960	0.01	89.59
5	0.80	5224	0.01	52.23
6	0.85	3067	0.01	30.66
7	0.90	1761	0.01	17.60
8	0.95	965	0.01	9.64
9	1.00	594	0.01	5.93

Table 5.4. Process fractional orders, number of samples, sampling period, and time length that have been used in this example for processes $P_{1,i}$ ($i = 1,\ldots, 9$).

j	Method #	x_2	Set of points
1	1	25%	(10-25-90%)
2	2	30%	(10-30-90%)
3	3	35%	(10-35-90%)
4	4	40%	(10-40-90%)
5	5	45%	(10-45-90%)
6	6	50%	(10-50-90%)
7	7	55%	(10-55-90%)
8	8	60%	(10-60-90%)
9	9	65%	(10-65-90%)
10	10	70%	(10-60-90%)
11	11	75%	(10-75-90%)

Table 5.5. Symmetrical sets of points used for determining the influence of x_2 location on the accuracy of the FFOPDT model.

The following conclusions have been drawn from Figure 5.9:

1. The maximum value of $S(\bar{\theta}_{i,j})$ is always obtained for $x_2 = 25\%$ ($j = 1$).
2. The value of $S(\bar{\theta}_{i,j})$ decreases substantially as x_2 increases, i.e., for larger values of j.
3. A minimum value of $S(\bar{\theta}_{i,j})$ located for $x_2 > 50\%$ can be identified in all curves.
4. More specifically, the minimum value of $S(\bar{\theta}_{i,j})$ for $\lambda_i \geq 0.75$ corresponds to a location $x_2 = 65\%$. While the location of the minimum for $\lambda_i < 0.75$ occurs for values slightly lower than $x_2 = 65\%$, although without significant differences with the latter.
5. The value of $S(\bar{\theta}_{i,j})$ increases significantly again from its minimum value for $\lambda_i < 0.8$. However, the increase of $S(\bar{\theta}_{i,j})$ is not significant for $\lambda_i \geq 0.8$.

These observations support that the accuracy of the estimated fractional-order model can be improved using the FFOPDT model identification method for symmetrical sets of points by setting the value of the central point x_2 around 65%. In this regard, Figure 5.10 shows the relative performance indices between method #9 ($x_2 = 65\%$) and method #6 ($x_2 = 50\%$) for all values of λ_i ($i = 1, ..., 9$).

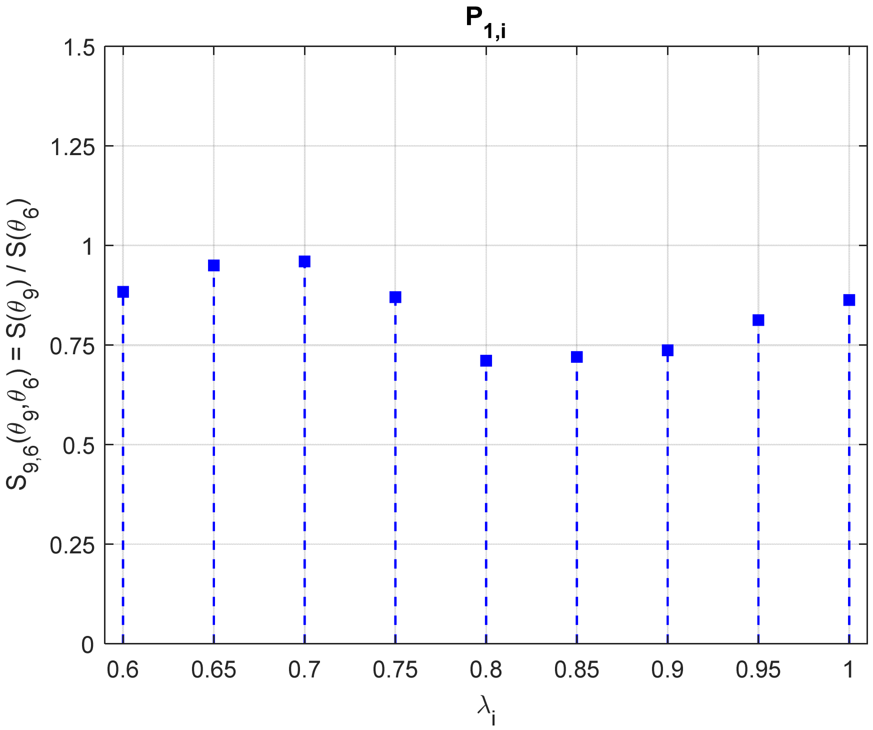

Figure 5.10. Relative performance index values $S_{9,6}(\theta_9, \theta_6)$ for each value of λ_i ($i = 1, \ldots, 9$), which represent the ratio between model performance indices with method #9 ($x_2 = 65\%$) and with method #6 ($x_2 = 50\%$).

The case $i = 5$ ($\lambda_5 = 0.80$) for the above considered processes $P_{1,i}$, which has been treated in Chapter 4 for the symmetrical set of points (x-50-(100–x)%), is used below for illustrative purposes.

The process reaction curve for the model $P_{1,5}$ is illustrated in Figure 5.11. Data information required for the identification procedure and the corresponding FFOPDT model parameters $\bar{\theta}_{5,j} = \{K_{5,j}, T_{5,j}, L_{5,j}, \alpha_{5,j}\}$, have been obtained in Tables 5.6 and 5.7, respectively, for cases $j = 6$ ($x_2 = 50\%$) and $j = 9$ ($x_2 = 65\%$). In this regard, the results obtained with the set of points (10-50-90%), which has been recommended in Chapter 4, and the ones obtained with (10-65-90%), which provides the minimum value in the performance index S, can be compared.

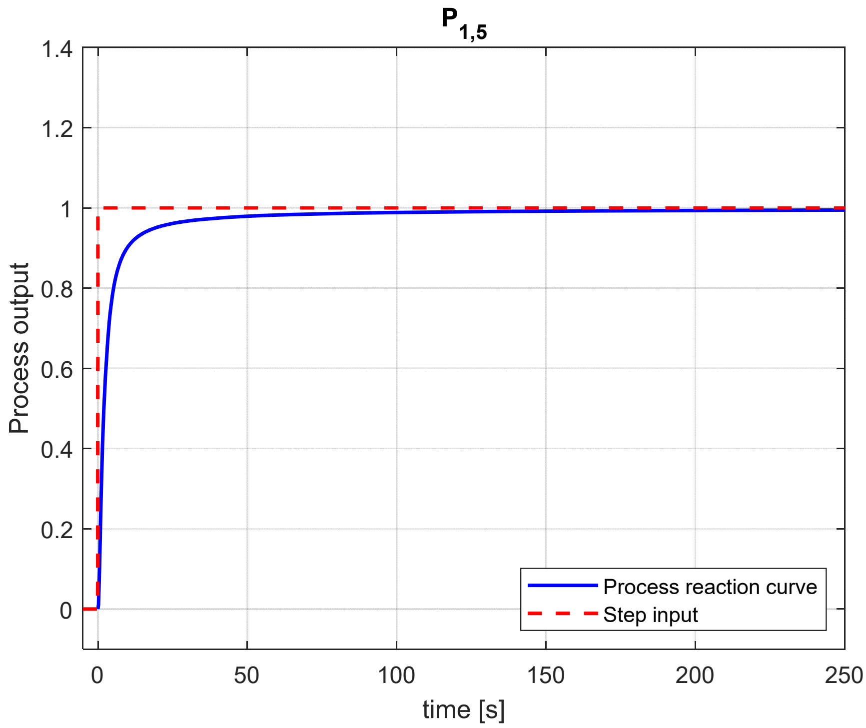

Figure 5.11. Step-input signal and process reaction curve for process $P_{1,5}$.

Method #6: FFOPDT (10-50-90%)	**Method #9: FFOPDT (10-65-90%)**
$\Delta u = 1.00$	
$\Delta y = 1.00$	
$t_{10} = 0.4890$ s	
$t_{50} = 1.9900$ s	$t_{65} = 2.6250$ s
$t_{90} = 9.7230$ s	

Table 5.6. Process information required for fractional-order model identification of process $P_{1,5}$.

Method #6: FFOPDT (10-50-90%)	Method #9: FFOPDT (10-65-90%)
$K_{5,6} = 1.00$	$K_{5,9} = 1.00$
$T_{5,6} = 2.2003$ s	$T_{5,9} = 2.0448$ s
$L_{5,6} = 0.3466$ s	$L_{5,9} = 0.3629$ s
$\alpha_{5,6} = 0.8447$	$\alpha_{5,9} = 0.8274$

Table 5.7. FFOPDT model parameters obtained for process $P_{1,5}$ with the considered identification method and sets of points (10-50-90%) and (10-65-90%), respectively.

Figures 5.12 and 5.13 show the step responses of the FFOPDT models with parameters $\bar{\theta}_{5,6}$ and $\bar{\theta}_{5,9}$, which have been obtained by using the proposed identification method with the set of points (10-50-90%) and (10-65-90%), respectively. Although in both cases there are good results obtained in comparison with the process reaction curve, one can observe that the response for the model with $x_2 = 65\%$ improves that of $x_2 = 50\%$. More specifically, the model performance index value obtained for $x_2 = 50\%$ is $S(\bar{\theta}_{5,6}) = 6.06 \cdot 10^{-5}$ and the one obtained for $x_2 = 65\%$ is $S(\bar{\theta}_{5,9}) = 4.31 \cdot 10^{-5}$, which implies a 30% reduction in the value of S, obtaining a more accurate model for the case $x_2 = 65\%$.

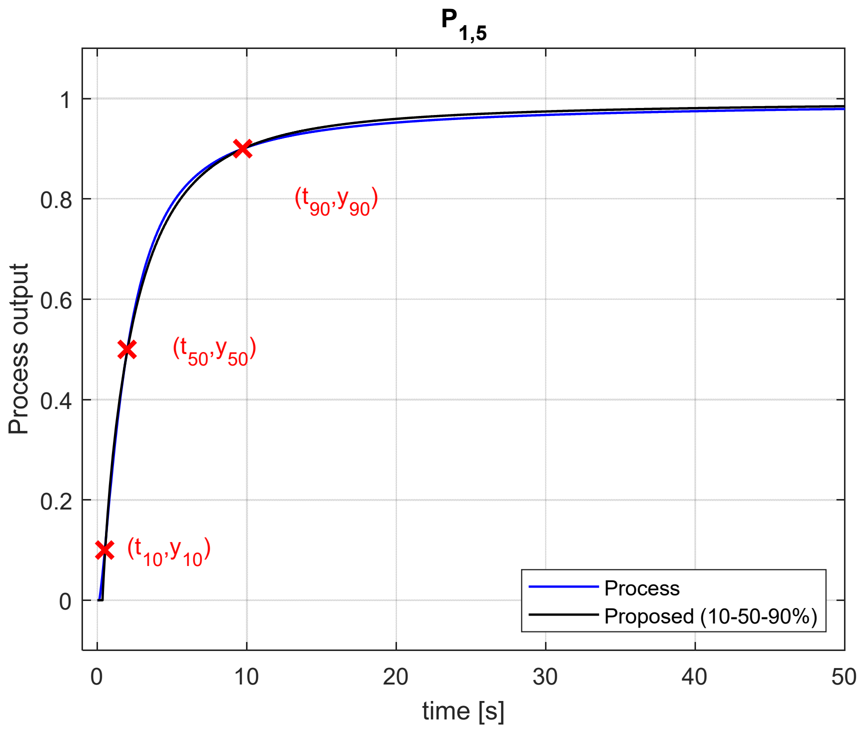

Figure 5.12. Process reaction curve and step response of the FFOPDT model obtained using method #6 (10-50-90%) for process $P_{1,5}$.

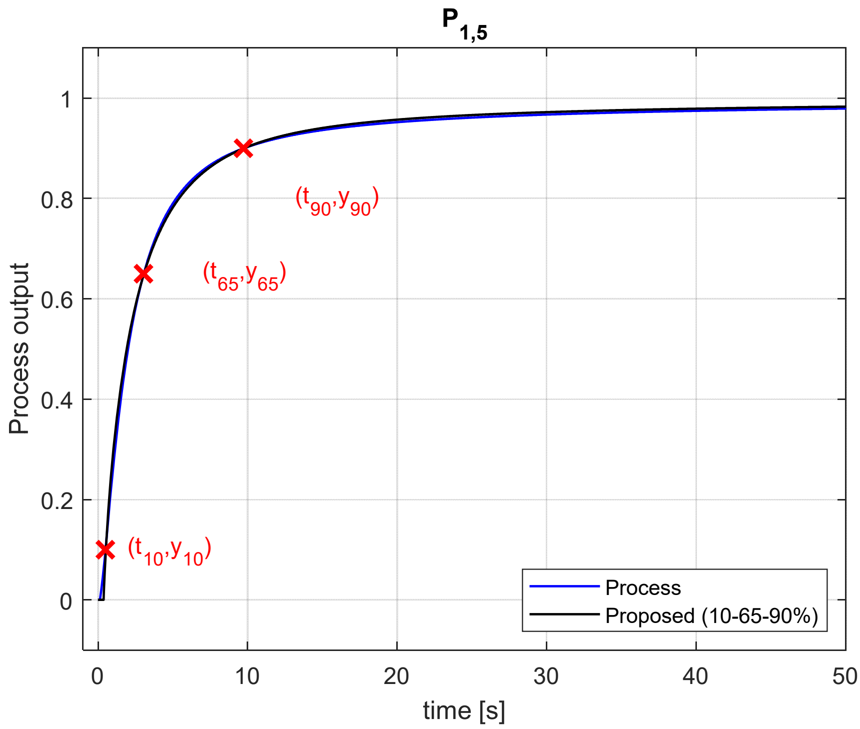

Figure 5.13. Process reaction curve and step response of the FFOPDT model obtained using method #9 (10-65-90%) for process $P_{1,5}$.

In order to evaluate the effect of the location of x_2 on the accuracy of the estimated model, Figure 5.14 illustrates the model performance index values $S(\bar{\theta}_{5,j})$ for the 11 methods (j = 1, …, 11) considering the location of $x_2 \in [25, ..., 75\%]$. In this figure, it can be seen that the minimum value occurs for the case j = 9 ($x_2 = 65\%$).

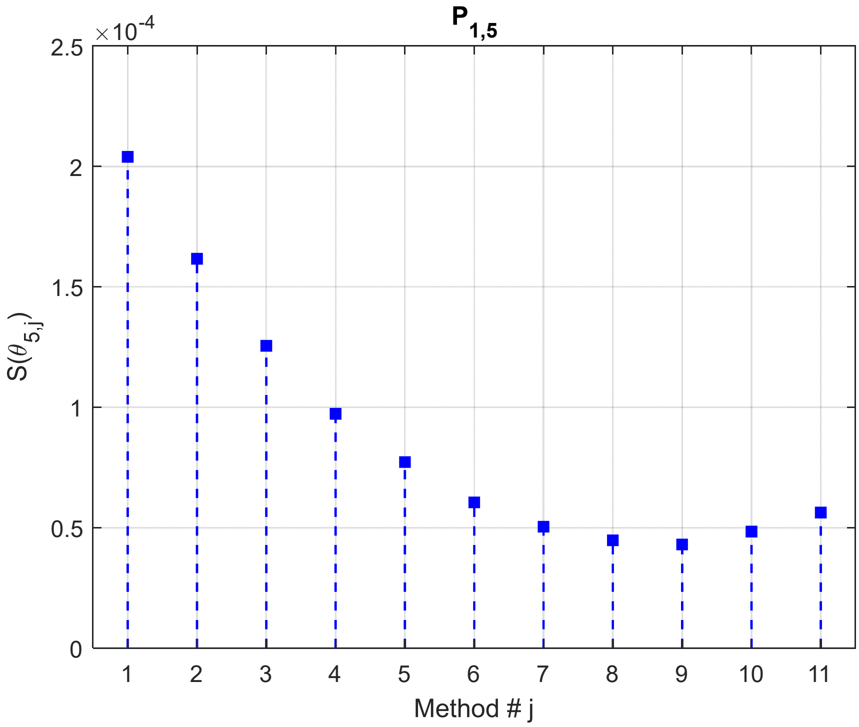

Figure 5.14. Model performance index values $S(\theta_{5,j})$ obtained with methods #1 – 11 for process $P_{1,5}$.

Figure 5.15 illustrates the values of the relative performance index $S_{9,j}(\bar{\theta}_{5,9}, \bar{\theta}_{5,j}) = S(\bar{\theta}_{5,9})/S(\bar{\theta}_{5,j})$ for the different locations of x_2 ($j=1, ...,11$) corresponding to the sets of points considered in Table 5.5. With this figure, it is possible to quantify the benefit when using a value of $x_2 = 65\%$ ($j = 9$) in the set of points when using the considered identification method with respect to the rest of possible locations of x_2 ($j = 1, ... 11$). On the one hand, for $x_2 < 65\%$ the benefit of using $x_2 = 65\%$ increases progressively up to 80% if compared to $x_2 = 25\%$. On the other hand, for $x_2 > 65\%$ the benefit of using $x_2 = 65\%$ also increases to almost 25% if compared to $x_2 = 75\%$.

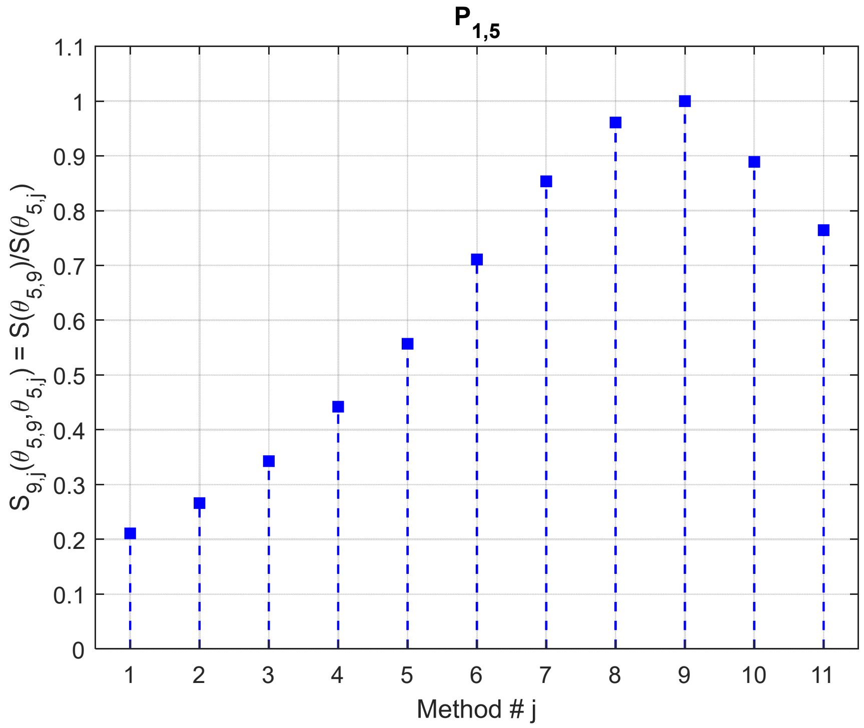

Figure 5.15. Relative performance index-based comparison between results obtained with methods #1 – 11 and the one obtained with method #9 for process $P_{1,5}$.

It is well known that fractional-order model identification methods provide better results in terms of accuracy than integer-order methods. In this regard, it has been demonstrated in Chapter 4 that the FFOPDT model obtained using the identification method for the set of points (10-50-90%) for this same example outperforms those obtained for well-recognized integer-order models. Since the FFOPDT model obtained for $x_2 = 65\%$ is more accurate than the one obtained for $x_2 = 50\%$, the aforementioned results obtained in Chapter 4 are also applicable to this case.

5.4.2. Example 2

In this example, the following lag-dominated higher-order fractional-order process model is selected:

$$P_2(s) = \frac{K_2}{(1 + T_2 s^{\lambda_2})^n} \tag{5.8}$$

where $K_2 = 2$, $T_2 = 1$ s, $n = 5$, and $\lambda_2 = 0.85$.

This model has been proposed in (Tavakoli-Kakhki, Haeri and Tavazoei 2010) and has been used in Chapter 4 as an illustrative example for verifying the effectiveness of this FFOPDT identification method for symmetrical set of points (x-50-(100–x)%). In this example, the FFOPDT model obtained by using the proposed identification method for $x_2 = 65\%$ is compared with the one obtained for $x_2 = 50\%$ and with other fractional-order models obtained with a well-recognized identification method.

Figure 5.16 shows the result of an open-loop step-input test applied to process P_2. From these data, the process information required for the identification of the FFOPDT models for sets of points (10-50-90%) and (10-65-90%), respectively, are summarized in Table 5.8.

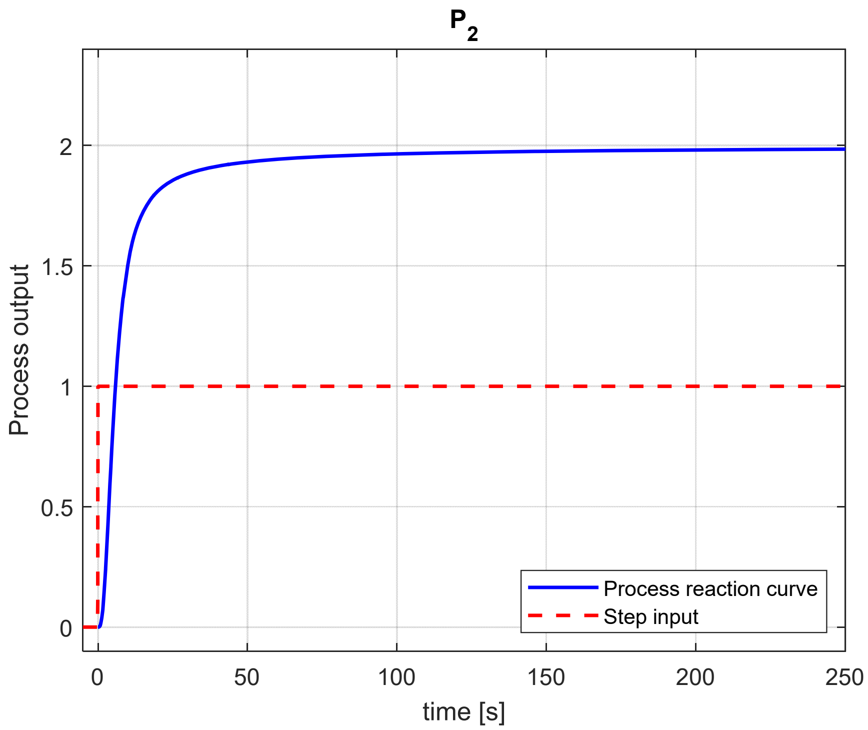

Figure 5.16. Step-input signal and process reaction curve for process P_2.

Method #6: FFOPDT (10-50-90%)	Method #9: FFOPDT (10-65-90%)
$\Delta u = 1.00$	
$\Delta y = 2.00$	
$t_{10} = 2.3450$ s	
$t_{50} = 5.8450$ s	$t_{65} = 7.8050$ s
$t_{90} = 19.2050$ s	

Table 5.8. Process information required for fractional-order model identification of process P_2.

Table 5.9 shows the FFOPDT model parameters $\bar{\theta}_{2,j} = \{K_{2,j}, T_{2,j}, L_{2,j}, \alpha_{2,j}\}$ for methods j = 6 ($x_2 = 50\%$) and j = 9 ($x_2 = 65\%$). At the same time, Table 5.10 shows the parameters of the approximated FFOPDT models according to the three strategies proposed by Tavakoli-Kakhki in (Tavakoli-Kakhki, Haeri and Tavazoei 2010), where their fractional-order model parameters $\bar{\theta}_{2,j}$ for j = 12, 13, 14, correspond to methods #12 – 14.

Method #6: FFOPDT (10-50-90%)	Method #9: FFOPDT (10-65-90%)
$K_{2,6} = 2.00$	$K_{2,9} = 2.00$
$T_{2,6} = 5.0713$ s	$T_{2,9} = 4.3409$ s
$L_{2,6} = 1.8860$ s	$L_{2,9} = 1.9975$ s
$\alpha_{2,6} = 0.9119$	$\alpha_{2,9} = 0.8798$

Table 5.9. FFOPDT model parameters obtained for process P_2 with the considered identification method and sets of points (10-50-90%) and (10-65-90%), respectively.

Method #12: FFOPDT Tavakoli-Kakhki (Strategy 1)	Method #13: FFOPDT Tavakoli-Kakhki (Strategy 2)	Method #14: FFOPDT Tavakoli-Kakhki (Strategy 3)
$K_{2,12} = 2.00$	$K_{2,13} = 2.00$	$K_{2,14} = 2.00$
$T_{2,12} = 5.00$ s	$T_{2,13} = 5.00$ s	$T_{2,14} = 4.48$ s
$L_{2,12} = 1.50$ s	$L_{2,13} = 0.69$ s	$L_{2,14} = 1.50$ s
$\alpha_{2,12} = 0.85$	$\alpha_{2,13} = 0.85$	$\alpha_{2,14} = 0.85$

Table 5.10. FFOPDT model parameters for the different strategies proposed by Tavakoli-Kakhki in (Tavakoli-Kakhki, Haeri and Tavazoei 2010).

The corresponding step responses of the approximated models that have been considered for methods #6 ($x_2 = 50\%$), #9 ($x_2 = 65\%$), and those proposed by Tavakoli-Kakhki (methods #12 – 14) have been compared with the process reaction curve and have been illustrated in Figures 5.17 – 5.21, respectively.

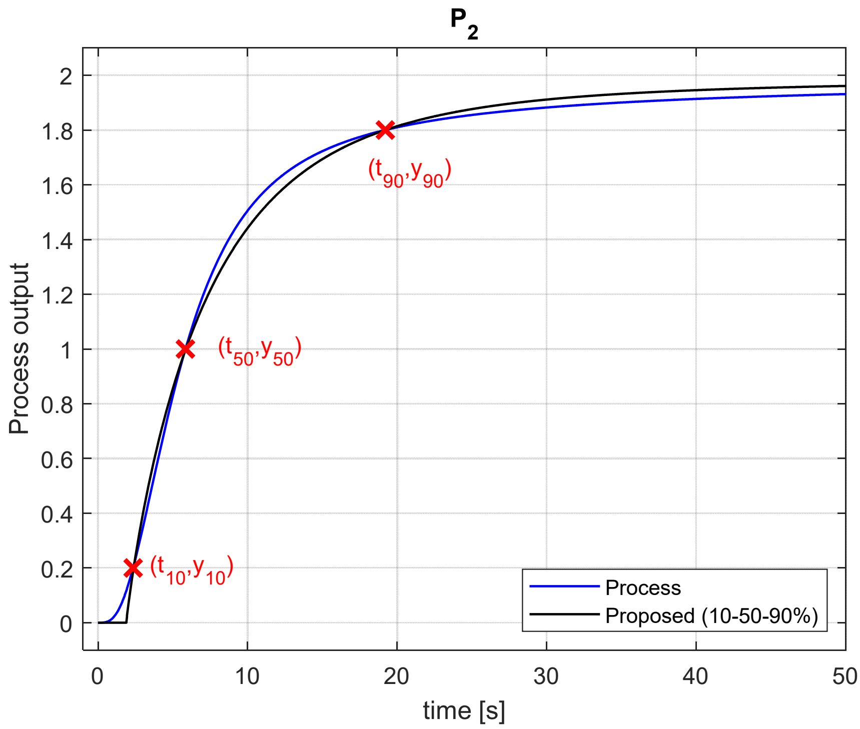

Figure 5.17. Process reaction curve and step response of the FFOPDT model obtained using method #6 (10-50-90%) for process P_2.

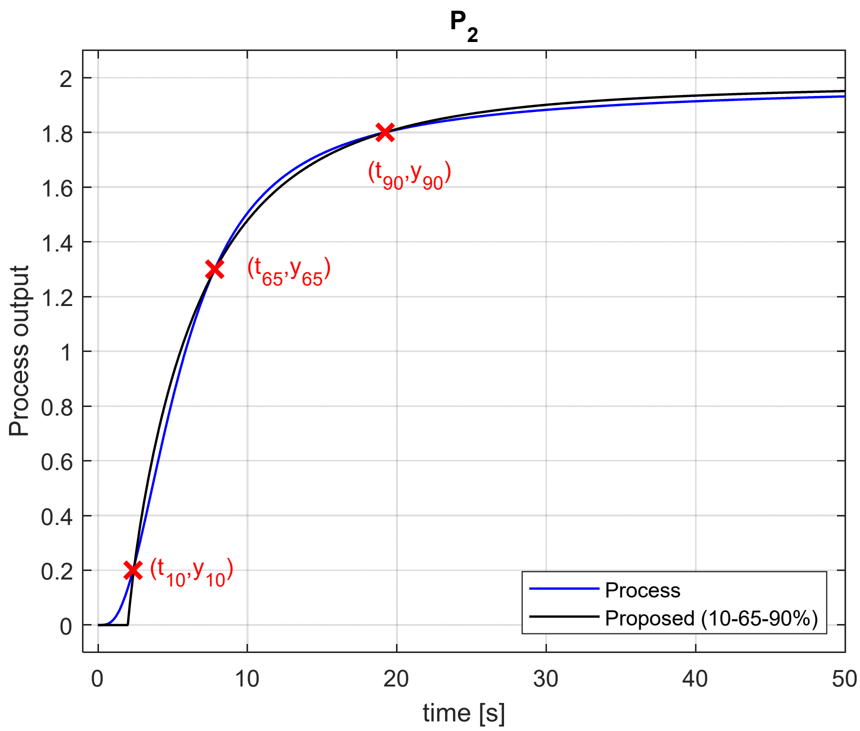

Figure 5.18. Process reaction curve and step response of the FFOPDT model obtained using method #9 (10-65-90%) for process P_2.

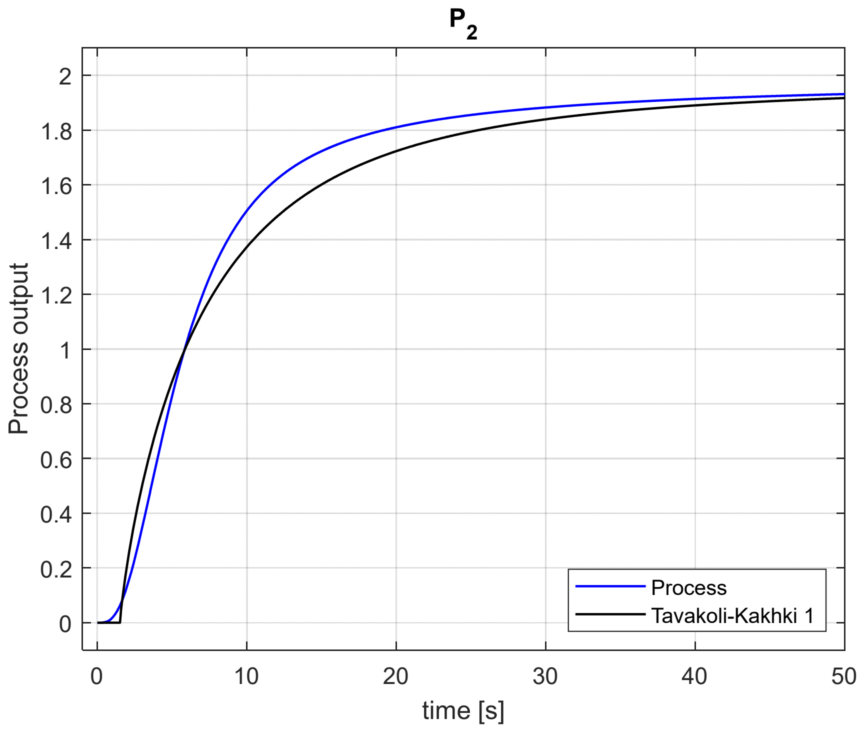

Figure 5.19. Process reaction curve and step response of the FFOPDT model obtained using the identification method (strategy 1) proposed by Tavakoli-Kakhki in (Tavakoli-Kakhki, Haeri and Tavazoei 2010) for process P_2.

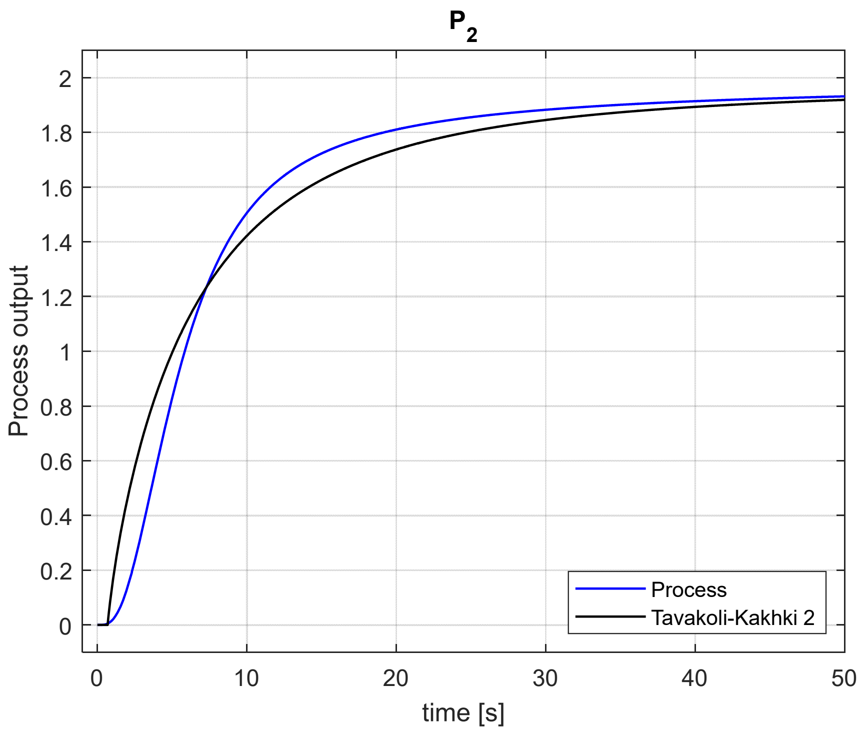

Figure 5.20. Process reaction curve and step response of the FFOPDT model obtained using the identification method (strategy 2) proposed by Tavakoli-Kakhki in (Tavakoli-Kakhki, Haeri and Tavazoei 2010) for process P_2.

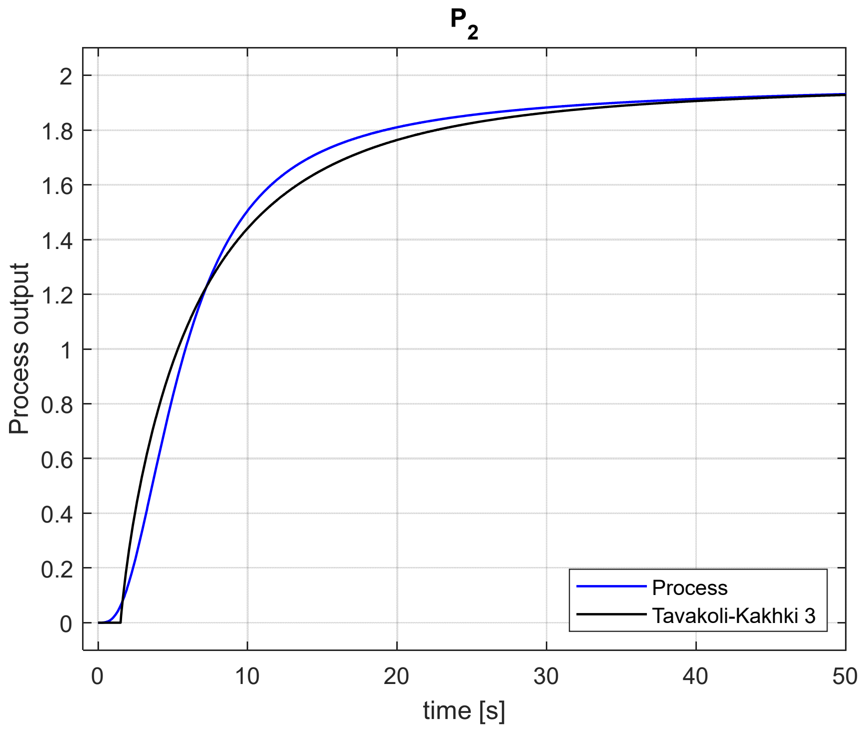

Figure 5.21. Process reaction curve and step response of the FFOPDT model obtained using the identification method (strategy 3) proposed by Tavakoli-Kakhki in (Tavakoli-Kakhki, Haeri and Tavazoei 2010) for process P_2.

In order to evaluate the accuracy of the different FFOPDT models obtained, the time-domain model performance index values $S(\bar{\theta}_{2,j})$ for the models obtained with the considered identification methods ($j = 1, \ldots, 14$) applied to the process P_2 are shown in Table 5.11.

j	Identification method	x_2	Set of points	Model	$S(\theta_{2,j})$
1	Method #1	25%	(10-25-90%)	FFOPDT	$1.50 \cdot 10^{-3}$
2	Method #2	30%	(10-30-90%)	FFOPDT	$1.10 \cdot 10^{-3}$
3	Method #3	35%	(10-35-90%)	FFOPDT	$9.01 \cdot 10^{-4}$
4	Method #4	40%	(10-40-90%)	FFOPDT	$7.09 \cdot 10^{-4}$
5	Method #5	45%	(10-45-90%)	FFOPDT	$5.56 \cdot 10^{-4}$
6	Method #6	50%	(10-50-90%)	FFOPDT	$4.49 \cdot 10^{-4}$
7	Method #7	55%	(10-55-90%)	FFOPDT	$3.66 \cdot 10^{-4}$
8	Method #8	60%	(10-60-90%)	FFOPDT	$3.13 \cdot 10^{-4}$
9	Method #9	65%	(10-65-90%)	FFOPDT	$2.86 \cdot 10^{-4}$
10	Method #10	70%	(10-70-90%)	FFOPDT	$2.89 \cdot 10^{-4}$
11	Method #11	75%	(10-75-90%)	FFOPDT	$3.22 \cdot 10^{-4}$
12	Tavakoli-Kakhki 1	–	–	FFOPDT	$1.10 \cdot 10^{-3}$
13	Tavakoli-Kakhki 2	–	–	FFOPDT	$1.90 \cdot 10^{-3}$
14	Tavakoli-Kakhki 3	–	–	FFOPDT	$6.56 \cdot 10^{-4}$
Number of samples					$N_S = 25001$

Table 5.11. Time-domain model performance indices $S(\theta_{2,j})$ for the models obtained with the considered identification methods ($j = 1, \ldots, 14$) applied to process P_2.

In the same context, the values of the relative performance index $S_{9,j}(\bar{\theta}_{2,9}, \bar{\theta}_{2,j})$, which shows the comparison between the models obtained using methods #1 – 14 with the one obtained with method #9 ($x_2 = 65\%$), are listed in Table 5.12. Note that $\bar{\theta}_{2,9}$ is the vector of model parameters obtained using method #9 for process P_2 and $\bar{\theta}_{2,j}$ is the one obtained using method #j, $j = 1, \ldots, 14$, for process P_2. The information in Table 5.12 is illustrated in Figures 5.22 and 5.23 below.

Compared methods	$S_{9,j} = S_9/S_j$
method #9 – method #1	0.1976
method #9 – method #2	0.2499
method #9 – method #3	0.3182
method #9 – method #4	0.4047
method #9 – method #5	0.5156
method #9 – method #6	0.6391
method #9 – method #7	0.7832
method #9 – method #8	0.9176
method #9 – method #9	1.0000
method #9 – method #10	0.9927
method #9 – method #11	0.8910
method #9 – method #12	0.2501
method #9 – method #13	0.1526
method #9 – method #14	0.4369

Table 5.12. Relative performance index-based comparison between some considered fractional-order models for process P_2.

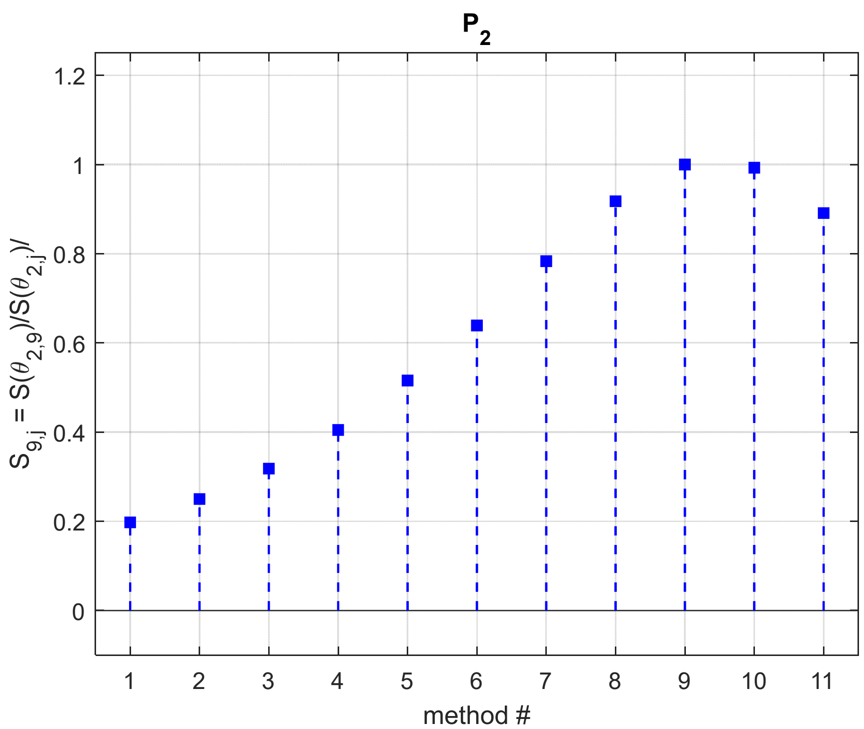

Figure 5.22 Relative performance index-based comparison between results obtained with methods #1 – 11 and the one obtained with method #9 for process P_2.

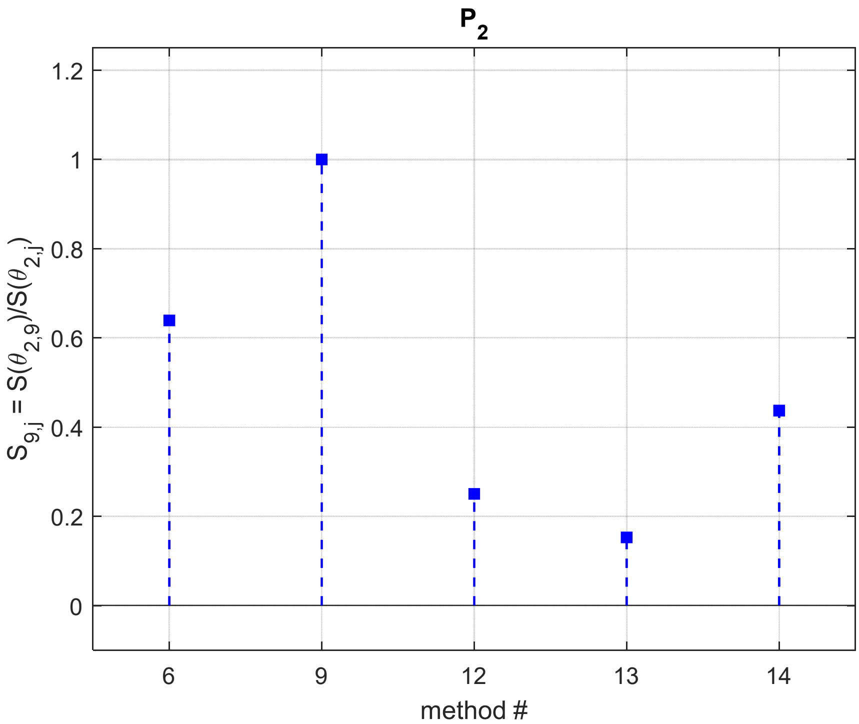

Figure 5.23. Relative performance index-based comparison between results obtained with methods # 6 and #12 – 14 and the one obtained with method #9 for process P_2.

On the one hand, Figure 5.22 illustrates the relative performance index values $S_{9,j}$ for models obtained using methods #1 – 11 ($j = 1, ..., 11$) compared to the one for method #9. The value of S for $x_2 < 65\%$ increases substantially up to 80% for $x_2 = 25\%$. For values of $x_2 > 65\%$, with $x_2 = 70\%$ the value of S is very similar to the one with $x_2 = 65\%$ and increases slightly up to 11% with $x_2 = 75\%$.

On the other hand, Figure 5.23 illustrates the relative performance index values $S_{9,j}$ for models obtained using methods #6, 12, 13, and 14 (j = 6, 12, 13, and 14) compared to the one for method #9. This figure shows that method #9 ($x_2 = 65\%$) reduces by 36% the value of S with respect to method #6 ($x_2 = 50\%$) and reduces by 75, 85, and 57%, respectively, the value of S with respect to models #12 – 14 proposed by Tavakoli-Kakhki.

In summary, this example also shows that moving the central point x_2 of the set of points to a value around 65% provides significant improvement in the accuracy of the estimated model.

5.4.3. Example 3

In this example, a higher-order lag-dominated fractional-order process model is selected:

$$P_3(s) = \frac{K_3}{\prod_{i=1}^{3}(1 + T_i s^{\lambda_3})} \tag{5.9}$$

where $K_3 = 3$, $T_1 = 1$ s, $T_2 = 2$ s, $T_3 = 3$ s, and $\lambda_3 = 0.88$.

This model has been proposed in (Tavakoli-Kakhki, Haeri and Tavazoei 2010) and will be used in Chapter 6 as an illustrative example in order to validate the proposed FFOPDT model identification procedure not only for symmetrical, but also for asymmetrical sets of points.

In this example, the FFOPDT model obtained by using the considered identification method for $x_2 = 65\%$ is compared with the one obtained for $x_2 = 50\%$ and with other integer- and fractional-order models obtained with well-known identification methods characterized for being based on the process reaction curve.

The step signal applied to the considered process P_3 as an open-loop test and the reaction curve obtained for this fractional-order model are depicted in Figure 5.24. Table 5.13 summarizes the process information required for the identification of the FFOPDT models for sets of points (10-50-90%) and (10-65-90%), respectively.

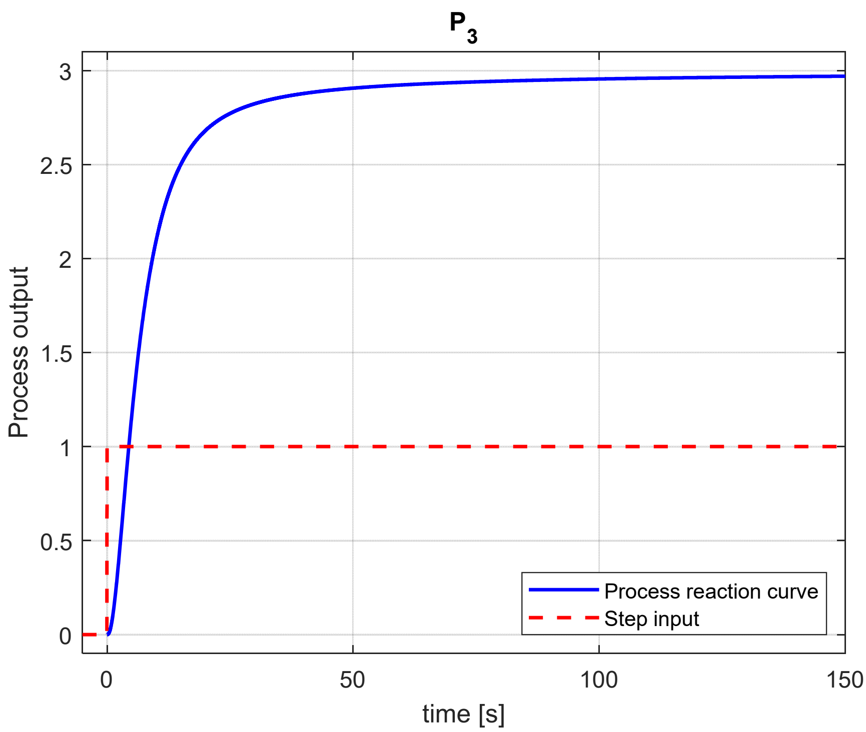

Figure 5.24. Step-input signal and process reaction curve for process P_3.

Method #6: FFOPDT (10-50-90%)	Method #9: FFOPDT (10-65-90%)
$\Delta u = 1.00$	
$\Delta y = 3.00$	
$t_{10} = 2.0290$ s	
$t_{50} = 6.3850$ s	$t_{65} = 8.8640$ s
$t_{90} = 20.8030$ s	

Table 5.13. Process information required for fractional-order model identification of process P_3.

Table 5.14 contains the FFOPDT model parameters $\bar{\theta}_{3,j} = \{K_{3,j}, T_{3,j}, L_{3,j}, \alpha_{3,j}\}$ for methods $j = 6$ ($x_2 = 50\%$) and $j = 9$ ($x_2 = 65\%$). Additionally, process (5.9) has also been approximated using several integer- and fractional-order models. More specifically, it has been approximated using an FFOPDT model obtained with the identification procedure described by Tavakoli-Kakhki in (Tavakoli-Kakhki, Haeri and Tavazoei 2010), using an FFOPDT model determined with the optimization-based procedure described by Guevara et al. in (Guevara, et al. 2015), and using an optimal FOPDT model. The parameters of the models $\bar{\theta}_{3,j}$ for j = 12, 13, 14, which correspond to methods #12 – 14, are shown in Table 5.15.

Method #6: FFOPDT (10-50-90%)	Method #9: FFOPDT (10-65-90%)
$K_{3,6} = 3.00$	$K_{3,9} = 3.00$
$T_{3,6} = 6.6709$ s	$T_{3,9} = 5.9386$ s
$L_{3,6} = 1.3436$ s	$L_{3,9} = 1.4627$ s
$\alpha_{3,6} = 0.9477$	$\alpha_{3,9} = 0.9240$

Table 5.14. FFOPDT model parameters obtained for process P_3 with the considered identification method and sets of points (10-50-90%) and (10-65-90%), respectively.

Method #12: FFOPDT Tavakoli-Kakhki	Method #13: FFOPDT Guevara et al.	Method #14: FOPDT Optimal
$K_{3,12} = 3.00$	$K_{3,13} = 2.00$	$K_{3,14} = 3.00$
$T_{3,12} = 6.30$ s	$T_{3,13} = 5.00$ s	$T_{3,14} = 8.7412$ s
$L_{3,12} = 1.00$ s	$L_{3,13} = 0.69$ s	$L_{3,14} = 0.00$ s
$\alpha_{3,12} = 0.9200$	$\alpha_{3,13} = 0.85$	–

Table 5.15. FFOPDT model parameters obtained for process P_3 with the identification methods proposed by Tavakoli-Kakhki in (Tavakoli-Kakhki, Haeri and Tavazoei 2010), by Guevara et al. in (Guevara, et al. 2015), and the optimal ones obtained for an FOPDT model.

The corresponding step responses of the approximated models considered for methods #6 ($x_2 = 50\%$), #9 ($x_2 = 65\%$) and the process reaction curve are illustrated in Figures 5.25 and 5.26, respectively. The corresponding symmetrical representative points, (x-x_2-($100-x$)%), are also included in these figures.

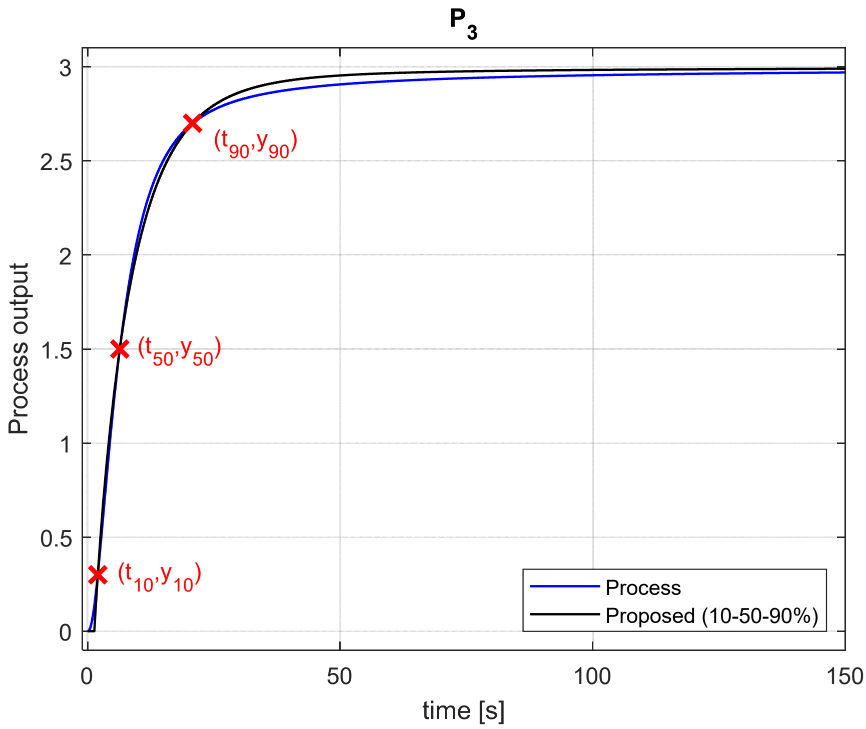

Figure 5.25. Process reaction curve and step response of the FFOPDT model obtained using method #6 (10-50-90%) for process P_3.

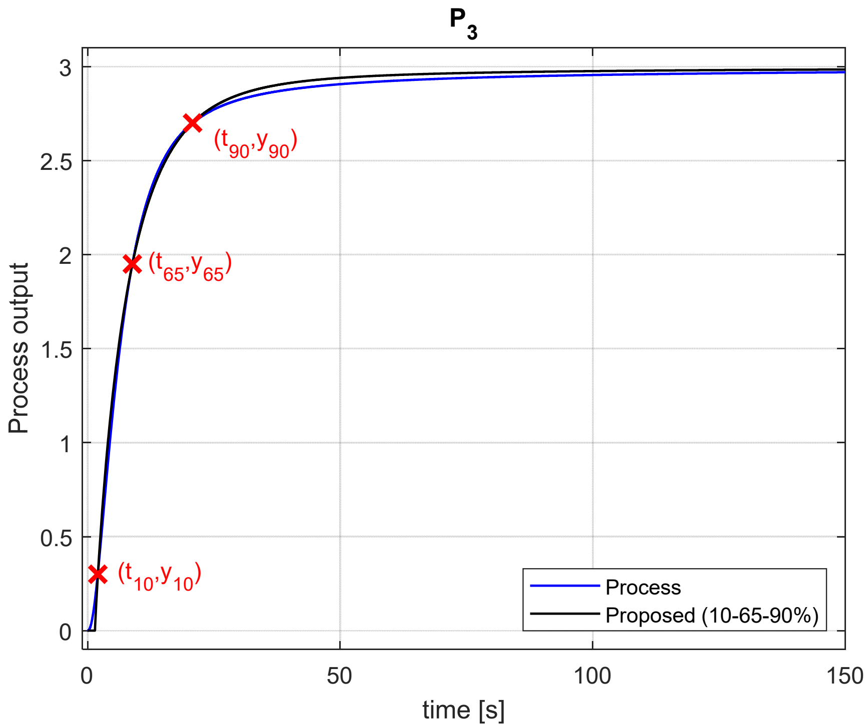

Figure 5.26. Process reaction curve and step response of the FFOPDT model obtained using method #9 (10-65-90%) for process P_3.

In addition, the step responses of the FFOPDT model using the method #12, the one obtained using the method #13, and the optimal FOPDT model (method #14) are compared with the process reaction curve, respectively, in Figures 5.27 – 5.29.

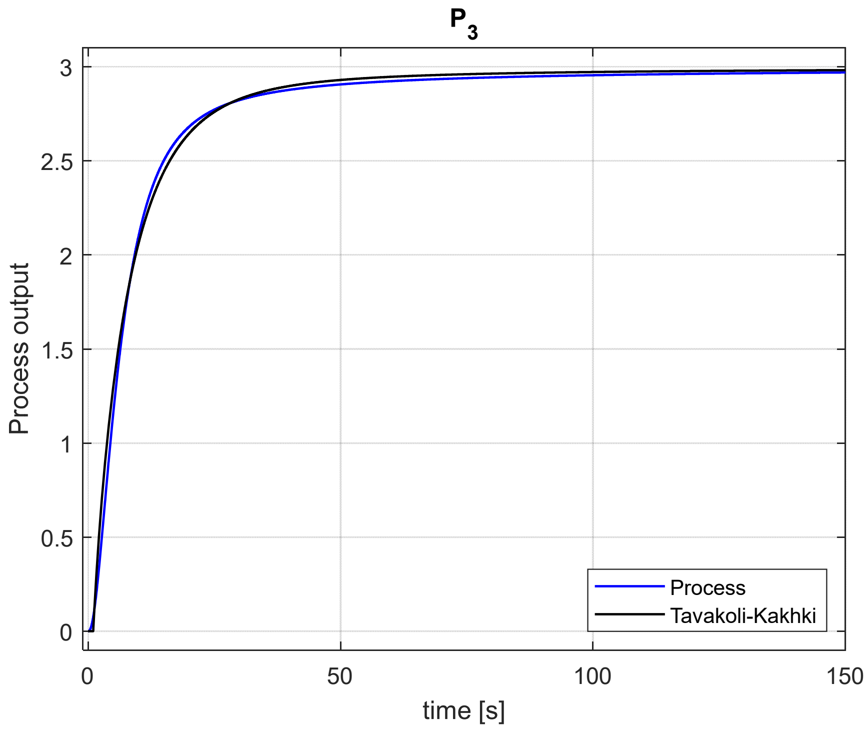

Figure 5.27. Process reaction curve and step response of the FFOPDT model obtained using the identification method proposed by Tavakoli-Kakhki in (Tavakoli-Kakhki, Haeri and Tavazoei 2010) for process P_3.

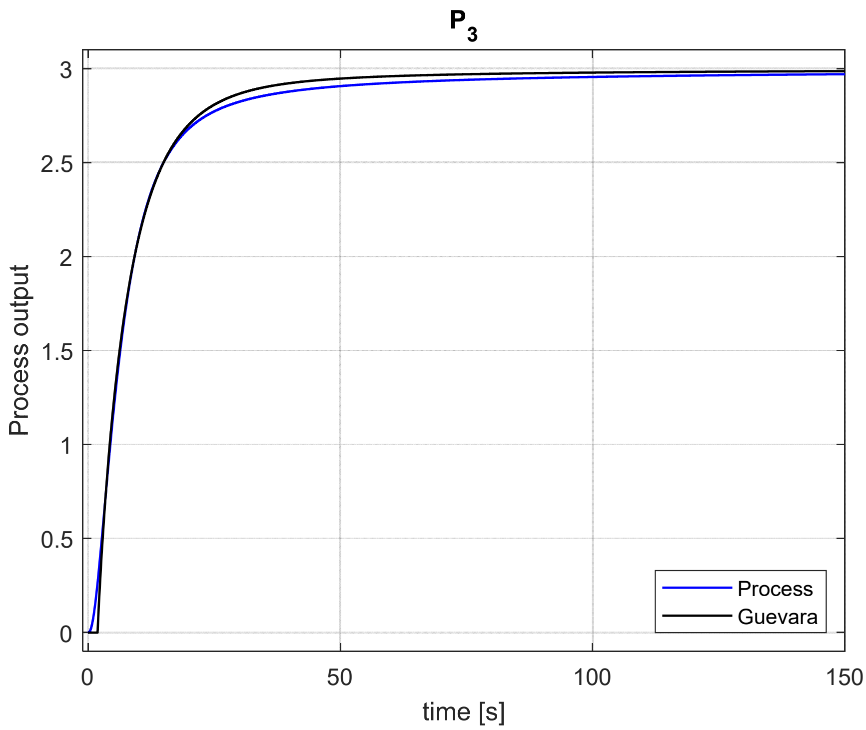

Figure 5.28. Process reaction curve and step response of the FFOPDT model obtained using the identification method proposed by Guevara et al. in (Guevara, et al. 2015) for process P_3.

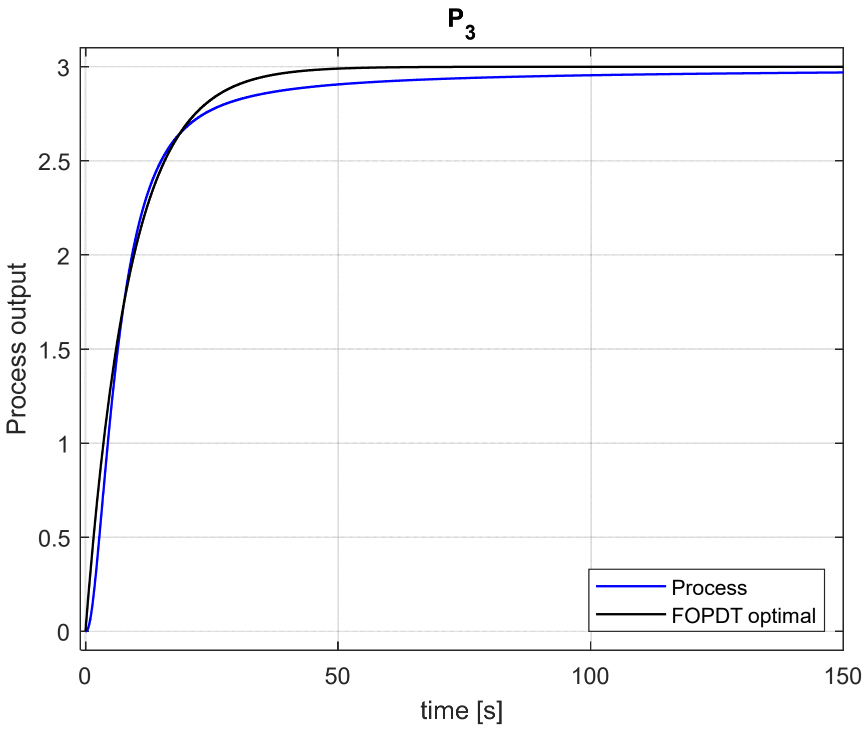

Figure 5.29. Process reaction curve and step response of the optimal FOPDT model for process P_3.

In order to evaluate the accuracy of the different models that have been obtained, Table 5.16 illustrates the time-domain model performance index values $S(\overline{\theta}_{3,j})$ for the models obtained with the considered identification methods ($j = 1, \ldots, 14$) applied to the considered process P_3.

j	Identification method	x_2	Set of points	Model	$S(\theta_{3,j})$
1	Method #1	25%	(10-25-90%)	FFOPDT	$3.80 \cdot 10^{-3}$
2	Method #2	30%	(10-30-90%)	FFOPDT	$3.00 \cdot 10^{-3}$
3	Method #3	35%	(10-35-90%)	FFOPDT	$2.40 \cdot 10^{-3}$
4	Method #4	40%	(10-40-90%)	FFOPDT	$2.00 \cdot 10^{-3}$
5	Method #5	45%	(10-45-90%)	FFOPDT	$1.60 \cdot 10^{-3}$
6	Method #6	50%	(10-50-90%)	FFOPDT	$1.30 \cdot 10^{-3}$
7	Method #7	55%	(10-55-90%)	FFOPDT	$1.10 \cdot 10^{-3}$
8	Method #8	60%	(10-60-90%)	FFOPDT	$9.55 \cdot 10^{-4}$
9	Method #9	65%	(10-65-90%)	FFOPDT	$8.65 \cdot 10^{-4}$
10	Method #10	70%	(10-70-90%)	FFOPDT	$8.44 \cdot 10^{-4}$
11	Method #11	75%	(10-75-90%)	FFOPDT	$8.68 \cdot 10^{-4}$
12	Tavakoli-Kakhki	–	–	FFOPDT	$1.40 \cdot 10^{-3}$
13	Guevara	–	–	FFOPDT	$1.10 \cdot 10^{-3}$
14	Optimal	–	–	FOPDT	$5.30 \cdot 10^{-3}$
	Number of samples				$N_S = 15001$

Table 5.16. Time-domain model performance indices $S(\theta_{3,j})$ for the models obtained with the considered identification methods ($j = 1, \ldots, 14$) applied to process P_3.

Figure 5.30 demonstrates that the accuracy of the estimated FFOPDT model can be significantly improved by increasing x_2 around to $x_2 = 65\%$. Beyond that value there is no additional benefit in increasing x_2.

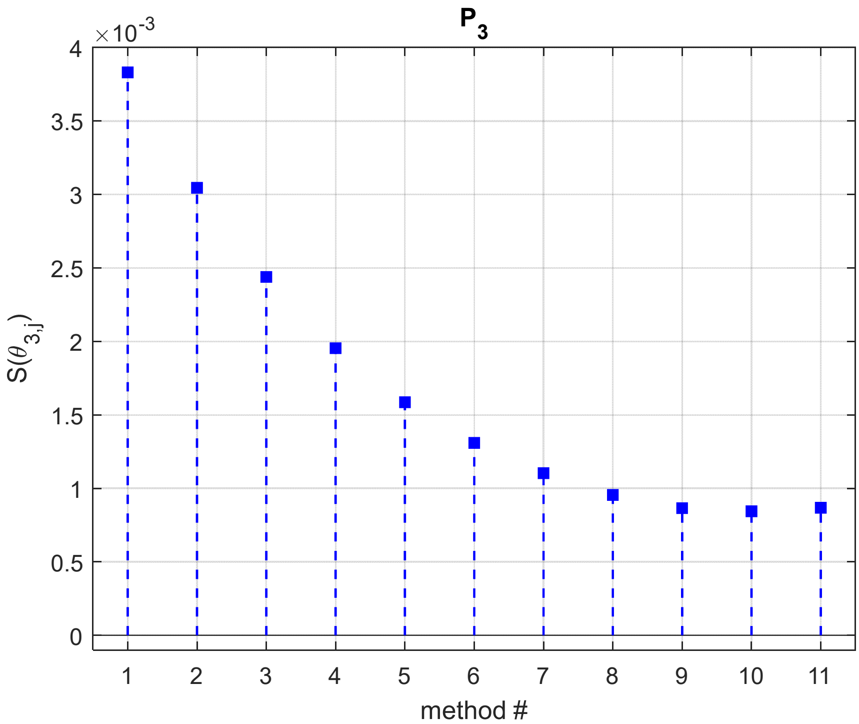

Figure 5.30. Model performance index values $S(\theta_{3,j})$ obtained with methods #1 – 11 for process P_3.

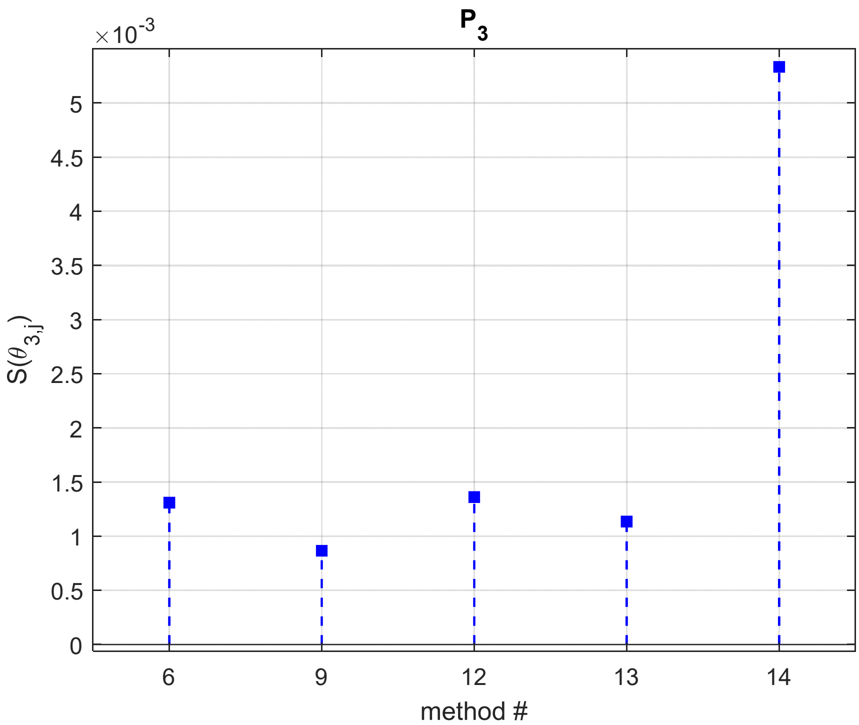

Figure 5.31. Model performance index values $S(\theta_{3,j})$ obtained with methods #6, 9, and 12 – 14 for process P_3.

A comparison in terms of the model performance index $S(\bar{\theta}_{3,j})$ between methods #6, 9, 12, 13, and 14 ($j = 6, 9, 12, 13, 14$) is shown in Figure 5.31. On the one hand, method #14 has been included to show that even the optimal FOPDT model gives significantly worse results than an FFOPDT model. On the other hand, it can be seen that method #9 ($x_2 = 65\%$) gives better results than the other methods, even than methods #13 and 14, which are based on optimization.

In the same context, the values of the relative performance index $S_{9,j}(\bar{\theta}_{3,9}, \bar{\theta}_{3,j})$, which shows the comparison between the performance index for the models obtained using methods #1 – 14 with the one obtained for method #9 ($x_2 = 65\%$), are listed in Table 5.17. Note that $\bar{\theta}_{3,9}$ is the vector of model parameters obtained using method #9 for process P_3 and $\bar{\theta}_{3,j}$ is the one obtained using method #j, j = 1, ..., 14, for process P_3. The information in Table 5.17 is illustrated in Figures 5.32 and 5.33 below.

Compared methods	$S_{9,j} = S_9/S_j$
method #9 – method #1	0.2259
method #9 – method #2	0.2842
method #9 – method #3	0.3549
method #9 – method #4	0.4430
method #9 – method #5	0.5457
method #9 – method #6	0.6609
method #9 – method #7	0.7844
method #9 – method #8	0.9058
method #9 – method #9	1.0000
method #9 – method #10	1.0257
method #9 – method #11	0.9971
method #9 – method #12	0.6359
method #9 – method #13	0.7623
method #9 – method #14	0.1623

Table 5.17. Relative performance index-based comparison between some considered fractional-order models for process P_3.

On the one hand, Figure 5.32 illustrates the relative performance index values $S_{9,j}$ for methods #1 – 11 ($j = 1, ..., 11$) compared to method #9. The value of S for $x_2 < 65\%$ increases substantially nearly up to 80% for $x_2 = 25\%$. The model accuracy in terms of S for $x_2 \geq 65\%$ is very similar. There is no apparent benefit in increasing x_2 above this value.

On the other hand, Figure 5.33 illustrates the relative performance index values $S_{9,j}$ for methods #6, 12, 13, and 14 ($j = 6, 12, 13$, and 14) compared to method #9. This figure shows that method #9 ($x_2 = 65\%$) reduces by 34% the value of S with respect to method #6 ($x_2 = 50\%$) and reduces by 36, 24, and 84%, respectively, the value of S with respect to models #12 – 14.

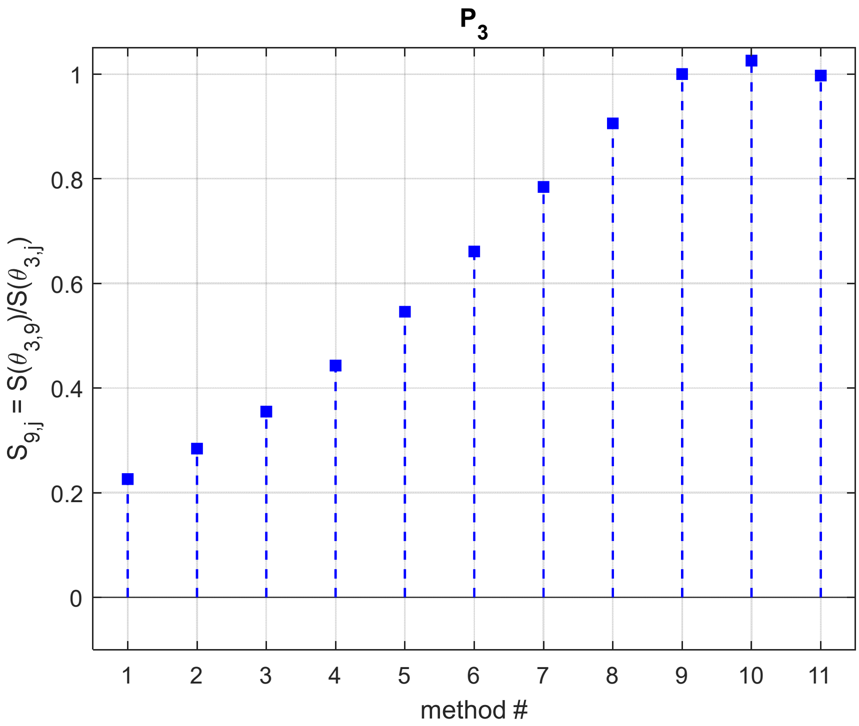

Figure 5.32. Relative performance index-based comparison between results obtained with methods #1 – 11 and the one obtained with method #9 for process P_3.

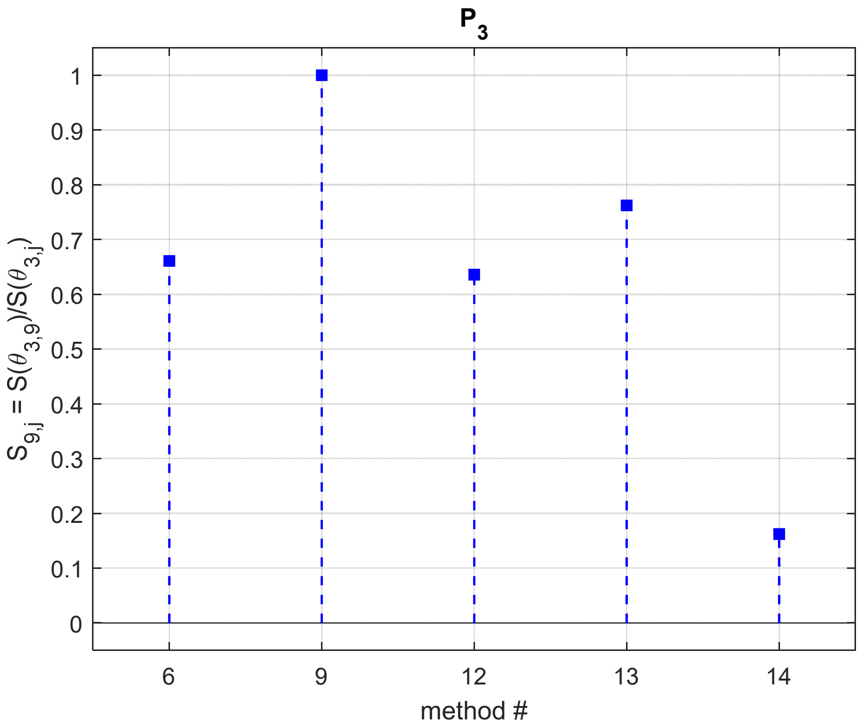

Figure 5.33. Relative performance index-based comparison between results obtained with methods #6 and #12 – 14 and the one obtained with method #9 for process P_3.

As a summary, this example also demonstrates that moving the central point x_2 of the set of points on the reaction curve to a value around 65% provides a significant improvement in the accuracy of the estimated fractional-order model.

5.4.4. Algorithm for determining FFOPDT model parameters

In the same way as in Chapter 4, there is a significant interest that the fractional-order model identification procedure can be implemented on a hardware platform. Therefore, the development of an algorithm is intended to facilitate software implementation of the identification method proposed in this chapter.

In this method, the variation in input signal Δu and process output Δy, and times necessary to reach $x\%$ (t_x), $x_2\%$ (t_{x2}), and $(100–x)\%$ ($t_{100–x}$) of the total change of the process output on the reaction curve must be collected in order to determine FFOPDT model parameters $\theta_P = \{K, T, L, \alpha\}$.

Chapter 8 will present the corresponding algorithm and show the results of applying the algorithm, when implemented on a microprocessor-based hardware, to an experimental temperature setup.

5.4.5. Discussion

In this section, several fractional-order process models have been selected in order to demonstrate the effectiveness of the considered identification method in estimating an approximated fractional-order model (3.21) and to gain insight into the effect of moving the central point x_2 of the set of representative points $(x\text{-}x_2\text{-}(100–x)\%)$ on the accuracy of the estimated FFOPDT model.

Note that this work is restricted to the identification of processes exhibiting fractional behaviour, characterized by a monotonic S-shaped response and with an order in the range $0.50 \leq \alpha \leq 1.00$. Such processes with essentially monotonic step responses are very common in the area of process control (Åström and Hägglund 2006).

In the framework of identification procedures that are based on the process reaction curve, it is well-known in the academic community that the accuracy of the identified model is sensitive to the position of the representative points on the process reaction curve (Huang and Jeng 2005). However, in the case of classical integer-order model identification methods, the selection of these points is somewhat arbitrary: in some cases, no explanation is given for the selection (Vitecková, Vitecek and Smutny 2000); in others, significant points closely related to the model parameters are selected (Smith 1972). In some other methods, see, e.g., (Alfaro 2006), these points have been carefully chosen to optimize the identified model parameters. In contrast to the above, in the case of fractional-order identification methods, such influence of the representative points will be verified in Chapter 6 for both asymmetrical and symmetrical sets of points, and in Chapter 4 and in (Gude and García Bringas 2022) for the symmetrical ones.

In this work, only the symmetrical case that has been presented in Chapter 4 is considered. In the context of the symmetry considerations of the identification procedure, it is important to note that the set of representative points (x_1-x_2-x_3%) on the process reaction curve are selected with the requirement of selecting the optimal location of one of the extreme points, $x_1 = x\%$, since the other is immediately determined by the symmetry requirement, $x_3 = (100–x)\%$, with respect to the centre of the output range. Being, therefore, the location of the central point x_2 the object of study in this paper. In this regard, the process reaction curve is well fitted by the step response of FFOPDT models estimated using the identification procedure for symmetrical sets of points, especially in the interval [x - (100–x)], as discussed in Chapter 4. It is worth noting that the smaller value of x, the wider the interval [x - (100–x)] and, hence, will better fit the process reaction curve, resulting in a lower value in the model performance index S.

One of the main results of this chapter is to verify that the accuracy of the identified FFOPDT model is sensitive to the location of the set of representative points and that a significant improvement on the accuracy of the identified fractional-order model can be obtained by moving the central point x_2 to another location different from $x_2 = 50\%$, while keeping the extreme points $x_1 = x\%$ and $x_3 = (100–x)\%$. More specifically, the author has verified that the behaviour described in Section 5.4 in which the accuracy of the identified model exhibits a minimum value for $x_2 > 50$ and around 65% is common to several fractional-order dynamics in the considered order range $0.50 \leq \alpha \leq 1.00$.

To conclude, it has already been proven in Chapter 4 that good results have been obtained using the considered FFOPDT model identification procedure for symmetrical set of points compared to other integer- and fractional-order model identification methods.

In this section, it has been shown using several fractional-order process models that a significant improvement in the accuracy of the estimated model can be obtained by setting the value $x_2 = 65\%$. Thus, the effectiveness of the identification procedure is improved while maintaining its main features:

1. It is an analytical method, which simplifies considerably its implementation on a hardware device, as will be presented in Chapter 8.
2. Simplicity. This feature is mainly due to the fact that identification methods based on fitting various points on the process reaction curve have a straightforward physical interpretation and are typically easy to implement and apply.
3. Effectiveness. This identification method is very effective, as discussed above, increasing even more the accuracy of the identified model.

In addition, other important aspects that are not covered in this chapter are measurement noise and model uncertainty. The author refers the reader to Chapter 6, where these aspects will be discussed in detail in the context of the considered identification procedure.

Furthermore, the practical implementation on a microprocessor-based hardware device of the FFOPDT model identification procedures presented in this dissertation will be discussed in detail in Chapter 8.

Therefore, the verification of the results obtained in this chapter using a temperature-based experimental prototype and implementing the identification algorithm on a hardware platform will be performed later in the dissertation.

5.5. Conclusions

This chapter deals with a FFOPDT model identification procedure based on the location of three symmetrical points (x-x_2-$(100–x)\%$) on the process reaction curve. More specifically, the possibility of improving the accuracy of the fractional-order model by modifying the location of the central point x_2 has been explored, while maintaining the symmetry of the extreme points with respect to the centre of the total range.

The results of this work confirm that the accuracy of the estimated FFOPDT model is sensitive to the position of the central point within the symmetrical set of points of the process reaction curve. It has also been demonstrated how a more accurate identified model can be obtained, verifying that increasing the x_2 around 65% can significantly improve the accuracy of the identified model in the context of the considered identification procedure. New insights have also been offered on this selection of the central point x_2.

Several simulation examples have been utilized to demonstrate the applicability and effectiveness of this method for identifying FFOPDT models and to gain insight into the influence of the location of central point x_2 on the accuracy of the identified fractional-order model.

The results obtained in this chapter will also be applied to a temperature-based experimental prototype to confirm its validity and applicability when the identification algorithm is implemented on a microprocessor-based control hardware. The author refers the reader to Chapter 8 for this purpose.

With respect to the applicability of the considered identification procedure in an industrial framework, it is important to highlight that this identification method is analytical, which requires less computational effort in comparison to more complicated identification algorithms usually based on optimization. In the industrial context, large process industries are generally composed of hundreds or thousands of control loops. Therefore, the simplicity offered by methods such as the one used in this chapter is of major interest when identifying a process model for control purposes.

In the author's opinion, identification methods that provide an emphasis on simplicity will help to bridge the existing gap between theoretical studies about fractional-order models and their practical application at the industrial level, encouraging their use in the process industry. This expectation is one of the main motivations for the present work.

Seldom is asymmetry merely the absence of symmetry…

Hermann Weyl (1885 – †1955)
Symmetry

CHAPTER

6

Fractional-order model identification method: the asymmetrical case

CHAPTER 4 has presented a general identification procedure for FFOPDT models based on fitting three points on the process reaction curve. The aim of the present chapter is to validate this general identification procedure by considering both symmetrical and asymmetrical sets of points on the process reaction curve. Some numerical examples are provided to show the straightforwardness and effectiveness of the proposed procedure. Good results have been obtained in comparison with other well-known identification methods, especially when simplicity is emphasized. A discussion is also provided about the effect of the location of the three points on the accuracy of the identified fractional-order model. Finally, some comments and reflections on practical issues related to industrial practice are given.

6.1. Introduction

The academic and industrial community recognizes that PID controller is the most widely used option in the process industry, having become an industry standard for process control (Åström and Hägglund 2006). Although the most commonly used models for tuning PID controllers are the FOPDT, DPPDT, and SOPDT ones, they are not able to represent the process dynamics with the required accuracy in some cases, as suggested, e.g., in (Åström and Hägglund 2004).

Due to this, increasing the robustness of the control system can introduce issues in the well-known robustness/performance trade-off, constraining the desired performance (Garpinger, Hägglund and Åström 2014). Therefore, obtaining more accurate models of the controlled process is expected to improve performance.

In the technical literature, there are a wide variety of identification procedures for integer-order models that are based on an open-loop step-test experiment; see, e.g., the identification methods detailed in (Liu and Gao 2012), (Huang and Jeng 2005), (Ljung 2002), and (Tan, et al. 1999), and the references cited therein. In general, these types of identification procedures are characterized by being performed with very little information about the plant, which makes them ideal for their use in industry. More specifically, some references also described identification algorithms that are based on fitting different points on the reaction curve; see, e.g., (Alfaro 2006), (Rangaiah and Krishnaswamy 1996), and (Huang, Lee and Chen 2001).

Generally, identification methods for integer-order models that are based on the location of two or three points on the process reaction curve use FOPDT, DPPDT, and SOPDT models.

Considering both two-point and three-point methods separately, in the first group, the following methods can be considered (Alfaro 2006), (Ho, Hang and Cao 1995), (Smith 1972), and (Vitecková, Vitecek and Smutny 2000), while in the second group, methods (Jahanmiri and Fallahi 1997), (Mollenkamp 1984), and (Rangaiah and Krishnaswamy 1994) can be examined. The identification method proposed in (Alfaro 2006), which is used as a two-point method for FOPDT and DPPDT models, can also be used as a three-point method for SOPDT models. In a recent paper, the method proposed in (Alfaro 2006) has been also extended for identifying a multiple-pole with dead-time model (Alfaro and Vilanova 2021).

Note that in the case of two-point methods considered above, the sets of points are asymmetrical with respect to the central point on the reaction curve (50%). The only method with a symmetrical set of points is 123c identification method proposed by Alfaro in (Alfaro 2006). For the considered three-point methods, (Jahanmiri and Fallahi 1997) and (Rangaiah and Krishnaswamy 1994) and present asymmetrical sets of points, while (Alfaro 2006) for SOPDT models and (Mollenkamp 1984) provide sets of points that are symmetrical, although for the latter the central point does not match the central value on the reaction curve.

In recent decades, the advent of fractional calculus and new computational techniques have made possible a major academic and industrial effort focused on the transition from classical models and controllers to those described by non-integer order differential equations. Thus, fractional-order dynamic models and controllers were introduced; see, e.g., (Monje, Chen, et al. 2010) and (Tepljakov 2017).

The apparent benefit of fractional calculus in the field of modelling has been justified from an industrial point of view. However, it has been more difficult to convey the advantages of fractional calculus on the controller side because of implementation issues (Tepljakov, Alagoz, et al. 2018). That is why the adoption of fractional-order PID controllers in the industry is currently low, even though these controllers offer clear advantages in comparison with integer-order ones.

In the technical literature there is a wide range of methods for identifying fractional-order models based on the process reaction curve, however, there are not many that are analytical techniques and whose main feature is simplicity of implementation. Some strategies to estimate the FFOPDT model parameters by using step-response data have been proposed in (Tavakoli-Kakhki, Haeri and Tavazoei 2010). It combines numerical computation and graphical estimation. Integral-based estimation methods, whose main feature is their robustness to the presence of measurement noise, are proposed in (Tavakoli-Kakhki and Tavazoei 2014) and (Tavakoli-Kakhki, Tavazoei and Mesbahi 2013).

The most common approach in industrial practice is based on nonlinear optimization; see, e.g., (Guevara, et al. 2015), (Malek, Luo and Chen 2013), (Alagoz, et al. 2019), and (Ahmed 2015). These methods are generally applied by minimizing the error between the fractional-order model step response and the process reaction curve. These techniques are characterized by the fact that they require more computational effort compared to other existing analytical methods.

Despite the fact that the fractional-order model has been demonstrated to be technologically superior on multiple occasions, the industrial adoption of the fractional-order approach requires further analysis (Tepljakov, Alagoz, et al. 2021).

Considering all the above, the existence of identification methods for simple-structure fractional-order models is of major relevance and results to be very helpful in the practical design of integer- and fractional-order control systems.

There are multiple reaction curve-based methods for identifying integer-order models, as discussed previously. This is mainly due to the fact that the step response of a process has a straightforward physical interpretation and that identification methods for integer-order models based on fitting several points of the process reaction curve are very easy to implement and apply. Therefore, one may consider appropriate to extend such methods for fractional-order models. To that end, an FFOPDT model identification method, which is based on fitting three points on the reaction curve, has been conducted in Chapter 4. However, that study has been restricted to considering that the central point is located in the center of the reaction curve (50%), and that the extreme points are located symmetrically with respect to this central point.

It is the author's opinion that it is of significant interest to extend the identification method proposed in Chapter 4 to any set of points on the process reaction curve.

Therefore, the objective of this work is to verify and validate this identification procedure for three asymmetrical points on the reaction curve and to get insight into the selection of such points and their influence on the accuracy of the identified fractional-order model.

This chapter is organized as follows. Section 6.2 summarizes the general identification procedure for FFOPDT models based on three arbitrary points on the process reaction curve. This general method is particularized for several symmetrical and asymmetrical sets of points on the process reaction curve. The results of some numerical simulations are presented in Section 6.3, illustrating the effectiveness and simplicity of the proposed method for both symmetrical and asymmetrical sets of points in comparison to well-known identification methods. This section also provides a discussion about the results obtained and some concluding remarks on the practical issues of the identification procedure that has been presented in this part of the dissertation. Finally, Section 6.4 presents the conclusions of this chapter.

6.2. Materials and methods

An analytical method of identifying the FFOPDT model based on three arbitrary points (x_1-x_2-x_3%) on the process reaction curve has been developed in Chapter 4. This method has also been discussed restricted to the case where the points are symmetrical with respect to the central point.

In Chapter 5, an approach has been employed in which the central point x_2 can be moved along the reaction curve while maintaining the symmetry of the extreme points ($x_1 = x$ and $x_3 = 100–x$) with respect to the central value of the range (50%).

The objective of this chapter is to validate this general identification procedure considering three asymmetrical points on the reaction curve in comparison with the symmetrical case.

Figure 6.1 shows the general scheme of the complete procedure for obtaining the expressions for the identification of the FFOPDT model parameters, $\theta_P = \{K, T, L, \alpha\}$, from three arbitrary points of the process reaction curve.

This procedure is summarized in the following steps, as depicted in Figure 6.1.

1. From the normalized process output (4.3), $\tilde{y}_\alpha(\tau)$, the values of the normalized times $\{\tau_{x1}, \tau_{x2}, \tau_{x3}\}$ of the three considered points on the process reaction curve are obtained for the different values of α, $0.50 \leq \alpha \leq 1.10$.
2. Data sets $\{\Delta, \alpha\}$, $\{\alpha, a^\alpha\}$, and $\{\alpha, (\tau_{x3})^{1/\alpha}\}$ are obtained for the considered set of points (x_1-x_2-x_3%) by using the values of the corresponding normalized times.

Note that this procedure is general and admits the points x_1, x_2, and x_3 to be arbitrary. In this chapter, both a symmetrical and an asymmetrical location of the points on the process reaction curve will be considered.

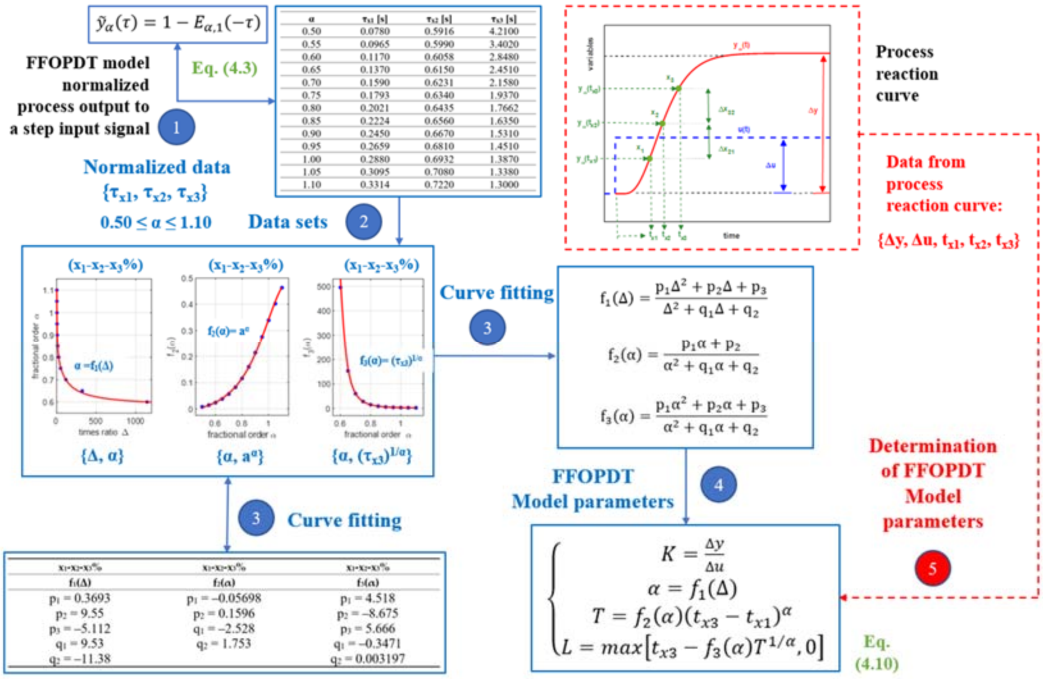

Figure 6.1. Scheme of the complete procedure for identifying the parameters of the fractional-order model considering three arbitrary points on the process reaction curve. Note that the blue part of the scheme represents the general procedure to obtain expressions (4.10) that allow to determine the parameters of the FFOPDT model for any three points (x_1, x_2, and x_3) on the process reaction curve. On the other hand, the red part of the scheme indicates how to estimate the parameters $\theta_P = \{K, T, L, \alpha\}$ from the information collected from the process reaction curve $\{\Delta y, \Delta u, t_{x1}, t_{x2}, t_{x3}\}$.

3. By means of a curve-fitting procedure, the values of the parameters $\{p_i, q_i\}$ for the rational functions $f_1(\Delta)$, $f_2(\alpha)$, and $f_3(\alpha)$, respectively, are obtained.
4. By means of a curve-fitting procedure, the values of the parameters $\{p_i, q_i\}$ for the rational functions $f_1(\Delta)$, $f_2(\alpha)$, and $f_3(\alpha)$, respectively, are obtained.
5. From the rational functions $f_1(\Delta)$, $f_2(\alpha)$, and $f_3(\alpha)$ obtained in the previous step, the expressions for the FFOPDT model parameters (4.10) are completed.

Once the numerical values of α, f_2, and f_3 are determined, the values of the FFOPDT model parameters, $\theta_P = \{K, T, L, \alpha\}$, are calculated using expressions (4.10) and experimental data collected from the process reaction curve, $\{\Delta y, \Delta u, t_{x1}, t_{x2}, t_{x3}\}$.

For a more detailed development of equations (4.10), the reader is referred to Chapter 4, where these equations are obtained and subsequently particularized for the case in which the three points on the process reaction curve are symmetrical with respect to the central point.

A detailed algorithm for estimating the FFOPDT model parameters, $\theta_P = \{K, T, L, \alpha\}$, from the information collected from the process reaction curve is provided in Chapter 8, where hardware implementation issues and results of fractional-order model estimation algorithms will be discussed.

Table 6.1 includes the numerical values of the normalized times τ_5, τ_{10}, τ_{20}, τ_{25}, τ_{50}, τ_{55}, τ_{60}, τ_{75}, τ_{90}, and τ_{95}, respectively. These data will be used indistinctly as τ_x, τ_{50}, or τ_{100-x} in Section 6.2.1 for a symmetrical set of points (x-50-(100–x)%), and τ_{x1}, τ_{x2}, or τ_{x3} in Section 6.2.2 for an asymmetrical set of points (x_1-x_2-x_3%), respectively, and constitute the main source of data to determine the corresponding data sets $\{\Delta, \alpha\}$, $\{\alpha, a^\alpha\}$, and $\{\alpha, (\tau_{x3})^{1/\alpha}\}$ or $\{\alpha, (\tau_{100-x})^{1/\alpha}\}$, needed to determine expressions for the functions $f_1(\Delta)$, $f_2(\alpha)$, and $f_3(\alpha)$.

α	τ_5 [s]	τ_{10} [s]	τ_{20} [s]	τ_{25} [s]	τ_{50} [s]	τ_{55} [s]	τ_{60} [s]	τ_{75} [s]	τ_{90} [s]	τ_{95} [s]
0.5	0.046	0.096	0.211	0.278	0.769	0.922	1.107	2.052	5.5556	11.36
0.6	0.046	0.096	0.210	0.275	0.740	0.881	1.048	1.873	4.7612	9.344
0.7	0.047	0.097	0.211	0.275	0.718	0.847	0.999	1.713	3.9916	7.416
0.8	0.048	0.099	0.213	0.277	0.703	0.822	0.960	1.576	3.2873	5.589
0.9	0.049	0.102	0.217	0.281	0.694	0.806	0.933	1.466	2.7112	4.019
1.0	0.051	0.105	0.223	0.288	0.693	0.799	0.916	1.3863	2.3026	2.996
1.1	0.053	0.110	0.231	0.297	0.699	0.800	0.911	1.3334	2.0419	2.456

Table 6.1. Numeric values of normalized times τ_5, τ_{10}, τ_{20}, τ_{25}, τ_{50}, τ_{55}, τ_{60}, τ_{75}, τ_{90}, and τ_{95}, respectively, for different values of α, with $0.5 \le \alpha \le 1.1$.

6.2.1. Symmetrical set of points (x-50-(100–x)%)

This case can be considered as a simplification of the general identification procedure, where only points that are symmetrically located on the process reaction curve are selected. Note that the central point or centroid will be located in the middle of the range, $x_2 = 50\%$, ($t_{x2} = t_{50}$, $y_\alpha(t_{50})$), as depicted in Figure 5.3. The remaining two points could be located arbitrarily on the reaction curve, but symmetrically located with respect to the central point ($\Delta x_{32} = \Delta x_{21}$). One of the extreme points will be denoted $x_1 = x$, the other being $x_3 = 100-x$. In this case, the times to be determined will be $t_{x1} = t_x$ and $t_{x3} = t_{100-x}$, where t_x and t_{100-x} denote the time required to reach x% ($y_\alpha(t_x)$) and (100–x)% ($y_\alpha(t_{100-x})$) of the total process output change, respectively, considering the following range $0 < x < 50$.

In this section, the sets of points indicated in Table 6.2 will be considered. For the case of symmetrical points, sets #1 and #2 have been chosen because the accuracy of the fractional-order model is improved for low values of x. In particular, the influence of the location of the symmetrical representative points of the reaction curve on the accuracy of the identified model is explained in detail in Chapter 4. In addition, set #3 has been chosen because it gives very good results for integer- or close to integer-order models; see also Chapter 4. This behaviour has already been observed in the technical literature in some identification methods for integer-order models, e.g., the aforementioned 123c method (Alfaro 2006) uses time sets (25–75%) to identify FOPDT and DPPDT models and (25–50–75%) for SOPDT models; and in (Alfaro and Vilanova 2021), points (25–50–75%) are proposed to identify multiple-pole with dead-time models.

Set #	Symmetrical points	centroid	distance from centroid
1	(5-50-95%)	$x_2 = 50\%$	$\Delta x_{21} = \Delta x_{32} = 45\%$
2	(10-50-90%)	$x_2 = 50\%$	$\Delta x_{21} = \Delta x_{32} = 40\%$
3	(25-50-75%)	$x_2 = 50\%$	$\Delta x_{21} = \Delta x_{32} = 25\%$

Table 6.2. Sets of symmetrical points that have been considered.

Then, the procedure summarized in Figure 6.1 is followed for the symmetrical case. Data sets $\{\Delta, \alpha\}$, $\{\alpha, a^{\alpha}\}$, and $\{\alpha, (\tau_{100-x})^{1/\alpha}\}$ for $0.5 \le \alpha \le 1.1$, and the functions $f_1(\Delta)$, $f_2(\alpha)$, and $f_3(\alpha)$ obtained by curve fitting for the different sets of symmetrical points, respectively, are shown in Figure 6.2. Remark that Δ depends on normalized times $\{\tau_x, \tau_{50}, \text{and } \tau_{100-x}\}$ and has a significant dependence on α parameter, that $f_2(\alpha) = a^{\alpha}$ depends on α and normalized times τ_x and τ_{100-x}, and that $f_3(\alpha) = (\tau_{100-x})^{1/\alpha}$ depends on α and normalized time τ_{100-x}.

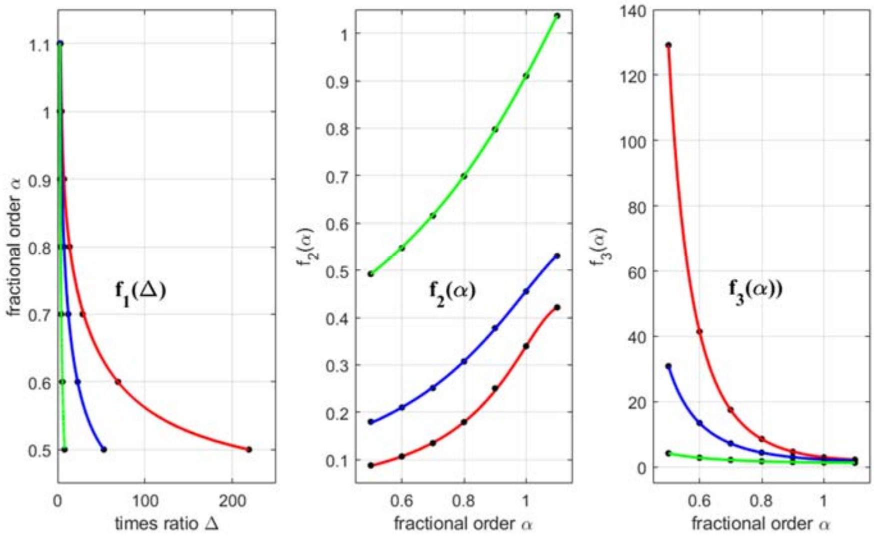

(a) (b) (c)

Figure 6.2. Data sets and results of curve fitting for symmetrical sets of points, (5-50-95%), (10-50-90%), and (25-50-75%), respectively: (a) Data sets $\{\Delta, \alpha\}$ and curve fitting for $f_1(\Delta)$; (b) Data sets $\{\alpha, a^{\alpha}\}$ and curve fitting for $f_2(\alpha)$; (c) Data sets $\{\alpha, (\tau_{100-x})^{1/\alpha}\}$ and curve fitting for $f_3(\alpha)$. Note that in each graph curve fitting for (5-50-95%) is represented in red, (10-50-90%) in blue, and (25-50-75%) in green, respectively.

The following rational functions have been used for curve fitting of functions $f_1(\Delta)$, $f_2(\alpha)$, and $f_3(\alpha)$, respectively:

$$f_1(\Delta) = \frac{p_1\Delta^2 + p_2\Delta + p_3}{\Delta^2 + q_1\Delta + q_2} \tag{6.1}$$

$$f_2(\alpha) = \frac{p_1\alpha + p_2}{\alpha^2 + q_1\alpha + q_2} \tag{6.2}$$

$$f_3(\alpha) = \frac{p_1\alpha^2 + p_2\alpha + p_3}{\alpha^2 + q_1\alpha + q_2} \tag{6.3}$$

The Levenberg–Marquardt least-squares curve-fitting algorithm has been used for fitting data in all graphs in Figure 6.2. The values of the corresponding parameters $\{p_i, q_i\}$ for functions $f_1(\Delta)$, $f_2(\alpha)$, and $f_3(\alpha)$, and each one of the selected sets of symmetrical points are shown in Tables 6.3, 6.4, and 6.5, respectively.

(5-50-95%)	(10-50-90%)	(25-50-75%)
$p_1 = 0.4259$	$p_1 = 0.3808$	$p_1 = 0.2676$
$p_2 = 38.78$	$p_2 = 13.57$	$p_2 = 1.756$
$p_3 = 14.34$	$p_3 = -3.067$	$p_3 = -2.578$
$q_1 = 45.33$	$q_1 = 14.69$	$q_1 = -0.7042$
$q_2 = -27.8$	$q_2 = -15.9$	$q_2 = -1.289$

Table 6.3. Parameters $\{p_i, q_i\}$ of the rational function $f_1(\Delta)$ for the different sets of symmetrical points.

(5-50-95%)	(10-50-90%)	(25-50-75%)
$p_1 = -0.0337$	$p_1 = -0.05698$	$p_1 = -0.3443$
$p_2 = 0.0595$	$p_2 = 0.1596$	$p_2 = 0.7806$
$q_1 = -2.328$	$q_1 = -2.528$	$q_1 = -3.017$
$q_2 = 1.404$	$q_2 = 1.753$	$q_2 = 2.496$

Table 6.4. Parameters $\{p_i, q_i\}$ of the rational function $f_2(\alpha)$ for the different sets of symmetrical points.

(5-50-95%)	(10-50-90%)	(25-50-75%)
$p_1 = 10.43$	$p_1 = 4.518$	$p_1 = 3.901$
$p_2 = -22.09$	$p_2 = -8.675$	$p_2 = -4.833$
$p_3 = 13.14$	$p_3 = 5.666$	$p_3 = 4.546$
$q_1 = -0.586$	$q_1 = -0.3471$	$q_1 = 2.239$
$q_2 = 0.07943$	$q_2 = 0.003197$	$q_2 = -0.6319$

Table 6.5. Parameters $\{p_i, q_i\}$ of the rational function $f_3(\alpha)$ for the different sets of symmetrical points.

6.2.2. Asymmetrical set of points (x_1-x_2-x_3%)

In this section, the general identification procedure is applied to three arbitrary points asymmetrically located on the reaction curve (x_1, x_2, and x_3), as shown in Figure 5.1. This means that the times to be determined will be t_{x1}, t_{x2}, and t_{x3}, where they denote the time needed to reach x_1% ($y_\alpha(t_{x1})$), x_2% ($y_\alpha(t_{x2})$), and x_3% ($y_\alpha(t_{x3})$) of the total process output change, respectively.

The origin of the asymmetry comes not only from the fact that, in general, the centroid x_2 will not be located in the middle of the range ($0 - 100$%) of the process output, but also from the fact that the distance from the centroid x_2 to the extreme points x_1 and x_3, respectively, is different, i.e., $\Delta x_{21} \neq \Delta x_{32}$.

As discussed previously, the objective is to validate this identification procedure for the asymmetrical case and to get insight into the selection of representative points of the reaction curve and their influence on the accuracy of the identified model.

In this section, the sets of points indicated in Table 6.6 will be considered.

Set #	Asymmetrical points	centroid	distance from centroid
4	(10-55-90%)	$x_2 = 55\%$	$\Delta x_{21} = 45\%$, $\Delta x_{32} = 35\%$
5	(20-60-95%)	$x_2 = 60\%$	$\Delta x_{21} = 40\%$, $\Delta x_{32} = 35\%$
6	(20-75-95%)	$x_2 = 75\%$	$\Delta x_{21} = 55\%$, $\Delta x_{32} = 25\%$

Table 6.6. Sets of asymmetrical points that have been considered.

The selection of these three sets of points (x_1-x_2-x_3%) is based on experimentation. A large amount of experiments has been performed in order to draw the following observations:

1. The three sets of points have been chosen with a high x_3 value, where $x_3 = 90\%$ or 95%, because the obtained model fits better the reaction curve, especially in the final part. In this regard, it has been shown in Chapter 4 that the step response of the identified models gives a good fit with the process reaction curve for the symmetrical case, particularly in the interval $[x - (100–x)]$. Due to the symmetry exhibited by this method, the interval $[x - (100–x)]$ is larger for lower values of x and, therefore, the step response of these models fits better the process reaction curve, which translates into a lower value in the performance index S for this fractional-order model.
2. In general, the selection of x_1 affects the accuracy of the model in the initial part and, together with x_3, allows better fitting of T parameter.
3. With respect to the centroid x_2, set #4 has been chosen in order to test the effect of moving the centroid x_2, increasing Δx_{21} and decreasing Δx_{32}, in comparison with the symmetrical set #2. Sets #5 and #6 have been chosen because the effect of moving the centroid x_2, while keeping the extreme values x_1 and x_3, can be observed. In particular, set #5 allows to analyze the effect of increasing x_1, with asymmetrical distances $\Delta x_{21} = 40\%$ and $\Delta x_{32} = 35\%$, while set #6 shows the effect of increasing x_2, with asymmetric distances $\Delta x_{21} = 55\%$ and $\Delta x_{32} = 25\%$.

Although the sets of points could have been chosen considering other criteria, in the author's opinion, these are the ones that best reflect the effect of their position on the model's accuracy.

In the following section, several examples will be used to verify that these observations are met.

Then, the procedure summarized in Figure 6.1 is followed for the asymmetrical case. Data sets $\{\Delta, \alpha\}$, $\{\alpha, a^\alpha\}$, and $\{\alpha, (\tau_{100-x})^{1/\alpha}\}$ for $0.5 \leq \alpha \leq 1.1$, and the functions $f_1(\Delta)$, $f_2(\alpha)$, and $f_3(\alpha)$ obtained by curve fitting for the different sets of asymmetrical points, i.e. (10-55-90%), (20-60-95%), and (20-75-95%), respectively, are shown in Figure 6.3.

Remark that Δ depends on normalized times $\{\tau_{x1}, \tau_{x2}, \text{and } \tau_{x3}\}$ and has a significant dependence on α, that $f_2(\alpha) = a^\alpha$ depends on α and normalized times τ_{x1} and τ_{x3}, and that $f_3(\alpha) = (\tau_{x3})^{1/\alpha}$ depends on α and normalized time τ_{100-x}.

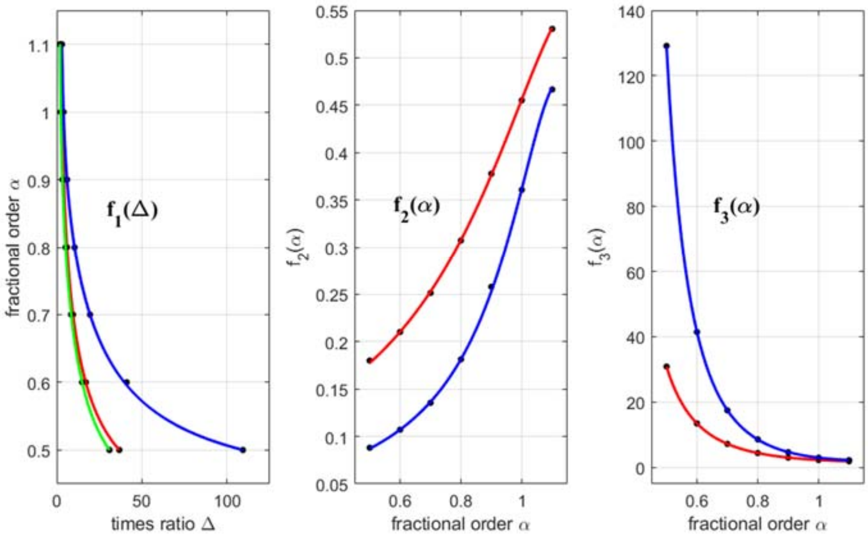

(a) (b) (c)

Figure 6.3. Data sets and results of curve fitting for asymmetrical sets of points, (10-55-90%), (20-60-95%), and (20-75-95%), respectively: (a) Data sets $\{\Delta, \alpha\}$ and curve fitting for $f_1(\Delta)$; (b) Data sets $\{\alpha, a^\alpha\}$ and curve fitting for $f_2(\alpha)$; (c) Data sets $\{\alpha, (\tau_{x3})^{1/\alpha}\}$ and curve fitting for $f_3(\alpha)$. Note that in each graph curve fitting for (10-55-90%) is represented in red, (20-60-95%) in blue, and (20-75-95%) in green, respectively. Note also that sets #5 (20-60-95%) and #6 (20-75-95%) have the same functions $f_2(\alpha)$ and $f_3(\alpha)$.

The Levenberg–Marquardt least-squares curve-fitting algorithm has been used in for fitting data in all graphs in Figure 6.3. The same rational functions (6.1) – (6.3) have been used for obtaining functions $f_1(\Delta)$, $f_2(\alpha)$, and $f_3(\alpha)$, respectively, by using curve fitting.

The values of the corresponding parameters $\{p_i, q_i\}$ for functions $f_1(\Delta)$, $f_2(\alpha)$, and $f_3(\alpha)$, and each one of the selected sets of asymmetrical points are shown in Tables 6.7, 6.8, and 6.9, respectively.

Note that the obtained values of T, L, and α, which are determined by using equations (4.10), depend on functions $f_1(\Delta)$, $f_2(\alpha)$, and $f_3(\alpha)$. These functions thus play a relevant role in the identification method as the features of normalized step responses (4.3) can be well characterized due to their respective contribution. It is important to emphasize that, for any different choice of times set $\{t_{x1}\ t_{x2}, t_{x3}\}$ to reach three points $\{y_\alpha(t_{x1}), y_\alpha(t_{x2}), y_\alpha(t_{x3})\}$ on the reaction curve, the accuracy of the identification results only depends upon the fitting precision. In this context, an accurate determination of α-value is of primary importance since, subsequently, functions f_2 and f_3 –and therefore T and L– depend on the estimated value of α.

(10-55-90%)	(20-60-95%)	(20-75-95%)
$p_1 = 0.3693$	$p_1 = 0.4165$	$p_1 = 0.3665$
$p_2 = 9.55$	$p_2 = 18.5$	$p_2 = 7.191$
$p_3 = -5.112$	$p_3 = -15.5$	$p_3 = -8.393$
$q_1 = 9.53$	$q_1 = 18.69$	$q_1 = 5.838$
$q_2 = -11.38$	$q_2 = -25.6$	$q_2 = -8.767$

Table 6.7. Parameters $\{p_i, q_i\}$ of the rational function $f_1(\Delta)$ for the different sets of asymmetrical points.

(10-55-90%)	(20-60-95%)	(20-75-95%)
$p_1 = -0.05698$	$p_1 = -0.03498$	$p_1 = -0.03498$
$p_2 = 0.1596$	$p_2 = 0.05957$	$p_2 = 0.05957$
$q_1 = -2.528$	$q_1 = -2.33$	$q_1 = -2.33$
$q_2 = 1.753$	$q_2 = 1.398$	$q_2 = 1.398$

Table 6.8. Parameters $\{p_i, q_i\}$ of the rational function $f_2(\alpha)$ for the different sets of asymmetrical points. Note that the parameters for (20-60-95%) and (20-75-95%) are the same since their x_1 and x_3-values are the same ($x_1 = 20\%$ and $x_3 = 95\%$).

(10-55-90%)	(20-60-95%)	(20-75-95%)
$p_1 = 4.518$	$p_1 = 10.43$	$p_1 = 10.43$
$p_2 = -8.675$	$p_2 = -22.09$	$p_2 = -22.09$
$p_3 = 5.666$	$p_3 = 13.14$	$p_3 = 13.14$
$q_1 = -0.3471$	$q_1 = -0.586$	$q_1 = -0.586$
$q_2 = 0.003197$	$q_2 = 0.07943$	$q_2 = 0.07943$

Table 6.9. Parameters $\{p_i, q_i\}$ of the rational function $f_3(\alpha)$ for the different sets of asymmetrical points. Note that the parameters for (20-60-95%) and (20-75-95%) are the same since their x_3-values are the same ($x_3 = 95\%$).

6.3. Results and discussion

In this section, the identification method proposed in this work has been proved for several models that exhibit fractional behaviour.

Process models (6.4), (6.5), and (6.6) have been selected to test the effectiveness of the proposed method in obtaining a FFOPDT model (3.21) in comparison with several identification methods for integer- and fractional-order models.

$$P_1(s) = \frac{1}{(1+s^{0.75})^2} e^{-0.1s} \tag{6.4}$$

$$P_2(s) = \frac{3}{(1+3s^{0.88})(1+2s^{0.88})(1+s^{0.88})} \tag{6.5}$$

$$P_3(s) = e^{-\sqrt{s}} \tag{6.6}$$

On the one hand, process P_1 has been used to evaluate the proposed identification method for several symmetrical and asymmetrical sets of points in comparison with several well-known identification methods for integer-order model and to get insight into the influence of the location of asymmetrical points on the accuracy of the identified model.

On the other hand, processes P_2 and P_3 have been used to evaluate the model performance of the proposed procedure for symmetrical and asymmetrical points with other fractional-order methods.

These examples selected in this section have been also used to validate the proposed identification method for both symmetrical and asymmetrical points on the process reaction curve.

The experimental procedure followed is as follows: A step signal has been applied to the input of these processes and the reaction curve has been registered. Then the process output responses of the processes have been used to obtain the parameters of the different models using the different proposed identification methods. The sampling period used in all the experiments is $Ts = 10$ ms.

Finally, it is required to evaluate the accuracy of the model parameters that have been identified and the effectiveness of the model structure that has been adopted. A wide variety of model validation methods and fitting objective functions for system identification are available in the technical literature (Liu and Gao 2012).

Although another objective function could have been used, the Mean Squared Error (MSE) (4.20) has been used as a time-domain fitting criterion as a measure of performance for the identified model.

The Mean Absolute Error (MAE), which expression is (6.7), has also been calculated in the following examples for illustrative purposes.

$$E(\bar{\theta}) = \frac{1}{N_s}\sum_{k=1}^{N_s}\left|e(kT_s,\bar{\theta})\right| = \frac{1}{N_s}\sum_{k=1}^{N_s}\left|y(kT_s) - y_m(kT_s,\bar{\theta})\right| \tag{6.7}$$

In the same context, it may be interesting to evaluate the goodness of fit of the identified model at different intervals of the reaction curve. For this reason, the index $S_{x_i-x_j}(\bar{\theta})$ is introduced in this paper, where $\bar{\theta}$ is the vector of identified model parameters.

This performance index represents the time-domain performance index $S(\bar{\theta})$ restricted to the interval $[x_i - x_j]$ on the reaction curve, where x_i and x_j are two specific points on the reaction curve as depicted in Figure 4.3. Remark that if the step response of the identified model is divided into p intervals $[x_i - x_j]$, the model performance index $S(\bar{\theta})$ and the p performance indices $S_k(\bar{\theta})$ $(k = 1, \ldots, p)$ of each of the intervals satisfy the following expression:

$$S(\bar{\theta}) = \frac{1}{N_s} \sum_{k=1}^{p} S_k(\bar{\theta}) \cdot N_{sk} \quad (6.8)$$

where $p \in \mathbb{Z}^{+}$ is the number of intervals into which the model step response is divided, and N_{Sk} is the number of samples of the model step response in the corresponding k interval.

The simulation results obtained in this section have been performed using FOTF MATLAB toolbox, which is a set of built-in functions that extends the control toolbox to deal with fractional-order systems (Chen, Petras and Xue 2009). For a deeper knowledge of the FOTF toolbox, the reader is referred to the reference text in (Xue 2017).

6.3.1. Example 1

In this example, the fractional-order process model (6.4) is selected. This model is a lag-dominated FSOPDT, providing some modelling deviation from the model structure selected in the proposed identification method, which is a FFOPDT dynamics.

This same model but for different α-values in the range $0.60 \leq \alpha \leq 1.00$ has been used in Chapter 4, on the one hand, as a batch of processes to validate the proposed identification procedure for different sets of symmetrical points and, on the other hand, to get insight into the influence of the location of symmetrical points on the accuracy of the identified model.

The objective in this case is to validate the identification procedure for asymmetrical points on the process reaction curve and to get insight into the influence of the location of such asymmetrical points on the accuracy of the fractional-order identified model. A comparison between the proposed method and several well-known identification methods for integer-order models is also provided in this section.

The process reaction curve for this model and the step-input signal are shown in Figure 6.4.

The process information summarized in Table 6.10 for the different proposed identification methods is collected from data in Figure 6.4.

With the information collected from Table 6.10, the following FFOPDT model parameters $\bar{\theta}_{1,i} = \{K_{1,i}, T_{1,i}, L_{1,i}, \alpha_{1,i}\}$, for $i = 1, \ldots, 6$, have been obtained in Table 6.11 for the different sets of points proposed in Tables 6.2 and 6.6.

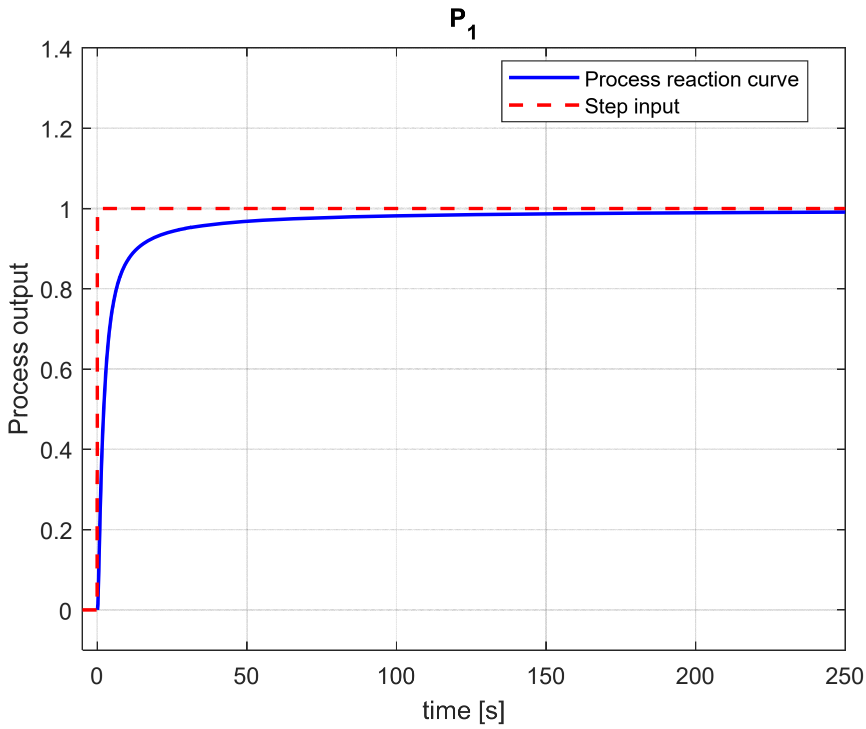

Figure 6.4. Process reaction curve for process P_1 and step-input signal.

Symmetrical methods			Asymmetrical methods		
Method #1: (5-50-95%)	**Method #2: (10-50-90%)**	**Method #3: (25-50-75%)**	**Method #4: (10-55-90%)**	**Method #5: (20-60-95%)**	**Method #6: (20-75-95%)**
$\Delta u = 1.00$					
$\Delta y = 1.00$					
$t_5 = 0.3020$ s	$t_{10} = 0.4540$ s	$t_{25} = 0.9300$ s	$t_{10} = 0.4540$ s	$t_{20} = 0.7620$ s	$t_{20} = 0.7620$ s
$t_{50} = 2.0910$ s	$t_{50} = 2.0910$ s	$t_{50} = 2.0910$ s	$t_{55} = 2.4400$ s	$t_{60} = 2.8590$ s	$t_{75} = 4.9730$ s
$t_{95} = 29.1410$ s	$t_{90} = 13.2640$ s	$t_{75} = 4.9730$ s	$t_{90} = 13.2640$ s	$t_{95} = 29.1410$ s	$t_{95} = 29.1410$ s

Table 6.10. Process information collected from the reaction curve for fractional-order model identification of process P_1.

Symmetrical methods			Asymmetrical methods		
Method #1: (5-50-95%)	**Method #2: (10-50-90%)**	**Method #3: (25-50-75%)**	**Method #4: (10-55-90%)**	**Method #5: (20-60-95%)**	**Method #6: (20-75-95%)**
$K_{1,1} = 1.00$	$K_{1,2} = 1.00$	$K_{1,3} = 1.00$	$K_{1,4} = 1.00$	$K_{1,5} = 1.00$	$K_{1,6} = 1.00$
$T_{1,1} = 2.3137$ s	$T_{1,2} = 2.2492$ s	$T_{1,3} = 2.1890$ s	$T_{1,4} = 2.1963$ s	$T_{1,5} = 2.0223$ s	$T_{1,6} = 1.8807$ s
$L_{1,1} = 0.2745$ s	$L_{1,2} = 0.2782$ s	$L_{1,3} = 0.3901$ s	$L_{1,4} = 0.2791$ s	$L_{1,5} = 0.3139$ s	$L_{1,6} = 0.2921$ s
$\alpha_{1,1} = 0.7791$	$\alpha_{1,2} = 0.7888$	$\alpha_{1,3} = 0.8088$	$\alpha_{1,4} = 0.7836$	$\alpha_{1,5} = 0.7580$	$\alpha_{1,6} = 0.7463$

Table 6.11. Fractional-order model settings for the symmetrical and asymmetrical sets of points (5-50-95%), (10-50-90%), (25-50-75%), (10-55-90%), (20-60-95%), and (20-75-95%), respectively.

The FFOPDT model step responses for (5-50-95%), (10-50-90%), (25-50-75%), (10-55-90%), (20-60-95%), and (20-75-95%), respectively, are compared with the process reaction curve and illustrated in Figures 6.5 – 6.10. In each figure the corresponding representative points, symmetrical (x-50-(100–x)%) and asymmetrical (x_1-x_2-x_3%), respectively, are also displayed.

Figures 6.5 – 6.10 show that the step responses of the fractional-order models identified with the proposed method, for both the symmetrical and asymmetrical case, give good fit with the process reaction curve, which confirms the validity of this identifica-tion method also for the asymmetrical case.

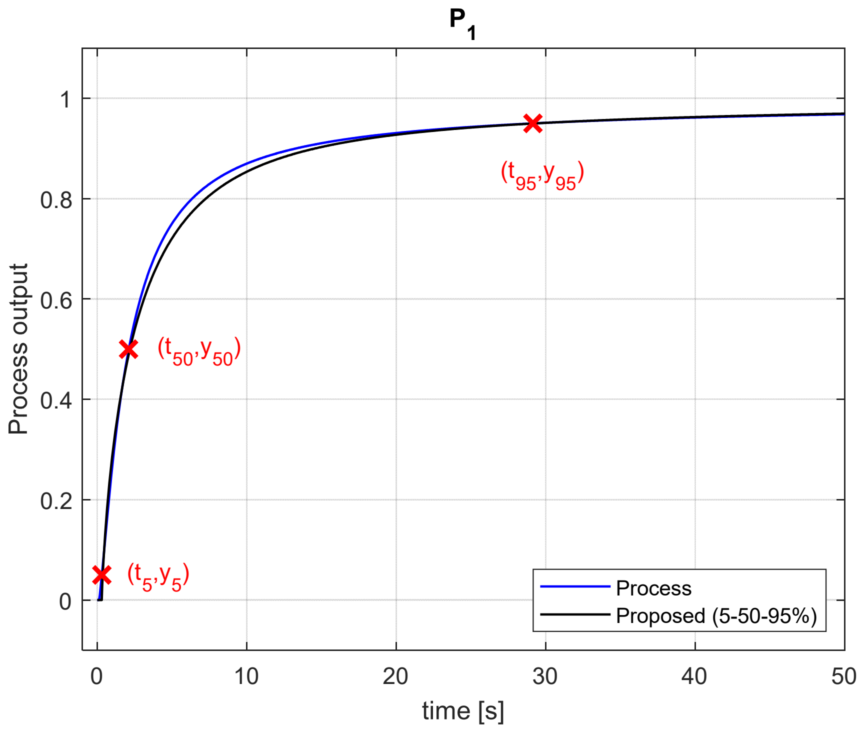

Figure 6.5. FFOPDT model step response using the proposed identification method for process P_1 and process reaction curve: Symmetrical set of points (5-50-95%).

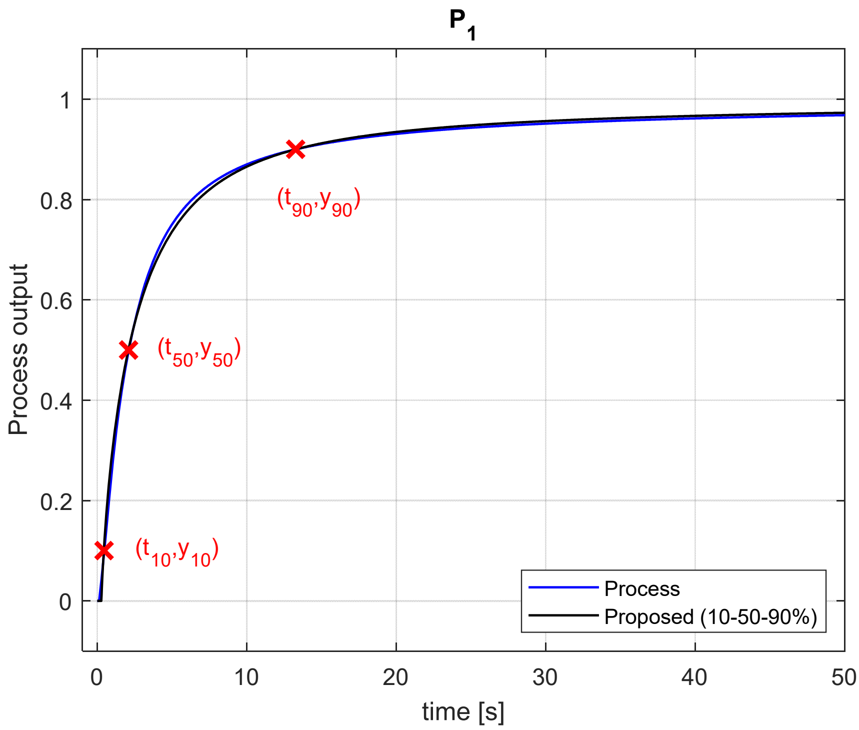

Figure 6.6. FFOPDT model step response using the proposed identification method for process P_1 and process reaction curve: Symmetrical set of points (10-50-90%).

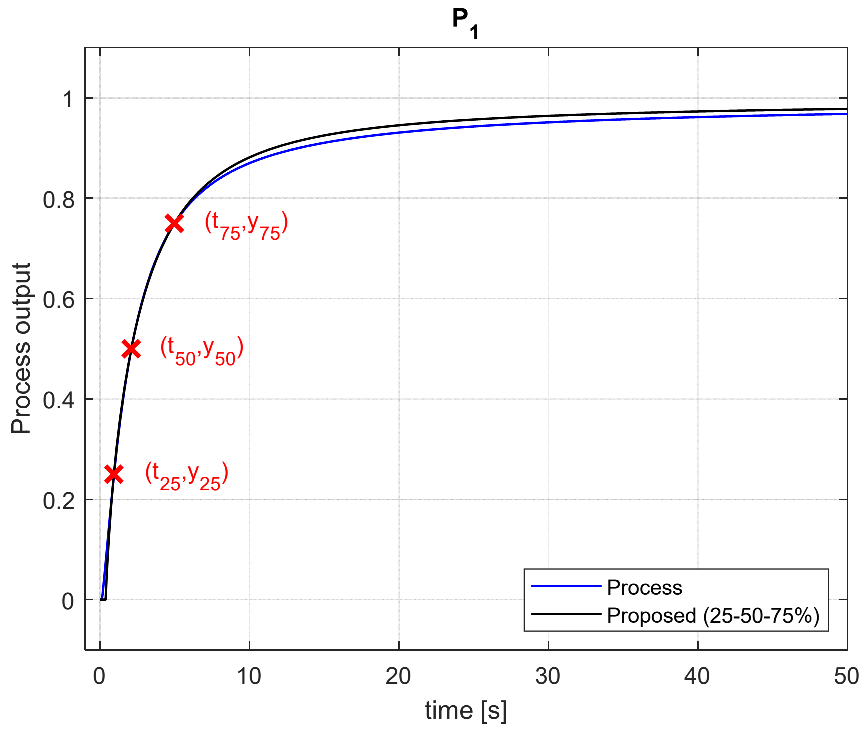

Figure 6.7. FFOPDT model step response using the proposed identification method for process P_1 and process reaction curve: Symmetrical set of points (25-50-75%).

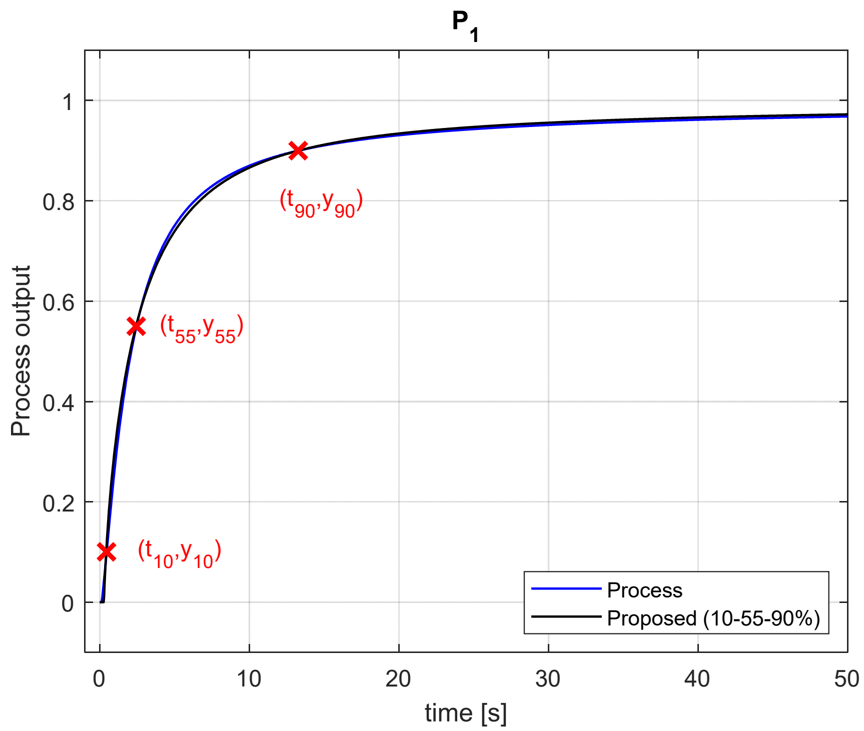

Figure 6.8. FFOPDT model step response using the proposed identification method for process P_1 and process reaction curve: Asymmetrical set of points (10-55-90%).

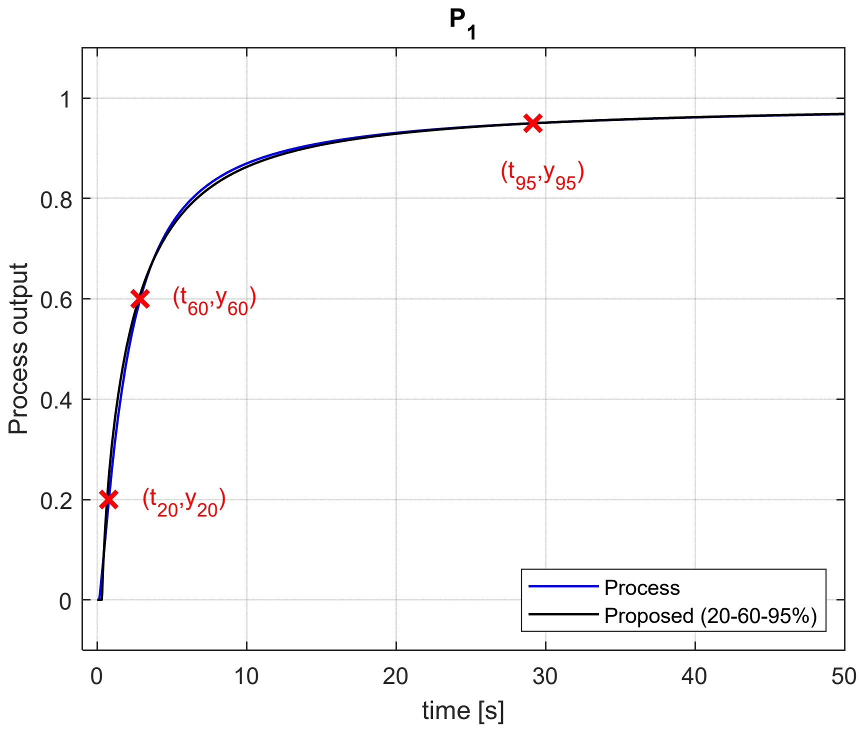

Figure 6.9. FFOPDT model step response using the proposed identification method for process P_1 and process reaction curve: Asymmetrical set of points (20-60-95%).

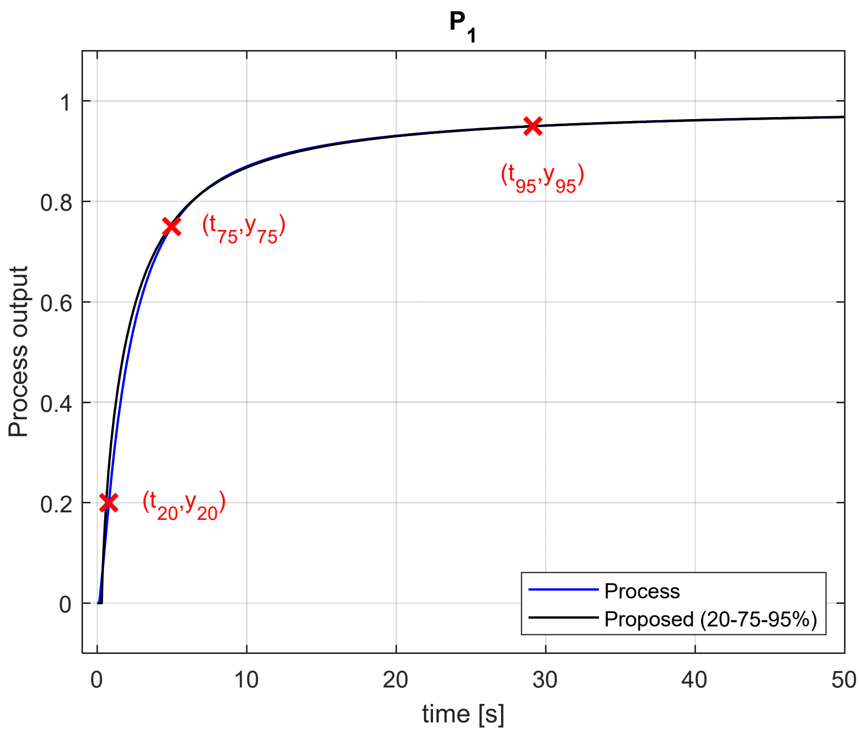

Figure 6.10. FFOPDT model step response using the proposed identification method for process P_1 and process reaction curve: Asymmetrical set of points (20-75-95%).

Note that the identification method for the symmetrical case has been studied in detail and its validity for the identification of FFOPDT models has also been confirmed in Chapter 4.

Table 6.12 shows the process parameters identified for FOPDT and DPPDT models obtained using the methods proposed by Alfaro in (Alfaro 2006), and by Vitecková et al. in (Vitecková, Vitecek and Smutny 2000), and the ones for SOPDT obtained using methods proposed by Stark in (Mollenkamp 1984) and by Jahanmiri and Fallahi in (Jahanmiri and Fallahi 1997), respectively, using two or three points from the process reaction curve.

The corresponding integer-order model step responses for the considered classical identification methods are compared with the process reaction curve and illustrated in Figures 6.11 and 6.12 for FOPDT and DPPDT models and in Figure 6.13 for SOPDT models, respectively.

FOPDT		DPPDT		SOPDT	
Alfaro (25-75%)	**Vitecková (33-70%)**	**Alfaro (25-75%)**	**Vitecková (33-70%)**	**Stark (15-45-75%)**	**Jahanmiri-Fallahi (2-70-90%)**
$K_{1,7} = 1.00$	$K_{1,8} = 1.00$	$K_{1,9} = 1.00$	$K_{1,10} = 1.00$	$K_{1,11} = 1.00$	$K_{1,12} = 1.00$
$T_{1,7} = 3.68$ s	$T_{1,8} = 3.51$ s	$T_{1,9} = 2.24$ s	$T_{1,10} = 2.33$ s	$T_{1,11a} = 3.52$ s	$T_{1,12a} = 5.61$ s
$L_{1,7} = 0.00$ s	$L_{1,8} = 0.00$ s	$L_{1,9} = 0.00$ s	$L_{1,10} = 0.00$ s	$T_{1,11b} = 0.34$ s	$T_{1,12b} = 0.0072$ s
–	–	–	–	$L_{1,11} = 0.00$ s	$L_{1,12} = 0.20$ s

Table 6.12. FOPDT, DPPDT, and SOPDT model settings obtained for the considered integer-order identification methods.

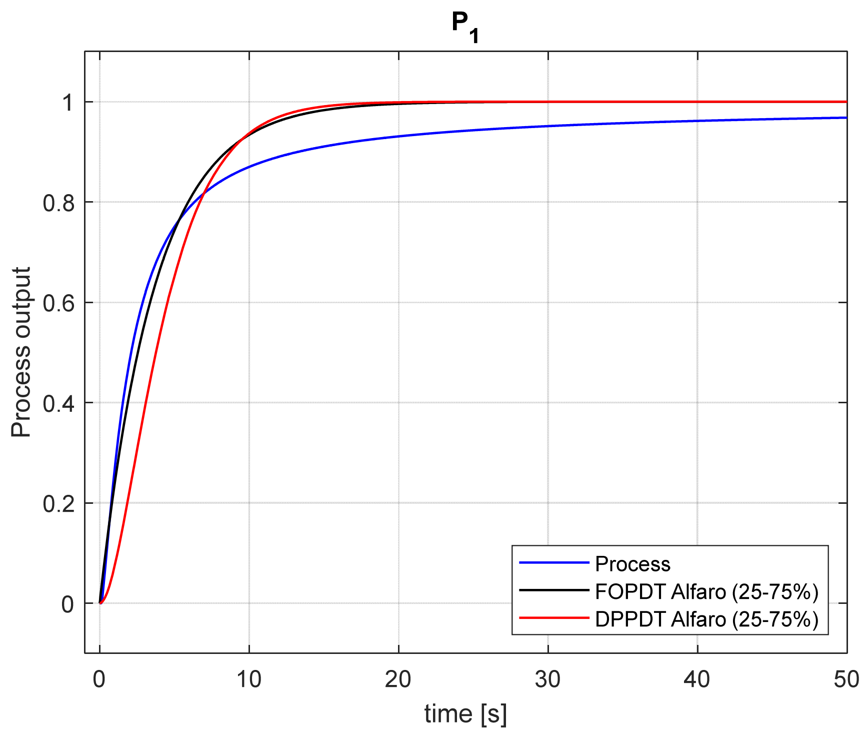

Figure 6.11. FOPDT and DPPDT model step responses using integer-order model identification methods for process P_1 and process reaction curve: Alfaro (25-75%) (Alfaro 2006).

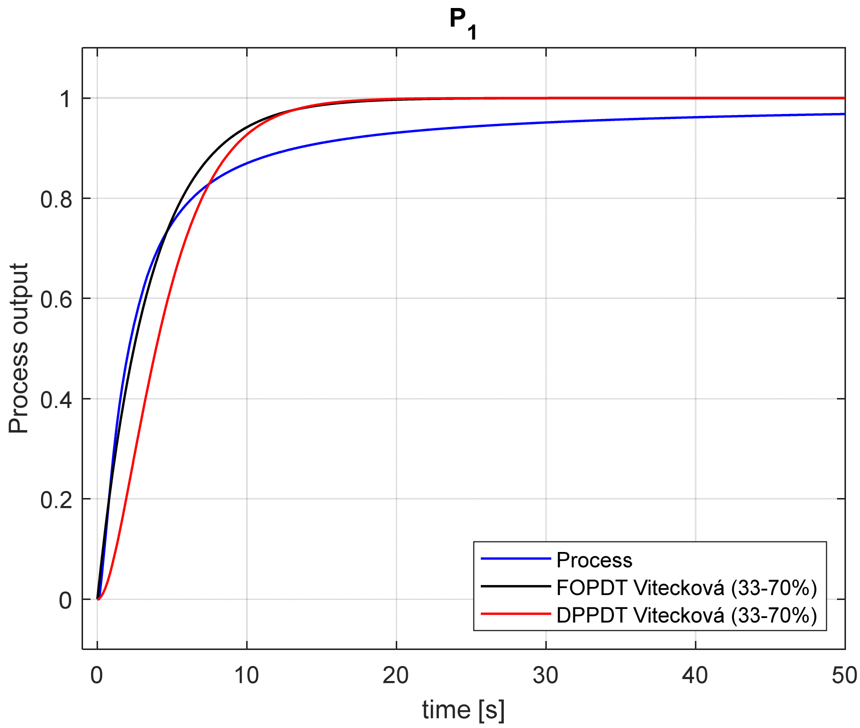

Figure 6.12. FOPDT and DPPDT model step responses using integer-order model identification methods for process P_1 and process reaction curve: Vitecková et al. (33-70%) (Vitecková, Vitecek and Smutny 2000).

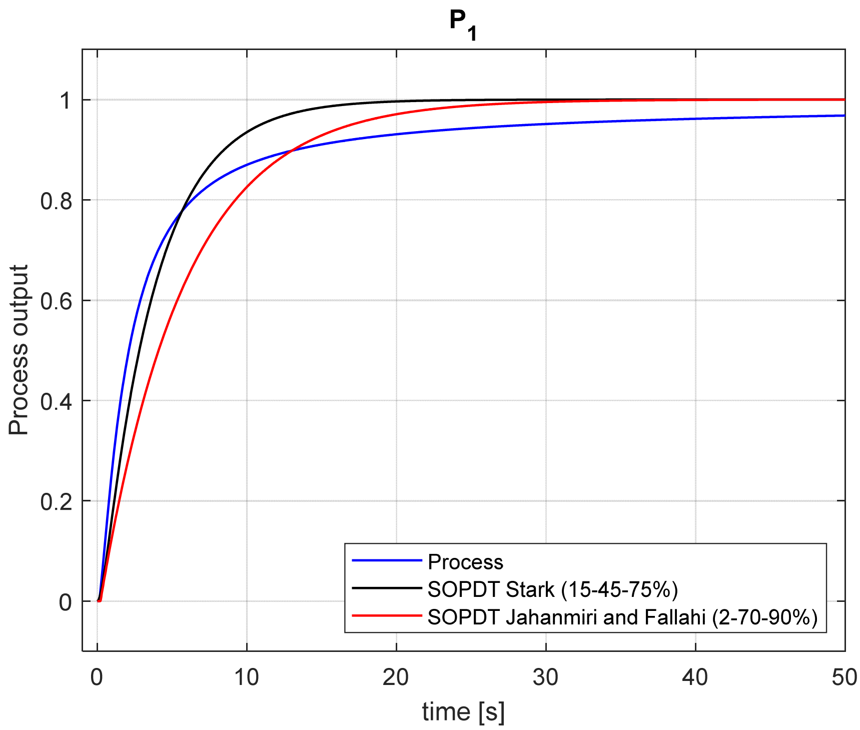

Figure 6.13. SOPDT model step responses using methods proposed by Stark (15-45-75%) (Mollenkamp 1984) and by Jahamiri and Fallahi (2-70-90%) (Jahanmiri and Fallahi 1997), and process reaction curve.

Figures 6.11 – 6.13 illustrate that FOPDT, DPPDT, and SOPDT models, respectively, approximate process P_1 with insufficient accuracy compared to FFOPDT models obtained with the proposed method. It has been illustrated from Figures 6.5 – 6.13 that the proposed identification method outperforms significantly the considered methods for integer-order models.

Table 6.13 shows the values of the time-domain performance indexes $S(\bar{\theta}_{1,i})$ and $E(\bar{\theta}_{1,i})$ for process P_1, and the ones corresponding to the intervals [0–50%], $S_{0-50}(\bar{\theta}_{1,i})$, and [50–100%], $S_{50-100}(\bar{\theta}_{1,i})$, of the total process output total change, respectively, for the different models considered in this example. In this table, i = 1, …, 6, and represents the different sets of points considered in the proposed identification method, and i = 7, …, 12 represents the different identification methods for integer-order models.

Time-domain performance indexes in both intervals, $S_{0-50}(\bar{\theta}_{1,i})$ and $S_{50-100}(\bar{\theta}_{1,i})$, give information about the effect of the location of the different set of points on the accuracy of the identified models. Since the step response of the identified models can be divided into the two aforementioned intervals, the accuracy of the identified models can be quantified and the one for the first and second half of the total interval can be also determined from data in Table 6.13. The number of samples for the model step responses in the whole range, N_S, and in both intervals, N_{S1} and N_{S2}, respectively, are also provided in Table 6.13.

i	Method	Set of points	$S_{0-50}(\bar{\theta}_{1,i})$	$S_{50-100}(\bar{\theta}_{1,i})$	$S(\bar{\theta}_{1,i})$	$E(\bar{\theta}_{1,i})$
1	FFOPDT Proposed #1	(5-50-95%)	$3.07\cdot10^{-4}$	$2.24\cdot10^{-5}$	$2.48\cdot10^{-5}$	$2.4\cdot10^{-3}$
2	FFOPDT Proposed #2	(10-50-90%)	$4.63\cdot10^{-4}$	$1.45\cdot10^{-5}$	$1.83\cdot10^{-5}$	$3.6\cdot10^{-3}$
3	FFOPDT Proposed #3	(25-50-75%)	$4.75\cdot10^{-4}$	$5.36\cdot10^{-5}$	$5.72\cdot10^{-5}$	$6.7\cdot10^{-3}$
4	FFOPDT Proposed #4	(10-55-90%)	$6.86\cdot10^{-4}$	$1.09\cdot10^{-5}$	$1.65\cdot10^{-5}$	$3.2\cdot10^{-3}$
5	FFOPDT Proposed #5	(20-60-95%)	$1.30\cdot10^{-3}$	$3.46\cdot10^{-6}$	$1.44\cdot10^{-5}$	$1.2\cdot10^{-3}$
6	FFOPDT Proposed #6	(20-75-95%)	$3.20\cdot10^{-3}$	$6.86\cdot10^{-6}$	$3.34\cdot10^{-5}$	$9.7\cdot10^{-4}$
7	FOPDT Alfaro	(25-75%)	–	–	$7.32\cdot10^{-4}$	$2.19\cdot10^{-2}$
8	FOPDT Viteckova	(33-70%)	–	–	$7.54\cdot10^{-4}$	$2.20\cdot10^{-2}$
9	DPPDT Alfaro	(25-75%)	–	–	$1.50\cdot10^{-3}$	$2.51\cdot10^{-2}$
10	DPPDT Viteckova	(33-70%)	–	–	$1.60\cdot10^{-3}$	$2.53\cdot10^{-2}$
11	SOPDT Stark	(15-45-75%)	–	–	$8.26\cdot10^{-4}$	$2.26\cdot10^{-2}$
12	SOPDT Jahanmiri-Fallahi	(2-70-90%)	–	–	$1.40\cdot10^{-3}$	$2.35\cdot10^{-2}$
	Number of samples:		$N_{S1} = 210$	$N_{S2} = 24791$	$N_S = 25001$	$N_S = 25001$

Table 6.13. Comparison between the performance indexes obtained for the proposed method with different sets of points, symmetrical and asymmetrical, and the ones for several well-known methods for integer-order models. The number of samples N_S for the whole range and for each interval are also displayed.

Note that from expression (6.8) the following relation that must be fulfilled can be particularized for this case:

$$S(\bar{\theta}_{1,i}) = S_{0-100}(\bar{\theta}_{1,i}) = \frac{1}{N_s}\left[S_{0-50}(\bar{\theta}_{1,i}) \cdot N_{s1} + S_{50-100}(\bar{\theta}_{1,i}) \cdot N_{s2}\right] \qquad (6.9)$$

The results of Table 6.13 for the proposed identification method in terms of $S_{0–50}(\bar{\theta}_{1,i})$, $S_{50–100}(\bar{\theta}_{1,i})$, and $S(\bar{\theta}_{1,i})$, for $i = 1, \ldots, 6$, are also shown graphically in Figure 6.14.

Next, the results obtained in Table 6.13 and illustrated in Figure 6.14 for the FFOPDT models identified for process P_1 will be analyzed in order to gain insights into the location of the points for the asymmetrical case and their effect on the accuracy of the identified model.

The following observations can be drawn from the above results:

1. Methods with low values of x_1 for the asymmetrical case, or x in the symmetrical case, allow obtaining low values of $S_{0–50}$, as can be seen in Figure 6.14 for methods #1, #2, and #4, compared to #5 and #6, which give worse results in that interval.
2. Methods with high values of x_3 for the asymmetrical case allow better fitting of the model to the reaction curve in the final part of the response, as verified by the low values of $S_{50–100}$ for methods #4, #5, and #6. For the symmetrical case, a high value of $(100–x)$ implies a low value of x, thus better fitting the model to the reaction curve in the initial and final parts of the response, as illustrated by the low values of $S_{0–50}$ and $S_{50–100}$, respectively, for methods #1 and #2.
3. Comparing methods #2 and #4, it can be seen that the effect of increasing the value of x_2, while keeping x_1 and x_3 constant, is to reduce the value of S as a result of a reduction in the value of $S_{50–100}$, even though the value of $S_{0–50}$ is slightly increased.
4. Comparing methods #5 and #6, the effect of increasing the value of x_2 can also be observed, while keeping x_1 and x_3 constant. Note that the value of x_1 in this case is higher than for methods #2 and #4. The value of S for method #5 is reduced as a result of a very good fit in the interval [50–100%], as shown in Figure 6.14. The value of S corresponding to method #6 increases substantially due to a poorer fit in the interval [0–50%] despite the good result for $S_{50–100}$.

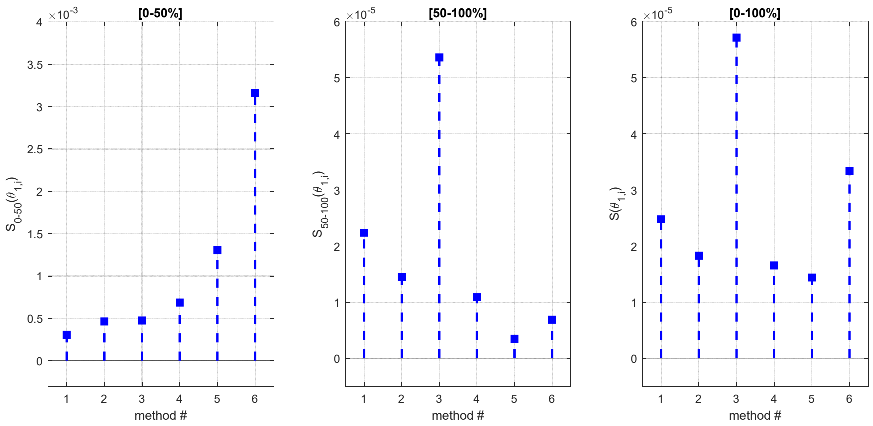

Figure 6.14. Graphical representation of the data given in Table 6.13 for process P_1. From left to right the performance indexes $S_{0\text{–}50}(\bar{\theta}_{1,i})$, $S_{50\text{–}100}(\bar{\theta}_{1,i})$, and $S(\bar{\theta}_{1,i})$, $i = 1, \ldots, 6$, are shown, respectively, for each of the considered methods.

As discussed previously, the step response of the identified model can be divided into different intervals to evaluate the effect that the selection of different sets of points (x_1-x_2-x_3%) has on the model's accuracy in each interval.

Interval #	Interval	Method #2: (10-50-90%)	Method #4: (10-55-90%)	N_S
1	[0–10%]	$S_{0\text{–}10}(\bar{\theta}_{1,2}) = 2.61\cdot10^{-4}$	$S_{0\text{–}10}(\bar{\theta}_{1,4}) = 2.64\cdot10^{-4}$	46
2	[10–55%]	$S_{10\text{–}55}(\bar{\theta}_{1,2}) = 4.31\cdot10^{-4}$	$S_{10\text{–}55}(\bar{\theta}_{1,4}) = 6.76\cdot10^{-4}$	198
3	[55–90%]	$S_{55\text{–}90}(\bar{\theta}_{1,2}) = 8.11\cdot10^{-5}$	$S_{55\text{–}90}(\bar{\theta}_{1,4}) = 4.90\cdot10^{-5}$	1117
4	[90–100%]	$S_{90\text{–}100}(\bar{\theta}_{1,2}) = 1.14\cdot10^{-5}$	$S_{90\text{–}100}(\bar{\theta}_{1,4}) = 9.06\cdot10^{-6}$	23674
–	[0–100%]	$S(\bar{\theta}_{1,2}) = 1.83\cdot10^{-5}$	$S(\bar{\theta}_{1,4}) = 1.65\cdot10^{-5}$	25001

Table 6.14. Comparison between methods #2 and #4 in terms of time-domain model performance indices for different intervals of the process reaction curve for both identified models. The time-domain performance index for the whole response is also included in this table. N_S represents the number of points for each interval.

Interval #	Interval	Method #5: (20-60-95%)	Method #6: (20-75-95%)	N_S
1	[0–20%]	$S_{0\text{–}20}(\bar{\theta}_{1,5}) = 7.65\cdot10^{-4}$	$S_{0\text{–}20}(\bar{\theta}_{1,6}) = 1.60\cdot10^{-3}$	77
2	[20–50%]	$S_{20\text{–}50}(\bar{\theta}_{1,5}) = 1.60\cdot10^{-3}$	$S_{20\text{–}50}(\bar{\theta}_{1,6}) = 4.10\cdot10^{-3}$	133
3	[50–75%]	$S_{50\text{–}75}(\bar{\theta}_{1,5}) = 9.31\cdot10^{-5}$	$S_{50\text{–}75}(\bar{\theta}_{1,6}) = 5.69\cdot10^{-4}$	288
4	[75–100%]	$S_{75\text{–}100}(\bar{\theta}_{1,5}) = 2.40\cdot10^{-6}$	$S_{75\text{–}100}(\bar{\theta}_{1,6}) = 2.45\cdot10^{-7}$	24503
–	[0–100%]	$S(\bar{\theta}_{1,5}) = 1.44\cdot10^{-5}$	$S(\bar{\theta}_{1,6}) = 3.34\cdot10^{-5}$	25001

Table 6.15. Comparison between methods #5 and #6 in terms of time-domain model performance indices for different intervals of the process reaction curve for both identified models. The time-domain performance index for the whole response is also included in this table. N_S represents the number of points for each interval.

In this regard, Table 6.14 allows the comparison of method #2 with #4 for the intervals [0–10%], [10–55%], [55–90%], and [90–100%], respectively. The comparison of methods #5 and #6 for the intervals [0–20%], [20–50%], [50–75%], and [75–100%], respectively, is shown in Table 6.15.

6.3.2. Example 2

The model (6.5) proposed in (Tavakoli-Kakhki, Haeri and Tavazoei 2010) is considered in this example. This process exhibits a higher-order lag-dominated fractional-order dynamics. The proposed identification method for symmetrical and asymmetrical sets of points are compared with other well-recognized methods for FFOPDT models, which is also based on the process reaction curve, and the optimal FOPDT.

The step-input signal and the process reaction curve for this model are shown in Figure 6.15. The process information summarized in Table 6.16 for the different identification methods is collected from data in Figure 6.15.

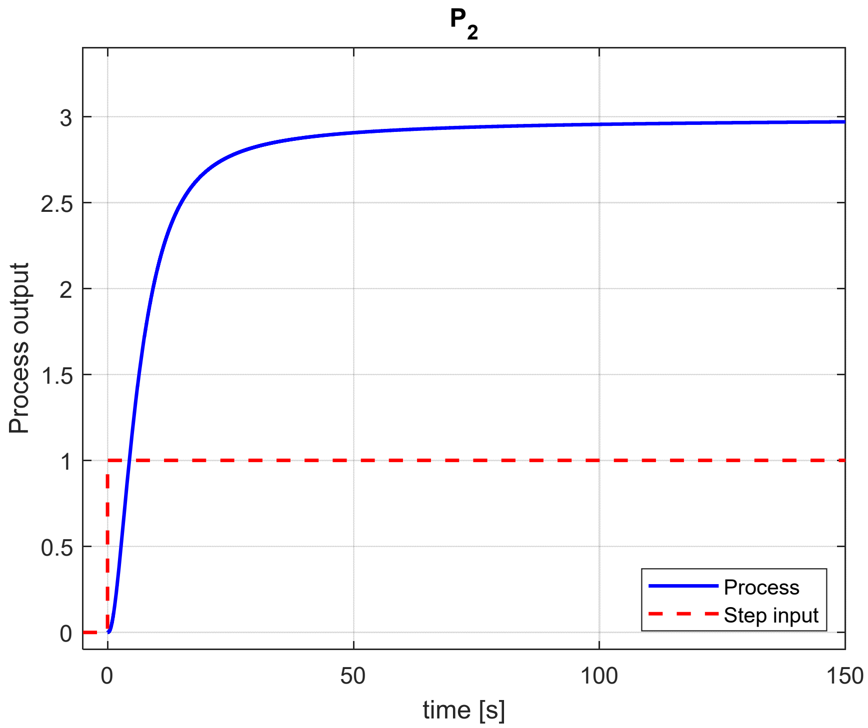

Figure 6.15. Process reaction curve for process P_2 and step-input signal.

With the information collected from Table 6.16, the following FFOPDT model parameters $\bar{\theta}_{2,i} = \{K_{2,i}, T_{2,i}, L_{2,i}, \alpha_{2,i}\}$, for $i = 1, \ldots, 6$, have been obtained in Table 6.17 for the different sets of points, i.e., (5-50-95%), (10-50-90%), (25-50-75%), (10-55-90%), (20-60-95%), and (20-75-95%), respectively.

Symmetrical methods			Asymmetrical methods		
Method #1: (5-50-95%)	**Method #2: (10-50-90%)**	**Method #3: (25-50-75%)**	**Method #4: (10-55-90%)**	**Method #5: (20-60-95%)**	**Method #6: (20-75-95%)**
$\Delta u = 1.00$					
$\Delta y = 3.00$					
$t_5 = 1.4140$ s	$t_5 = 1.4140$ s	$t_5 = 1.4140$ s	$t_5 = 1.4140$ s	$t_5 = 1.4140$ s	$t_5 = 1.4140$ s
$t_{50} = 6.3850$ s	$t_{50} = 6.3850$ s	$t_{50} = 6.3850$ s	$t_{50} = 6.3850$ s	$t_{50} = 6.3850$ s	$t_{50} = 6.3850$ s
$t_{95} = 33.929$ s	$t_{95} = 33.9290$ s	$t_{95} = 33.9290$ s	$t_{95} = 33.9290$ s	$t_{95} = 33.9290$ s	$t_{95} = 33.9290$ s

Table 6.16. Process information collected from the reaction curve for fractional-order model identification of process P_2.

Symmetrical methods			Asymmetrical methods		
Method #1: (5-50-95%)	**Method #2: (10-50-90%)**	**Method #3: (25-50-75%)**	**Method #4: (10-55-90%)**	**Method #5: (20-60-95%)**	**Method #6: (20-75-95%)**
$K_{2,1} = 3.00$	$K_{2,2} = 3.00$	$K_{2,3} = 3.00$	$K_{2,4} = 3.00$	$K_{2,5} = 3.00$	$K_{2,6} = 3.00$
$T_{2,1} = 6.406$ s	$T_{2,2} = 6.6381$ s	$T_{2,3} = 6.6817$ s	$T_{2,4} = 6.3850$ s	$T_{2,5} = 5.1733$ s	$T_{2,6} = 4.6914$ s
$L_{2,1} = 1.263$ s	$L_{2,2} = 1.3955$ s	$L_{2,3} = 1.6203$ s	$L_{2,4} = 1.4329$ s	$L_{2,5} = 2.4042$ s	$L_{2,6} = 2.5096$ s
$\alpha_{2,1} = 0.9189$	$\alpha_{2,2} = 0.9470$	$\alpha_{2,3} = 0.9802$	$\alpha_{2,4} = 0.9391$	$\alpha_{2,5} = 0.8901$	$\alpha_{2,6} = 0.8759$

Table 6.17. Fractional-order model settings for the symmetrical and asymmetrical sets of points (5-50-95%), (10-50-90%), (25-50-75%), (10-55-90%), (20-60-95%), and (20-75-95%), respectively.

Process (6.5) is also approximated by a FFOPDT model following the method proposed by Tavakoli-Kakhki in (Tavakoli-Kakhki, Haeri and Tavazoei 2010), by a FFOPDT model obtained using the optimization-based method proposed by Guevara et al. in (Guevara, et al. 2015), and by the optimal FOPDT model, where model parameters, $\bar{\theta}_{2,i}$, for $i = 7, 8$, and 9, respectively, are given in Table 6.18.

Note that the method proposed in (Guevara, et al. 2015) is based on optimization, where the function to be minimized is $E(\bar{\theta})$ (6.7). In this method, the approximation of the fractional term s^{α} is developed using the Oustaloup method; see (Monje, Chen, et al. 2010). In contrast, the parameters obtained in the optimal FOPDT model are those that minimize the function $S(\bar{\theta})$ (4.20).

Method #7: FFOPDT Tavakoli-Kakhki	**Method #8: FFOPDT Guevara *et al.***	**Method #9: FOPDT optimal**
$K_{2,7} = 3.00$	$K_{2,8} = 3.0000$	$K_{2,9} = 3.0000$
$T_{2,7} = 6.30$ s	$T_{2,8} = 5.6285$ s	$T_{2,9} = 8.7412$ s
$L_{2,7} = 1.00$ s	$L_{2,8} = 1.8833$ s	$L_{2,9} = 0.0000$ s
$\alpha_{2,7} = 0.92$	$\alpha_{2,8} = 0.9263$	–

Table 6.18. FFOPDT model parameters obtained using methods proposed by Tavakoli-Kakhki (Tavakoli-Kakhki, Haeri and Tavazoei 2010) and by Guevara et al. (Guevara, et al. 2015), and optimal FOPDT model parameters, respectively, for process P_2.

The step responses of the considered approximated models for (5-50-95%), (10-50-90%), (25-50-75%), (10-55-90%), (20-60-95%), and (20-75-95%), respectively, are compared with the process reaction curve and illustrated in Figures 6.16 – 6.21. The corresponding representative points, symmetrical (x-50-(100–x)%) and asymmetrical (x_1-x_2-x_3%), respectively, are also displayed in these figures. Moreover, the process re-action curve and the step responses of the FFOPDT model proposed by Tavakoli-Kakhki, the FFOPDT model obtained using the method proposed by Guevara et al., and the optimal FOPDT model, respectively, are shown in Figure 6.22.

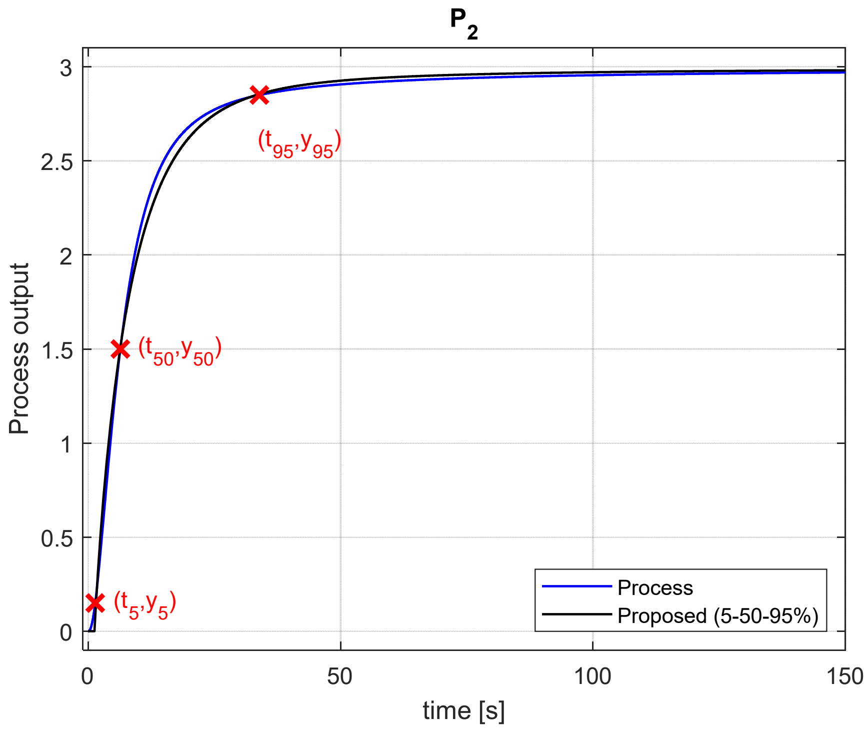

Figure 6.16. FFOPDT model step response using the proposed identification method for process P_2 and process reaction curve: Symmetrical set of points (5-50-95%); (b) Symmetrical set of points (10-50-90%).

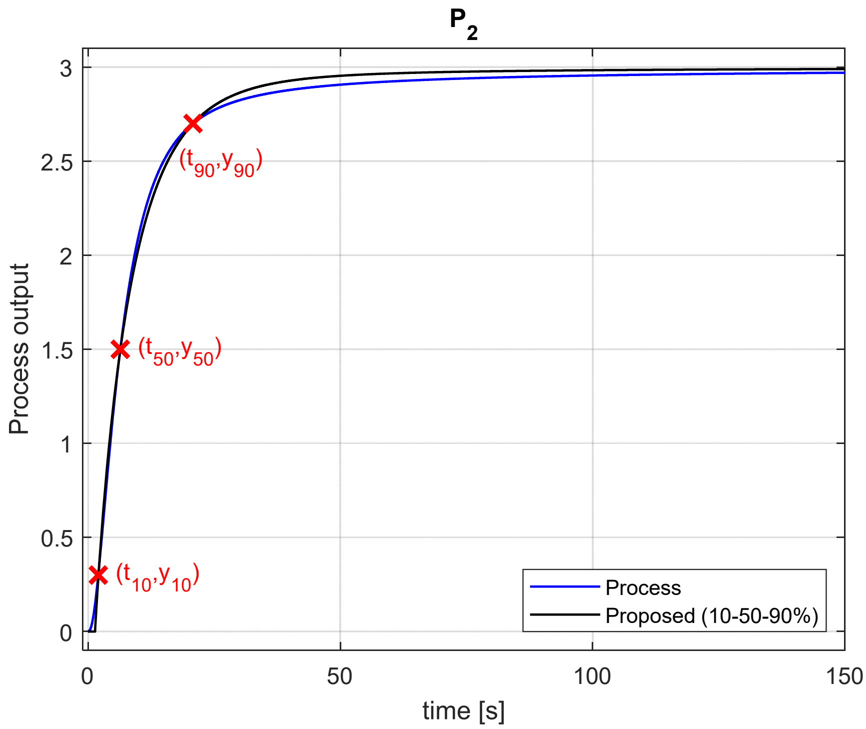

Figure 6.17. FFOPDT model step response using the proposed identification method for process P_2 and process reaction curve: Symmetrical set of points (10-50-90%).

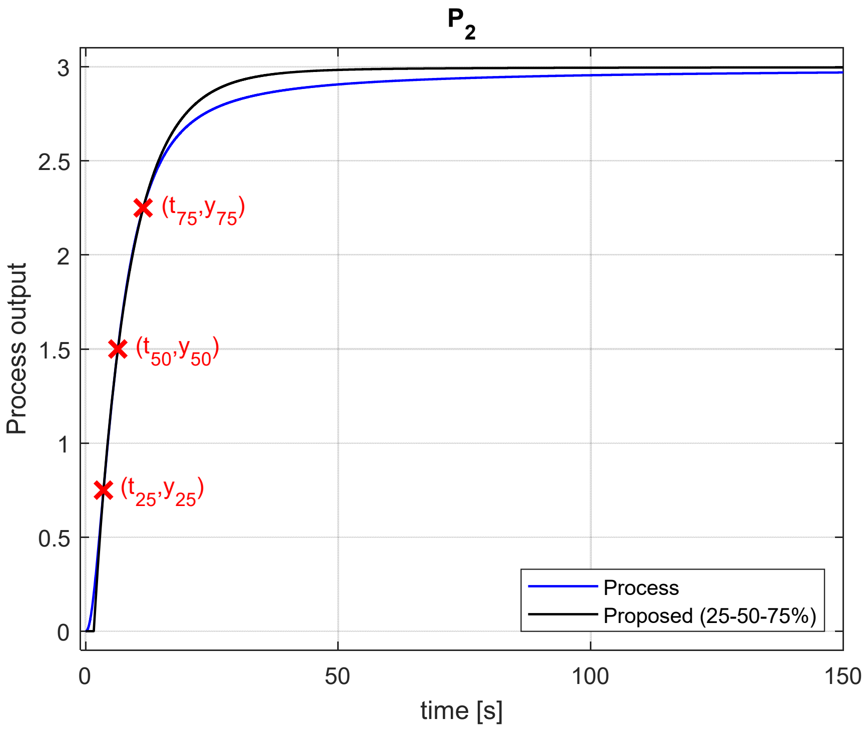

Figure 6.18. FFOPDT model step response using the proposed identification method for process P_2 and process reaction curve: Symmetrical set of points (25-50-75%).

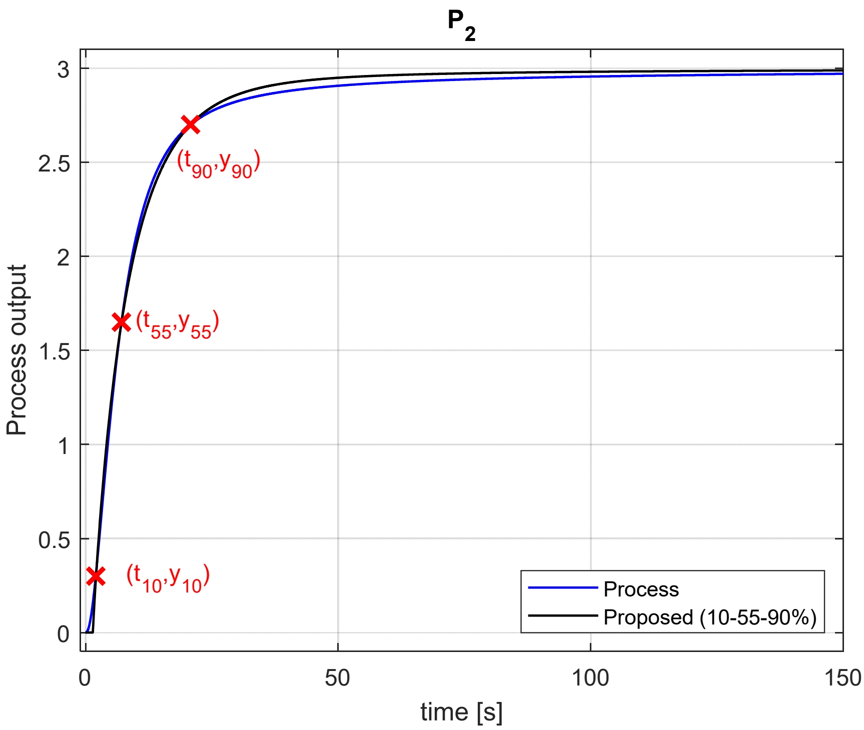

Figure 6.19. FFOPDT model step response using the proposed identification method for process P_2 and process reaction curve: Asymmetrical set of points (10-55-90%).

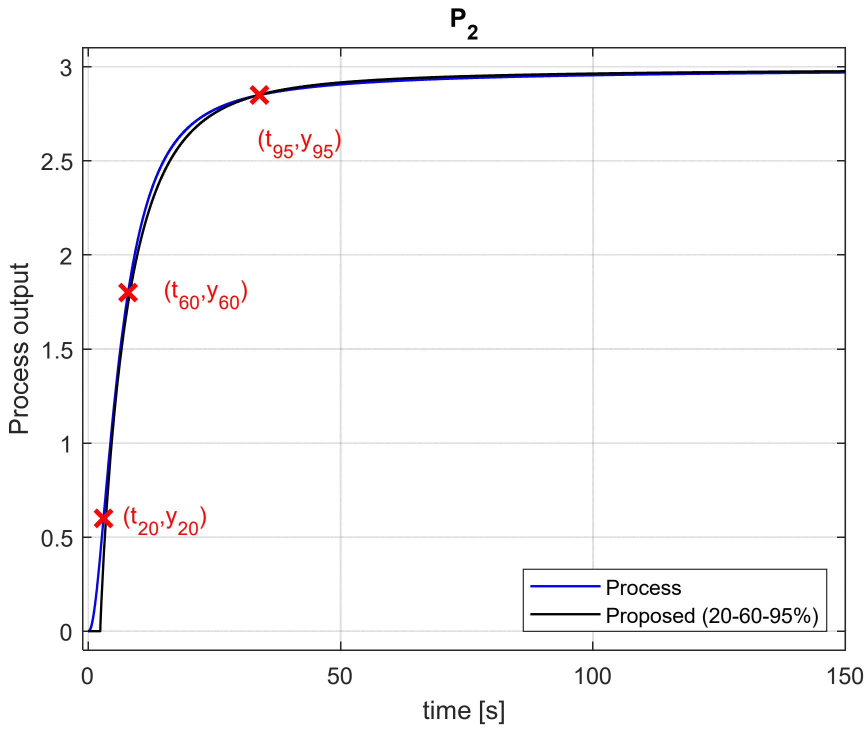

Figure 6.20. FFOPDT model step response using the proposed identification method for process P_2 and process reaction curve: Asymmetrical set of points (20-60-95%).

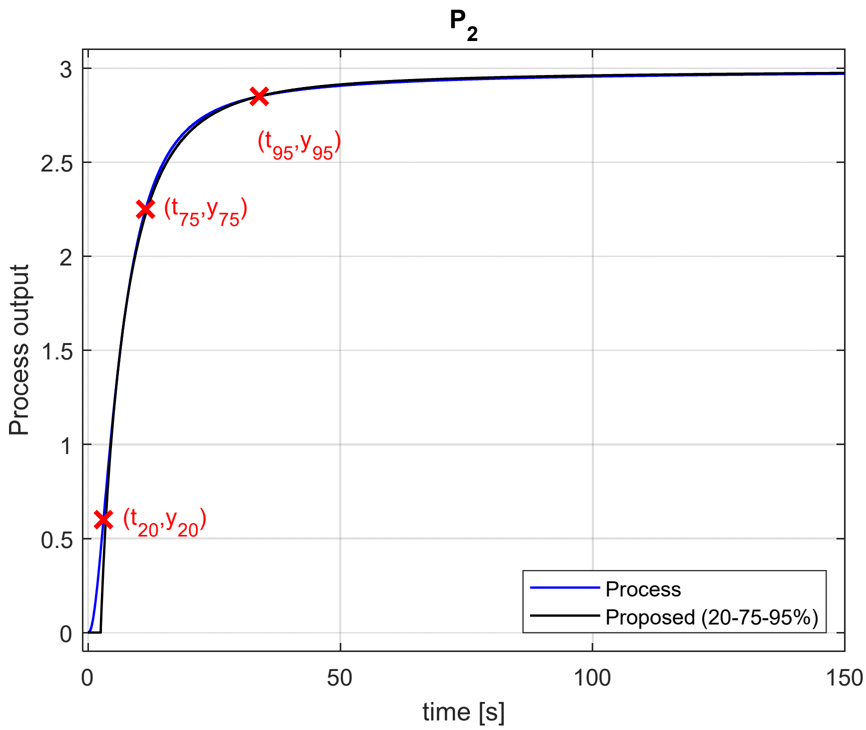

Figure 6.21. FFOPDT model step response using the proposed identification method for process P_2 and process reaction curve: Asymmetrical set of points (20-75-95%).

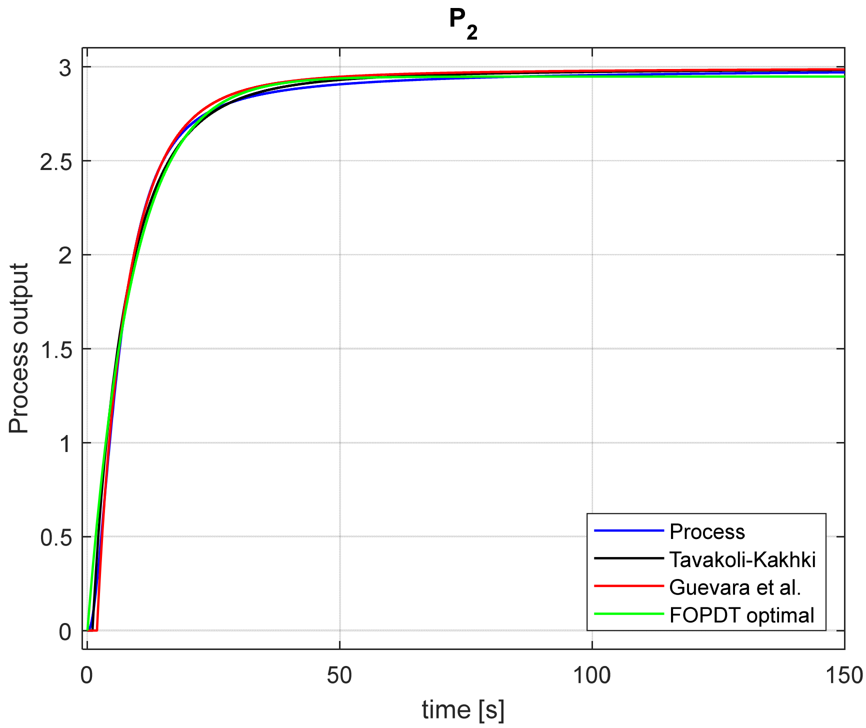

Figure 6.22. Step response of the FFOPDT model obtained using methods #7, #8, and #9 for process P_2 and process reaction curve.

In this example, a high-order process model has been utilized to demonstrate the effectivity and applicability of the proposed identification procedure in the task of estimating FFOPDT-type model parameters.

Similarly to the previous example, Figures 6.16 – 6.21 illustrate that the models obtained with the proposed method, for both the symmetrical and asymmetrical case, provide a good fit with the process reaction curve also for a higher-order lag-dominated fractional-order process in comparison with the results obtained using the well-recognized method proposed by Tavakoli-Kakhki, and even in comparison with optimization-based methods for FFOPDT and FOPDT models. These results are shown in Figure 6.22.

Figures 6.16 – 6.18 show that the proposed method for the symmetrical case gives good results in the interval $[x - (100–x)\%]$. For this reason, better results are obtained for low values of x, as discussed in Chapter 4. Figures 6.19 – 6.21 show that by moving the points x_1, x_2, and x_3 of the reaction curve it is possible to obtain a FFOPDT model which step response can be better fitted to the reaction curve in certain intervals, as will be shown below. Table 6.19 shows the values of the time-domain performance indexes $S(\overline{\theta}_{2,i})$ and $E(\overline{\theta}_{2,i})$ for process P_2, and the ones corresponding to the intervals $[0–50\%]$, $S_{0–50}(\overline{\theta}_{2,i})$, and $[50–100\%]$, $S_{50–100}(\overline{\theta}_{2,i})$, of the total process output change, respectively, for the different models considered in this example. In this table, $i = 1, …, 6$ represents the different sets of points considered in the proposed identification method, and $i = 7, 8$, and 9 represents methods #7 and #8 for FFOPDT models, and #9 for FOPDT, respectively.

Note that from expression (6.8) the following relation that must be fulfilled can be particularized for this case:

$$S(\bar{\theta}_{2,i}) = S_{0-100}(\bar{\theta}_{2,i}) = \frac{1}{N_s}\left[S_{0-50}(\bar{\theta}_{2,i}) \cdot N_{s1} + S_{50-100}(\bar{\theta}_{2,i}) \cdot N_{s2}\right] \tag{6.10}$$

Table 6.19 shows that the accuracy of models obtained with methods #1, #5, and #6 is better in terms of E than the one obtained for methods #7 and #8. The proposed method for all the sets of points except #3 provides models with lower values of E than for the optimal FOPDT model.

i	Method	Set of points	$S_{0-50}(\bar{\theta}_{1,i})$	$S_{50-100}(\bar{\theta}_{1,i})$	$S(\bar{\theta}_{1,i})$	$E(\bar{\theta}_{1,i})$
1	FFOPDT Proposed #1	(5-50-95%)	$5.80\cdot10^{-3}$	$8.78\cdot10^{-4}$	$1.10\cdot10^{-3}$	$2.40\cdot10^{-2}$
2	FFOPDT Proposed #2	(10-50-90%)	$2.80\cdot10^{-3}$	$1.20\cdot10^{-3}$	$1.30\cdot10^{-3}$	$3.34\cdot10^{-2}$
3	FFOPDT Proposed #3	(25-50-75%)	$4.40\cdot10^{-3}$	$3.33\cdot10^{-3}$	$3.30\cdot10^{-3}$	$5.14\cdot10^{-2}$
4	FFOPDT Proposed #4	(10-55-90%)	$3.80\cdot10^{-3}$	$9.58\cdot10^{-4}$	$1.10\cdot10^{-3}$	$3.02\cdot10^{-2}$
5	FFOPDT Proposed #5	(20-60-95%)	$2.78\cdot10^{-2}$	$4.53\cdot10^{-4}$	$1.60\cdot10^{-3}$	$1.92\cdot10^{-2}$
6	FFOPDT Proposed #6	(20-75-95%)	$2.88\cdot10^{-2}$	$1.01\cdot10^{-4}$	$1.30\cdot10^{-3}$	$1.24\cdot10^{-2}$
7	FFOPDT Tavakoli-Kakhki	–	$2.02\cdot10^{-2}$	$5.25\cdot10^{-4}$	$1.40\cdot10^{-3}$	$2.47\cdot10^{-2}$
8	FFOPDT Guevara	–	$8.30\cdot10^{-3}$	$8.23\cdot10^{-4}$	$1.10\cdot10^{-3}$	$2.82\cdot10^{-2}$
9	FOPDT optimal	–	$4.55\cdot10^{-2}$	$9.07\cdot10^{-4}$	$2.80\cdot10^{-3}$	$2.95\cdot10^{-2}$
	Number of samples		$N_{S1} = 639$	$N_{S2} = 14362$	$N_S = 15001$	$N_S = 15001$

Table 6.19. Comparison between the performance indexes obtained for the proposed method with different sets of points, symmetrical and asymmetrical, and the ones for several methods for FFOPDT and FOPDT models. The number of samples N_S for the whole range and for each interval are also displayed.

For the sake of simplicity in the interpretation of results, information taken from Table 6.19 is depicted in Figure 6.23.

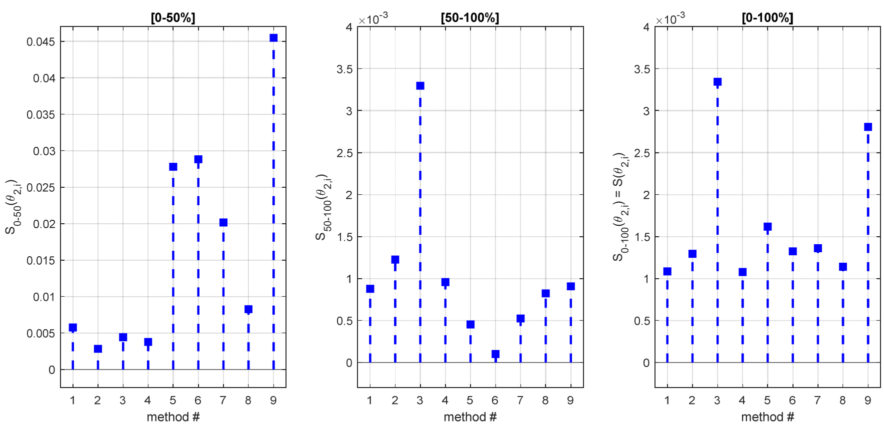

Figure 6.23. Graphical representation of data given in Table 6.19 for process P_2. From left to right the performance indices $S_{0-50}(\bar{\theta}_{2,i})$, $S_{50-100}(\bar{\theta}_{2,i})$, and $S(\bar{\theta}_{2,i})$, i = 1, …, 9, are shown, respectively, for each of the considered methods.

Figure 6.23 illustrates that the accuracy of the models obtained with the proposed method for the symmetrical and asymmetrical case is similar to the one obtained using the method proposed by Guevara et al., and even better than that obtained with a well-known identification method such as the one proposed by Tavakoli-Kakhki, or than the optimal FOPDT model. Note that the method proposed by Guevara et al. is based on optimization, while the method proposed in this paper is analytical.

Specifically, the value of the time-domain model performance index of methods #1, #2, #4, and #6 are lower than the one proposed by Tavakoli-Kakhki, confirming the effectiveness of the proposed method for both the symmetrical and the asymmetrical case. Furthermore, the proposed method not only gives better results than the Tavakoli-Kakhki’s method in terms of S, but in the authors' opinion it is easier to apply.

The S-value of the model obtained with method #5 is slightly higher than the one by Tavakoli-Kakhki, while the one obtained with method #3 is substantially higher than the rest. This fact has already been discussed above and also in Chapter 4 for the symmetrical case and the choice of this method among the symmetrical methods allows to determine that the accuracy of models obtained is improved for low values of x in the symmetrical case, and high values of x_3 for the asymmetrical case.

Results in Table 6.19 confirm the same observations taken from Example 1:

1. Methods with low values of x_1 for the asymmetrical case, or x in the symmetrical case, present low values of S_{0-50}, as can be seen in Figure 6.19 for methods #1, #2 and #4.
2. Methods with high values of x_3 for the asymmetric case present a lower value of S_{50-100}, as can be observed for methods #4, and especially for #5 and #6. For the symmetrical case, methods #1 and #2, with low values of x and high values of $(100–x)$, present good values of S_{0-50} and S_{50-100}, as expected.
3. Comparison of methods #2 and #4 yields the same conclusions as for Example 1.
4. The observations drawn from Example 1 for the comparison of methods #5 and #6 are also extensible to Example 2.

The comparison of method #7 with the methods providing the best results in terms of S is then performed by dividing the reaction curve and the respective step responses of the obtained models into different intervals.

It can be extracted from data taken from Table 6.19 that the best results in terms of S are those obtained with models determined using method #1 for the symmetrical case and #4 for the asymmetrical case. Then, the step responses of the models obtained us-ing methods #1, #4, and #7 are divided into 4 intervals, i.e., [0–10%], [10–50%], [50–90%], and [90–100%], respectively. Table 6.20 provides a comparison of these methods for the aforementioned intervals.

#	Interval	Method #1: (5-50-95%)	Method #4: (10-55-90%)	Method #7	N_S
1	[0–10%]	$S_{0-10}(\bar{\theta}_{2,1}) = 2.8\cdot10^{-3}$	$S_{0-10}(\bar{\theta}_{2,4}) = 5.70\cdot10^{-3}$	$S_{0-10}(\bar{\theta}_{2,7}) = 4.80\cdot10^{-3}$	203
2	[10–50%]	$S_{10-50}(\bar{\theta}_{2,1}) = 7.2\cdot10^{-3}$	$S_{10-50}(\bar{\theta}_{2,4}) = 2.9\cdot10^{-3}$	$S_{10-50}(\bar{\theta}_{2,7}) = 2.73\cdot10^{-2}$	436
3	[50–90%]	$S_{50-90}(\bar{\theta}_{2,1}) = 6.1\cdot10^{-3}$	$S_{50-90}(\bar{\theta}_{2,4}) = 1.3\cdot10^{-3}$	$S_{50-90}(\bar{\theta}_{2,7}) = 2.30\cdot10^{-3}$	1442
4	[90–100%]	$S_{90-100}(\bar{\theta}_{2,1}) = 3\cdot10^{-4}$	$S_{90-100}(\bar{\theta}_{2,4}) = 9.2\cdot10^{-5}$	$S_{90-100}(\bar{\theta}_{2,7}) = 3.26\cdot10^{-4}$	12920
–	[0–100%]	$S(\bar{\theta}_{2,1}) = 1.10\cdot10^{-3}$	$S(\bar{\theta}_{2,4}) = 1.10\cdot10^{-3}$	$S(\bar{\theta}_{2,7}) = 1.40\cdot10^{-3}$	15001

Table 6.20. Comparison between methods #1, #4, and #7 in terms of time-domain model performance indexes for different intervals of the process reaction curve for both identified models. The time-domain performance index for the whole response is also included in this table. N_S represents the number of points for each interval.

Note that from expression (6.8) the following relation must be fulfilled:

$$S(\bar{\theta}_{2,i}) = S_{0-100}(\bar{\theta}_{2,i}) = \\ = \frac{1}{N_s}\left[S_{0-10}(\bar{\theta}_{2,i})\cdot N_{s1} + S_{10-50}(\bar{\theta}_{2,i})\cdot N_{s2} \\ + S_{50-90}(\bar{\theta}_{2,i})\cdot N_{s3} + S_{90-100}(\bar{\theta}_{2,i})\cdot N_{s4}\right] \tag{6.11}$$

Figure 6.24 represents graphically the information taken from Table 6.20, which simplifies the interpretation of results.

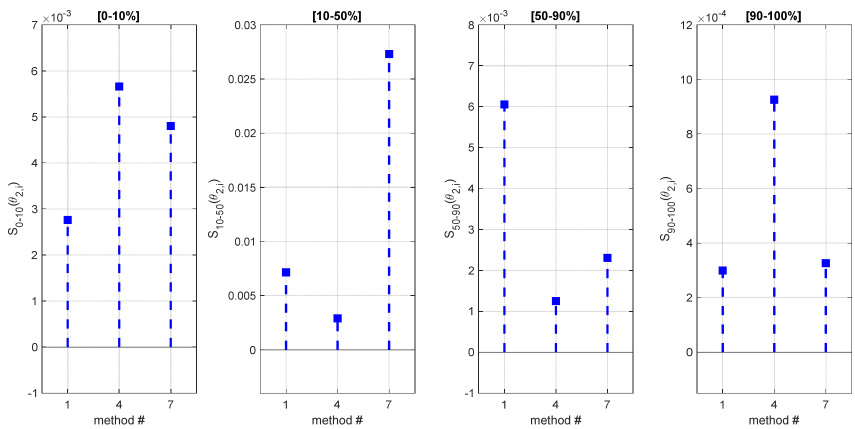

Figure 6.24. Graphical representation of data given in Table 6.20 for process P_2. From left to right the performance indexes $S_{0-10}(\bar{\theta}_{2,i})$, $S_{10-50}(\bar{\theta}_{2,i})$, $S_{50-90}(\bar{\theta}_{2,i})$, and $S_{90-100}(\bar{\theta}_{2,i})$, are shown for methods #1, #4, and #7, respectively.

Information about the accuracy of the model obtained at the different intervals of the reaction curve can be extracted from Table 6.20. Specifically, it can be seen that method #1 provides a model that fits the reaction curve very well in the intervals [0–10%], [10–50%] and [90–100%], while the fit is worse in the interval [50–90%], as can also be seen in Figure 6.16. This method provides the best results of the three compared methods in the intervals [0–10%] and [90–100%].

The model for method #4 fits very well in the intervals [10–50%] and [50–90%], where it presents the lowest values of the three compared methods. In contrast, the value of S increases outside these intervals, as can also be seen in Figure 6.19.

The model proposed by Tavakoli-Kakhki provides a good fit in the intervals [50–90%] and [90–100%], while the results for the rest of intervals are worse, particularly for [10–50%].

6.3.3. Example 3

The model (6.6), which has been proposed in (Åström and Hägglund 2000) as part of a collection of systems that are suitable for testing PID controllers, is considered in this example.

Physically, this transfer function describes how temperature evolves over time in a solid medium, which assumes that the temperature is distributed in only one spatial coordinate and the heat is transferred in the direction in which the temperature decreases. This ideal transfer function contains the irrational operator $\sqrt{s}$ which may cause difficulties in a further analytical analysis.

In general, temperature control is a widespread application in the process industry, and, in particular, thermal conduction is a very common dynamic in process control.

Traditionally, FOPDT model has been utilized to approximate this dynamic, however, with insufficient accuracy. Since a growing body of evidence has suggested that fractional-order models are able to describe dynamic processes with higher accuracy, the proposed identification method will be used to more accurately model this process, which exhibits fractional behaviour.

In order to evaluate the effectiveness of the proposed method, the estimated models for the symmetrical and asymmetrical cases will be compared with the optimal FOPDT and FFOPDT models, respectively.

Following the same procedure used in previous examples, the following FFOPDT model parameters $\bar{\theta}_{3,i} = \{K_{3,i}, T_{3,i}, L_{3,i}, \alpha_{3,i}\}$ for $i = 1, \ldots, 6$, have been obtained in Table 6.21 for the different sets of points, i.e., (5-50-95%), (10-50-90%), (25-50-75%), (10-55-90%), (20-60-95%), and (20-75-95%), respectively. Model parameters for optimal FFOPDT and FOPDT models have also been calculated. Process (6.6) has also been approximated by the optimal FFOPDT and FOPDT models, where model parameters $\bar{\theta}_{3,i}$ for $i = 7$ and 8, respectively, are given in Table 6.21. Note that the parameters obtained in the optimal models are those that minimize the function $S(\bar{\theta})$ (4.20). Since the Taylor series expansion for the irrational transfer function (6.6) give a polynomial of half order integrators $s^{0.5}$, $\alpha_{3,7}$ has been considered to be 0.5.

Method #1: (5-50-95%)	Method #2: (10-50-90%)	Method #3: (25-50-75%)	Method #4: (10-55-90%)	Method #5: (20-60-95%)	Method #6: (20-75-95%)
$K_{3,1}$ = 1.00	$K_{3,2}$ = 1.00	$K_{3,3}$ = 1.00	$K_{3,4}$ = 1.00	$K_{3,5}$ = 1.00	$K_{3,6}$ = 1.00
$T_{3,1}$ = 1.26 s	$T_{3,2}$ = 1.26 s	$T_{3,3}$ = 1.22 s	$T_{3,4}$ = 1.22 s	$T_{3,5}$ = 1.13 s	$T_{3,6}$ = 1.08 s
$L_{3,1}$ = 0.00 s	$L_{3,2}$ = 0.60 s	$L_{3,3}$ = 0.22 s	$L_{3,4}$ = 0.67 s	$L_{3,5}$ = 0.00 s	$L_{3,6}$ = 0.00 s
$\alpha_{3,1}$ = 0.5368	$\alpha_{3,2}$ = 0.9545	$\alpha_{3,3}$ = 0.5598	$\alpha_{3,4}$ = 0.5401	$\alpha_{3,5}$ = 0.5206	$\alpha_{3,6}$ = 0.5140

Table 6.21. Fractional-order model settings for the symmetrical and asymmetrical sets of points (5-50-95%), (10-50-90%), (25-50-75%), (10-55-90%), (20-60-95%), and (20-75-95%), respectively, for process P_3.

#7: FFOPDT optimal	#8: FOPDT optimal
$K_{3,7}$ = 1.02	$K_{3,8}$ = 0.91
$T_{3,7}$ = 1.23 s	$T_{3,8}$ = 2.24 s
$L_{3,7}$ = 0.0001 s	$L_{3,8}$ = 0.00 s
$\alpha_{3,7}$ = 0.5000	–

Table 6.22. Optimal FFOPDT and FOPDT model parameters for process P_3.

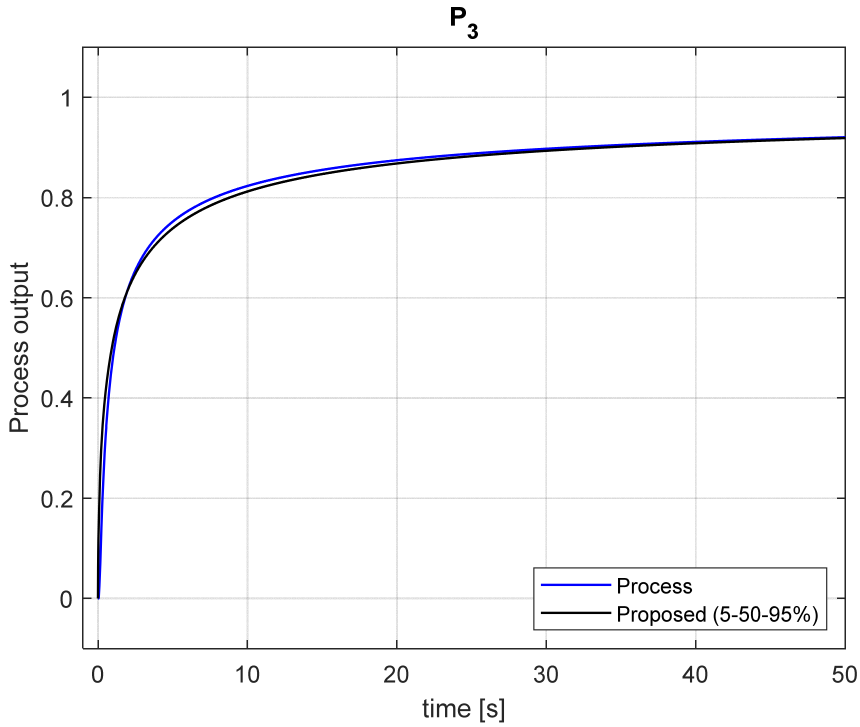

Figure 6.25. FFOPDT model step response using the proposed identification method for process P_3 and process reaction curve: Symmetrical set of points (5-50-95%).

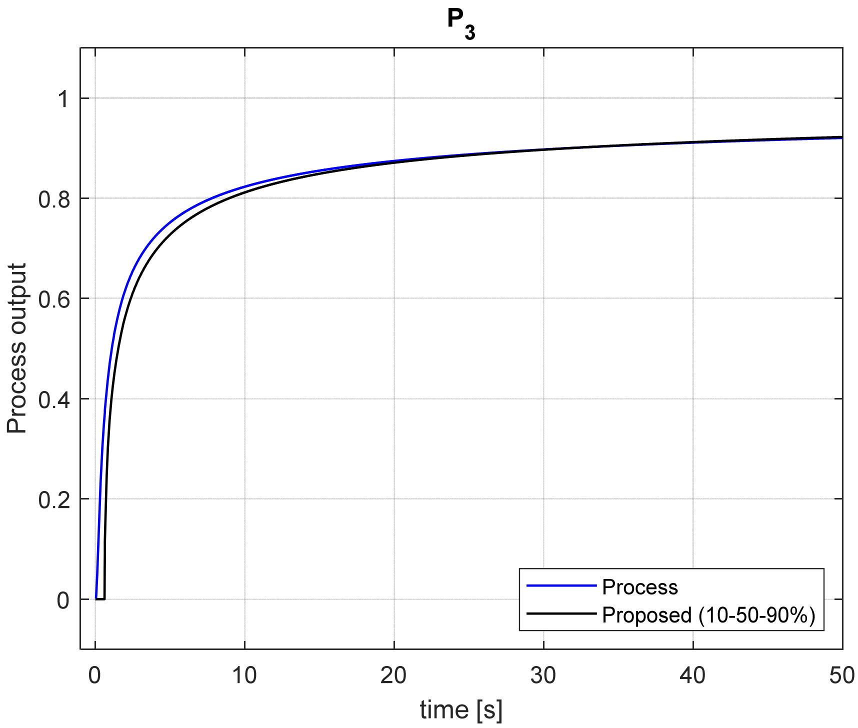

Figure 6.26. FFOPDT model step response using the proposed identification method for process P_3 and process reaction curve: Symmetrical set of points (10-50-90%).

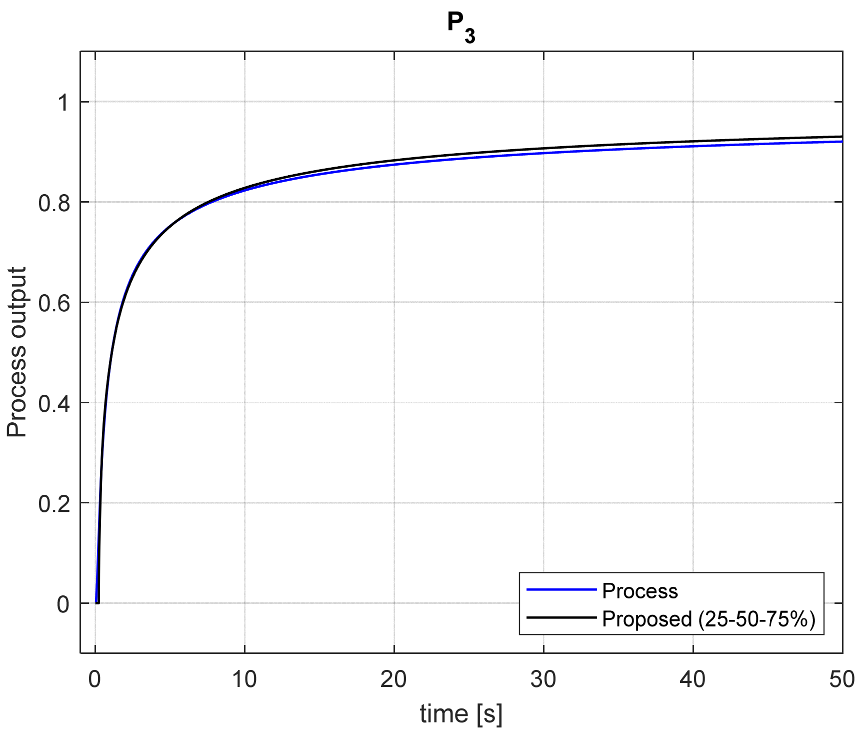

Figure 6.27. FFOPDT model step response using the proposed identification method for process P_3 and process reaction curve: Symmetrical set of points (25-50-75%).

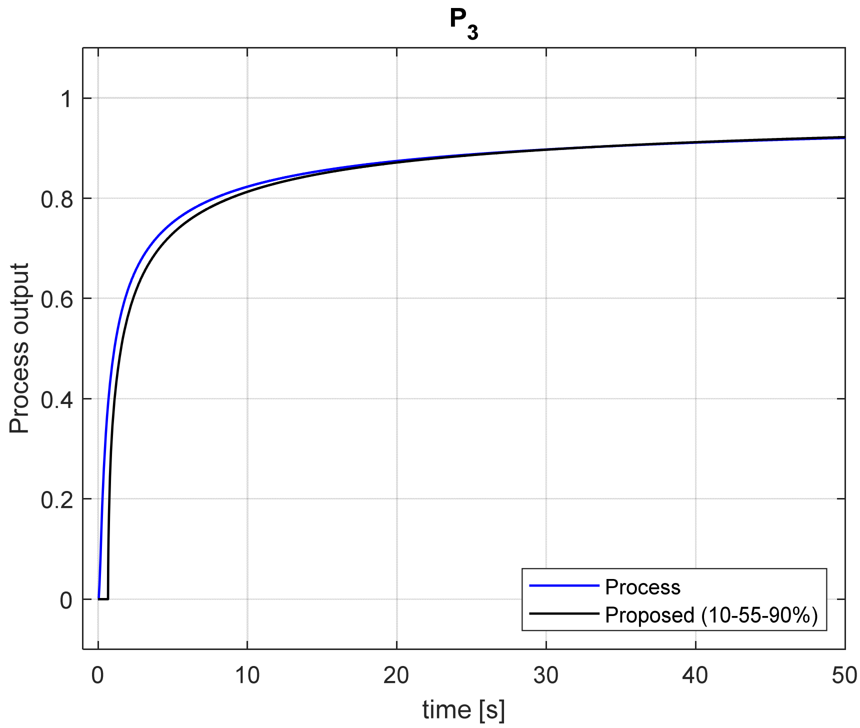

Figure 6.28. FFOPDT model step response using the proposed identification method for process P_3 and process reaction curve: Asymmetrical set of points (10-55-90%).

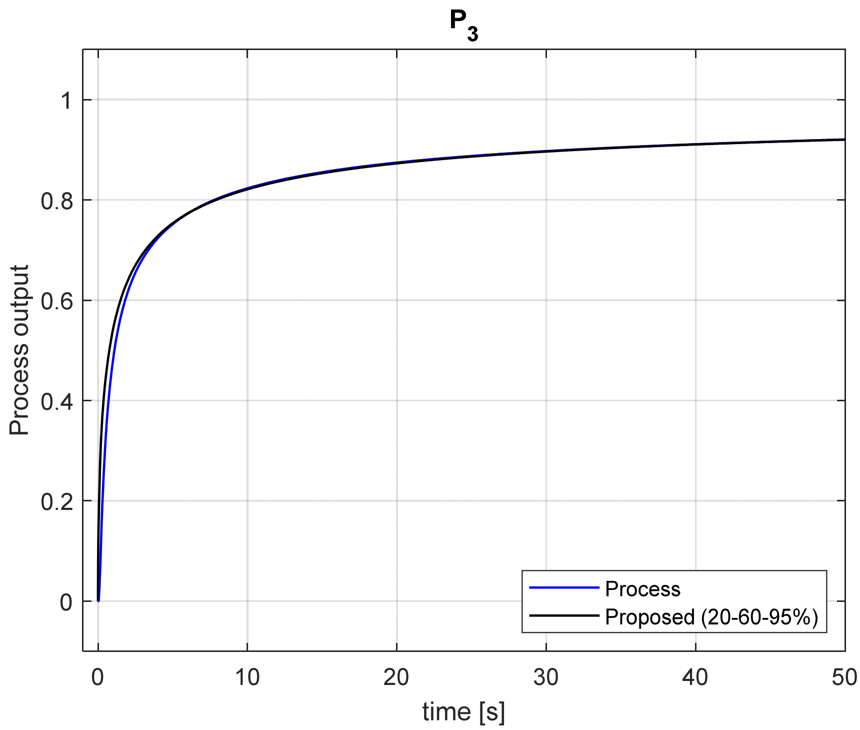

Figure 6.29. FFOPDT model step response using the proposed identification method for process P_3 and process reaction curve: Asymmetrical set of points (20-60-95%).

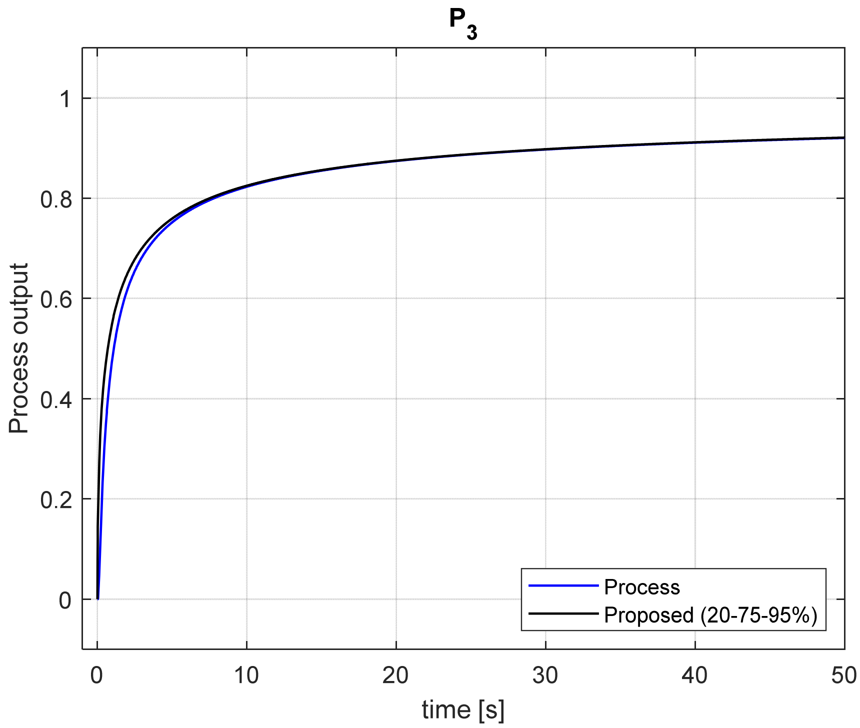

Figure 6.30. FFOPDT model step response using the proposed identification method for process P_3 and process reaction curve: Asymmetrical set of points (20-75-95%).

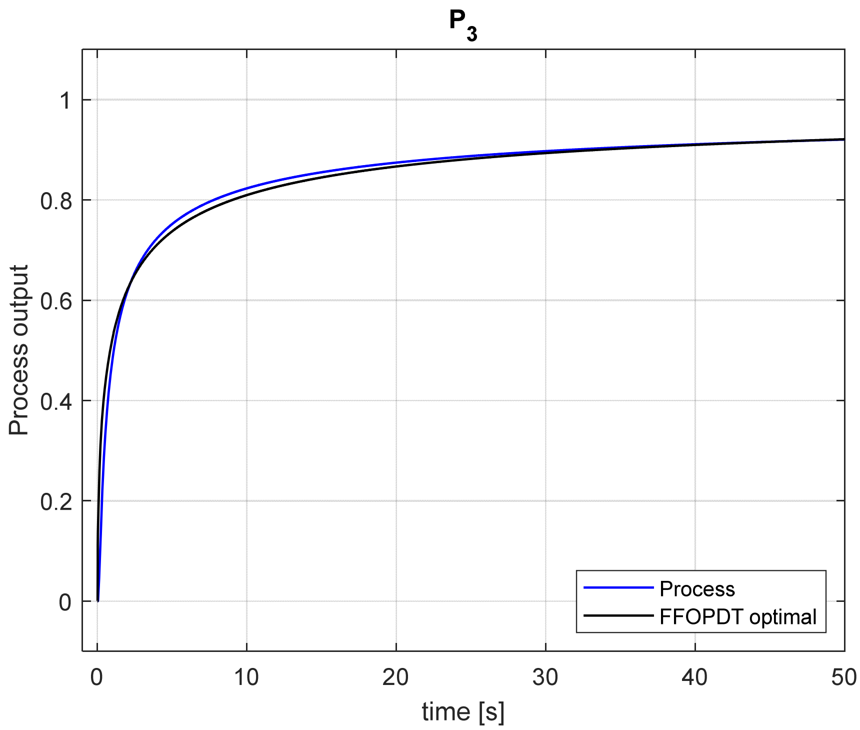

Figure 6.31. Optimal FFOPDT model step response using the proposed identification method for process P_3 and process reaction curve.

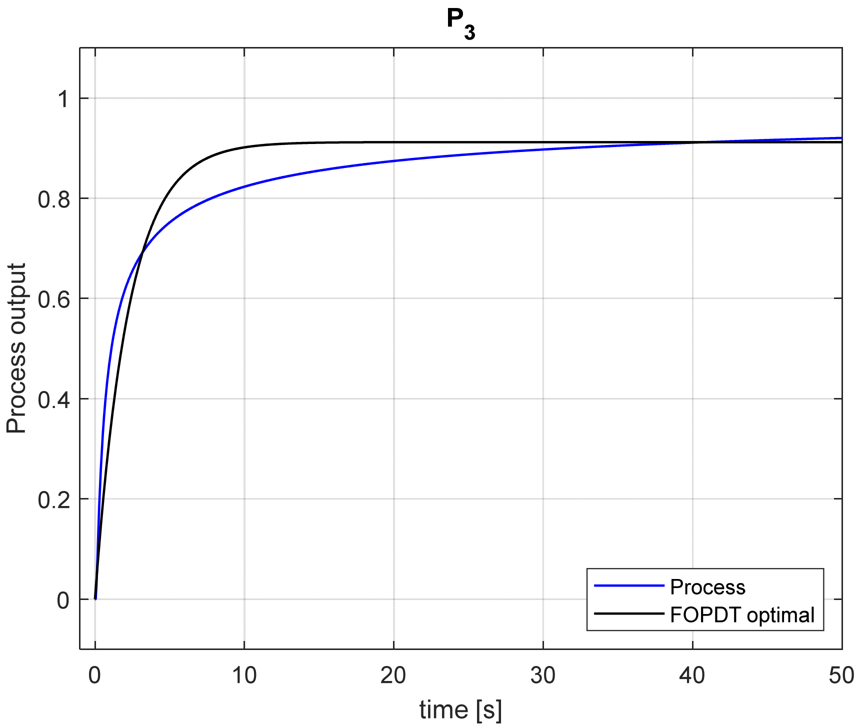

Figure 6.32. Optimal FOPDT model step response using the proposed identification method for process P_3 and process reaction curve.

Figures 6.25 – 6.30 illustrate that the models obtained with the proposed method, for both the symmetrical and asymmetrical case, provide a good fit with the process reaction curve compared to the results obtained using the optimal FFOPDT, which is shown in Figure 6.31. It can also be observed that the proposed method outperforms the results obtained using the optimal FOPDT model, which is shown in Figure 6.32.

Table 6.23 shows the values of the time-domain performance indexes $S(\bar{\theta}_{3,i})$ and $E(\bar{\theta}_{3,i})$ for process P_3, for the different models considered in this example. In this table, $i = 1, \ldots, 6$ represents the different sets of points considered in the proposed identification method, and $i = 7$ and 8 represents optimal FFOPDT and FOPDT models, respectively.

Table 6.23 shows that methods #1, #5, and #6 provide E values comparable to that obtained for the optimal FFOPDT model. On the other hand, it is also observed that the FOPDT model approximates the process dynamics with insufficient accuracy. In fact, for example, methods #1, #5, and #6 have E values that are 10.3, 15.4, and 12.3 times lower than that obtained by the optimal FOPDT model.

i	Method	Set of points	$S(\overline{\theta}_{3,i})$	$E(\overline{\theta}_{3,i})$
1	FFOPDT Proposed #1	(5-50-95%)	$1.00 \cdot 10^{-4}$	$3.00 \cdot 10^{-3}$
2	FFOPDT Proposed #2	(10-50-90%)	$3.60 \cdot 10^{-4}$	$5.70 \cdot 10^{-3}$
3	FFOPDT Proposed #3	(25-50-75%)	$8.97 \cdot 10^{-5}$	$8.90 \cdot 10^{-3}$
4	FFOPDT Proposed #4	(10-55-90%)	$4.19 \cdot 10^{-4}$	$5.40 \cdot 10^{-3}$
5	FFOPDT Proposed #5	(20-60-95%)	$1.41 \cdot 10^{-4}$	$2.00 \cdot 10^{-3}$
6	FFOPDT Proposed #6	(20-75-95%)	$1.73 \cdot 10^{-4}$	$2.50 \cdot 10^{-3}$
7	FFOPDT optimal	–	$1.47 \cdot 10^{-4}$	$6.40 \cdot 10^{-3}$
8	FOPDT optimal	–	$1.40 \cdot 10^{-3}$	$3.08 \cdot 10^{-2}$
	Number of samples		**N_S = 15001**	**N_S = 15001**

Table 6.23. Comparison between the performance indexes obtained for the proposed method with different sets of points, symmetrical and asymmetrical, and the ones for optimal methods for FFOPDT and FOPDT models. The number of samples N_S is also displayed.

6.3.4. Discussion and final remarks

This section provides some final remarks and discussion about the results obtained in this chapter.

Remark 1: Measurement noise

The main disadvantage provided by the use of feedback is that measurement noise is injected into the loop. Noise generally generates undesirable motion of the final controlling elements, which may cause wear and possible break down.

It is common practice that open-loop model identification procedures use process information based on noise-free process reaction curve; see, e.g., (Liu and Gao 2012) for integer-order systems, and (Tavakoli-Kakhki, Haeri and Tavazoei 2010) for fractional-order systems. However, it is usual in an industrial environment that the controlled process feedback signal includes measurement noise that must be properly filtered for model identification and control purposes.

It is important to take into account that the filter dynamics will be an integral part of the controlled process to be identified. As this will influence and add a lag to the loop dynamics, measurement filter must be set before any controlled process model identification and/or controller tuning (Alfaro and Vilanova 2021).

In this context, it is very difficult to derive general conclusions about the influence of measurement noise on the identification procedure, because this will depend on the measurement noise and filter characteristics.

The results of the experiment conducted in this section serve to demonstrate the applicability of the proposed identification method on a laboratory equipment and its implementation on an industrial control hardware, which presents similarities with the industrial environment.

Remark 2: Model uncertainty

In the industrial context, processes exhibit nonlinearities, i.e., the dynamic characteristics of the process and therefore those of the identified FFOPDT model –gain, time constant, apparent dead-time and fractional order– will change with the operating point. The operating point of a control system may vary due to a change in the setpoint or as a result of the effect of disturbances.

Therefore, it must be considered that there is an implicit uncertainty in the nominal model.

In general, there are two approaches in the technical literature when considering the parametric uncertainty of the plant in an identification method; see Chapter 4.

1. The first approach is to incorporate the uncertainty explicitly into the model. This typically makes the identification procedure to become more complicated.
2. The second approach consists of taking into account the potential changes in the controlled process dynamics and model uncertainties in the design phase of the controller; see, e.g., (Åström and Hägglund 2006) for integer-order controllers and (Monje, Chen, et al. 2010) for fractional-order controllers. A common application of this second approach is to ensure a certain degree of robustness of the designed control system to guarantee its stability under variations in the process characteristics.

In the context of this work, the primary use of the identified fractional-order model is for control purposes. Consequently, the approach to be used will be the second one.

Rules of thumb in selecting sets of points

In Sections 6.2.1 and 6.2.2 some rules of thumb, which are based on experimentation, have been provided to get insight about the selection of the points for the symmetrical and asymmetrical case, respectively, in the context of the proposed identification method.

Based on the results obtained in examples 1 – 3 in Section 6.3, a recommendation on the selection of the set of points for the proposed identification method can be provided:

1. In the symmetrical case, the set of points in method #1 gives the best results in terms of the performance index E.
2. In the asymmetrical case, the set of points in methods #5 and #6 give quite similar results in terms of E, although #6 is slightly better.

Final comments and discussion

In this section, a discussion is made about the usefulness and improvement obtained by using a FFOPDT model instead of an integer-order model, being FOPDT, DPPDT, and SOPDT models the most commonly used in the industrial context.

In this chapter, an identification method for FFOPDT models has been presented. This method is focused on processes characterized by an S-shaped response (monotonic) that exhibits a fractional behaviour.

There is no exact definition to describe a fractional dynamic behaviour in the technical literature. According to (Sabatier 2021), a system has a fractional behaviour if its input and output are linked by a function of the form $t^{\upsilon-1}$, $\upsilon \in \mathbb{R}, \upsilon < 1$.

Although an implicit link exists in the literature between fractional behaviours and fractional-based models, they are two distinct concepts. One designates a property or a particular behaviour of a physical system, while the other refers to a model class that can capture fractional behaviours.

Fractional behaviours appear in many physical-, biological-, or thermal-based processes, among others; see, e.g., (Monje, Chen, et al. 2010) and (Tepljakov 2017). In spite of the slow dynamics, real processes exhibiting fractional behaviour with values of α in the range proposed in this paper can be found in electrical engineering, motion controls, and process control, being thermal-based processes the most important type encountered in the process industry (Yuan, et al. 2022).

Since these kinds of behaviours are ubiquitous, the existence of methods for identification of simple-structure fractional-order models is of significant interest.

The main issue of adopting fractional-order models in industry can be summarized in the form of the following question: "Is the additional effort to consider a fractional-order model worth to obtaining a more accurate model and, eventually, a better control performance?"

In the industrial context, the apparent benefit of using fractional calculus has been justified in the literature in terms of a more precise modelling; see, e.g., (Tepljakov 2017), (Guevara, et al. 2015), (Alagoz, et al. 2019).

More specifically in the context of this work, the proposed identification method for symmetrical and asymmetrical sets of points has been compared with several two- and three-point identification methods for integer-order models, which are based on data collected from the process reaction curve. It has been illustrated that the proposed method outperforms significantly methods for integer-order models. In some cases, even better results are obtained with the estimated fractional-order model than with the optimal integer-order model.

If the process reaction curve exhibits fractional behaviour, the estimated FFOPDT model will more accurately fit the reaction curve compared to the integer-order model. Note that the proposed identification method allows characterizing the existence of fractional behaviour in measured data collected from the process reaction curve. The identification procedure presented in this dissertation is intended for control purposes, as considered previously. In the industrial context, large process industries have hundreds or thousands of control loops. In order for such an identification procedure to have a significant impact in the industrial environment, simplicity is a fundamental feature.

In the context of this work, there is a trade-off between accuracy and computational effort. Although this identification procedure provides good results in comparison with other well-known integer- and fractional-order identification methods, it is possible to find methods that improve further the accuracy of the estimated fractional-order model at a cost of more complex algorithms or a higher computational effort. Another aspect to highlight is that the proposed method is analytical, which facilitates its applicability in terms of a lower computational effort compared to complicated identification algorithms generally based on optimization.

6.4. Conclusions

In this chapter, an identification procedure for FFOPDT models, which is based on the information obtained from three points on the process reaction curve, is presented. This identification procedure has been validated for both cases, considering three symmetrical and asymmetrical points on the reaction curve.

Three simulation examples, with processes exhibiting different dynamics, have been used to verify the simplicity and effectiveness of this identification procedure for the symmetrical and asymmetrical cases. Good results have been obtained in comparison with other well-recognized integer- and fractional-order identification methods which is also based on information taken from the process reaction curve, especially when simplicity is emphasized.

A thermal process-based experimental setup has also been used, where the proposed identification procedure has been implemented in a microprocessor-based control hardware, confirming the applicability of this method in an industrial equipment. Besides effectiveness, the main characteristic exhibited by this method is simplicity. This feature is of significant importance in the industrial context, where easy-to-implement identification methods are required.

Some comments and reflections have been offered in the context of industrial practice. It is worth pointing out that the identification method proposed in this chapter is restricted to values of the fractional order in the range $0.5 \leq \alpha \leq 1.0$, and as a future work, this method is being extended using the same methodology for processes with underdamped step response, extending the range of the fractional order to $1.0 \leq \alpha \leq 2.0$.

Who would be satisfied with a navigator or engineer, who had no practice or experience whereby to carry on his scientific conclusions out of their native abstract into the concrete and the real?

Saint John Henry Newman (1801 – †1890)
An Essay in Aid of a Grammar of Assent, VIII 1, 2

PART

II

Implementation issues

Enormous technological advances have marked a new stage in the field of process control in the process industries. The last three decades have witnessed a remarkable development in the use of fractional calculus for modelling and control.

However, laboratory equipment and hardware resources are required for training and research in applied fractional calculus.

Part I of this dissertation has presented different methods for identifying fractional-order models based on the process reaction curve.

Part II of this dissertation provides the required resources for the practical implementation of the identification procedures developed in Part I.

Consequently, this part supports, on the one hand, the practical implementation of fractional-order model identification algorithms on real-time hardware platforms and, on the other hand, bridges the gap between software-based fractional controller simulations and real-time hardware solutions.

Thus, one of the contributions of this thesis is verified, which is to provide an efficient and practical hardware architecture for implementing integer- and fractional-order identification and control algorithms in different control technologies.

In this part of the dissertation:

Chapter 7 presents the conceptualization of a novel control hardware architecture aimed to the practical implementation of fractional-order identification and control algorithms. The experimental thermal-based prototype that has been designed and built to test the performance of the control hardware architecture proposed in this dissertation is also described in detail.

Chapter 8 shows the results obtained by applying the identification algorithms presented in Part I of this dissertation on a temperature-based experimental setup and implemented using the hardware architecture described in Chapter 7.

Chapter 9 evaluates the effectiveness and applicability of the control hardware architecture presented in Chapter 7 through the practical implementation of integer- and fractional-order PID control algorithms on two real-time targets, i.e., on microprocessor- and FPGA-based hardware.

Hardware can't argue.

C. A. Higgins (1991 – …)
Lightless

CHAPTER

7

A novel control hardware architecture for fractional-order systems

THIS chapter presents the conceptualization of a control hardware architecture aimed to the implementation of integer- and fractional-order identification and control algorithms. The proposed hardware architecture combines the capability of implementing PC-based control applications with embedded applications in microprocessor- and FPGA-based real-time targets. The potential advantages of this hardware architecture over other available alternatives are discussed from different perspectives.

The experimental prototype that has been designed and built to test the performance of the control hardware architecture proposed in this thesis is also described in detail. The thermal-based process taking place in the prototype is characterized for being reconfigurable and exhibiting fractional behaviour, which results in a suitable equipment for the purpose of fractional-order identification and control.

7.1. Introduction

Enormous advances in technology have marked a new stage in the field of process control in the process industries. Laboratory equipment plays a significant role in control engineering research and education.

The lack of adequate equipment to bring students closer to the reality in industry is one of the main problems encountered by a Faculty of Engineering in the practical education in the field of control engineering.

Due to this situation, there is a gap between the technical-practical and the theoretical education of the university graduates, which increases the deep-rooted distrust that companies have in academia because generally the practical training in these institutions does not meet industrial demands; see, e.g., (Gude and Kahoraho 2010a) and (Rossiter, et al. 2018).

The past three decades have witnessed remarkable development in the use of fractional calculus in various fields, such as process control and modelling. It is now an important tool for the international industrial and scientific communities; see, e.g., (Podlubny 1999a); (Tepljakov 2017); and (Monje, Chen, et al. 2010). The development of fractional calculus has enabled a major industrial and academic effort centered on the transition from conventional modelling and control to those described by fractional-order differential equations. It has also been shown that fractional calculus in the design of control systems results in controllers that are more efficient in comparison with traditional integer-order controllers. However, the use of fractional-order control algorithms in industry is currently low, despite the fact that fractional PID controllers provide significant benefits over integer-order ones. The well-known implementation issues have contributed to the difficulties in conveying in industry the advantages of fractional-order controllers (Tepljakov, Alagoz, et al. 2018).

Therefore, there is a need for laboratory equipment for training and researching in applied fractional calculus. To bridge the gap existing between theoretical fractional-order identification and control algorithms and their practical implementation in a control hardware device, this chapter proposes a control hardware architecture that simplifies their real implementation in a real-time target. Training in implementation and tuning methods for fractional-order controllers is of major interest for making them more convenient and attractive for industry, thus facilitating their transition from state-of-art to state-of-use, see (Chevalier, et al. 2019).

The objective of this chapter is only to introduce and present how a novel control hardware architecture has been conceived, whose features and available control technologies are particularly suitable for the practical implementation of fractional-order identification and control algorithms. In addition, this chapter also includes a detailed description of the temperature-based experimental prototype that has been recently designed and built at the University of Deusto. Chapters 8 and 9 will test the applicability and performance of the proposed hardware architecture applied on the temperature-based experimental setup by implementing several integer- and fractional-order identification and control algorithms, respectively, on the different control technologies offered by the control hardware.

Chapter 7 is organized as follows. In Section 7.2, a description of the temperature experimental prototype is made, explaining the process that takes place and emphasizing its characteristics as a reconfigurable controlled process. The proposed control hardware architecture is presented in Section 7.3, detailing the different control technologies available and their potential capabilities for implementation of fractional-order identification and control algorithms in each of them. Finally, this chapter is concluded with a discussion on the advantages of this hardware architecture over other available alternatives.

7.2. Temperature experimental prototype

This section presents the temperature-based experimental setup that is to be used to demonstrate the effectiveness and applicability of the control hardware architecture proposed in this chapter.

The section is divided into the following parts: First, the temperature prototype to be used in this thesis is described. Then, a detailed description of the thermal process that takes place in the prototype is provided. Finally, as the thermal process can be configured with three different settings, its possibilities as a reconfigurable controlled process are considered in detail.

7.2.1. Description of the prototype

The prototype can be divided into two clearly different parts, as shown in Figure 7.1.

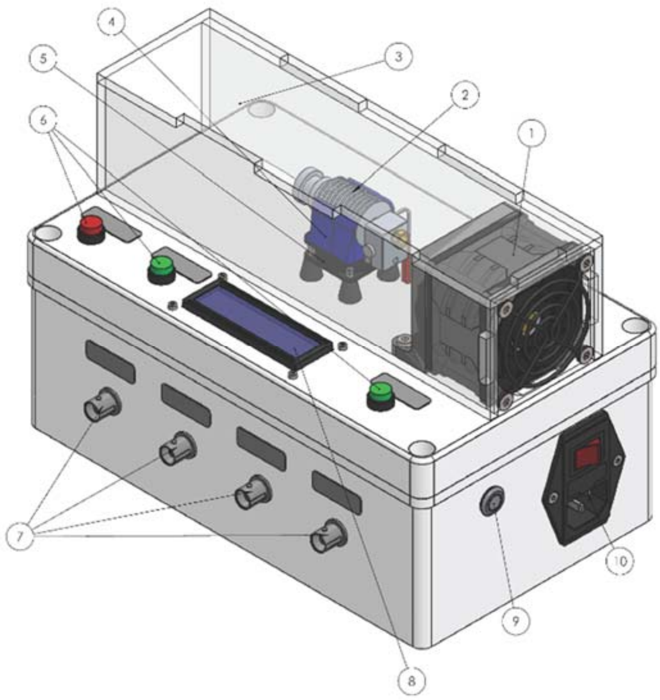

Figure 7.1. 3D-model layout of the Deusto-Heater Experimental Setup.

#	Component
1	Air Fan
2	3D-printer extruder head
3	Acrylic duct
4	Plastic duct covering heat sink
5	Forced convection fan
6	User LEDs
7	BNC output connectors
8	LCD display
9	User button
10	IEC Power connector

Table 7.1. Deusto Heater Experimental Setup – List of the main external components of the prototype.

- This prototype has a 3D-printer extruder head, which is inside a methacrylate duct, and an air fan installed in front of the hot end. Outside the enclosure there is an LCD display, LEDs, BNC output connectors for displaying process variables on an external device, such as an oscilloscope, and a user button. The list of the main external components of the prototype is shown in Table 7.1.
- The power source and all electrical and hardware components required for the proper functioning of the prototype are located in the inner part of the enclosure. A 34-way standard IDC connector, located on one side of the enclosure, is also used to connect input and output signals to the proposed control hardware.

Deusto Heater Experimental Setup (Deusto HES) is the name of this equipment and has been built by using simple components, which makes this prototype affordable. Its technical characteristics, its size, and weight make it portable and suitable to work with it at home, which is a very important characteristic for a Faculty of Engineering (Rossiter, et al. 2018).

This lab equipment has been designed and built in the *Laboratory of Measuring Systems and Control*, and in *Deusto FabLab*, both belonging to the Faculty of Engineering, University of Deusto. The total cost of the Deusto HES platform, without including the hardware device, is estimated to be around EUR 250.

7.2.2. Thermal-based process

Figure 7.2 details the various components of the extruder head, which is the area of the apparatus where the thermal process of interest takes place. The figure also illustrates the different thermodynamic phenomena taking place that are the origin of the fractional-order behaviour exhibited by the thermal-based process, as will be discussed in Chapter 8.

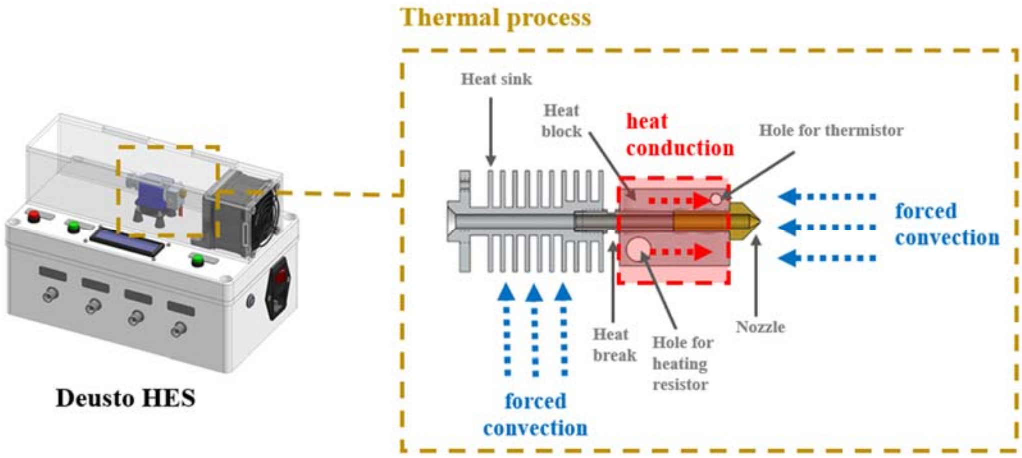

Figure 7.2. 3D-model layout of the Deusto-Heater Experimental Setup.

It is important to note that no extrusion process takes place in the 3D-printer head, since it is only used as a heating element.

The four parts of the extruder head, which is shown in Figure 7.2, are described in the following way:

- Heat block. It is constituted by a high-conductivity aluminum. A heating resistor is embedded inside it, which provides the main heat inflow into the system, increasing the nozzle temperature. A thermistor-type temperature sensor is embedded in the block inside a second hole. Its main function is to monitor the evolution of the temperature in the extruder head.
- Nozzle. This part is heated by conduction from the heat block. In a real 3D-printer the hot extrusion is directly developed in it.
- Heat break. This is the first of the protection measures provided by the extruder head. This component minimizes heat conduction towards the heat sink, since it is constituted by a low-conductivity stainless steel. This is why it is directly attached to the heat block. Nevertheless, dissipation by forced convection is needed, since this barrier is generally not enough. For that purpose, the heat sink is covered using a plastic duct with a fan running at a constant speed.
- Heat sink. It is a finned surface that promotes heat dissipation by convection. This part, together with the aforementioned heat break, contributes to decrease the temperature along the extruder head body.

Figure 7.2 also shows the thermodynamic phenomena of heat conduction in the heat block due to the action of the heating resistor and forced convection due to the action of the air fan. Both, the airflow in the air fan and the heating power can be controlled by modifying the duty cycle of both PWM signals sent by the control hardware.

7.2.3. Reconfigurable controlled process

The control objective is to bring the heat block temperature $T(t)$ to the desired value, T_{SP}, in spite of any disturbances that could affect the controlled process.

Considering that there is no change in the physical properties, only the influence of the air fan and the heating power of the resistance on the controlled variable $T(t)$ need to be taken into account.

Consequently, from a control point of view, the unique heating source in the process is the heat conduction generated by the heating resistance. Moreover, the forced convection of the air flow caused by the fan over the heat block is the other phenomenon involved in the thermal process, see (Bergman, et al. 2017); (Skogestad 2009).

Since both of these phenomena can be controlled using the control hardware, the configuration of the controlled process can be easily established by using software.

Therefore, considering all the above considerations, the controlled process can be configured to control the temperature in the heat block under the following three settings:

1. Configuration #1: The heating element is used in this configuration as the final control element while maintaining the air fan speed constant. The block diagram corresponding to this configuration for the controlled process is shown in Figure 7.3.
2. Configuration #2: The controlled process in this configuration utilizes the air fan as the final control element while maintaining the heating power of the resistance constant, as shown in Figure 7.4.
3. Configuration #3: Figure 7.5 shows how in this configuration both the heating element and the air fan are used as the final control elements.

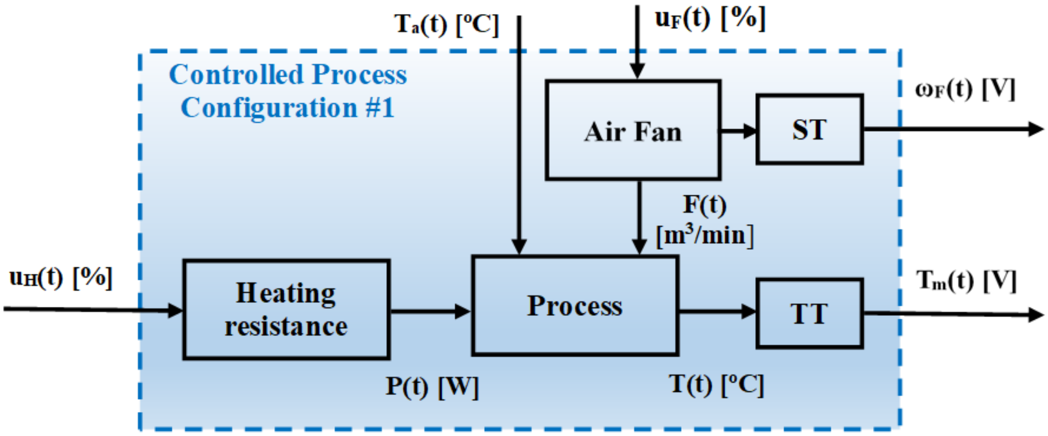

Figure 7.3. Block diagram corresponding to configuration #1 for the controlled process.

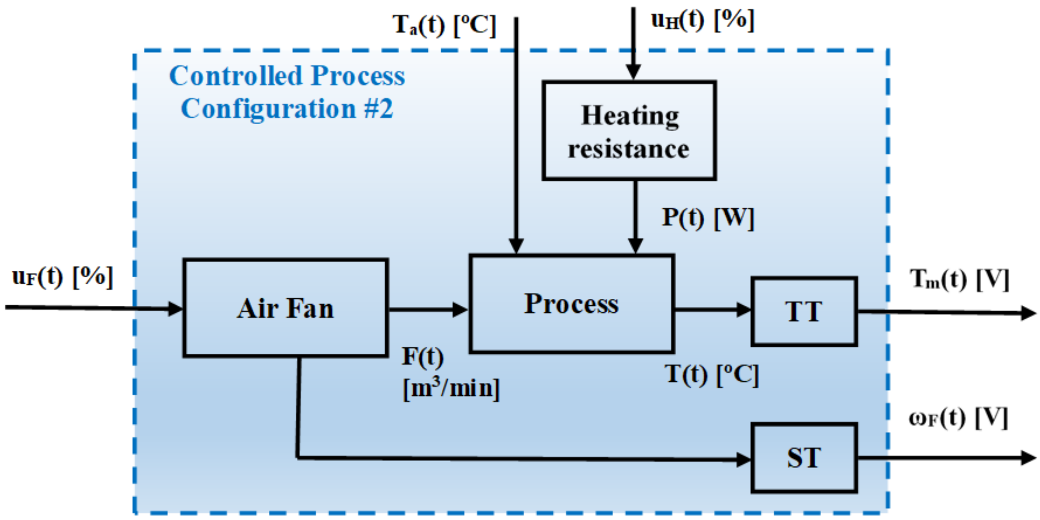

Figure 7.4. Block diagram corresponding to configuration #2 for the controlled process.

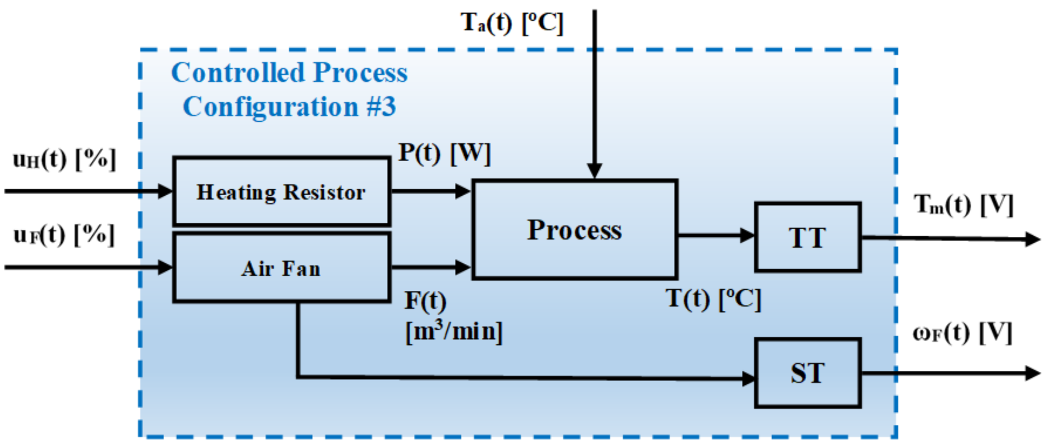

Figure 7.5. Block diagram corresponding to configuration #3 for the controlled process.

The main process variables including their units in each of the different configurations are those shown in Table 7.2.

Process variables or components	Controlled Process Configuration #1	Controlled Process Configuration #2	Controlled Process Configuration #3
Controlled variable	Temperature in the heat block T(t) [ºC]		
Manipulated variable(s)	Power delivered to the heat block by the heating resistance P(t) [W]	Airflow F(t) [m^3/min]	Power delivered to the heat block by the heating resistance P(t) [W] and airflow F(t) [m^3/min]
Measured variable(s)	Temperature measured by the thermistor $T_m(t)$ [V] Rotational speed of fan $\omega_F(t)$ [V]		
Control signal	Output of the controller $u_H(t)$ [V]	Output of the controller $u_F(t)$ [V]	Output of the controller $u_H(t)$ [V] or $u_F(t)$ [V]
Final control element(s)	Heating resistance	Air fan	Heating resistance and air fan
Measurement Devices	Temperature transmitter (TT) and Frequency transmitter (ST)		
Disturbance(s)	Ambient temperature $T_a(t)$ [ºC], command signal to air fan $u_F(t)$ [%]	Ambient temperature $T_a(t)$ [ºC], Command signal to heating resistance $u_H(t)$ [%]	Ambient temperature $T_a(t)$ [ºC], command signal to air fan $u_F(t)$ [%] (when $u_H(t)$ is applied) or command signal to heating resistance $u_H(t)$ [%] (when $u_F(t)$ is applied)

Table 7.2. Main components and process variables depending on the controlled process configuration.

In configurations #1 and #2, a simple feedback control loop can be considered as the control structure, while in configuration #3 a split-range control can be used.

7.3. Control hardware architecture

The main objective of this section is to present a novel control hardware architecture that facilitates the implementation of integer- and fractional-order identification and control algorithms on a real-time target.

For that purpose, this section is divided into the following parts: First, a review of the different control hardware usually applied in industry is described. Then, an overview of the real-time target used in this dissertation and its technical capabilities and features are provided. Finally, the proposed control hardware architecture is described in detail, showing the interaction between hardware components and software.

7.3.1. Review of control hardware technologies

Nowadays, as computers have become even more popular, control technology has progressed to be combined with computer technology for more accurate and faster methods of computation. Hence, new control methods for real-time systems are progressively being introduced in industry and taught in institutions. Generally speaking, one can find many different approaches to process control technology in the literature. These usually vary based on the software and hardware architecture used. The most frequent types can be divided into the following major categories, as shown in Figure 7.6.

In addition to the specific references that will be included below in each section devoted to modelling and implementation of fractional-order dynamic systems, respectively, some recent and significant references for each hardware technology have also been included in each category in the context of this chapter.

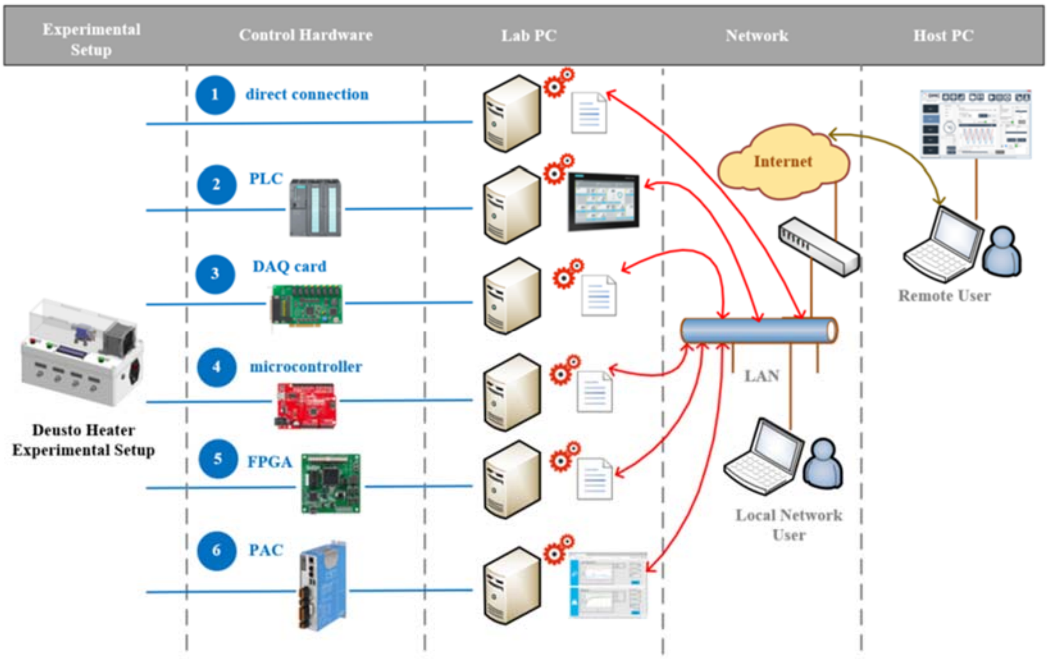

Figure 7.6. Review of the most frequently approaches to control hardware applied in industry.

1. Direct connection (Figure 7.6 – Case 1). This type of architecture is commonly found when a direct connection between the experimental setup and the lab PC (e.g., by serial or USB port) is used. In this case, the experimental apparatus incorporates some form of DAQ equipment and the appropriate software for controlling this device must be provided to the lab PC.

2. Programmable Logic Controller (PLC) (Figure 7.6 – Case 2). A SCADA system with a control hardware, generally a PLC or another hardware controller, is one of the most widely used industrial approaches. Most SCADA systems provide variable control capabilities and connectivity, data acquisition, and HMI as their main and common features. (Możaryn, Petryszyn and Ozana 2021) describes the implementation of a fractional-order PI controller in a PLC, which is used for positioning of an electrohydraulic drive with servo valve. (Monje, Vinagre and Santamaría, et al. 2009) describes the design, parameter tuning, and experimental evaluation of a PLC-based fractional-order PID temperature control in a pipeline with induced air-flow in a laboratory test bench. Regarding the development and implementation of tuning algorithms, the implementation of an auto-tuning method for fractional-order PID controllers using a PLC and a position servo motor has been carried out in (Rybarczyk 2016).
3. DAQ device (Figure 7.6 – Case 3). This architecture is often used in a situation when it is not possible to directly interconnect the experimental setup and the PC. In this case, the acquisition device, which is usually a DAQ card, is a separate part of the architecture. Proper software for data acquisition and control of the experimental setup must be provided to the lab PC. The following two references to works that fall into this category are given below: In (Malek, Luo and Chen 2013), it is verified that a FFOPDT model represents a more accurate model than the standard FOPDT model for a Heat Flow Equipment (HFE). In this work, an integer-order PID controller and two fractional-order PI controllers have been designed for FFOPDT systems. Both fractional controllers guarantee robustness against loop gain variations. (Monje, Vinagre and Feliu, et al. 2008) develops a synthesis method of fractional-order PID controllers to meet five different design specifications for the closed-loop system, guaranteeing a robust behaviour of the controlled system against gain and noise changes. In addition, a self-tuning method for the fractional-order PID controller using the relay test has been proposed.

In recent years, industrial processes are controlled using other very popular approaches that are based on programmable targets, such as microcontrollers, cheap alternatives to standard computers, and FPGAs. Another common approach in industry is the use of certain PACs, which is an industrial technology focused on automated control, prototyping and measurement.

4. Microcontroller (Figure 7.6 – Case 4). A standard microcontroller can be interfaced to the experimental setup and programmed to operate a control system or collect and perform data operations. In this case, the microcontroller usually has the appropriate hardware for DAQ and a lab PC with specific software is typically required.

One of the first monographs devoted to the implementation of fractional-order controllers in various hardware devices is (Caponetto, et al. 2010). This reference includes not only this category, but also the following ones. Another more recent book where fractional-order PID control algorithms are implemented on a microprocessor-based real-time target is (Tepljakov 2017). (Oprzedkiewicz, Rosół and Zeglen-Włodarczyk 2021) presents the time, frequency and real-time properties of a fractional-order PID implemented on a microprocessor-based real-time platform. The results obtained can be used in building embedded fractional control systems implemented on resource-constrained platforms.

5. FPGA (Figure 7.6 – Case 5). The implementation of control systems on FPGA devices by using optimal hardware resources is one of the challenging research areas in control engineering. In this approach, a standard FPGA is used for operating and implementing real-time control systems for the experimental device. In this case, the FPGA provides interface and quick access to real-world I/O at several levels. Although a stand-alone application can be programmed in the FPGA, a lab PC with specific software is typically required for HMI operations. A recent monograph that provides a simple, step-by-step procedure for the implementation of fractional-order PID controllers on an FPGA-based real-time target is (Copot, Ionescu and Muresan 2020). Other significant examples are the following: In (Muresan, Folea, et al. 2013), a fractional-order PI controller for DC motor speed control on an FPGA target is proposed and implemented. FPGA implementation issues and the advantages of using FPGA devices to implement robust fractional-order PI controllers are addressed. The same authors present in (Muresan, Folea and Mois 2013) the design of two advanced control algorithms are implemented on FPGA and applied to the speed control of a DC motor and evaluated in terms of closed-loop robustness, power consumption, execution times and resource minimization. In (Wang, et al. 2022), a fractional-order PI controller is designed to control the speed of the permanent magnet synchronous motor (PMSM), and the accuracy of the numerical implementation of the fractional-order PI controller is evaluated.
6. PAC (Figure 7.6 – Case 6). PAC devices combine the control reliability of a PLC with the monitoring and computational flexibility of a PC. Certain PACs often include technologies covered in categories 4 and 5. Although any other PAC could be used, a NI myRIO device has been selected in this thesis. This approach exhibits enhanced flexibility, since the hardware architecture proposed and implemented in this device incorporates categories 3, 4, and 5 explained above. The main references for this category are provided in Chapter 9.

In general, in any of the considered approaches the lab PC can be connected to the Internet so that the control hardware can be easily accessed from a local or a host PC. In this way, any of these architectures allow the integration of the experimental device in a remote laboratory, as indicated, e.g., in (Kalúz, et al. 2015).

7.3.2. Control hardware overview

In this section, a NI myRIO device has been selected as a control hardware for operation of the temperature-based experimental setup and implementation of integer- and fractional-order identification and control algorithms in various control technologies, as will be explained later.

The NI myRIO 1900 is a reconfigurable and reusable device that features AI, AO, DIO, power output, and secondary digital functions (such as SPI, I2C, UART, quadrature encoder input, and PWM) in a compact embedded device, see (National Instruments, 2022). It also features a 667 MHz dual core ARM Cortex-A9 programmable processor and custom Xilinx FPGA I/O which can be used by users to start system development and solve design problems faster. The NI myRIO device allows final user to interface with the Zynq-7010 System on a Fully Programmable Chip (SoC) to develop real-time (RT) and FPGA-level applications.

The flexibility in the configuration and access to the available hardware that has been addressed in the design of the control hardware architecture allows to exploit the RT and FPGA capabilities of the device to implement identification and control algorithms, as will be discussed in the following chapters.

Figure 7.7 represents a general scheme of the myRIO device used as a control hardware for operating and controlling the prototype. This figure also depicts the different control technologies and specific software that has been configured to be used as a part of the proposed hardware architecture.

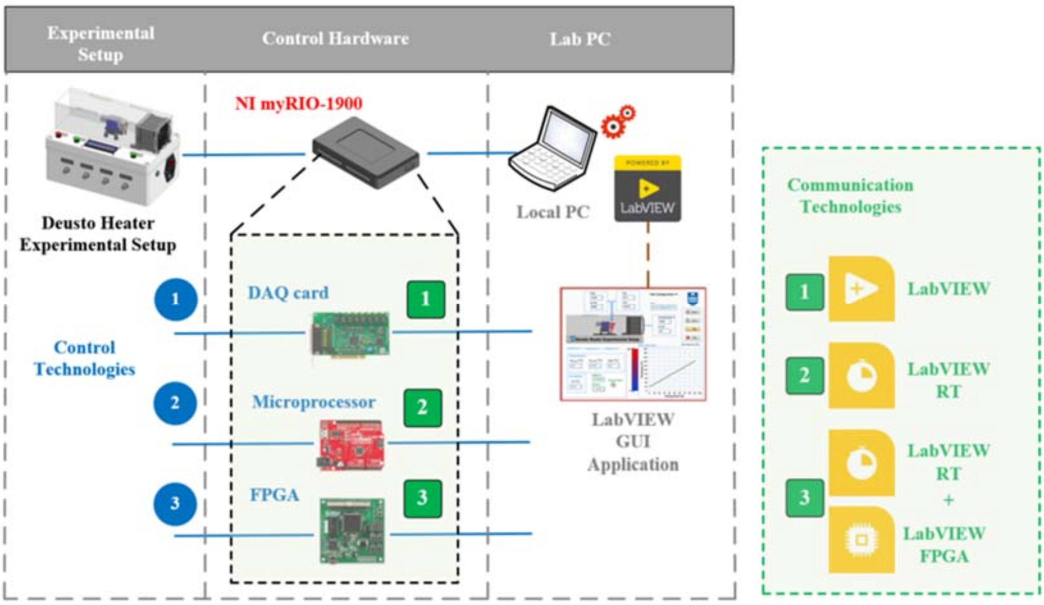

Figure 7.7. General scheme of the prototype using myRIO as a control hardware device. The different hardware technologies contained in the device and the software used are also depicted.

7.3.3. Proposed control hardware architecture

The prototype is designed to naturally integrate a control hardware unit through a standard 34-pin IDC connector. Although any other control hardware or microprocessor could have been easily incorporated, a NI myRIO-1900 device has been used as a control hardware equipment.

Figure 7.8 shows in detail the scheme of the hardware components available in myRIO devices, showing the I/O connections and the different interactions between hardware components and software.

The flexibility and transparency provided by this control hardware offer the ability to enable the following control hardware architecture for the practical implementation of advanced control and identification algorithms. Thus, hardware components are accessed using LabVIEW software to constitute the control hardware architecture that enables the following control modes or technologies (Gude and García Bringas 2021):

1. PC-based mode. In this mode, the identification or control algorithms can be implemented using a non-deterministic LabVIEW application on the user PC. Special functions that use the I/O functions of the myRIO toolkit have been implemented to access transparently the I/O signals of the myRIO device. This means that the control device is used as a DAQ card in this control mode.
2. Real-time microprocessor-based mode. This mode enables the RT processor of the myRIO device as a RT target to implement microprocessor-based deterministic applications. Identification or control algorithms are implemented by using LabVIEW RT and executed on the RT controller. LabVIEW RT also accesses the I/O ports through the FPGA interface and is responsible for communication with the host application, which is implemented in LabVIEW. A user can access or operate the control system from a local or remote PC.
3. FPGA-based mode. This mode enables the reconfigurable FPGA of the myRIO device as a RT target to implement FPGA-based deterministic applications. Identification or control algorithms are implemented using LabVIEW FPGA and executed on the reconfigurable FPGA. LabVIEW FPGA also is responsible to access the I/O ports through the FPGA interface. Communication between the FPGA and the local or remote PC is programmed in LabVIEW RT and executed in the real-time controller. A user can access or operate the control system from a local or remote PC.

Table 7.3 shows the signals from the output BNC connectors available for viewing on an oscilloscope. Tables 7.4 and 7.5 show the analog and digital input signals, and digital outputs, respectively, connected through the I/O Interface, as shown in Figure 7.8.

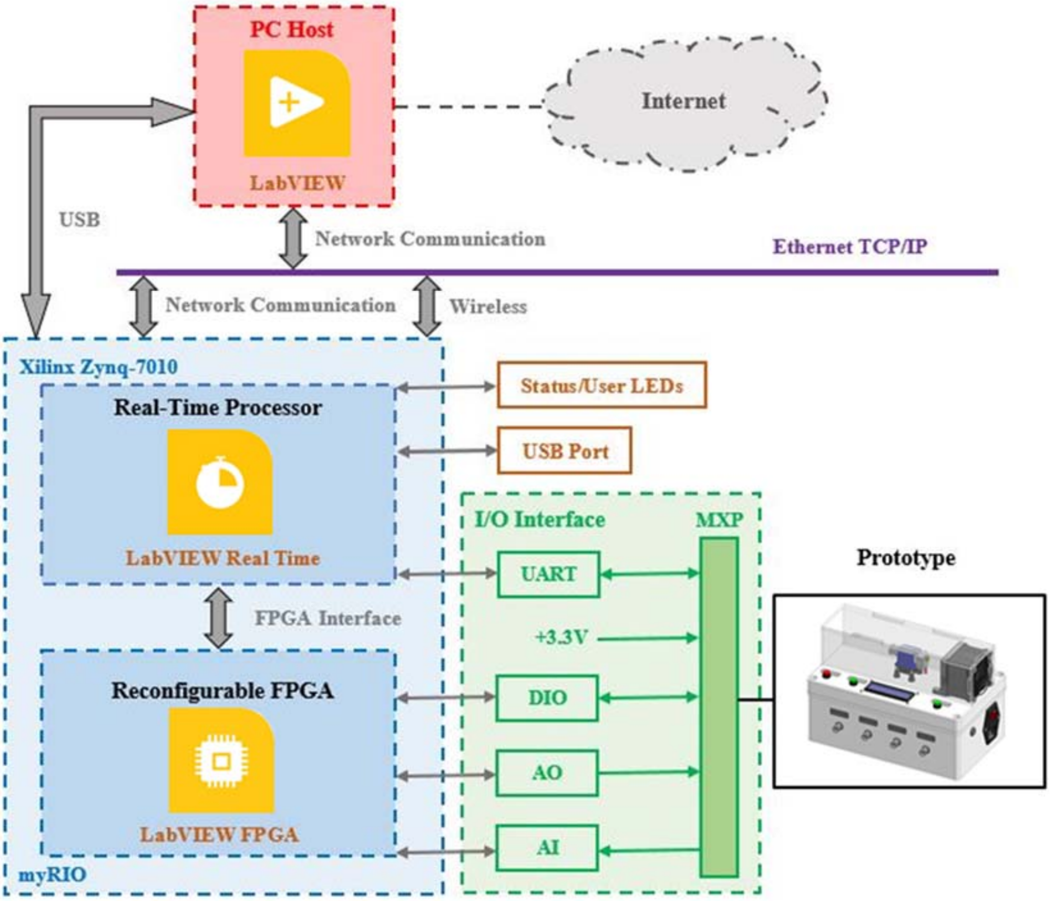

Figure 7.8. Proposal of hardware architecture applied to the laboratory prototype. The interaction between hardware and software is also illustrated.

BNC Output Connector	Signal
BNC1	command signal to air fan $u_F(t)$ [V]
BNC2	Rotational speed of Fan, $\omega_F(t)$ [V]
BNC3	command signal to heating resistance $u_H(t)$ [V]
BNC4	Temperature measured by the thermistor in the heat block $T_m(t)$ [V]

Table 7.3. Deusto Heater Experimental Setup – Signals in BNC output connectors in the prototype.

Analog or Digital Inputs	Signal
AI0	command signal to air fan $u_F(t)$ [V]
ENC.A	Rotational speed of Fan, $\omega_F(t)$ [V]
DIO13	User button

Table 7.4. Deusto Heater Experimental Setup – Analog and digital signals connected to the control hardware through the I/O interface.

Digital Outputs	Signal
PWM0	PWM signal to heating resistance $u_H(t)$ [V]
PWM1	PWM signal to air fan $u_F(t)$ [V]
DIO1	User LED 1
DIO2	User LED 2
DIO3	User LED 3

Table 7.5. Deusto Heater Experimental Setup – Digital output signals connected to the control hardware through the I/O interface.

7.4. Discussion

The previous section has presented the conceptualization of a hardware control architecture that combines the capability of implementing PC-based control applications with embedded applications on microprocessor- and FPGA-based real-time targets.

In what follows, the advantages of this hardware architecture over other available alternatives will be discussed.

Although there are several works in the technical literature that employ myRIO or compactRIO platforms to implement fractional-order PID controllers; see, e.g., (Koszewnik, Pawłuszewicz and Ostaszewski 2021); (Dastjerdi, Saikumar and HosseinNia 2018) and (Muresan, Folea, et al. 2013), none of the works have defined and utilized their hardware in the manner presented in this chapter. They are generally restricted to the implementation of the fractional-order PID algorithm on an FPGA-based real-time target.

Different hardware platforms, generally those based on microprocessor or FPGA, have also been used in the literature to implement fractional-order PID control algorithms. See, e.g., (Tepljakov 2017); (Caponetto, et al. 2010) and (Oprzedkiewicz, Rosół and Zeglen-Włodarczyk 2021). While each hardware architecture has its unique characteristics, the one proposed in this chapter provides some properties that are different from any other, such as:

1. It is a novel hardware control architecture that uniquely and efficiently exploits the different hardware available in myRIO device enabling their use indistinctly.
2. From the control hardware point of view, it features great flexibility since it can be configured to use the following technologies or control modes: PC-based, microprocessor-based, or FPGA-based control.

3. From the software point of view, it offers simplicity and transparency since the same programming language is used, regardless of the control hardware. Thus, instead of spending time developing user interfaces or debugging code syntax, end users can apply the LabVIEW graphical programming paradigm to focus on implementing their conventional or advanced identification and control algorithms without the added pressure of a complicated programming language for each hardware platform.
4. From a practical training perspective, the engineer has three hardware technologies on the same device for their use, without having to perform an experimental setup for each hardware platform to be used.

Hence, discussion on these directions involves novel interests.

The next two chapters will evaluate the effectiveness and applicability of this hardware control architecture for implementing fractional-order identification and control algorithms.

Nature is pleased with simplicity. And nature is no dummy.

Isaac Newton (1643 – †1727)

CHAPTER

8

Fractional-order model estimation: Implementation issues and results

THIS chapter discusses the implementation of fractional-order model identification methods on a real-time hardware platform. In Part I of this dissertation, different fractional-order model identification procedures based on the process reaction curve have been proposed. In this chapter, such identification procedures are implemented using the hardware control architecture presented in Chapter 7. Therefore, the performance of the hardware control architecture proposed in this dissertation for the implementation of fractional-order model identification algorithms is tested.

This chapter fulfils some of the objectives proposed in this work. On the one hand, the applicability of the proposed FFOPDT model identification procedures is verified and some of the conclusions obtained in this work are tested on a laboratory prototype. On the other hand, the practical issues related to the implementation of identification algorithms on an industrial control hardware are studied in depth.

8.1. Introduction

Fractional calculus has been considered for a long time as a pure mathematical field without many real applications. However, such a state of affairs has been changed in recent decades. In fact, it has been proven that fractional calculus can be useful and even powerful, especially in the area of modelling (Tepljakov 2017).

There is increasing evidence that certain dynamic processes can be described more accurately by using fractional-order models, see the applications in (Dzieliński, Sierociuk and Sarwas 2010) and (Tenreiro Machado, Silva, et al. 2010).

If the process reaction curve exhibits fractional behaviour as described in (Sabatier 2021), as in the case of processes involving thermal conduction, the use of an FFOPDT model has clear advantages over integer-order models (Podlubny 1999a), (Yuan, et al. 2022).

In this chapter, issues related to modelling of the thermal-based controlled process are described. Consequently, for the purposes of this chapter related to modelling considerations, it is sufficient to consider the dynamic and static characteristics of the controlled process and estimating integer- and fractional-order models at a certain operating point by using process information collected from the reaction curve.

This chapter is divided into the following parts: Section 8.2 presents the methodology and procedure to be used to obtain the experimental results, including the implemented identification algorithms to be applied to the thermal process taking place in the laboratory prototype. In Section 8.3, the experimental results obtained by implementing the identification procedures presented in the Part I of this dissertation (Chapters 4 – 6) are presented. These identification methods are implemented on a microprocessor-based hardware and applied to the temperature-based controlled process under configurations #1 and #2, respectively. These results are compared with those obtained using well recognized identification methods for integer- and fractional-order models. Section 8.4 presents the different applications implemented using LabVIEW to characterize the controlled process and implement the fractional-order model identification methods under an industrial hardware platform and applied to the laboratory prototype. And finally, Section 8.5 provides some concluding remarks and discussion about modelling issues in this context.

8.2. Materials and methods

Section 8.2 presents some details on the modelling of the thermal-based controlled process taking place in the laboratory prototype, and the methodology and procedure to be used to obtain the experimental results.

This section is divided into the following parts: First, the static and dynamic characteristics corresponding to the thermal process in its three different configurations are provided; Next, an overview of the general identification method presented in the Part I of this dissertation is provided; Then, the identification algorithms that will be subsequently implemented on a hardware platform are provided; Finally, the experimental procedure to be followed is detailed.

8.2.1. Temperature-based controlled process

The temperature-based process taking place in the laboratory prototype, which involves thermal conduction as detailed in Chapter 7, exhibits fractional behavior. This provides the laboratory prototype with very convenient features for the study of modelling and implementation of integer- and fractional-order model identification methods. For the purposes of this chapter, this section provides some details on the static and dynamic characteristics of the thermal controlled process under the three available configurations.

Controlled process configuration #1

Figure 8.1 represents the block diagram of the controlled process in configuration #1, where the different variables and units are listed in Table 7.2. The graph in Figure 8.2 illustrates the family of static characteristics for Process Configuration #1, namely the value of the controlled variable T [ºC] for each value of the control signal u_H [%], considering different values of u_F [%].

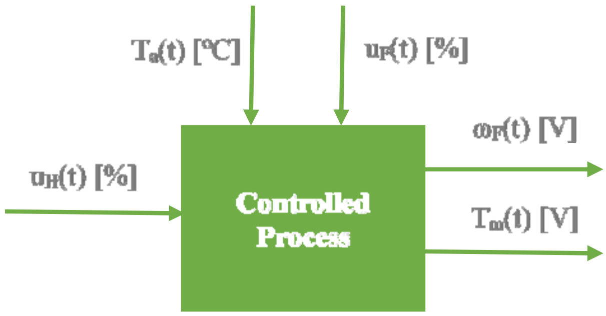

Figure 8.1. Block diagram for the controlled process configuration #1

Note that the behaviour of the characteristics (u_H, T) for different values of u_F is approximately linear, where the slope of each characteristic curve represents the gain or sensitivity of the controlled process under these operating conditions. Thus, the gain of the controlled process for the characteristic curves shown in Figure 8.2 is 1.85, 1.39, 1.03, 0.81, and 0.62°C/%, respectively, for u_F values of 0, 10, 30, 50, and 100%.

Besides, temperature gradient in each of the curves is greater for lower values of u_F, as can be seen in Figure 8.2. Consequently, the temperature variation in each curve for the whole range is 185.1, 139.2, 103.2, 81.3, and 62.3ºC, respectively, for decreasing values of u_F.

Figures 8.3 and 8.4 illustrate the input variables (control signal u_H and disturbance u_F) and the output variable (controlled variable T), respectively, in a typical staircase test. One can observe that the behaviour is clearly nonlinear, exhibiting different dynamic characteristics for the different operating points.

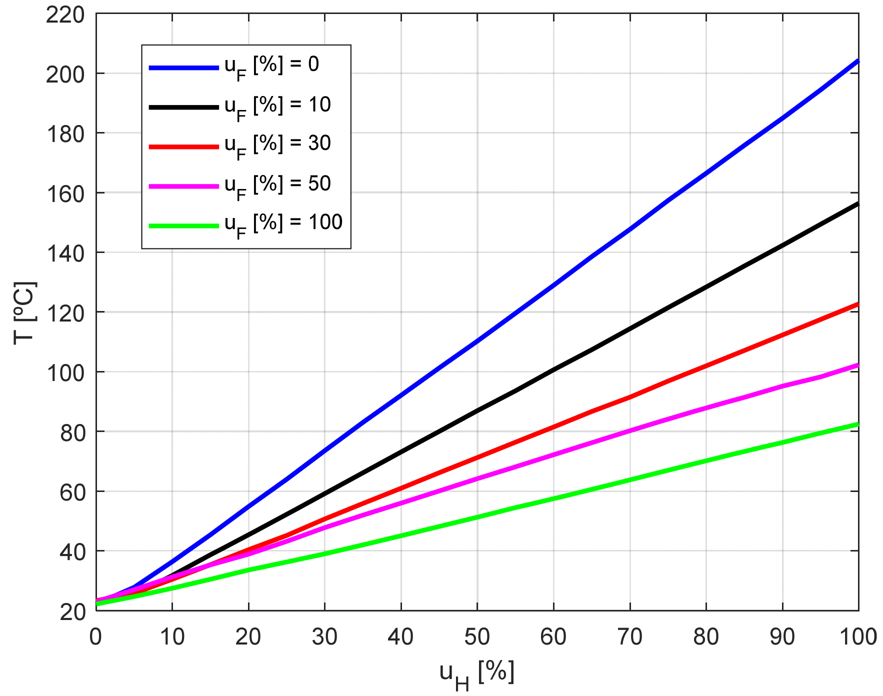

Figure 8.2. Static characteristics T [ºC] – u_H [%] for different values of u_F [%] (Process Configuration #1)

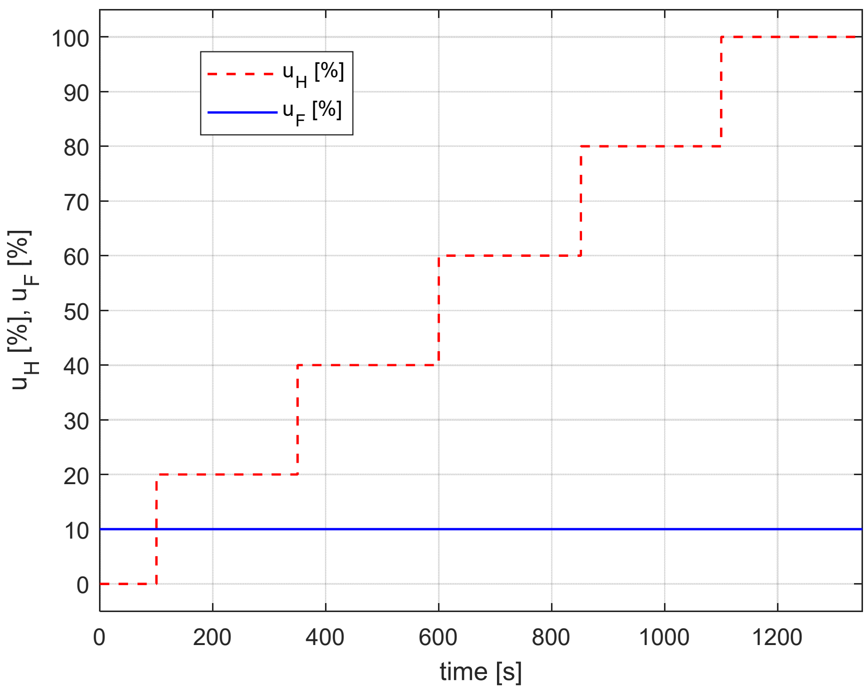

Figure 8.3. Dynamic characteristics in a typical staircase test (Process Configuration #1): input variables (control signal u_H and disturbance u_F).

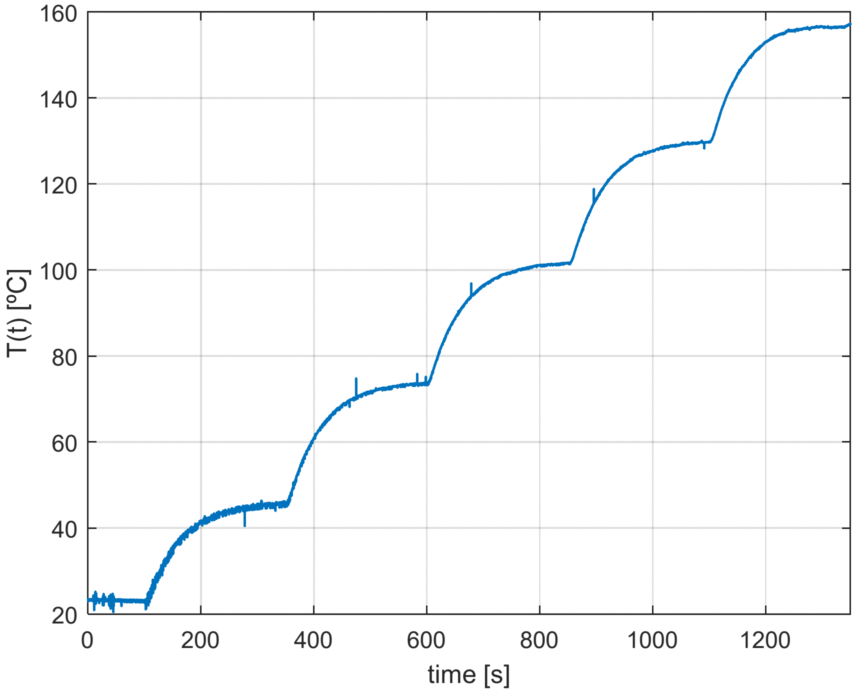

Figure 8.4. Dynamic characteristics in a typical staircase test (Process Configuration #1): output variable (controlled variable T).

Controlled process configuration #2

Figure 8.5 represents the block diagram of the controlled process in configuration #2, where the different variables and units are listed in Table 7.2. The static characteristic curves (u_F, T) for different values of u_H are shown in Figure 8.6, exhibiting a nonlinear behaviour throughout the operating range. Note that the gain of the controlled process for each one of the characteristic curves shown in Figure 8.6 decreases in a nonlinear way as the control signal u_F increases. In this case, a decrease of the temperature gradient for decreasing values of u_H can also be observed. Therefore, the temperature variation in each curve for the whole range is −124.6, −84.9, −55.1, and −25.4ºC, for u_H values of 100, 75, 50, and 25%, respectively.

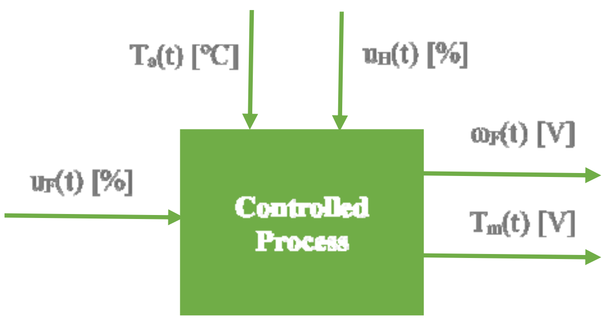

Figure 8.5. Block diagram for the controlled process configuration #2.

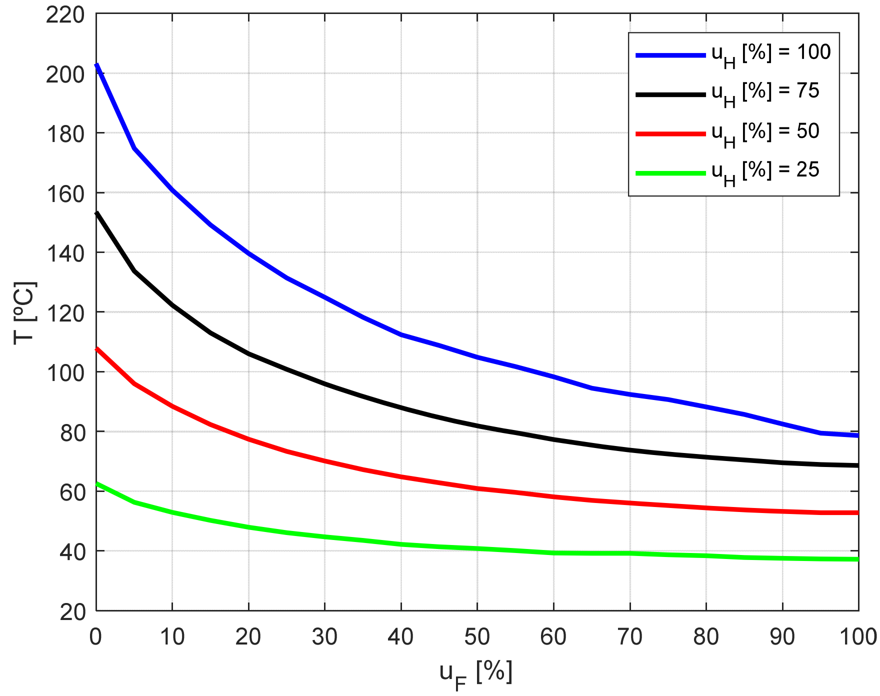

Figure 8.6. Static characteristics T [ºC] – u_F [%] for different values of u_H [%] (Process Configuration #2)

Figures 8.7 and 8.8 illustrate the input variables (control signal u_H and disturbance u_F) and the output variable (controlled variable T), respectively, in a typical staircase test. One can observe that the behaviour is clearly nonlinear, exhibiting different dynamic characteristics for the different operating points.

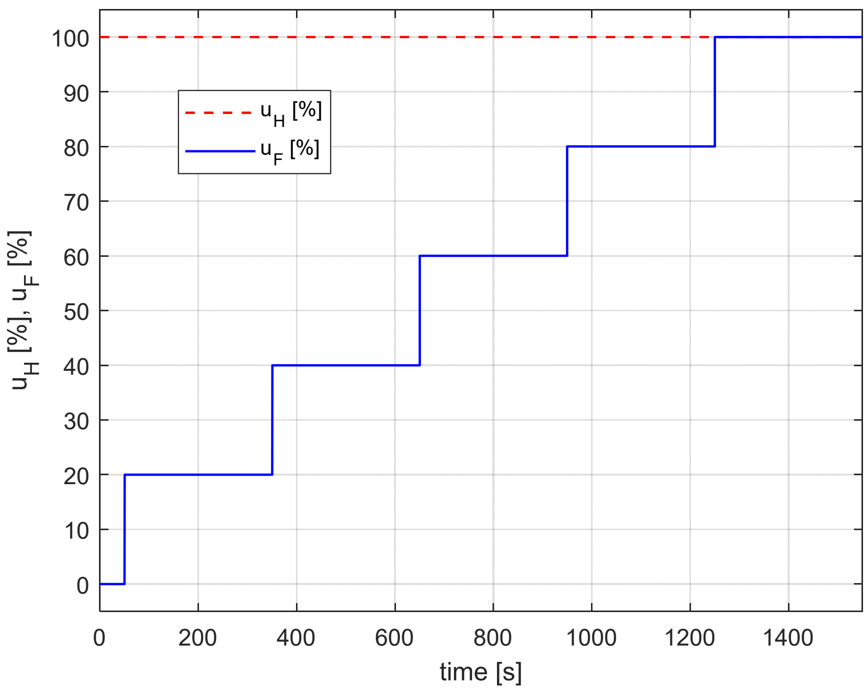

Figure 8.7. Dynamic characteristics in a typical staircase test (Process Configuration #2): input variables (control signal u_F and disturbance u_H).

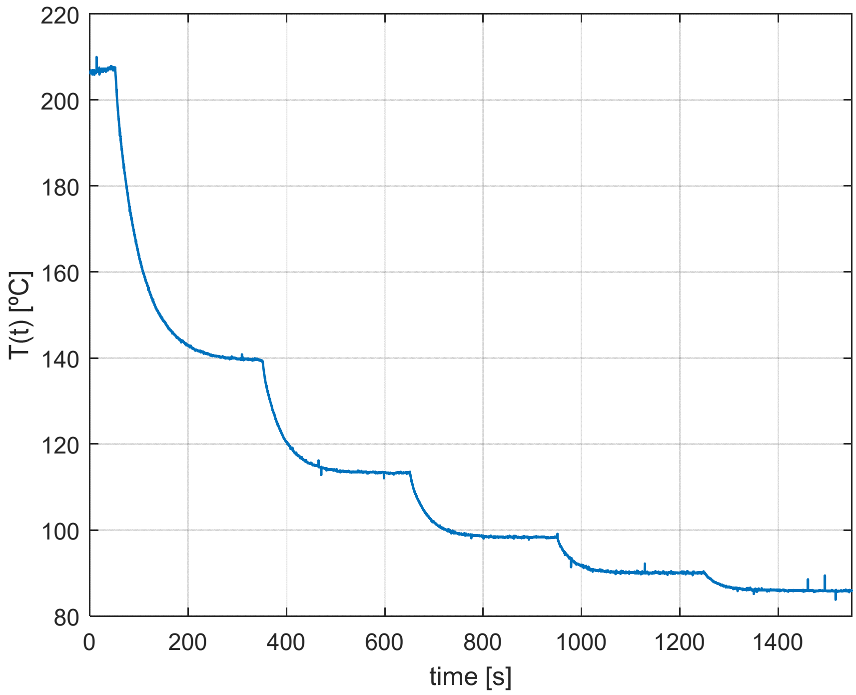

Figure 8.8. Dynamic characteristics in a typical staircase test (Process Configuration #2): output variable (controlled variable T).

Controlled process configuration #3

Figure 8.9 represents the block diagram of the controlled process in configuration #3, where the different variables and units are listed in Table 7.2. This process configuration exhibits the structure of a typical split-range control installation, where there are different ways to configure the final control elements so that they operate on two different ranges.

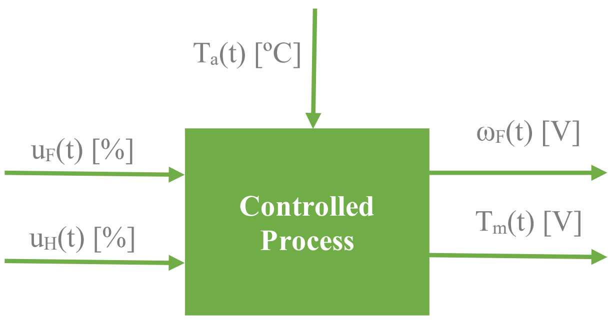

Figure 8.9. Block diagram for the controlled process configuration #3

Figure 8.10 shows an example for a possible operation of both final control elements in this configuration purely for illustrative purposes.

There, the 0 to 100% range of the controller output is splitted in two between both final control elements:

If the controller output is between 0 and 50%, the heating resistance operates. This heating power is a maximum when the controller output is 0% and at its medium value when the controller output is 50%.

If the controller output is between 50 and 100%, it is the air fan the one that is in operation. At 50%, the cooling fan starts to operate and it is at its maximum speed at 100% of the controller output.

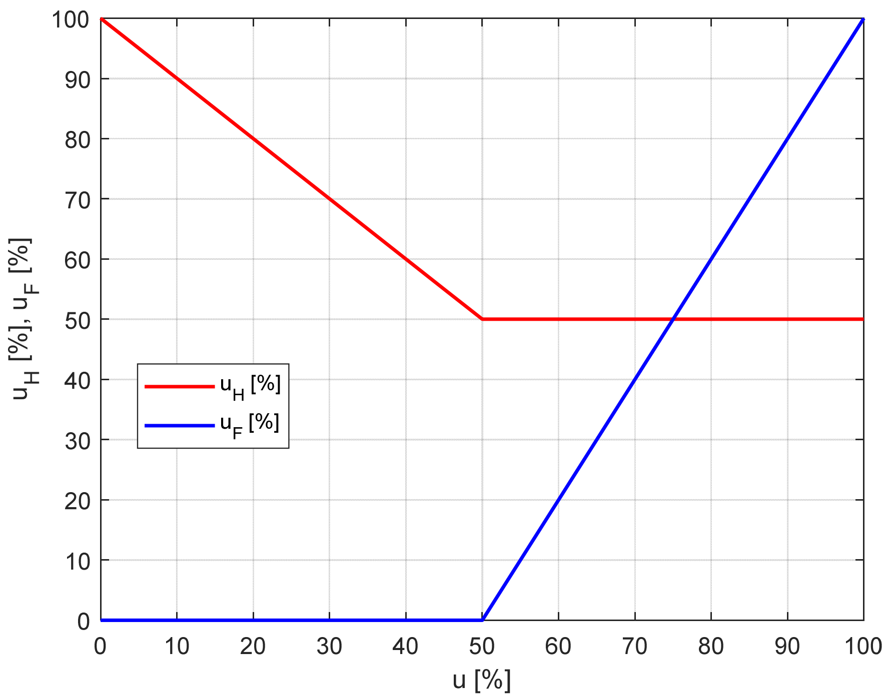

Figure 8.10. Example of the operation of both final control elements defined for the controlled process configuration #3

The static characteristic curves (u, T) for different values of the controller output u are shown in Figure 8.11, exhibiting a nonlinear behaviour throughout the operating range.

The equipment presented in Chapter 7 once again exhibits the flexibility of being able to modify in a very simple way via software the operating mode of the process, defining the operating ranges of both final control elements in a personalized way.

The static characteristic curve (u, T) for the operation defined in Figure 8.10 is shown in Figure 8.11, exhibiting a nonlinear behaviour in a part of the operating range. The gain of the controlled process for the characteristic curve shown in Figure 8.11 is $-1.85°C/\%$ for the range from 0 to 50%. The temperature variation in the characteristic curve for the range from 50 to 100% is $-58.1°C$, exhibiting a very highly nonlinear shape. The gain of the process decreases highly as u increases from 50 to 100%.

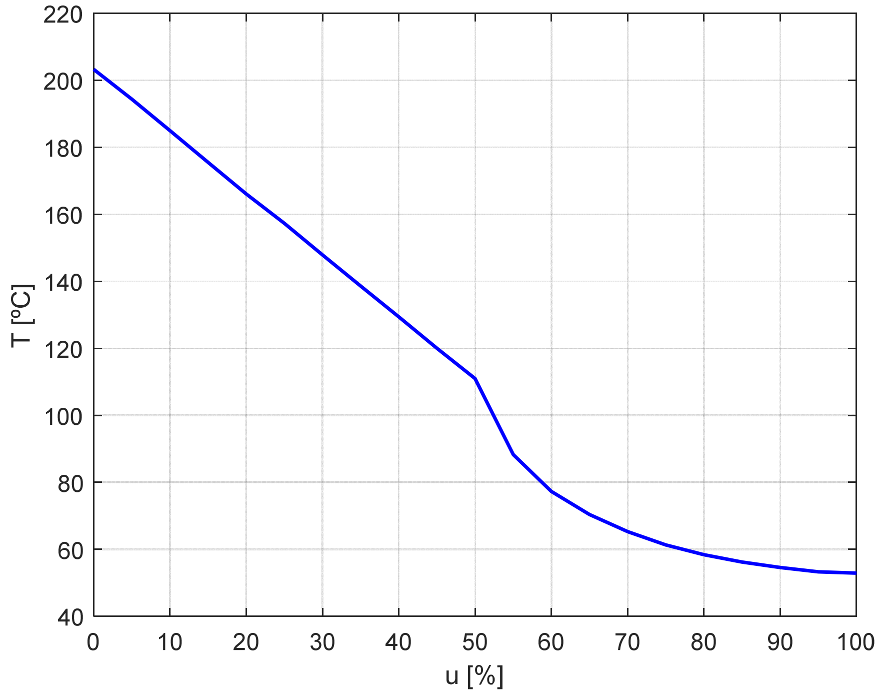

Figure 8.11. Static characteristic T [ºC] – u [%] (Process Configuration #3).

Figures 8.12 and 8.13 illustrate the input variables (control signals u_H and u_F, as functions of the controller output) and the output variable (controlled variable T), respectively, in a typical staircase test. The behaviour is clearly nonlinear, exhibiting different dynamic characteristics for the different operating points.

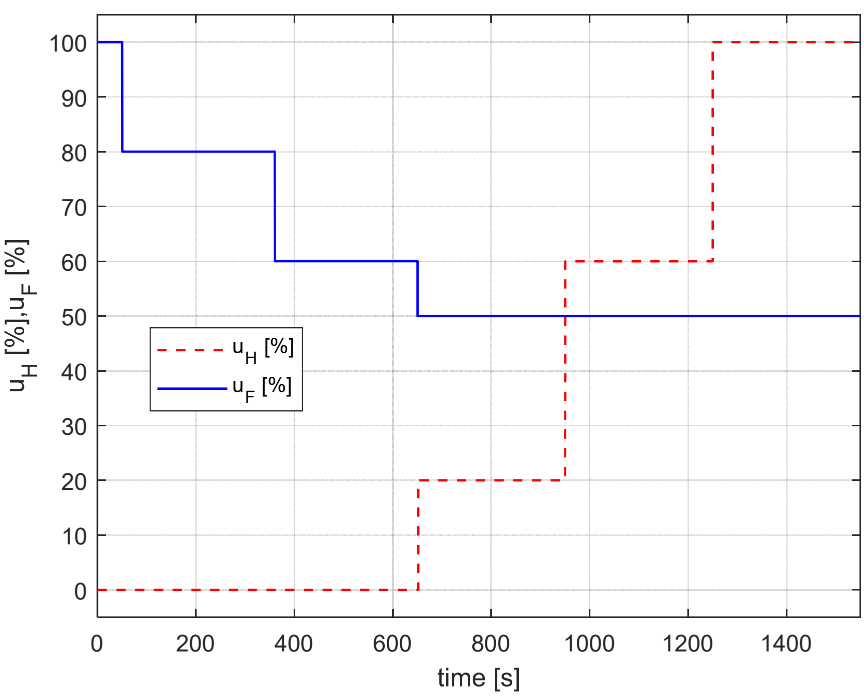

Figure 8.12. Dynamic characteristics in a typical staircase test (Process Configuration #3): input variables (control signals u_F and u_H).

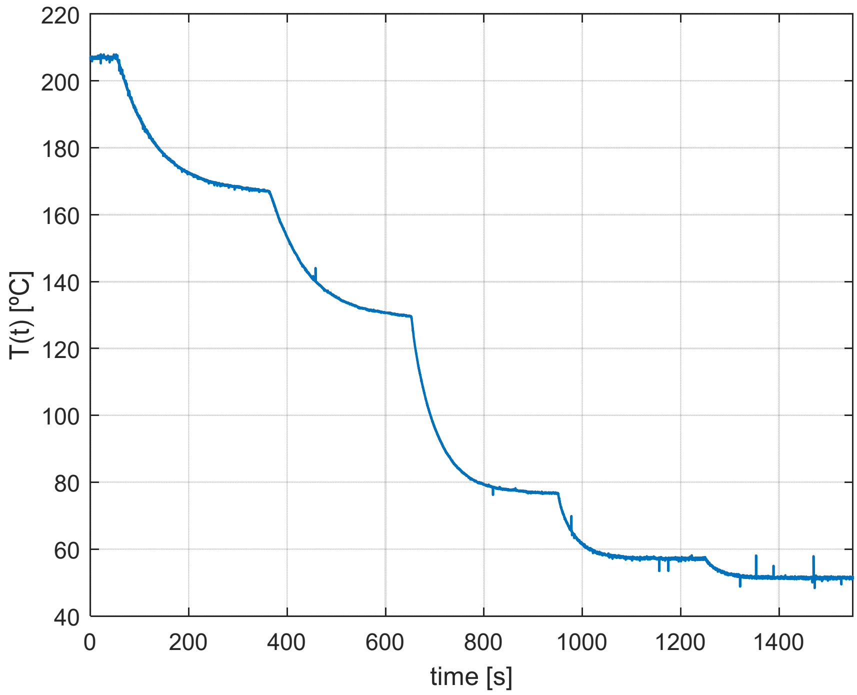

Figure 8.13. Dynamic characteristics in a typical staircase test (Process Configuration #3): output variable (controlled variable T).

8.2.2. Overview of the general identification method

Figure 8.14 illustrates the scheme that summarizes the procedure to identify the parameters of an FFOPDT model, $\theta_P = \{K, T, L, \alpha\}$, using three arbitrary points (x_1-x_2-x_3%) on the process reaction curve. Note that this is a general procedure and accepts that points x_1, x_2 and x_3 to be arbitrary, as illustrated in Figure 4.3.

This procedure admits both symmetrical and asymmetrical position of the points on the reaction curve, as explained in Chapter 6.

This scheme is divided into two different parts, as depicted in Figure 8.14.

Part A is the general procedure to determine rational expressions for functions $f_1(\Delta)$, $f_2(\alpha)$ and $f_3(\alpha)$, which depend on the location of the set of points (x_1-x_2-x_3%). It consists of the following steps:

1. The values of the normalized times $\{\tau_{x1}, \tau_{x2}, \tau_{x3}\}$ for the considered three arbitrary points are obtained from the normalized process output (4.3), $\tilde{y}_\alpha(\tau)$, for the different values of α, with $0.50 \leq \alpha \leq 1.10$.
2. Different data sets $\{\Delta, \alpha\}$, $\{\alpha, f_2(\alpha)\}$, and $\{\alpha, f_3(\alpha)\}$ are obtained using the values of the corresponding normalized times for the considered set of points (x_1-x_2-x_3%).
3. Using a curve-fitting procedure, rational functions are obtained for $f_1(\Delta)$, $f_2(\alpha)$, and $f_3(\alpha)$, respectively.

4. Considering the different rational functions $f_1(\Delta)$, $f_2(\alpha)$, and $f_3(\alpha)$, which have been determined in the previous step, the set of Equation (4.10) are completed.

Part B consists of the algorithm for identifying the FFOPDT model from the process reaction curve. It consists of the following steps:

1. Data required for the identification procedure are obtained from the process reaction curve $\{\Delta y, \Delta u, t_{x1}, t_{x2}, t_{x3}\}$.
2. The value of the ratio index Δ is calculated from the set of times $\{t_{x1}, t_{x2}, \text{and } t_{x3}\}$.
3. The value of α and the numerical values of f_2 and f_3 are estimated.
4. After determining the numerical values of α, f_2, and f_3, the FFOPDT model parameters, $\theta_P = \{K, T, L, \alpha\}$, are calculated by using the set of equations (4.10) and the process data taken from the process reaction curve $\{\Delta y, \Delta u, t_{x1}, t_{x2}, t_{x3}\}$.

This section only represents an overview of the general identification procedure to be used in this chapter. For a more detailed information the reader is referred to Chapter 6.

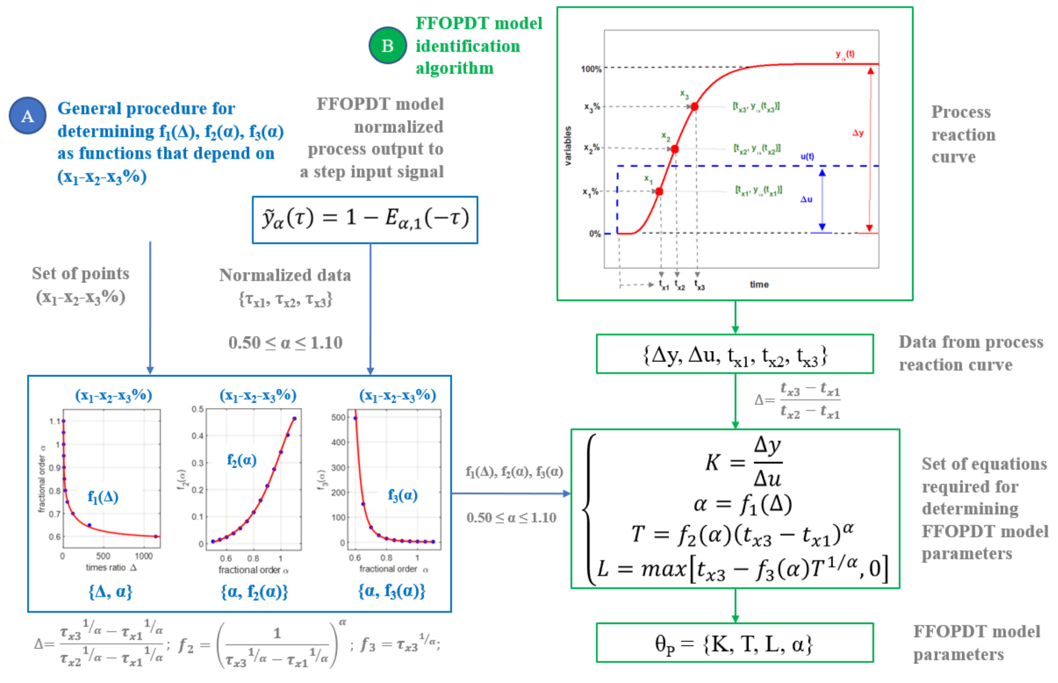

Figure 8.14. Scheme of the complete procedure for identifying a FFOPDT model considering three arbitrary points $(x_1\text{-}x_2\text{-}x_3\%)$ on the process reaction curve. Note that the scheme is divided into two parts: Part A represents the general procedure to obtain the set of equations for determining FFOPDT model parameters. These equations depend on the set of points $(x_1\text{-}x_2\text{-}x_3\%)$. Part B of the scheme illustrates the FFOPDT model identification algorithm for estimating model parameters $\theta_P = \{K, T, L, \alpha\}$ with the information collected from the process reaction curve $\{\Delta y, \Delta u, t_{x1}, t_{x2}, t_{x3}\}$.

8.2.3. Algorithms for determining FFOPDT model parameters

This section provides the FFOPDT model identification algorithms, which have been developed in Chapter 4 for a symmetrical set of points (x-50-(100–x)%), in Chapter 5 for a symmetrical set of points considering the central point x_2 to be arbitrary (x-x_2-(100–x)%), and in Chapter 6 for an asymmetrical set of points (x_1-x_2-x_3%), respectively.

As discussed throughout the dissertation, these procedures are analytical, which simplifies significantly their implementation on a hardware platform such as any of those considered in the hardware architecture presented in Chapter 7.

Therefore, the objective of these algorithms is to facilitate the software implementation of the proposed identification procedures.

Symmetrical set of points (x-50-(100–x)%)

In this method, the variation in input signal Δu and process output Δy, and times necessary to reach x% (t_x), 50% (t_{50}), and (100–x)% (t_{100-x}) of the process output total change on the process reaction curve must be collected in order to determine FFOPDT model parameters $\theta_P = \{K, T, L, \alpha\}$.

Table 8.1 illustrates the algorithm for determining the parameters of the FFOPDT model when three symmetrical points $\{t_x, t_{50}$ and $t_{100-x}\}$ on the process reaction curve are specified.

Algorithm: Symmetrical identification method
Input: $\{t_x, t_{50}$ and $t_{100-x}\}$, Δy, and Δu from the process reaction curve
Output: FFOPDT model parameters $\theta_P = \{K, T, L, \alpha\}$
1: Calculate the process gain K using (4.2).
2: Collect t_x, t_{50}, and t_{100-x} from the process reaction curve.
3: Calculate the value of Δ using equation (4.13).
4: Calculate the value of $\alpha = f_1(\Delta)$ using equation (4.15).
5: Calculate the value of functions $f_2(\alpha)$ and $f_3(\alpha)$ using equations (4.16) and (4.17), respectively.
6: Determine the value of $T = f_2(\alpha)\cdot(t_{100-x} - t_x)^{\alpha}$.
7: Determine the value of $L = \max[t_{100-x} - f_3(\alpha)\cdot T^{1/\alpha}, 0]$.

Table 8.1. Algorithm for determining FFOPDT model parameters $\theta_P = \{K, T, L, \alpha\}$ when three symmetrical points $\{t_x, t_{50}, t_{100-x}\}$ on the reaction curve are specified.

Symmetrical set of points with arbitrary central point x_2 (x-x_2-(100–x)%)

This method requires the variation in input signal Δu and process output Δy, and times necessary to reach x% (t_x), x_2% (t_{x2}), and (100–x)% (t_{100-x}) of the process output total change on the process reaction curve in order to determine FFOPDT model parameters $\theta_P = \{K, T, L, \alpha\}$.

Table 8.2 illustrates the algorithm for determining the parameters of the FFOPDT model when two symmetrical points and the arbitrary central point x_2 $\{t_x, t_{x2} \text{ and } t_{100-x}\}$ on the process reaction curve are specified.

Algorithm: Symmetrical identification method with arbitrary central point $\mathbf{x_2}$
Input: $\{t_x, t_{x2} \text{ and } t_{100-x}\}$, Δy, and Δu from the process reaction curve Output: FFOPDT model parameters $\theta_P = \{K, T, L, \alpha\}$
1: Calculate the process gain K using (4.2). 2: Collect t_x, t_{x2}, and t_{100-x} from the process reaction curve. 3: Calculate the value of $\Delta = (t_{100-x} - t_x)/(t_{x2} - t_x)$. 4: Calculate the value of $\alpha = f_1(\Delta)$ using equation (5.1). 5: Calculate the value of functions $f_2(\alpha)$ and $f_3(\alpha)$ using equations (5.2) and (5.3), respectively. 6: Determine the value of $T = f_2(\alpha)\cdot(t_{100-x} - t_x)^{\alpha}$. 7: Determine the value of $L = \max[t_{100-x} - f_3(\alpha)\cdot T^{1/\alpha}, 0]$.

Table 8.2. Algorithm for determining FFOPDT model parameters $\theta_P = \{K, T, L, \alpha\}$ when two symmetrical points and the central point $\{t_x, t_{x2}, t_{100-x}\}$ on the reaction curve are specified.

Asymmetrical set of points (x_1-x_2-x_3%)

In this method, the variation in input signal Δu and process output Δy, and times necessary to reach three arbitrary points x_1% (t_x), x_2% (t_{x2}), and x_3% (t_{x3}) on the process reaction curve must be collected in order to determine FFOPDT model parameters $\theta_P = \{K, T, L, \alpha\}$.

Table 8.3 illustrates the algorithm for determining the parameters of the FFOPDT model when three asymmetrical points $\{t_{x1}, t_{x2} \text{ and } t_{x3}\}$ on the process reaction curve are specified.

Algorithm: Asymmetrical identification method
Input: $\{t_{x1}, t_{x2} \text{ and } t_{x3}\}$, Δy, and Δu from the process reaction curve Output: FFOPDT model parameters $\theta_P = \{K, T, L, \alpha\}$
1: Select the corresponding symmetrical or asymmetrical method. 2: Collect process data $\{\Delta u, \Delta y, t_{x1}, t_{x2}, t_{x3}\}$ from the process reaction curve. 3: Calculate the process gain K using (4.2). 4: Calculate the value of $\Delta = (t_{x3} - t_{x1})/(t_{x2} - t_{x1})$. 5: Calculate the value of $\alpha = f_1(\Delta)$ using equation (6.1). 6: Calculate the value of functions $f_2(\alpha)$ and $f_3(\alpha)$ using equations (6.2) and (6.3), respectively. 7: Determine the value of $T = f_2(\alpha)\cdot(t_{100-x} - t_x)^{\alpha}$. 8: Determine the value of $L = t_{x3} - f_3(\alpha)\cdot T^{1/\alpha}$.

Table 8.3. Algorithm for determining FFOPDT model parameters $\theta_P = \{K, T, L, \alpha\}$ when three asymmetrical points $\{t_{x1}, t_{x2}, t_{x3}\}$ on the reaction curve are specified.

8.2.4. Experimental procedure

This section presents the methodology and experimental procedure used to verify and evaluate the effectiveness of the identification procedures developed in Part I of the dissertation when implemented using the hardware architecture presented in Chapter 7.

These identification methods have been applied to the thermal-based process presented in Chapter 7 under configurations #1 and #2.

Without loss of generality, for the results of this chapter an application has been developed in LabVIEW using a microprocessor-based hardware. Since the identification algorithms considered in Section 8.2.3 are analytical, their implementation on any of the control technologies available in the hardware architecture presented in Chapter 7 is simple and straightforward.

The experimental procedure followed in this chapter is as follows:

1. An open-loop step-text experiment has been applied to the input variable for both controlled process configurations (configuration #1 and #2) and the obtained process reaction curve has been recorded.
2. Afterwards, the parameters of the FFOPDT models have been determined using data taken from the process reaction curve and the following proposed identification methods:
    i. For symmetrical and asymmetrical sets of points.

       In this first case, the sets (5-50-95%) and (20-60-95%) are used because they are the symmetrical and asymmetrical sets, respectively, recommended in Chapter 6.
    ii. For symmetrical and symmetrical with arbitrary x_2 sets of points.

       In this second case, the sets (10-50-90%) and (10-65-90%) are used because they are are the sets recommended in Chapter 5.
3. Finally, the accuracy of the identified model parameters is evaluated in comparison with those obtained with other integer- and fractional-order models by means of the MAE (6.7).

Note that all the identification methods used in this section are analytical and based on the reaction curve, which means that they are simple to apply and the computational effort to implement them on a hardware device is low in all cases.

8.3. Experimental results

This section presents the results obtained by applying the different identification methods that have been developed in Part I of the dissertation, more specifically in Chapters 4 to 6, on the thermal-based process under configurations 1 and 2.

As discussed above, the different identification methods have been implemented on the microprocessor-based hardware, which is part of the hardware architecture presented in Chapter 7.

This section is divided into two parts: In the first part, the results obtained using the proposed identification method with symmetrical and asymmetrical sets of points, as discussed in Chapters 4 and 6, respectively, are compared. In the second part, the results obtained using the proposed identification method with both symmetrical and symmetrical with arbitrary x_2 set of points, as described in Chapter 5, are compared.

8.3.1. Symmetrical (x-50-(100–x)%) and asymmetrical (x_1-x_2-x_3%) methods

In this part, the identification methods will be applied to the thermal-based controlled process under configurations #1 and #2.

Controlled Process Configuration #1

In this part, the thermal-based laboratory setup considering controlled process configuration #1 is used. The scheme of the microprocessor-based experimental setup for this configuration is illustrated in Figure 8.15.

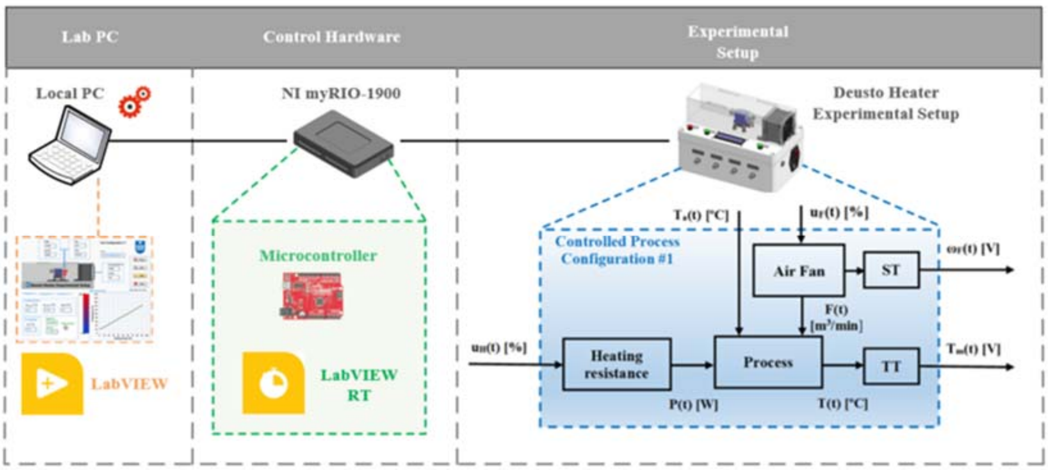

Figure 8.15. Scheme of microprocessor-based experimental setup for the implementation of fractional-order model identification procedures applied to Deusto HES with Controlled Process Configuration #1.

The open-loop step-test experiment is applied to the controlled process in this configuration as follows:

Initially, the control signal to the heating element and the command signal to fan are $u_H = 30\%$ and $u_F = 10\%$, respectively. A step input with amplitude $\Delta u_H = 30\%$ is applied at $t = 0$ s, while u_F is maintained constant, as illustrated in Figure 8.16. The measured variable T_m (measured temperature in the heat block), which is recorded in Figure 8.17, increases from 60.5 to 102.5 °C ($\Delta T_m = 42$ °C).

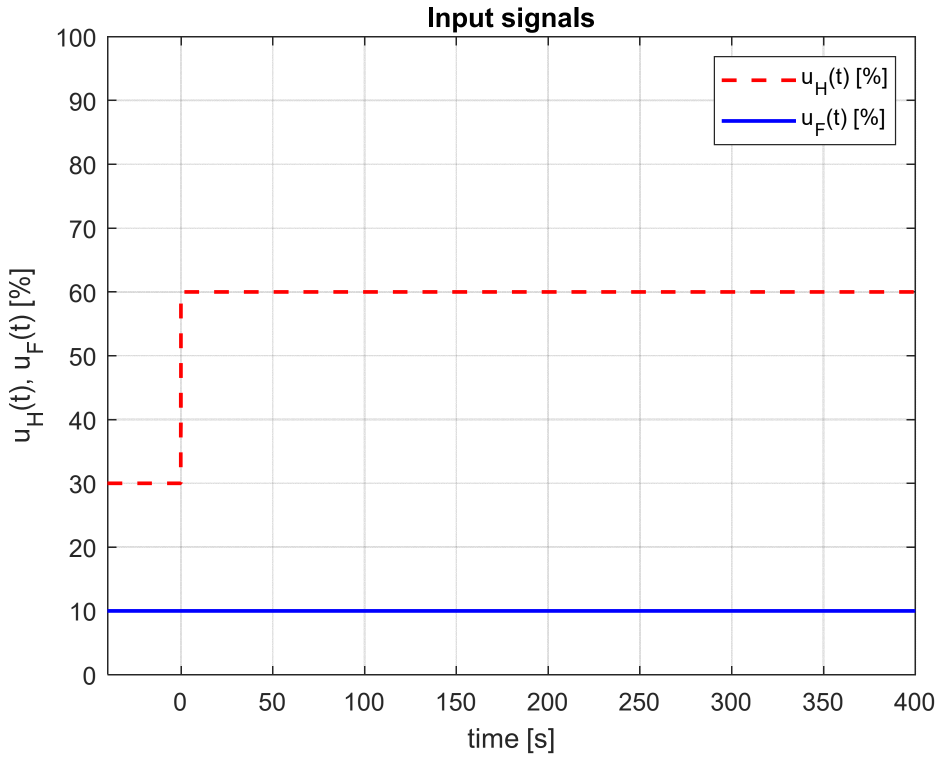

Figure 8.16. Experimental data obtained from a step test for identification of the process model in the Controlled Process Configuration #1: Control signal $u_H(t)$ [%] and command signal to air fan $u_F(t)$ [%].

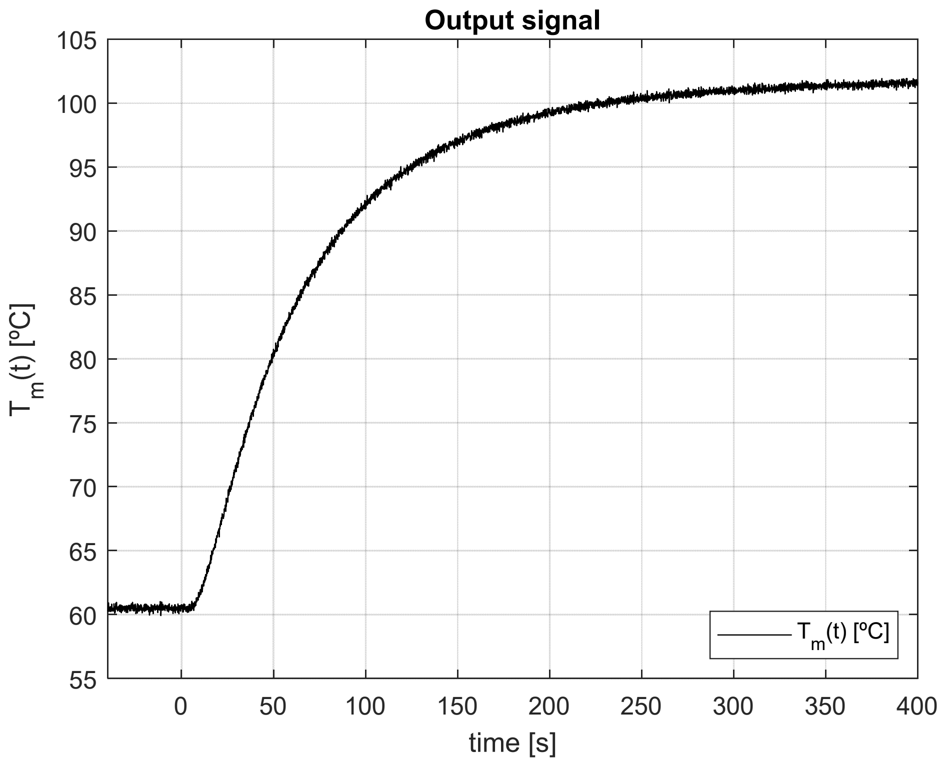

Figure 8.17. Experimental data obtained from a step test for identification of the process model in the Controlled Process Configuration #1: Process reaction curve $T_m(t)$ [°C] at a certain operating point.

Table 8.4 shows the process information required for applying the fractional-order identification method for the proposed set of points (5-50-95%) and (20-60-95%) and collected from the process reaction curve.

FFOPDT	
Symmetrical (5-50-95%)	**Asymmetrical (20-60-95%)**
$\Delta y = \Delta T_m = 42$ °C	
$\Delta u = \Delta u_H = 30\%$	
$t_5 = 12.40$ s	$t_{20} = 24.70$ s
$t_{50} = 53.30$ s	$t_{60} = 67.30$ s
$t_{95} = 251.60$ s	

Table 8.4. Process information for Configuration #1 for fractional-order model identification with sets of points (5–50–95%) and (20–60–95%).

Table 8.5 shows the FOPDT and FFOPDT model parameters for the thermal-based process obtained by using identification methods proposed by Alfaro in (Alfaro 2006) and Vitecková et al. in (Vitecková, Vitecek and Smutny 2000), respectively, and the ones obtained with the identification method proposed in Chapter 6 for (5-50-95%) and (20-60-95%), respectively.

FFOPDT (5-50-95%)	FFOPDT (20-60-95%)	FOPDT Vitecková (25-75%)	FOPDT Alfaro (33-70%)
$K_{1,1} = 1.4$ °C/%	$K_{1,2} = 1.4$ °C/%	$K_{1,3} = 1.4$ °C/%	$K_{1,4} = 1.4$ °C/%
$T_{1,1} = 49.02$ s	$T_{1,2} = 42.56$ s	$T_{1,3} = 64.26$ s	$T_{1,4} = 63.37$ s
$L_{1,1} = 10.55$ s	$L_{1,2} = 14.06$ s	$L_{1,3} = 10.20$ s	$L_{1,4} = 10.25$ s
$\alpha_{1,1} = 0.9418$	$\alpha_{1,2} = 0.9270$	-	-

Table 8.5. Model parameters obtained using the considered identification method for FFOPDT models using (5-50-95%) and (20-60-95%), and the ones using identification methods proposed by Alfaro and Vitecková for FOPDT models.

The step responses of the estimated models for FFOPDT models obtained with the symmetrical (5-50-95%) and asymmetrical (20-60-95%) case and the ones for FOPDT models obtained applying the considered classical methods, are then compared with the process reaction curve and plotted in Figures 8.18 – 8.21, respectively. These figures also show the corresponding representative points.

Figures 8.18 and 8.19 illustrates that both FFOPDT models obtained using the method proposed by the author fit the process reaction curve for the thermal process better than the results obtained for FOPDT models, which are illustrated in Figures 8.20 and 8.21.

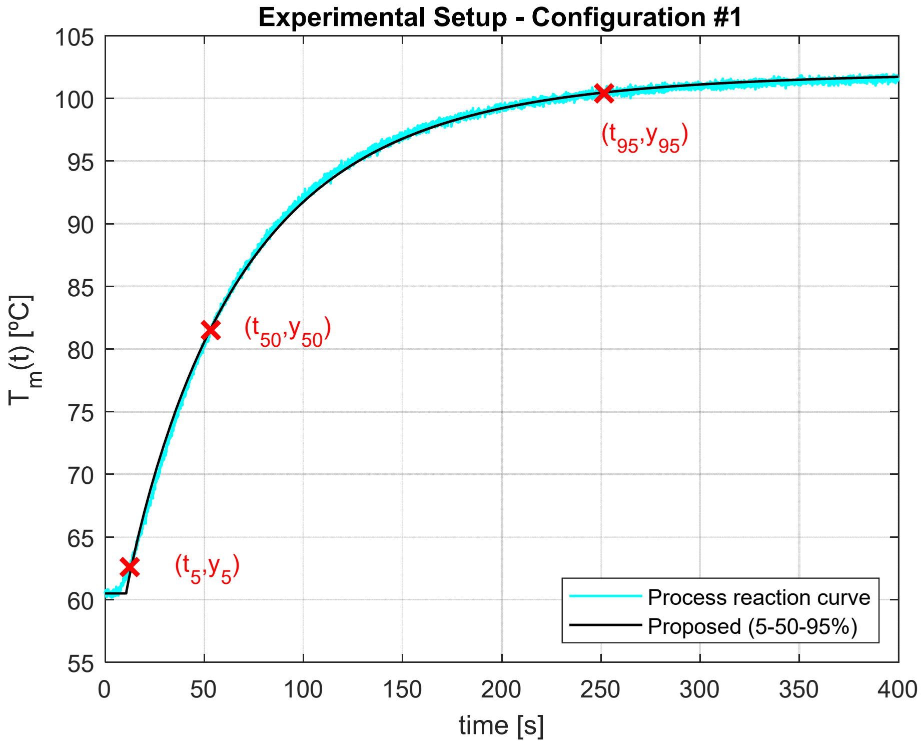

Figure 8.18. Process reaction curve in a certain operating point (Configuration #1) and FFOPDT model step response using the identification method proposed in Chapter 6 for the experimental setup: Symmetrical set of points (5-50-95%).

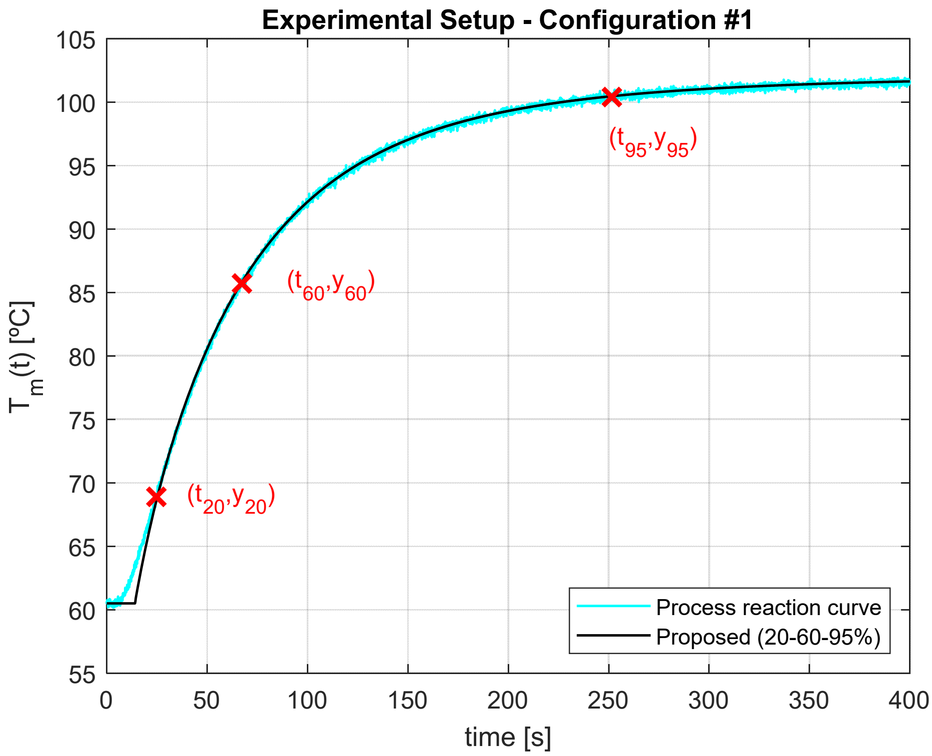

Figure 8.19. Process reaction curve in a certain operating point (Configuration #1) and FFOPDT model step response using the identification method proposed in Chapter 6 for the experimental setup: Asymmetrical set of points (20-60-95%).

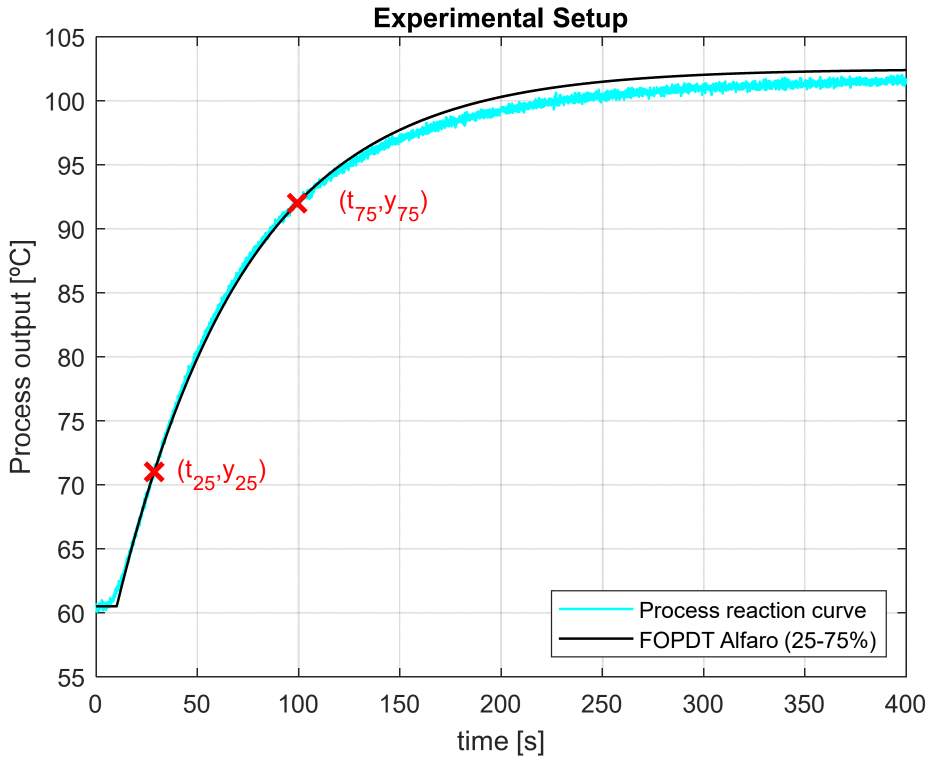

Figure 8.20. Process reaction curve in a certain operating point (Configuration #1) and FOPDT model step response using two-point identification methods for the experimental setup: (a) Method proposed by Alfaro in (Alfaro 2006).

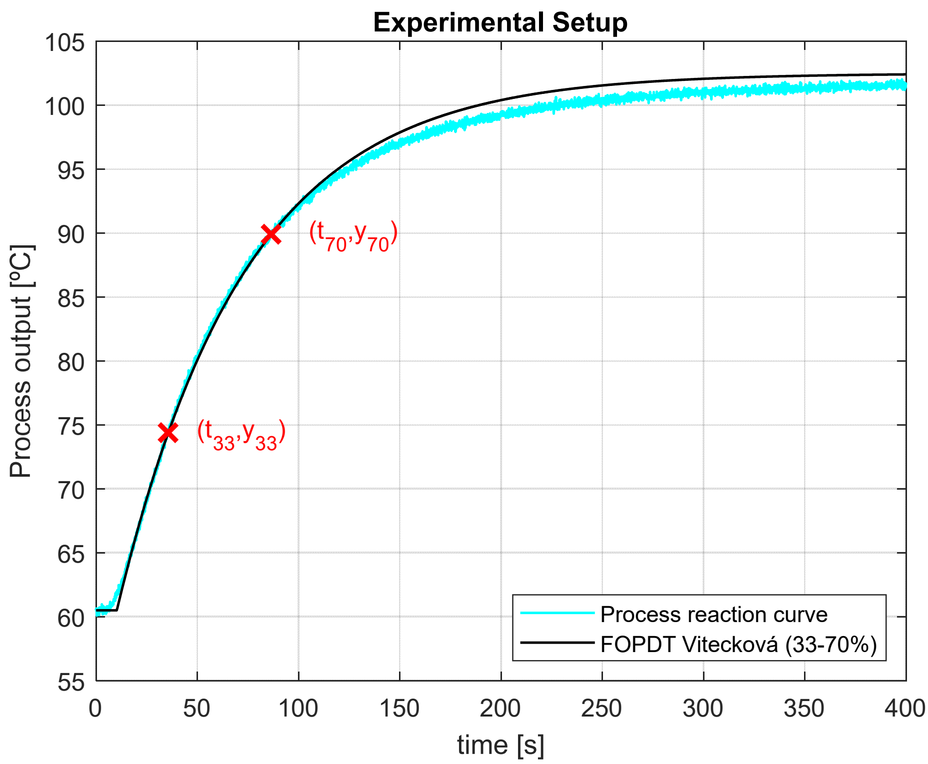

Figure 8.21. Process reaction curve in a certain operating point (Configuration #1) and FOPDT model step response using two-point identification methods for the experimental setup: Method proposed by Vitecková in (Vitecková, Vitecek and Smutny 2000).

Table 8.6 shows the values of the time-domain performance index $E(\bar{\theta}_{1,i})$ for the estimated models obtained with this configuration. Considering this table, one can observe that the result obtained with the asymmetrical set of points is better than the one obtained for the symmetrical case, more precisely, the value of E for the asymmetrical case is 1.6 times lower than the one obtained for the symmetrical case.

i	Identification Method	Set of Points	$E(\bar{\theta}_{1,i})$
1	FFOPDT Gude	(5-50-95%)	$6.60 \cdot 10^{-3}$
2	FFOPDT Gude	(20-60-95%)	$4.10 \cdot 10^{-3}$
3	FOPDT Alfaro	(25-75%)	$2.50 \cdot 10^{-2}$
4	FOPDT Vitecková	(33-70%)	$2.59 \cdot 10^{-2}$
	Number of samples:		$N_S = 4001$

Table 8.6. Model performance indexes obtained for the considered identification methods for FFOPDT and FOPDT models.

On the other hand, the results obtained using the method for FFOPDT models proposed by the author for the symmetrical and asymmetrical case provide better results in terms of E than the ones obtained for FOPDT models. More specifically, the FFOPDT model estimated for (5-50-95%) and for (20-60-95%) give E values 3.8 and 3.9, and 6.1 and 6.3 times lower than those obtained for FOPDT models proposed by Alfaro and Vitecková, respectively.

Controlled Process Configuration #2

In this part, the thermal-based laboratory setup considering controlled process configuration #2 is used. The scheme of the microprocessor-based experimental setup for this configuration is illustrated in Figure 8.22.

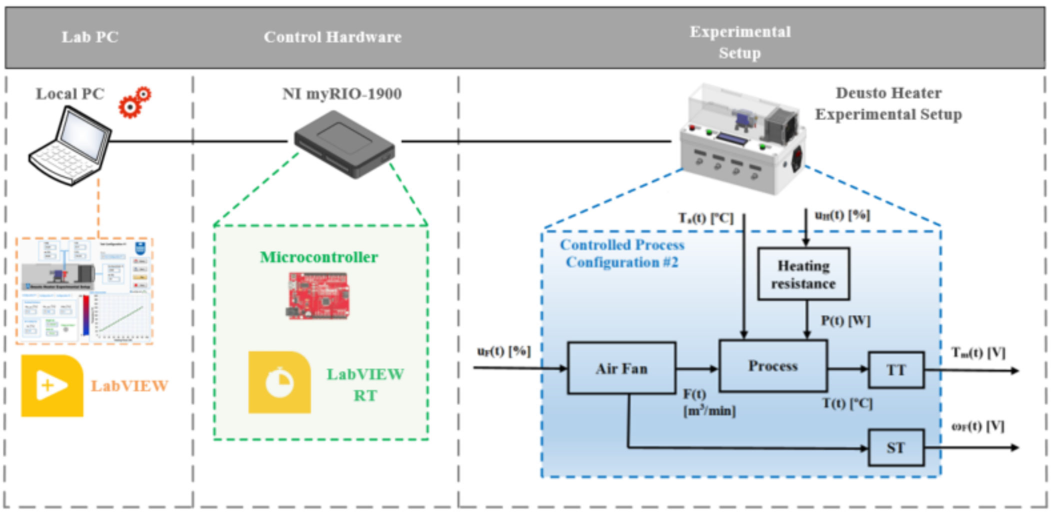

Figure 8.22. Scheme of microprocessor-based experimental setup for the implementation of fractional-order model identification procedures applied to Deusto HES with Controlled Process Configuration #2.

Note that the controlled process is reversed-action in this configuration and its dynamic characteristics are different from the previous case.

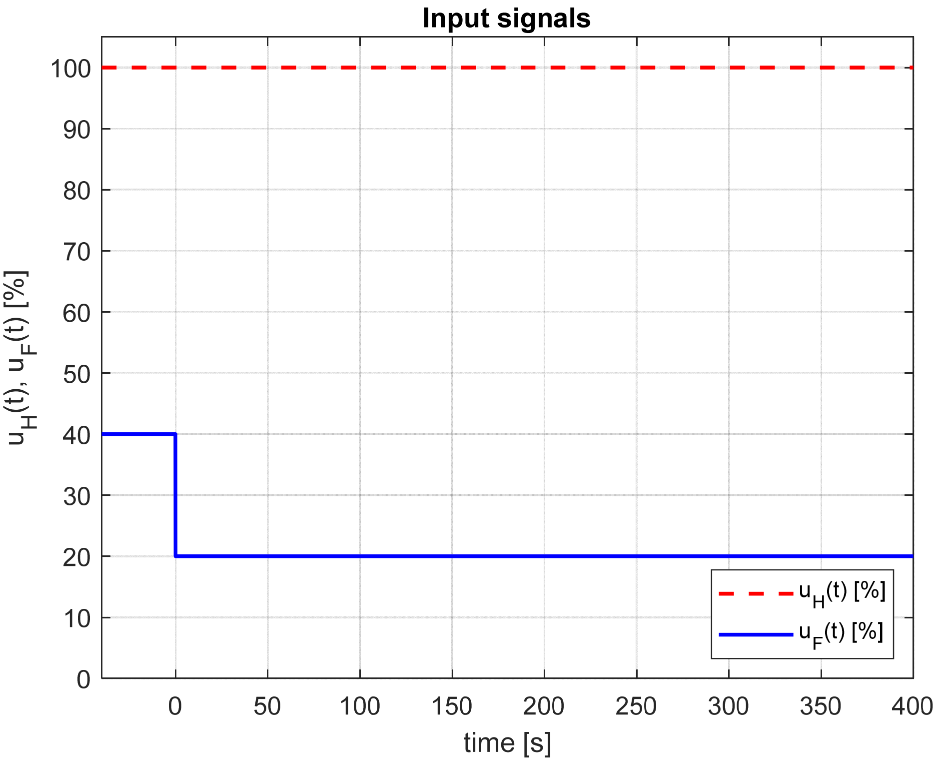

Figure 8.23. Experimental data obtained from a step test for identification of the process model in the Controlled Process Configuration #2: Control signal $u_F(t)$ [%] and command signal to heating resistance $u_H(t)$ [%].

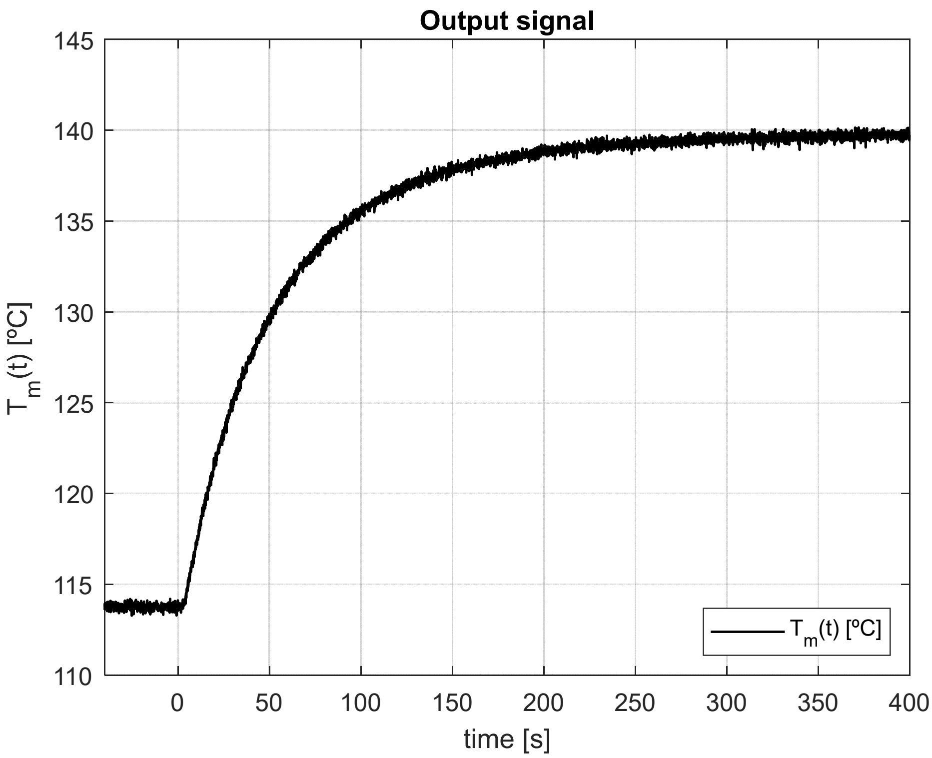

Figure 8.24. Experimental data obtained from a step test for identification of the process model in the Controlled Process Configuration #2: Process reaction curve $T_m(t)$ [°C] at a certain operating point.

The procedure followed in this case is similar to the one followed in the previous case. Initially, the control signal to the air fan is at $u_F = 40\%$ and the command signal to the heating element is at $u_H = 100\%$. A step input with amplitude $\Delta u_F = -20\%$ is applied at $t = 0$ s, while u_H is maintained constant, as depicted in Figure 8.23. The measured variable T_m (measured temperature in the heat block), which is recorded in Figure 8.24, changes from 113.75 to 139.75 °C ($\Delta T_m = 26$ °C).

Table 8.7 contains the process information required for applying the fractional-order identification method for the proposed set of points (5-50-95%) and (20-60-95%) and collected from the process reaction curve.

FFOPDT	
Symmetrical (5-50-95%)	**Asymmetrical (20-60-95%)**
$\Delta y = \Delta T_m = 26$ °C	
$\Delta u = \Delta u_F = -20\%$	
$t_5 = 5.69$ s	$t_5 = 5.69$ s
$t_{50} = 36.49$ s	$t_{50} = 36.49$ s
$t_{95} = 177.34$ s	

Table 8.7. Process information for Configuration #2 for fractional-order model identification with sets of points (5–50–95%) and (20–60–95%).

Table 8.8 shows the FOPDT and FFOPDT model parameters for the thermal-based process in configuration #2 by using the identification method proposed by the author in Chapter 6 for (5–50–95%) and (20–60–95%), respectively, and the ones obtained with methods proposed by Alfaro in (Alfaro 2006) and Vitecková et al. in (Vitecková, Vitecek and Smutny 2000), respectively.

FFOPDT (5-50-95%)	**FFOPDT (20-60-95%)**	**FOPDT Vitecková (25-75%)**	**FOPDT Alfaro (33-70%)**
$K_{2,1} = -1.3$ °C/%	$K_{2,2} = -1.3$ °C/%	$K_{2,3} = -1.3$ °C/%	$K_{2,4} = -1.3$ °C/%
$T_{2,1} = 39.20$ s	$T_{2,2} = 40.20$ s	$T_{2,3} = 52.54$ s	$T_{2,4} = 52.34$ s
$L_{2,1} = 4.10$ s	$L_{2,2} = 3.76$ s	$L_{2,3} = 1.37$ s	$L_{2,4} = 0.93$ s
$\alpha_{2,1} = 0.9523$	$\alpha_{2,2} = 0.9551$	-	-

Table 8.8. Model parameters obtained using the considered identification method for FFOPDT models using (5-50-95%) and (20-60-95%), and the ones using identification methods proposed by Alfaro and Vitecková for FOPDT models.

In this configuration, the step responses of the estimated FFOPDT models obtained using both the symmetrical (5-50-95%) and asymmetrical (20-60-95%) case and the ones for FOPDT models are then compared with the process reaction curve and plotted in Figures 8.25 – 8.28, respectively. These figures also show the corresponding representative points.

Figures 8.25 and 8.26 show that both FFOPDT models obtained with the method proposed by the author give a good fit to the process reaction curve compared with the results for FOPDT models, as illustrated in Figures 8.27 and 8.28.

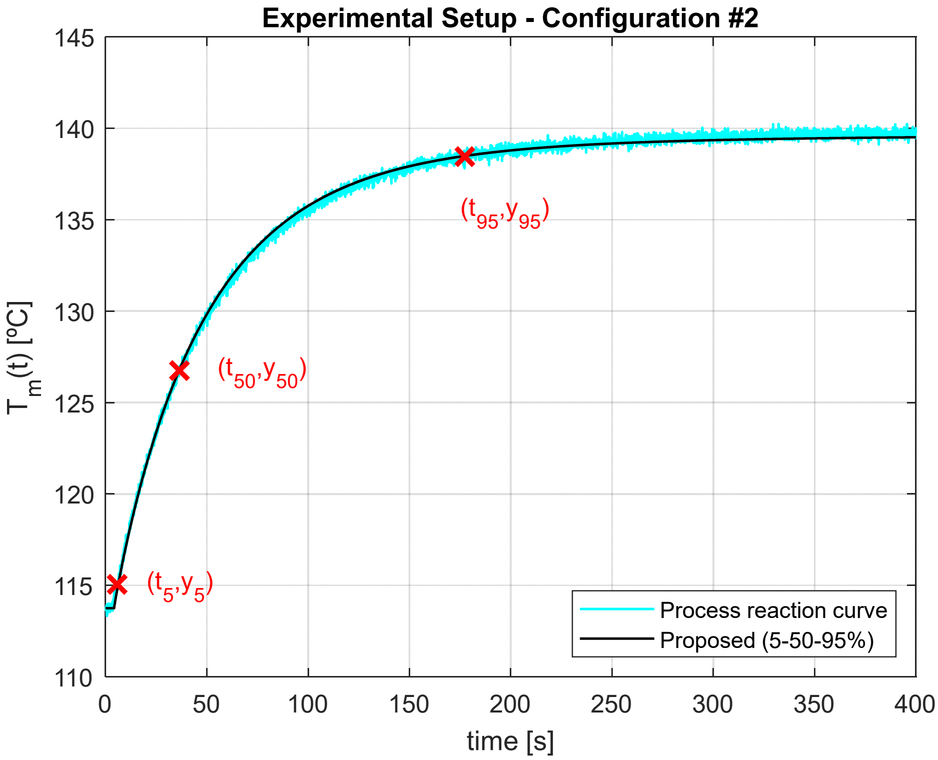

Figure 8.25. Process reaction curve in a certain operating point (Configuration #2) and FFOPDT model step response using the identification method proposed in Chapter 6 for the experimental setup: Symmetrical set of points (5–50–95%).

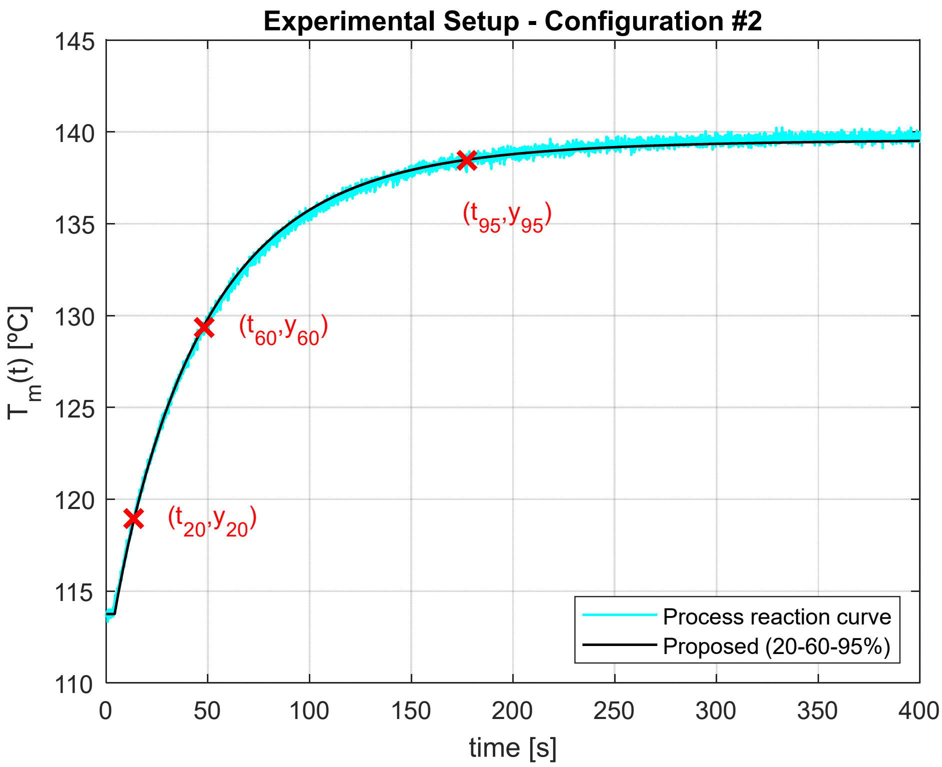

Figure 8.26. Process reaction curve in a certain operating point (Configuration #2) and FFOPDT model step response using the identification method proposed in Chapter 6 for the experimental setup: Asymmetrical set of points (20–60–95%).

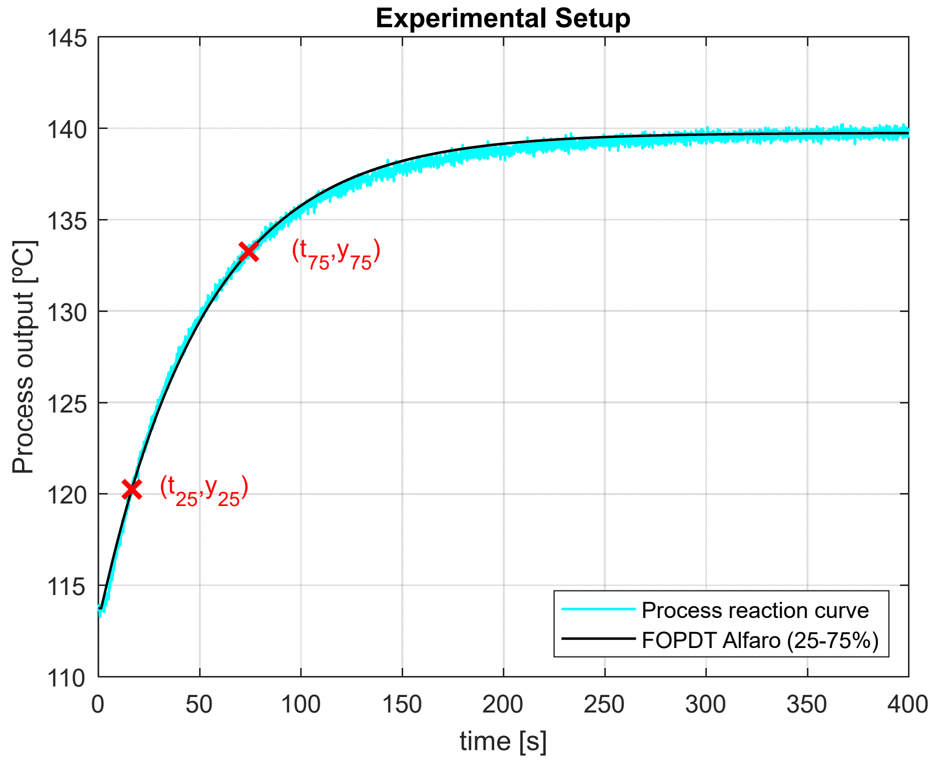

Figure 8.27. Process reaction curve in a certain operating point (Configuration #2) and FOPDT model step response using two-point identification methods for the experimental setup: Method proposed by Alfaro in (Alfaro 2006).

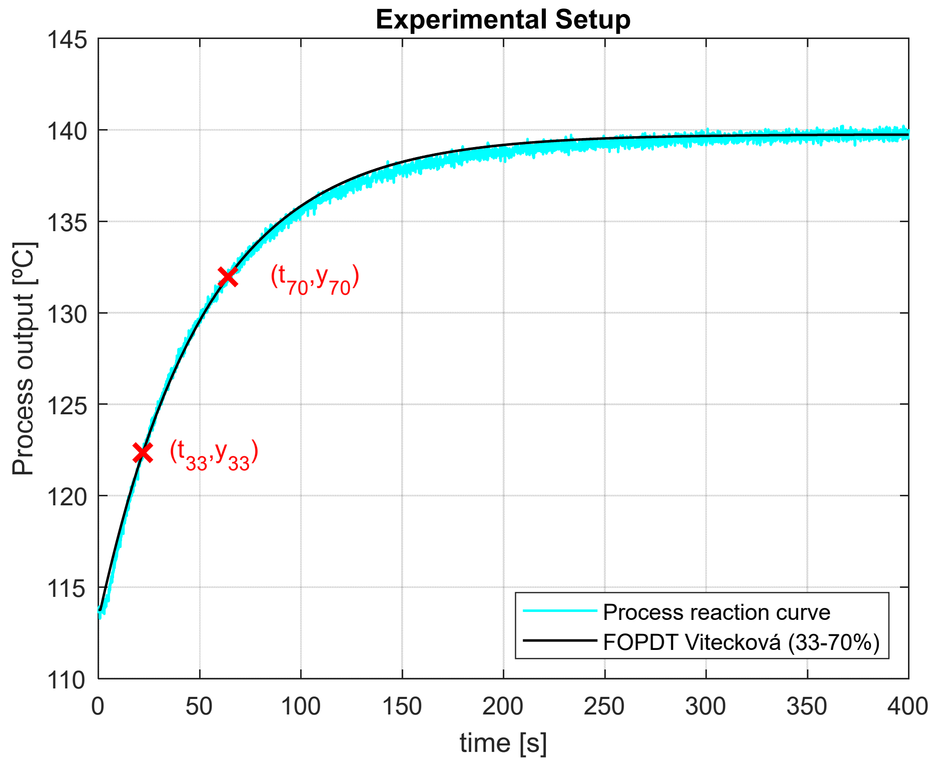

Figure 8.28. Process reaction curve in a certain operating point (Configuration #2) and FOPDT model step response using two-point identification methods for the experimental setup: Method proposed by Vitecková in (Vitecková, Vitecek and Smutny 2000).

Table 8.9 shows the values of the time-domain performance index $E(\overline{\theta}_{2,i})$ for the estimated models obtained with this configuration. Considering this table, one can observe that the result obtained with the asymmetrical set of points is slightly better than the one obtained with the symmetrical set of points. The results obtained using the method for FFOPDT models proposed by the author for the symmetrical and asymmetrical case provide better results in terms of E than the ones obtained for FOPDT models. More specifically, the FFOPDT model estimated for (5-50-95%) and for (20-60-95%) give E values 1.5 and 1.6, and 1.8 and 1.9 times lower than those obtained for FOPDT models proposed by Alfaro and Vitecková, respectively.

i	Identification Method	Set of Points	$E(\overline{\theta}_{2,i})$
1	FFOPDT Gude	(5-50-95%)	$7.20\cdot10^{-3}$
2	FFOPDT Gude	(20-60-95%)	$6.10\cdot10^{-3}$
3	FOPDT Alfaro	(25-75%)	$1.10\cdot10^{-2}$
4	FOPDT Vitecková	(33-70%)	$1.15\cdot10^{-2}$
	Number of samples:		$N_S = 4001$

Table 8.9. Model performance indexes obtained for the considered identification methods for FFOPDT and FOPDT models.

8.3.2. Symmetrical (x-50-(100–x)%) and symmetrical with arbitrary x_2 (x-x_2-(100–x)%) methods

In this part, the identification methods will be applied to the thermal-based controlled process under configuration #1.

Controlled Process Configuration #1

In this section, the thermal-based experimental setup considering the controlled process configuration #1 will be used. Figure 8.15 illustrates the complete layout of the microprocessor-based hardware architecture used to implement the fractional-order model identification algorithms considered in this dissertation. The figure also represents the controlled process in the form of a block diagram, including variables, units and the different components for this configuration.

The experimental data taken from an open-loop test for the identification of the process model at a certain operating point considering the controlled process configuration #1 are shown in Figures 8.16 and 8.17. These process data will be used to identify the FFOPDT models from the proposed procedure for the selected symmetrical set of points.

From the input and output signals of the open-loop step test shown in Figures 8.16 and 8.17, the process information shown in Table 8.10 has been determined, which shows the process information required to apply the identification method proposed in Chapter 5 for the symmetrical sets of representative points (10-50-90%) and (10-65-90%).

FFOPDT	
Method #6: (10-50-90%)	**Method #9: (10-65-90%)**
$\Delta y = \Delta T_m = 42$ °C	
$\Delta u = \Delta u_H = 30\%$	
$t_{10} = 16.80$ s	
$t_{50} = 53.30$ s	$t_{65} = 76.10$ s
$t_{90} = 174.50$ s	

Table 8.10. Process information for Configuration #1 for fractional-order model identification with sets of points (10–50–90%) and (10–65–90%).

The various FFOPDT model parameters obtained for the thermal-based process at the considered operating point using the identification method with the sets of points (10-50-90%) and (10-65-90%), respectively, are shown in Table 8.11.

Method #6: FFOPDT (10-50-90%)	**Method #9: FFOPDT (10-65-90%)**
$K_{3,6} = 1.40$ °C/%	$K_{3,9} = 1.40$ °C/%
$T_{3,6} = 49.83$ s	$T_{3,9} = 46.62$ s
$L_{3,6} = 11.08$ s	$L_{3,9} = 11.49$ s
$\alpha_{3,6} = 0.9468$	$\alpha_{3,9} = 0.9373$

Table 8.11. FFOPDT model parameters obtained for the experimental controlled process with the considered sets of points (10-50-90%) and (10-65-90%), respectively.

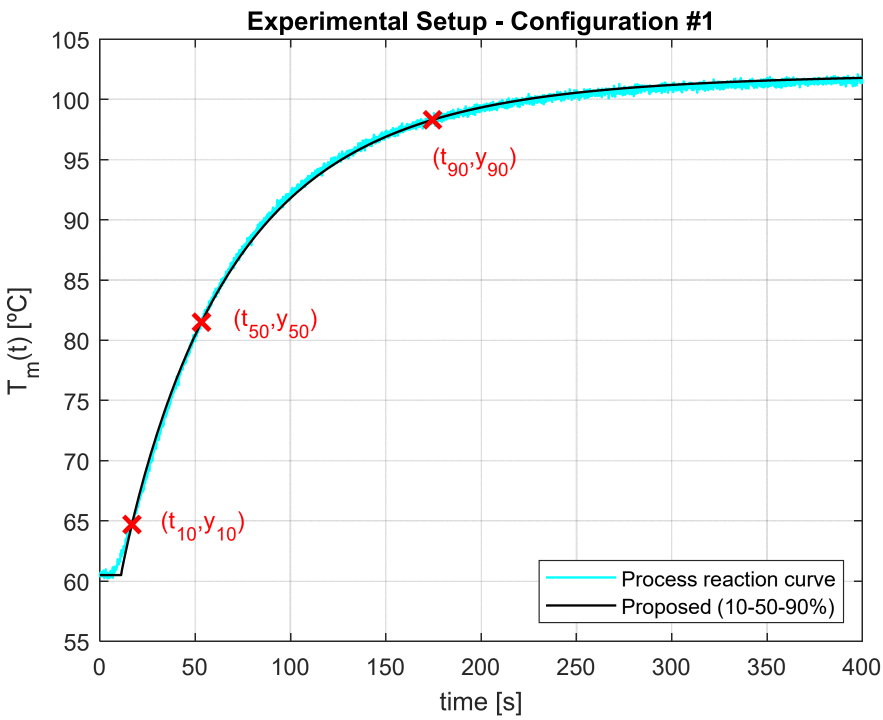

Figure 8.29. FFOPDT model step response using the proposed identification method for (10-50-90%) and process reaction curve.

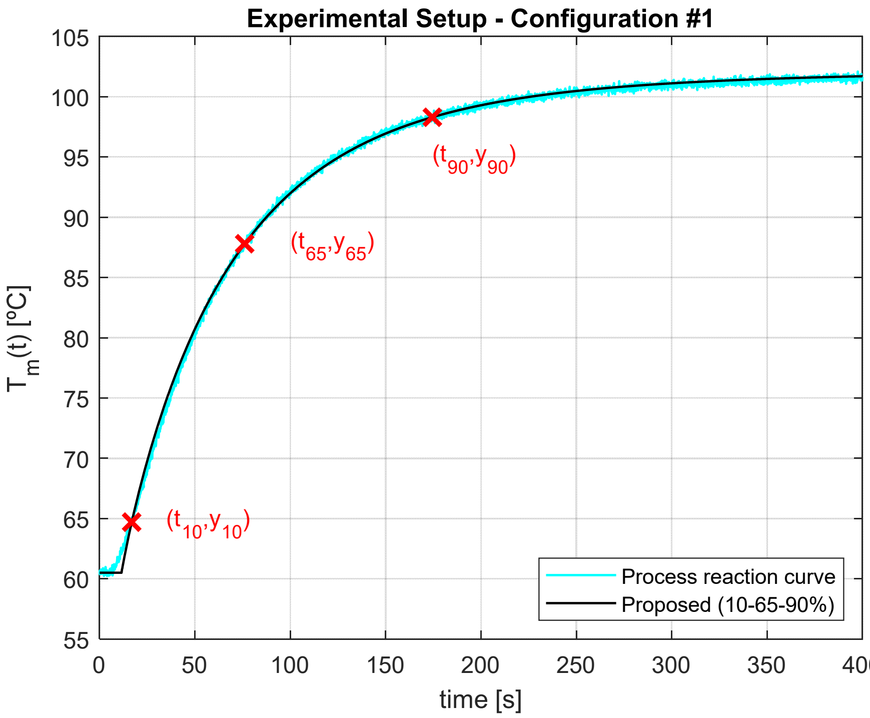

Figure 8.30. FFOPDT model step response using the proposed identification method for (10-65-90%) and process reaction curve.

The process reaction curve is then compared with the step responses of the corresponding FFOPDT models determined by considering the sets of points (10-50-90%) and (10-65-90%), and depicted in Figures 8.29 and 8.30, respectively. These figures also show the corresponding representative points on the process reaction curve.

The different models obtained using methods # 1 – 11 proposed in Chapter 5 have also been obtained. In order to evaluate the accuracy of these models, Table 8.12 shows the values of the time-domain model performance index $S(\bar{\theta}_{3,j})$ for the different identification methods ($j = 1, \ldots, 11$) applied to the thermal-based experimental controlled process.

Figure 8.31 shows graphically the information given in Table 8.12. Note that the behaviour for the temperature-based process is similar to the one for the illustrative examples shown in Chapter 5, exhibiting a minimum in $S(\bar{\theta}_{3,j})$ for a value of $x_2 > 50\%$. More specifically, the minimum value falls at $x_2 = 60\%$ ($j = 8$), although the difference with $x_2 = 65\%$ ($j = 9$) can be considered negligible. For values greater than $x_2 = 60\%$, the value of the performance index increases slightly, as described in Chapter 5. In this case, the benefit obtained by using $x_2 = 65\%$ instead of $x_2 = 50\%$ can be quantified in terms of an 8% reduction in the time-domain performance index S.

j	Identification method	x_2	Set of points	Model	$S(\theta_{3,j})$
1	Method #1	25%	(10-25-90%)	FFOPDT	$3.12 \cdot 10^{-4}$
2	Method #2	30%	(10-30-90%)	FFOPDT	$2.20 \cdot 10^{-4}$
3	Method #3	35%	(10-35-90%)	FFOPDT	$1.62 \cdot 10^{-4}$
4	Method #4	40%	(10-40-90%)	FFOPDT	$1.15 \cdot 10^{-4}$
5	Method #5	45%	(10-45-90%)	FFOPDT	$9.02 \cdot 10^{-5}$
6	Method #6	50%	(10-50-90%)	FFOPDT	$7.34 \cdot 10^{-5}$
7	Method #7	55%	(10-55-90%)	FFOPDT	$6.68 \cdot 10^{-5}$
8	Method #8	60%	(10-60-90%)	FFOPDT	$6.50 \cdot 10^{-5}$
9	Method #9	65%	(10-65-90%)	FFOPDT	$6.70 \cdot 10^{-5}$
10	Method #10	70%	(10-70-90%)	FFOPDT	$7.28 \cdot 10^{-5}$
11	Method #11	75%	(10-75-90%)	FFOPDT	$8.01 \cdot 10^{-5}$
		Number of samples			$N_S = 4001$

Table 8.12. Time-domain model performance indices $S(\theta_{3,j})$ for the experimental controlled process.

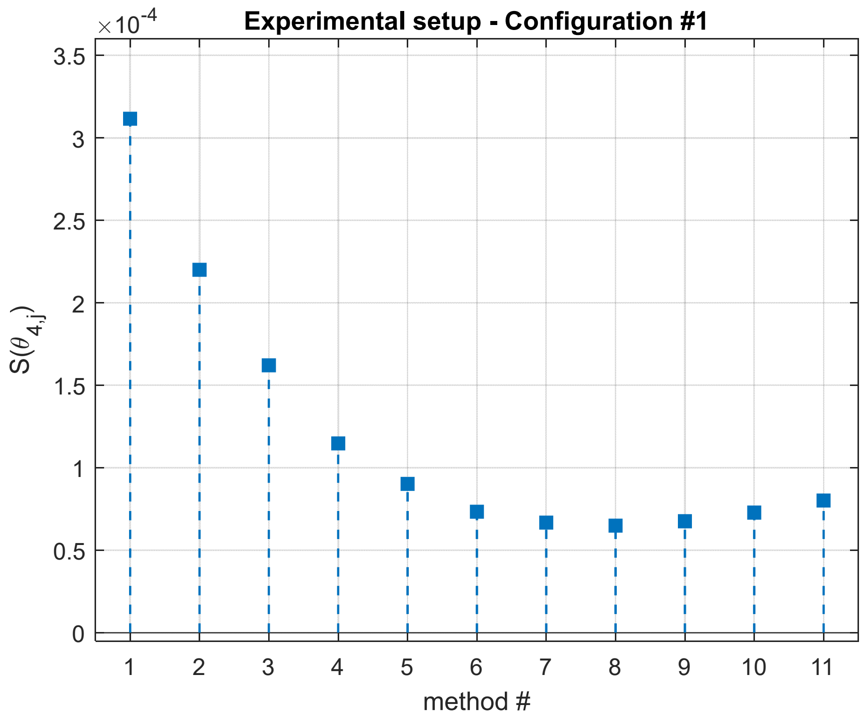

Figure 8.31. Model performance index values $S(\theta_{3,j})$ obtained with methods #1 – 11 for the experimental controlled process.

8.4. LabVIEW-based application

In this dissertation, the programming language LabVIEW has been selected as a tool to operate the experimental setup, estimate integer- or fractional-order model parameters, and implement integer- and fractional-order control algorithms on different hardware technologies, as has been discussed previously.

Nowadays, the graphical programming language LabVIEW can be considered as an industry standard. LabVIEW provides transparent access to hardware devices and, with the most advanced programming techniques, facilitates the application of various modelling approaches, as well as the practical implementation of both conventional and advanced control algorithms.

Figure 8.32 shows the main menu of the LabVIEW-based application that has been implemented to configure and operate with Deusto HES prototype.

In this figure, two different parts can be clearly observed:

1. Deusto HES Modelling: It includes the applications that determine the static characteristics, the dynamic characteristics, and estimate of the integer- or fractional-order model of the controlled process, respectively. This part will be dealt with in the following section.
2. Deusto HES Control: This includes the various control modes that use the different hardware technologies available in the proposed architecture. This part will be treated in Chapter 9.

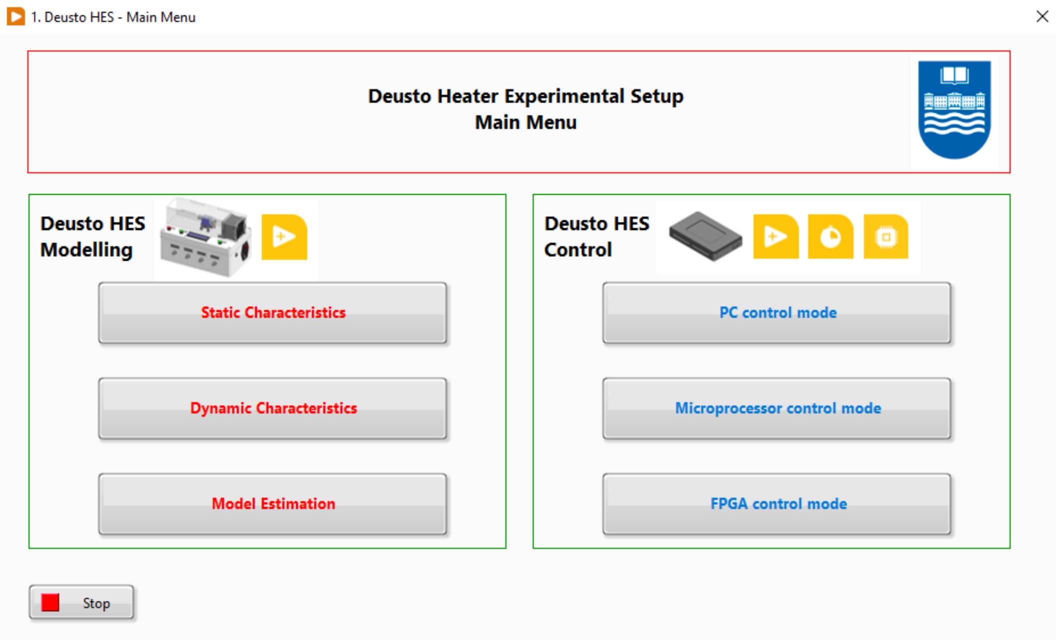

Figure 8.32. Main menu of the LabVIEW-based application to operate with Deusto HES prototype.

8.4.1. Deusto HES modelling

Three applications have been developed to characterize the controlled process in each one of the configurations:

1. Static characteristics. This application allows determining the static characteristics of the controlled process in the different available configurations, as shown in Figure 8.33.
2. Dynamic characteristics. It allows obtaining the evolution of the controlled variable when there is a change in the manipulated variable or disturbance, respectively. Figure 8.34 illustrates variation of $T_m(t)$ when the value of $u_F(t)$ is modified as a staircase while $u_H(t)$ is maintained constant. A nonlinear behaviour of the temperature in the heat block can be emphasized in this figure.
3. Model estimation. The values of the parameters for a simple-structure fractional-order model can be estimated numerically with this application.

Figure 8.35 illustrates the appearance of the LabVIEW-based application for estimation of fractional-order models by using the process reaction curve-based identification method proposed in the Part I of this dissertation for different symmetrical and asymmetrical sets of points.

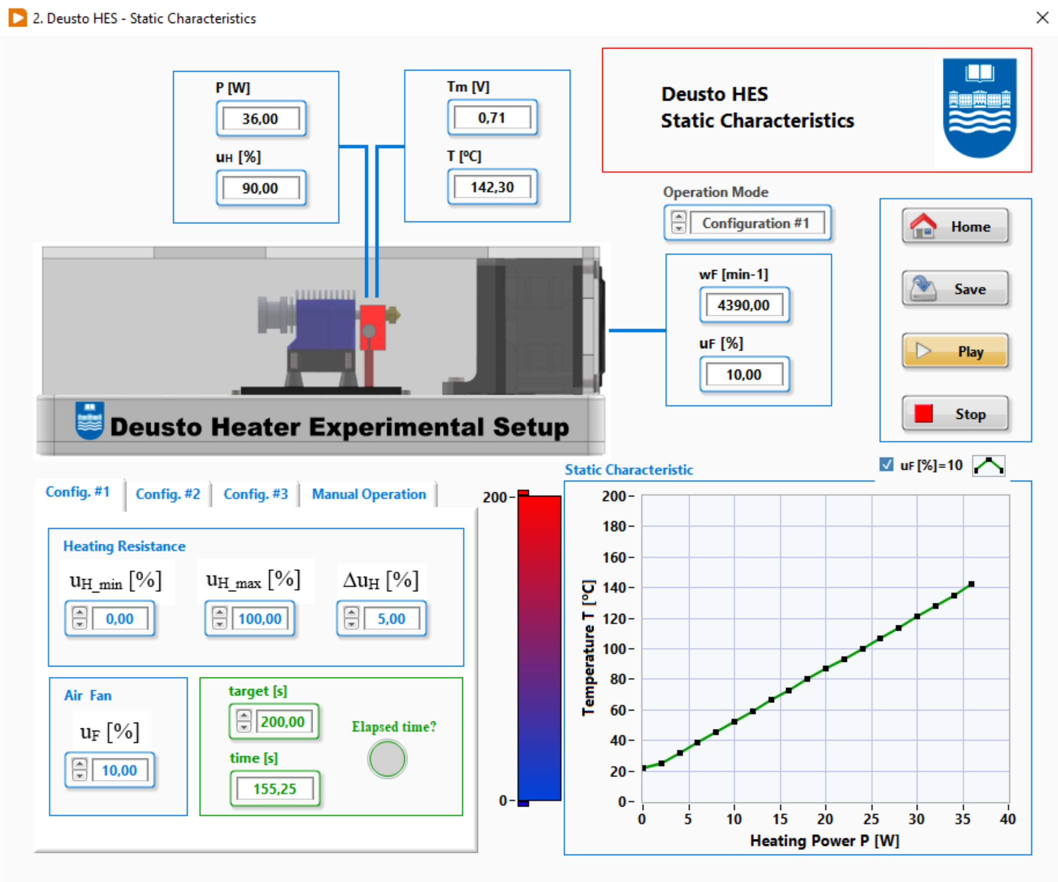

Figure 8.33. LabVIEW-based application for obtaining static characteristics for different configurations of the controlled process and different operating points.

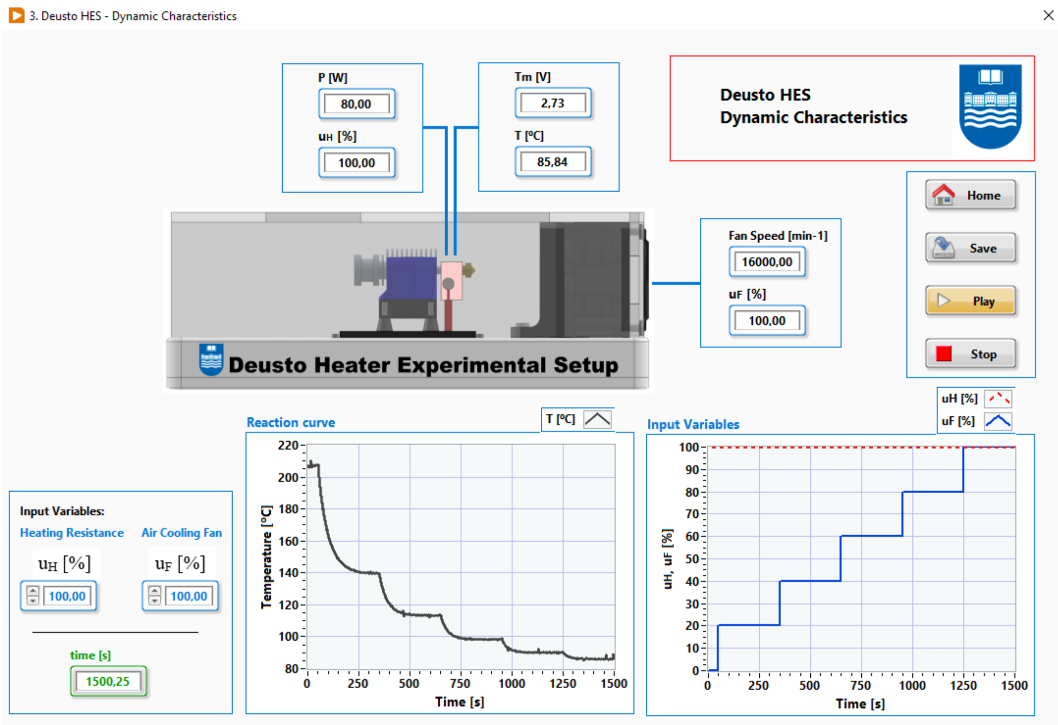

Figure 8.34. LabVIEW-based application for obtaining dynamic characteristics for different configurations of the controlled process and different operating points.

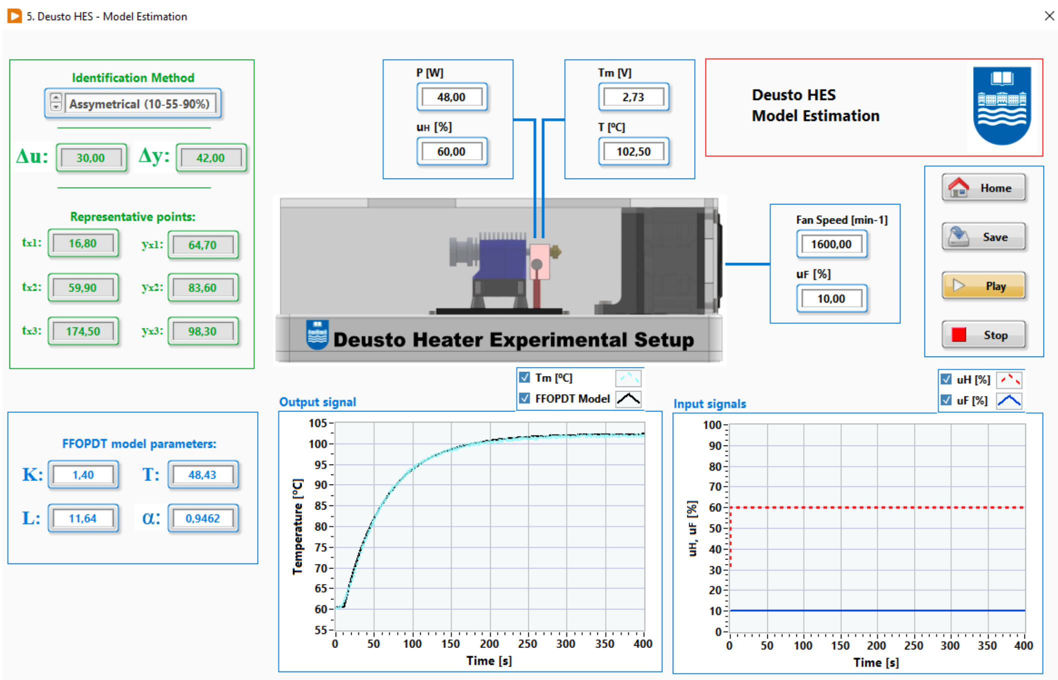

Figure 8.35. Application programmed with LabVIEW for the implementation of fractional-order identification algorithms.

This application presents the following features:

- Selection of the fractional-order identification method and set of points:
    - Symmetrical case (x-50-(100–x)%).
    - Symmetrical case with arbitrary central point x_2 (x-x_2-(100–x)%).
    - Asymmetrical case (x_1-x_2-x_3%).
- Determination of process data $\{\Delta u, \Delta y, t_{x1}, t_{x2}, t_{x3}\}$ taken from the process reaction curve.
- Identification of the fractional-order model parameters: $\theta_P = \{K, T, L, \alpha\}$. Note that FOPDT model parameters can be determined by using the same identification procedure, since FOPDT model can be considered as a particular case with $\alpha = 1$.
- Graphs for registering the process reaction curve $T_m(t)$ [ºC], the step response of the identified model, representative points of the process reaction curve $\{(t_{x1}, T_m(t_{x1})), (t_{x2}, T_m(t_{x2})), (t_{x3}, T_m(t_{x3}))\}$, the command signal to air fan $u_F(t)$ [%], and the command signal to heating resistance $u_H(t)$ [%].
- Export the experimental data in text- or excel-format.

8.5. Discussion

As mentioned in the previous chapter, one of the objectives of Part II of the dissertation is to develop a novel control hardware architecture for the implementation of integer- and fractional-order identification and control algorithms on a real-time target.

In this chapter, some of the objectives proposed in this dissertation are fulfilled. On the one hand, the proposed hardware architecture is used to validate its applicability and effectiveness for the implementation of fractional-order simple-structure model identification algorithms and tested on a laboratory prototype. On the other hand, insights into the practical issues related to the implementation of the identification algorithm in industrial control hardware are gained.

In this regard, the temperature-based process, which involves thermal conduction, exhibits fractional behaviour in the different configurations. Its nonlinear behaviour and the possibility of choosing multiple operating points with different dynamic characteristics are also remarkable. All these features make this laboratory setup suitable for training in aspects related to modeling and implementation of integer- and fractional-order model identification methods.

Since fractional behaviour is ubiquitous in the industrial context; see (Chen 2006) and (Sabatier 2021), the existence of methods for fractional-order model identification and the ability to be implemented on real-time targets is of major interest (Caponetto, et al. 2010), (Tavakoli-Kakhki, Haeri and Tavazoei 2010).

In the specific scope of this chapter, the implemented identification procedures described in the Part I of this dissertation have been compared with various well-recognized identification procedures for integer- and fractional-order systems that use process data taken from the process reaction curve.

It has been obtained that the estimated fractional-order models significantly outperform integer-order models in terms of accuracy. This confirms the well-known benefit obtained when using fractional calculus and justified in the technical literature in terms of more accurate modeling; see, e.g., (Tepljakov 2017), (Guevara, et al. 2015), and (Alagoz, et al. 2019).

In Chapter 6, there is an interesting discussion on whether the additional effort of considering fractional calculus is worth it to obtain a more accurate model and, eventually, a better control performance.

As far as the practical implementation is concerned, microprocessor-based hardware has been used for the implementation of fractional-order identification algorithms, which has made possible to verify their applicability in an industrial environment. Although in this chapter only analytical identification methods have been implemented, whose implementation is very simple and straightforward in any of the real-time targets available in the proposed hardware architecture, it is also possible to implement more complicated algorithms.

In this regard, it is important to note that a typical process plant involves hundreds or thousands of control loops and for an identification method of this type to have a potential impact in industry, a key requirement is simplicity. Also, having laboratory setups such as the one proposed in this dissertation supports training in the implementation of more complex identification algorithms, usually based on optimization.

In the author's opinion, the industry needs such identification procedures, especially when the emphasis is on simplicity, and that will help to bridge the existing gap between the practical implementation in industry and theoretical research on fractional-order modelling.

Experiment, fail, learn, and repeat.
Knowledge comes from experience.

Richard Feynman (1918 – †1988)

CHAPTER

9

Fractional-order control: Implementation issues and results

THE previous chapter has verified the applicability and performance of the hardware architecture proposed in Chapter 7 applied to the temperature-based experimental setup by implementing both integer- and fractional-order model identification algorithms.

In contrast, in this chapter, several examples using different hardware technologies have been presented to demonstrate the applicability and effectiveness of the proposed control hardware architecture for the implementation of fractional-order control algorithms on real-time targets. Some particular implementation issues of microprocessor-based and FPGA-based hardware are also discussed in the context of the proposed hardware architecture.

9.1. Introduction

In recent decades, it is widely recognized in both academia and industry that the new computational techniques and the development of fractional calculus have made possible significant advances in fractional-order modeling and control.

However, the existing problems with the implementation of fractional-order control algorithms in real-time targets has caused to become more challenging to convey the practical benefits of fractional calculus in the industrial field (Tepljakov, Alagoz, et al. 2018). Therefore, the use of fractional control algorithms in the industry is currently relatively low, despite the potential advantages offered by fractional-order PID controllers compared to integer-order ones.

In this chapter, various examples using different technologies have been presented in order to show the applicability and effectiveness of the proposed control hardware architecture in the implementation of fractional-order control algorithms. Some hardware implementation issues are also discussed.

Consequently, for the purposes of this chapter related to control considerations, it is enough to design and implement fractional-order PI controllers on two different real-time targets, i.e., on microprocessor- and FPGA-based hardware, respectively, thus verifying the applicability of the proposed hardware architecture and dealing with the specific implementation issues of each hardware platform.

One of the contributions of this dissertation lies in providing an efficient and practical hardware architecture for implementing fractional-order controllers in different control technologies. The main objective of this part of the dissertation is to help in filling the gap between real-time hardware solutions and software-based fractional-order controller simulations.

This chapter is divided into the following parts: First, Section 9.2 discusses hardware implementation issues. More specifically, aspects about microprocessor- and FPGA-based implementation are addressed. Then, in Section 9.3, the results of two examples are discussed for illustrative purposes, both considering the implementation of integer- and fractional-order PI controllers on microprocessor- and on FPGA-based mode, respectively. After that, Section 9.4 describes the application that has been implemented in LabVIEW in order to operate the experimental setup and for the implementation of fractional-order control algorithms in different control technologies. And, finally, some final remarks and a discussion about control issues in this context are provided in Section 9.5.

9.2. Hardware implementation issues

As was mentioned previously, fractional-order systems and controllers have been widely studied during the last two decades, and considerable advancements have been achieved in the analysis and theory of these systems. Moreover, a great deal of effort has been made in the hardware realization of such systems. As a general rule, the implementation of fractional-order control algorithms or systems typically requires the approximation of such systems as high-order rational systems. Consequently, in general it is difficult to translate them into hardware; see, e.g., (Tepljakov, Alagoz, et al. 2018).

Because of the particular practical issues in the approximation and implementation of fractional-order controllers, it is necessary to consider certain aspects, such as hardware cost and speed, and system performance, when choosing the hardware device (Caponetto, et al. 2010). Broadly speaking, implementation of fractional-order integrators and differentiators can be realized by considering analog or digital approximations.

In the analog realization, the considered fractional operator is then approximated as a rational higher-order system that keeps a constant phase within a selected frequency band (Krishna 2011); (Elwakil 2010); (Maundy, Elwakil and Freeborn 2011). The most commonly used analog approximations are based on Oustaloup's Recursive Approximation method and the Modified Oustaloup Filter (Monje, Chen, et al. 2010); (Oustaloup, et al. 2000), Continued Fraction Expansion (CFE) methods (Chen, Vinagre and Podlubny 2004), or Charef's method (Charef, et al. 1992). These CFE methods can be subdivided into low- and high-frequency methods, as well as Matsuda's and Carlson's methods (Vinagre, Podlubny, et al. 2000).

Otherwise, digital realizations of fractional operators, which are more suitable for a hardware implementation, can be performed by considering direct or indirect discretization methods.

Considering an indirect approach, the procedure consists of first doing the frequency-domain fitting in the continuous-time domain and then discretizing the fitted continuous-time transfer function.

Considering a direct approach, these can be based on CFE, power series expansion (PSE), and MacLaurin series expansion, in combination with an appropriate generating function that converts the continuous-time element into the equivalent discrete-time element.

The general formula for the generating function is as follows

$$w(z^{-1}) = \left(\frac{1}{\beta T_S}\frac{1 - z^{-1}}{\gamma + (1 - \gamma)z^{-1}}\right) \tag{9.1}$$

where $w(z^{-1})$ is the discrete equivalent element, T_s is the sampling period, and β and γ are the gain and phase tuning parameters of the generating function.

Several different types of such generating functions have been proposed in technical literature, such as Al-Alaoui, Simpson, recursive Tustin, mixed Tustin-Simpson, mixed Euler-Tustin-Simpson, impulse response-based, and other higher-order generating functions; see the following references (Chen, Vinagre and Podlubny 2004), (Vinagre, Podlubny, et al. 2000), (Tenreiro Machado, Galhano, et al. 2009), (Vinagre, Chen and Petras 2003), (Chen and Moore 2002), and (Gupta, Varshney and Visweswaran 2011).

The expansion formula together with the generating function defines the form of the approximation and the coefficients (Monje, Chen, et al. 2010). The expansion of the generating function can generally be performed through the PSE or CFE methods, which lead to approximations in the form of polynomial or rational functions, respectively. In case of using the PSE method, an approximation with only zeros is obtained for the fractional-order element:

$$s^{\alpha} \cong \mathrm{PSE}[w(z^{-1})^{\alpha}] = P_p(z^{-1}) \tag{9.2}$$

where P_p is the corresponding polynomial with degree p of variable z^{-1}.

In case of using the CFE method, an approximation with zeros and poles are obtained for the fractional-order element:

$$s^{\alpha} \cong \mathrm{CFE}[w(z^{-1})^{\alpha}] = \frac{P_p(z^{-1})}{Q_q(z^{-1})} \tag{9.3}$$

where P_p and Q_q are the corresponding polynomials with degrees p and q, respectively, of variable z^{-1}.

The CFE method is usually preferred over the PSE method because rational functions have the ability to model functions with zeros and poles, which converge faster and have a wider domain of convergence in the complex plane.

Moreover, direct discretization is in general the preferred approach for digital realization over its indirect counterpart (Das and Pan 2012). Note that the final choice for the most appropriate approximation should be connected to various aspects, among the most relevant are the accuracy required in the frequency or the time domain, the large the integer-order transfer functions may be, the maximum order of the transfer function, etc.

In the following, some practical aspects are discussed in particular for the cases where the implementation is performed on microprocessor- and FPGA-based hardware, respectively.

9.2.1. Microprocessor-based implementation

A survey of several fractional-order controller implementations based on microprocessor-based devices is presented in (Caponetto, et al. 2010). In this monograph, the fundamentals of the discrete approximations of a fractional-order operator are described, as well as the control algorithms for the implementation of the controllers. Three examples using discrete fractional-order controllers implemented on a PLC, on a PC with DAQ card, and on a PIC-type microcontroller, respectively, are also presented. For each of the cases considered, the results obtained are illustrated.

It is important to mention that controller realization generally is not equivalent to simulation or numerical evaluation of the fractional-order differential and integral operators.

In the controller realization case, it is worth taking into account some significant considerations:

1. Depending on the type of microprocessor, each system has its specific minimum value for the sampling period.
2. It is required to perform all the calculations required by the control law between two samples.

Because of this last point, obtaining good approximations with a minimum set of parameters is very important because as the number of parameters in the approximation increases, so does the speed and the amount of the required memory.

As a conclusion, the key point in the digital implementation of a fractional-order controller on a microprocessor-based device is the discretization of the fractional-order operators (Caponetto, et al. 2010).

9.2.2. FPGA-based implementation

One of the first monographs devoting to implementation of fractional-order systems in hardware devices is (Caponetto, et al. 2010). There, the basic operator s^{α}, where α is considered to be a real number, is approximated by the binomial expansion of the backward difference and then a hardware implementation of the differintegral operator is proposed using an FPGA. In this context, this building block can be considered as a basic element used to implement fractional-order control systems.

There are some recent references in the technical literature where the implementation of fractional-order operators in the LabVIEW environment is discussed. A systematic procedure for hardware implementation of the basic operators, i.e., fractional-order integrator and derivative, using the Grünwald–Letnikov definition, on FPGA in LabVIEW environment is presented in (Rana, et al. 2016). In (Muresan, Mois, et al. 2013), the authors proposed the implementation of the fractional-order PI controller on an FPGA for a DC motor speed control. The advantages of using FPGAs for implementing fractional-order PI controllers are addressed and the FPGA implementation issues of robust fractional-order PI controllers are discussed. However, several implementation-related issues were not resolved. Such implementation issues that may be encountered are mainly related to the data representation. On the one hand, calculations using floating-point data are generally very accurate, but are hard to be applied and implemented in hardware applications. In contrast, operations using fixed-point data offer the benefit of increased computation speed and are quite easy to be implemented. The main inconvenience of fixed-point data resides in the loss of accuracy. The comparative results obtained in the implementation of fractional-order controllers on two different FPGA real-time targets using various data representations have been presented in (Muresan, Folea, et al. 2013). The experimental results obtained in the application of speed control of a DC motor show that integer, double, and fixed-point data representation can be applied efficiently for control purposes.

It is widely acknowledged that FPGA implementations are up to one hundred times faster than microprocessor implementations; this additional speed may be further exploited to provide a higher performance in terms of digital approximations of fractional control algorithms. Overall, the implementation technique exploits versatility and the parallel structure of FPGA-based devices in order to obtain a low-cost implementation providing a higher performance.

9.3. Experimental results

Some recently published studies have pointed to fractional-order controllers, more specifically of PID type, as an emerging trend in the process industry; see, e.g., (Tepljakov, Alagoz, et al. 2018) and (Birs, et al. 2019). The main explanation for their popularity is the inherent robustness they provide by having a higher degree of freedom for operating and tuning controllers.

For the purposes of this chapter in relation to control considerations, it is sufficient to design and implement integer- and fractional-order PI controllers on the technologies offered by the proposed hardware architecture and applied for the temperature control of the Deusto HES prototype.

The transfer function of the fractional-order PI controller is:

$$G_{FO-PI}(s) = \frac{U(s)}{E(s)} = K_P\left(1 + \frac{1}{T_i s^{\lambda}}\right) = K_P + \frac{K_i}{s^{\lambda}} \tag{9.4}$$

where E and U are the Laplace transforms of the error and control signals, respectively, K_P is the proportional gain, K_i is the integral gain, T_i is the integral time, and λ is the non-integer order of the integrator. For the particular case where $\lambda = 1$, the fractional-order PI controller becomes the traditional integer-order PI controller.

This section is divided into two parts: In the first part, the considered integer- and fractional-order PI controllers are implemented in the microprocessor mode and applied to the controlled process in its configuration #1. Tuning rules based on an open-loop test are used to tune both controllers. While in the second part, the controllers are implemented in the FPGA mode and applied to the controlled process in its configuration #2. In this case, tuning methods based on the frequency response have been used.

Note that the objective of this section is not to perform an evaluation of any particular control algorithm or tuning method, but rather to test the applicability and effectiveness of the proposed hardware architecture for the implementation of integer- and fractional-order controllers.

9.3.1. Microprocessor-based control

In this subsection, results obtained with integer- and fractional-order PI controllers implemented on the microprocessor-based real-time target proposed in the hardware architecture are presented.

As the configuration #1 of the controlled process is used in this example, the power supplied to the heat block by the heating resistor $P(t)$ is the manipulated variable. This variable can be modified by varying the PWM signal in $u_H(t)$, which is the control signal in this configuration. The PWM signal to the air fan $u_F(t)$ can be used as a disturbance.

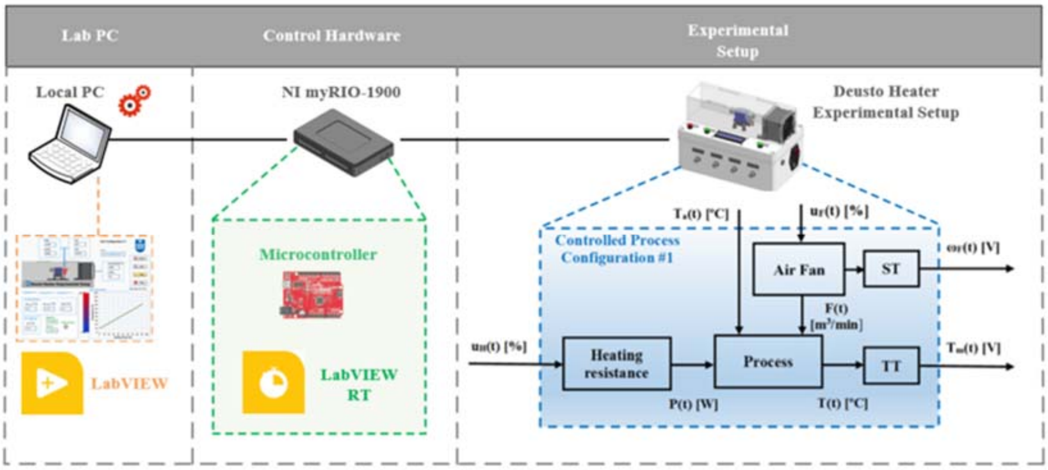

Figure 9.1. Scheme of microprocessor-based closed-loop implementation of temperature control with Controlled Process Configuration #1.

See Table 7.2 for a complete list of the main process variables for this configuration.

Figure 9.1 shows the scheme of the different software and hardware components used for the microprocessor-based closed-loop implementation of temperature control in this example.

As discussed in Chapter 8, the controlled process in configuration #1 exhibits fractional behaviour. Therefore, considering the process reaction curve in Figure 8.17, which has been obtained for a certain operating point by using a typical open-loop step-test experiment, the controlled process can be modeled by using an FFOPDT or an FOPDT model. Note that FFOPDT and FOPDT model identification methods have been implemented on the microprocessor-based hardware in Chapter 8.

Although there are a large number of tuning methods for such PI and fractional-order PI controllers, in this example the AMIGO and F-MIGO methods proposed by Hägglund and Åström in (Hägglund and Åström 2002) and by Bhaskaran et al. in (Bhaskaran, Chen and Xue 2007) will be used for PI and FO-PI controllers, respectively.

According to both tuning methods, the FOPDT model parameters and the normalized dead-time τ are used to design both an integer- and a fractional-order PI controller. AMIGO and F-MIGO methods provide the tuning rules for the PI and FO-PI controllers, respectively, as long as the controlled process step response has an S-shaped form that could be approximated by an FOPDT model. The transfer function of an FOPDT model is (3.23).

The identified parameters of the FOPDT model at this operating point, $\theta_P = \{K, T, L\}$, which are necessary to apply the considered tuning methods, are: $K = 1.40$ ºC/%, $T = 64.26$ s, and $L = 10.20$ s.

On the other hand, the normalized dead-time, which is defined in (3.25), has the property $0 \le \tau \le 1$ and is a parameter that can be used to characterize the difficulty of controlling a process. In the technical literature, some authors use the controllability index L/T to characterize the process, similar to the τ parameter; see, e.g., (Åström and Hägglund 2006). A process is lag-dominated if τ is small ($T >> L$), delay-dominated if τ is large ($L >> T$), and balanced if τ is around 0.5.

For the identified model, the normalized dead-time is $\tau = 0.1370$, and the controllability index is $L/T = 0.1587$.

Both AMIGO and F-MIGO are robust tuning methods that determine the optimum parameters for PI and FO-PI controllers, respectively, in such a way that the load disturbance rejection is optimized, with a constraint on the maximum sensitivity M_S.

Fractional MIGO (F-MIGO) is a popular tuning method, which is suitable for fractional-order PI controllers, and was developed as an extension of the MIGO (M_S con-strained integral gain optimization) method proposed in (Panagopoulos, Åström and Hägglund 2002).

According to (Bhaskaran, Chen and Xue 2007), the fractional order λ of the controller is practically independent of L, but is dependent on the normalized dead-time τ. For some practical situations, when $0.4 \le \tau < 0.6$, it is determined that an integer-order PI controller is more convenient for controlling the process. Proportional gain and integral time are defined as a function on the normalized dead-time τ.

The tuning rules for $M_S = 1.4$ can be summarized as follows:

$$\begin{gathered} K_P K = \frac{0.2978}{\tau + 0.00037} \\ \frac{T_i}{T} = \frac{0.8578}{\tau^2 - 3.402\tau + 2.405} \\ \lambda = \begin{cases} 1.1, & \tau \ge 0.6 \\ 1.0, & 0.4 \le \tau < 0.6 \\ 0.9, & 0.1 \le \tau < 0.4 \\ 0.7, & \tau < 0.1 \end{cases} \end{gathered} \tag{9.5}$$

Considering the estimated parameters of the FOPDT model and the value of the normalized dead-time for the controlled process, the controller parameters obtained with these tuning rules are $\theta_C = \{K_P, K_i, \lambda\}$, with $K_P = 1.5486$, $K_i = 0.055$, and $\lambda = 0.9$. In this case, the Oustaloup Recursive Approximation method (Monje, Chen, et al. 2010) with the following parameters: $N = 6$, $\omega_b = 10^{-2}$, $\omega_h = 10^2$ has been used to approximate the fractional-order operator. The continuous-time controller is then discretized.

The considered method for PI controllers is based on the MIGO method (Panagopoulos, Åström and Hägglund 2002). The tuning rules proposed in (Hägglund and Åström 2002) are obtained by finding simple relations between process parameters and controller parameters. The resulting design method is called AMIGO (Approximate MIGO based on step response data).

Most processes where the dynamics are the limiting factor for control design have a relation between dead-time L and time constant T that satisfy $0.15 < L/T < 1$. For these processes, the proposed tuning rules for $M_S = 1.4$ become particularly simple:

$$\begin{aligned} K_P K &= \frac{0.25T}{L} \\ \frac{T_i}{T} &= 0.8 \end{aligned} \tag{9.6}$$

Considering the estimated parameters of the FOPDT model for the controlled process, the controller parameters obtained with these tuning rules are $\theta_C = \{K_P, K_i\}$, with $K_P = 1.1250$ and $K_i = 0.0219$.

The closed-loop experimental results, obtained considering the operating point at which both the integer- and the fractional-order PI controllers have been designed, have been presented in Figure 9.2 for servo and regulatory control. In this example, the closed-loop test for servo control consists of a setpoint change T_{SP} from 60 to 80°C at time $t = 0$ s, while the closed-loop test for regulatory control consists of a change in the signal u_F from 10 to 30% at time $t = 250$ s. The corresponding control signals for both controllers, $u_{H\text{-}PI}$ and $u_{H\text{-}FO\text{-}PI}$, and disturbance signal u_F are given in Figure 9.3.

Figure 9.2 shows that both microprocessor-based implemented controllers give good performance, especially for regulatory control. Note that both tuning methods are robust approaches that seek to optimize load disturbance rejection.

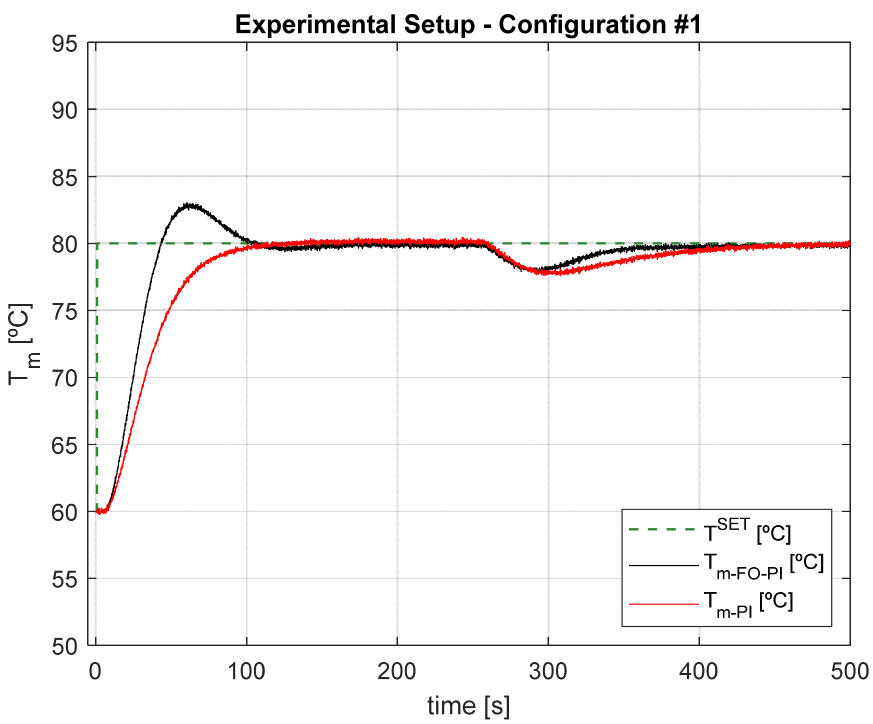

Figure 9.2. Closed-loop microprocessor-based experimental results for servo and regulatory control, considering a PI and a fractional-order PI controller: Temperature in the heat block.

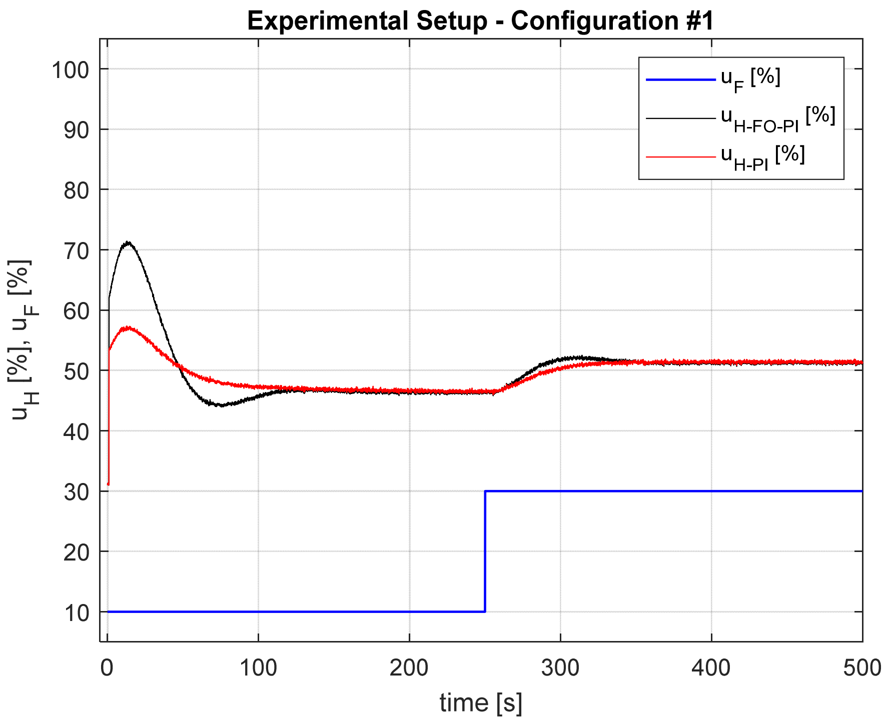

Figure 9.3. Closed-loop microprocessor-based experimental results for servo and regulatory control, considering a PI and a fractional-order PI controller: control signal u_H and disturbance u_F.

9.3.2. FPGA-based control

The design and FPGA-based implementation of an integer- and a fractional-order PI controller for the temperature control in Deusto HES is exemplified in this section. Therefore, the FPGA-based real-time target in the proposed hardware architecture is used.

As the configuration #2 of the controlled process is used in this example, the airflow generated by the air fan $F(t)$ is the manipulated variable. This variable can be modified by varying the PWM signal in $u_F(t)$, which is the control signal in this configuration. The PWM signal to the heating resistance $u_H(t)$ can be used as a disturbance. See Table 7.2 for a complete reference of the main process variables for this configuration.

Figure 9.4 illustrates the scheme of the different hardware and software components used for the FPGA-based closed-loop implementation of temperature control in this example.

Similar to the previous example, the controlled process in this configuration also exhibits a fractional behaviour. Considering the process reaction curve in Figure 8.24 obtained for a certain operating point by using a typical open-loop step-test experiment, the controlled process can be modeled by an FFOPDT or an FOPDT model, as detailed in Chapter 8.

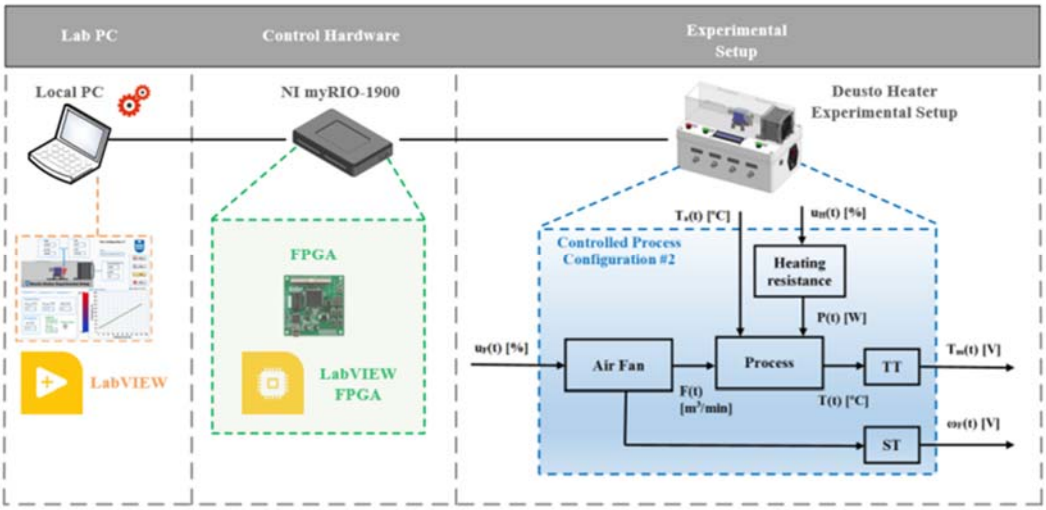

Figure 9.4. Scheme of FPGA-based closed-loop implementation of temperature control with Controlled Process Configuration #2.

In (Gude and Kahoraho 2009a) and (Gude and Kahoraho 2009b), tuning methods for PI and fractional-order PI controllers in the spirit of the kappa-tau tuning rules were presented. An extension of the well-known modified Ziegler-Nichols tuning rules for fractional-order PI controllers is presented in (Gude and Kahoraho 2010b), where an interpretation of these tuning rules as methods where one point of the Nyquist curve is positioned in a desired point is also given.

Without loss of generality, the tuning rules for PI and fractional-order PI controllers in the frequency domain proposed by Gude and Kahoraho in (Gude and Kahoraho 2009b) will be used in this example. When considering this frequency-domain method, the process dynamics is characterized by three simple parameters, i.e., the static gain K, and the gain K_{180} and the frequency ω_{180} where the process lag is 180^{o}.

For the time-domain methods in the previous section, the normalized dead-time τ has been used as a parameter to characterize the process. The corresponding frequency-domain parameter is the gain ratio κ, which is defined as follows:

$$\kappa = \frac{K_{180}}{K} = \frac{|G(\omega_{180})|}{G(0)} \tag{9.7}$$

where G(s) is the open-loop transfer function of the controlled process. This parameter gives useful information about the process. Processes with small κ can be considered easy to control and the difficulty in controlling the system increases as κ increases.

These tuning rules have been devised in order to minimize the performance criterion, which is mathematically expressed as a measure of the system ability to handle low-frequency load disturbances, with a robustness constraint on the maximum sensitivity function M_S.

According to the considered tuning method, the identified frequency-domain parameters of the controlled process at this operating point, $\theta_P = \{K, K_{180}, T_{180}\}$, which are necessary to apply the considered tuning methods, are: $K = -1.30$ ºC/%, $K_{180} = 0.053$, and $T_{180} = 13.93$ s. Therefore, the gain ratio is $\kappa = 0.041$.

The fractional order λ of the controller is practically constant for a certain range of κ, as indicated in (Gude and Kahoraho 2009b), and the tuning rules for a fractional-order PI controller and $M_S = 1.4$ can be summarized as follows:

$$\begin{gathered} K_P K_{180} = 0.29 - \frac{0.085}{\kappa + 0.34} \\ \frac{T_i}{T_{180}} = 0.086 + \frac{0.15}{\kappa + 0.058} \\ \lambda = 1.12 \end{gathered} \tag{9.8}$$

Considering the estimated process parameters and the value of the gain ratio for the controlled process, the controller parameters obtained with these tuning rules are $\theta_C = \{K_P, K_i, \lambda\}$, with $K_P = 1.2$, $K_i = 0.056$, and $\lambda = 1.12$.

On the other hand, the tuning rules for a PI controller and $M_S = 1.4$ can be summarized as follows:

$$\begin{gathered} K_P K_{180} = 0.19 - \frac{0.038}{\kappa + 0.25} \\ \frac{T_i}{T_{180}} = 0.11 + \frac{0.073}{\kappa + 0.022} \end{gathered} \tag{9.9}$$

Considering the estimated process parameters and the value of the gain ratio κ for the controlled process, the controller parameters obtained with these tuning rules are $\theta_C = \{K_P, K_i\}$, with $K_P = 1.12$ and $K_i = 0.063$.

In order to implement this fractional-order PI controller on the FPGA-based real-time target, its discrete form is required. The discretization approach that has been used consists in the ninth-order recursive Tustin method (Monje, Chen, et al. 2010), with a sampling period $T = 0.01$ s.

The discretization is based on the approximation of the fractional operator s^α with the Tustin generating function, which is given by:

$$s^\alpha = \left(\frac{2}{T}\right)^\alpha \left(\frac{1 - z^{-1}}{1 + z^{-1}}\right)^\alpha \tag{9.10}$$

By applying the Muir-recursion method (Monje, Chen, et al. 2010), the following approximation of the fractional-order operator is obtained:

$$s^\alpha = \left(\frac{2}{T}\right)^\alpha \frac{A(z^{-1}, \alpha)}{A(z^{-1}, -\alpha)} \tag{9.11}$$

where the polynomial A can be computed recursively according to the Muir-recursion method.

The discrete transfer function for the fractional-order PI controller will have the following structure:

$$G_{FO-PI}(z^{-1}) = \frac{a_0 + a_1 z^{-1} + a_2 z^{-2} + \cdots + a_{10} z^{-10}}{1 + b_0 + b_1 z^{-1} + b_2 z^{-2} + \cdots + b_{10} z^{-10}} \quad (9.12)$$

For the implementation of the fractional-order PI control algorithm on the FPGA target, a recursive relation for the control signal is derived (Caponetto, et al. 2010):

$$\begin{aligned} u(k) = a_0 e(k) + a_1 e(k-1) + \cdots + a_{10} e(k-10) - b_1 u(k-1) \\ - b_2 u(k-2) - \cdots - b_{10} u(k-10) \end{aligned} \quad (9.13)$$

where $u(k)$ and $e(k)$ are the control and error signals, respectively.

The closed-loop experimental results, obtained considering the operating point at which both the integer- and the fractional-order PI controllers have been designed, have been presented in Figure 9.5 for servo and regulatory control. In this example, the closed-loop test for servo control consists of a setpoint change T_{SP} from 115 to 135°C at time $t = 0$ s, while the closed-loop test for regulation consists of a change in the u_H signal from 100 to 80% at time $t = 250$ s. The corresponding control signals for both controllers, $u_{F\text{-}PI}$ and $u_{F\text{-}FO\text{-}PI}$, and disturbance signal u_H are given in Figure 9.6.

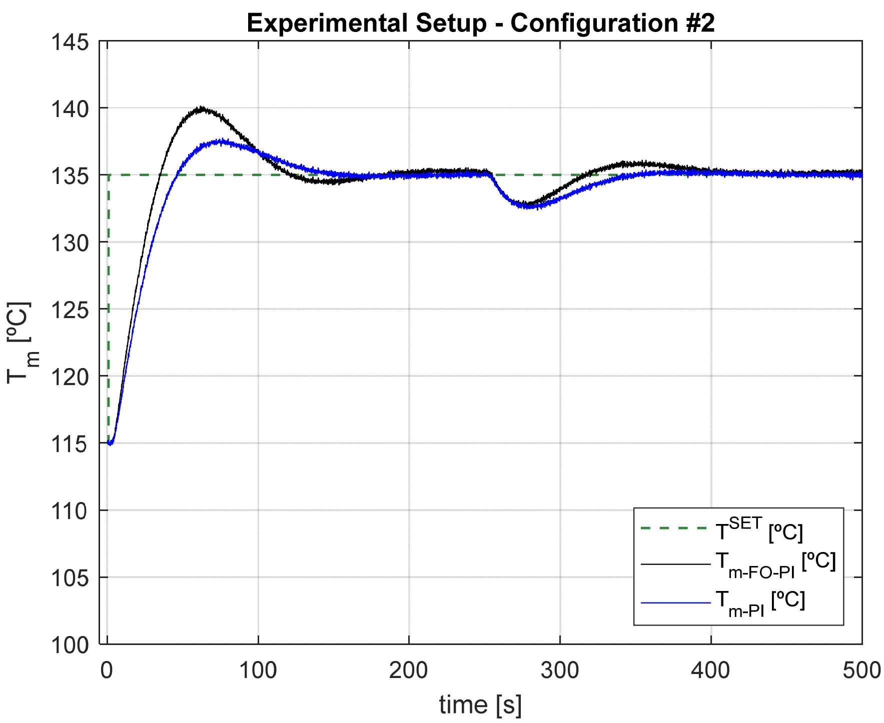

Figure 9.5. Closed-loop FPGA-based experimental results for servo and regulatory control, considering a PI and a fractional-order PI controller: Temperature in the heat block.

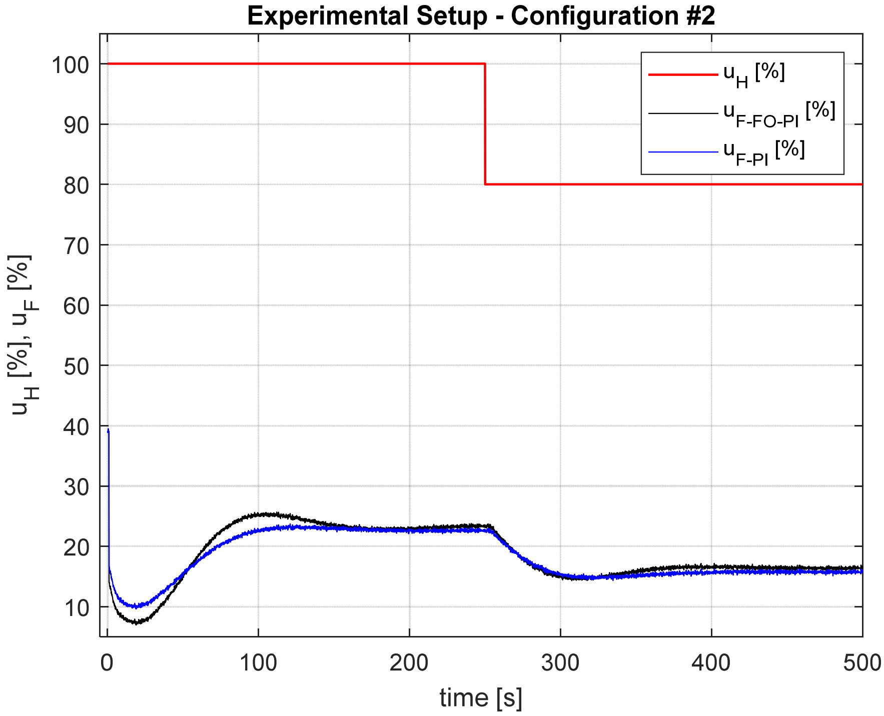

Figure 9.6. Closed-loop FPGA-based experimental results for servo and regulatory control, considering a PI and a fractional-order PI controller: control signal u_F and disturbance u_H.

Figure 9.5 shows that both FPGA-based implemented controllers offer good performance, especially for regulatory control since both tuning methods are robust approaches that seek to optimize load disturbance rejection.

9.3.3. Communication between Windows HMI, RT processor, and FPGA

As previously mentioned, in this section FPGA-based integer- and fractional-order controllers have been implemented using the proposed hardware architecture. However, for the complete operation and temperature control of the Deusto HES, different functionalities must be implemented at the FPGA, RT processor, and computer level, using the most advanced programming techniques of LabVIEW.

The objective of this part is to provide an overview of the communication between the different hardware resources, i.e. windows HMI, RT processor, and FPGA, in the context of the proposed control hardware architecture.

Figure 9.7 shows the complete scheme of functionalities implemented at software level using the hardware control architecture that has been proposed in this dissertation.

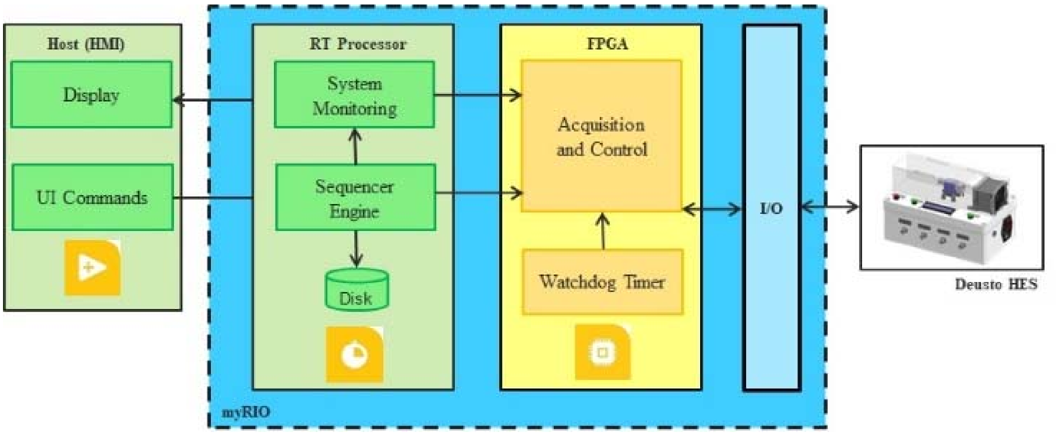

Figure 9.7. Scheme of the hardware architecture used for operation and implementation of control algorithms applied to the laboratory.

9.3.4. FPGA

The code on the FPGA is implemented using LabVIEW FPGA. The functions that are executed at the FPGA level include the deterministic data acquisition and control loops, which use low-level functions, i.e. implementation of the integer- and fractional-order control algorithm, and data acquisition through the FPGA I/O interface. Another function running on the FPGA is the watchdog timer, which provides a manner of setting the hardware device outputs into known safe-states in case of a system failure. This fail-safe feature provided by the watchdog timer safeguards the hardware connected to the experimental setup in case the control system stops operating as expected.

9.3.5. Real-time processor

Code running on the RT processor is implemented with LabVIEW RT. This code executes functions associated with system monitoring, sequencer engine, and data disk storage. A sequencer is a design pattern used for executing LabVIEW code sequentially. This software structure is a FIFO RT design pattern that manages the communication between host and FPGA.

9.3.6. Host (HMI)

The code that runs on the computer is implemented with LabVIEW. This code executes functions of the GUI, i.e. those related to the visualization of variables, states and graphs, and those related to the commands to be executed.

In this context, the following section deals with the GUI and shows the appearance of the FPGA-based application with the different functionalities and possibilities. All the functions available in the FPGA-based control application are also detailed.

Communication between the host and the hardware device is managed by the RT processor and is bidirectional:

- Data that is sent from the control hardware to the host for all those display tasks.
- UI commands sent from the GUI interface to the control hardware to be processed properly.

9.4. LabVIEW-based Application

In this section, the control-related applications implemented in LabVIEW for the different control technologies available in the control hardware architecture are described. The main features presented by each of the implemented applications are also illustrated.

9.4.1. Deusto HES control

Three different applications have been developed to control the controlled process with the considered laboratory setup in each one of the configurations, as shown in the right part of the main menu in Figure 8.32:

1. PC control mode.
2. Microprocessor control mode.
3. FPGA control mode.

The appearance of the GUI for the FPGA-based control application is shown in Figure 9.8 for illustrative purposes. However, the following functionalities are common for any of the available control modes, i.e., computer-, microprocessor-, and FPGA-based control:

- Select Controlled Process Configuration #1, #2, or #3 to operate the equipment.
- Set the instantaneous values of u_H [%] or u_F [%], which, depending on the configuration being used, can be considered as a disturbance to the process.
- Visualize time responses for temperature $T(t)$ [ºC] and set point $T_{SP}(t)$ [ºC] in a graph.
- Visualize time responses for signals $u_H(t)$ [%] and $u_F(t)$ [%] in another graph. In Figure 9.8, as configuration #1 is selected, u_H and u_F will be manipulated variable and disturbance, respectively.
- Select the control operation mode (manual or auto).
- Display the instantaneous value of the various process variables: P [W], u_H [%], T_m [V], T [ºC], ω_F [$\min^{-1}$], and u_F [%].
- Export data in graphs to a text- or an excel-format file.

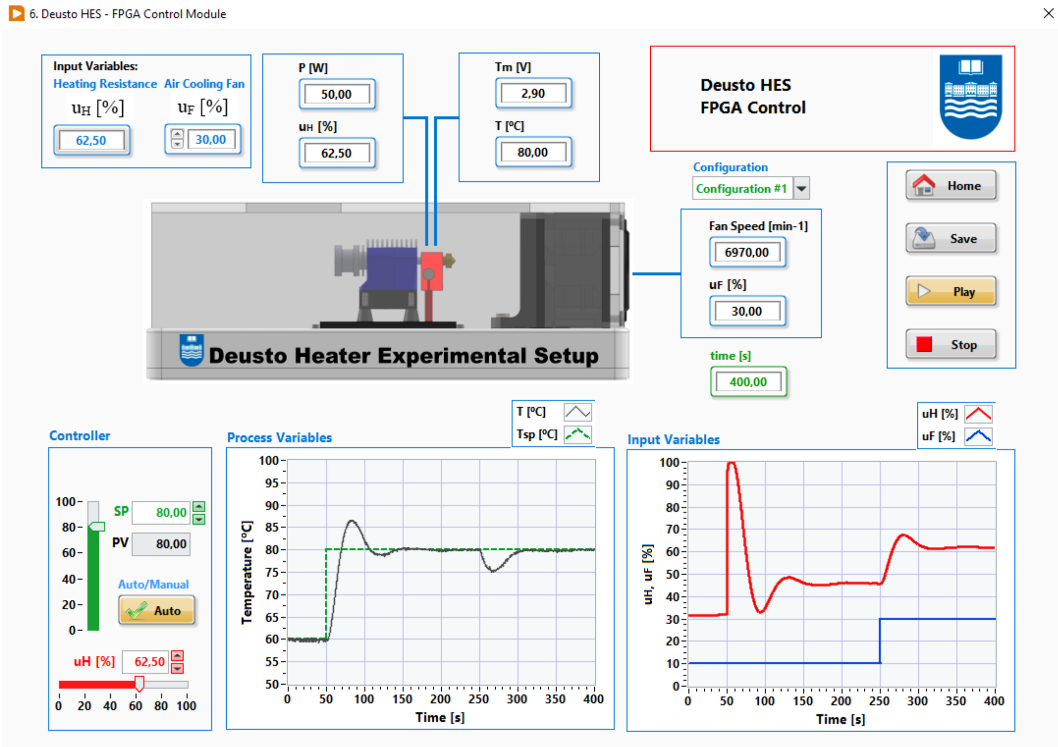

Figure 9.8. LabVIEW-based application for FPGA control.

9.5. Discussion

As mentioned above, one of the objectives of Part II of this dissertation is to present a novel control hardware architecture for the practical implementation of integer- and fractional-order control algorithms on a real-time target.

In this chapter, the proposed hardware control architecture has been used to validate its effectiveness for the implementation of integer- and fractional-order control algorithms. More specifically, integer- and fractional-order PI controllers have been implemented on microprocessor- and FPGA-based real-time targets, which constitute part of the proposed hardware architecture, and have been applied to the temperature-based experimental setup under two different configurations.

Note that the thermal process exhibits fractional-order behaviour in both configurations, whose dynamics in both cases are different and nonlinear since the process dynamics vary as a function of the operating point.

Although there is a wide variety of tuning methods for integer- and fractional-order PI controllers in the literature that use different approaches, without loss of generality, in order to design the PI controllers the tuning rules that have been used are characterized by their simplicity, and they are based on process information that can be determined using a simple step-input experiment for the time-domain method or using a relay-feedback experiment for the frequency-domain method. In both cases, the used tuning rules consider the well-known trade-off between performance and robustness.

In this chapter, the author have opted to focus on the implementation issues of integer- and fractional-order PI controllers on real-time targets, since the use of fractional-order PID controllers in industry is currently low mainly due to the aforementioned implementation issues. Some final remarks about the implementation of fractional-order controllers on real-time targets are discussed below.

Therefore, both integer- and fractional-order PI controllers have been implemented in microprocessor- and FPGA-based real-time targets, validating the effectiveness of the proposed hardware architecture for this purpose. In addition, a straightforward procedure for the development of a fractional-order PI controller has been provided and, at the same time, the implementation issues on both real-time platforms have been addressed.

The main advantage of this hardware architecture over other alternatives is that it provides three control technologies in the same hardware equipment, which increases significantly its possibilities for the training with the aforementioned technologies in the development of identification and control algorithms. In addition, all of these three control technologies use the same programming language: LabVIEW. In this way the engineer can concentrate on the implementation of control algorithms instead of being concerned with learning other programming languages for each hardware platform.

Fractional-order controllers present the fractional $s^{\pm\alpha}$ operators that involve infinite memory, i.e., an infinite number of terms are necessary to approximate their dynamic behaviour, either in the time or in the frequency domain. However, practical applications require realizing such operators with an algorithm of finite duration, which implies that, compared to the original, these realizations are valid only in a certain frequency range. If the case of real orders is considered, the main methods for realizing the fractional derivative and integral operators have been reviewed in this paper. Under this point of view, the discretization of the fractional-order controller takes on a key point in development of the final implementation, whatever the device on which it is to be implemented.

In the technical literature, one can verify that the implementation of control algorithms on microprocessor-based platforms is a widespread option and has become dominant in low-rate applications, which are characterized by not having major constraints in terms of power consumption or space saving. For some time now, FPGA devices have become more and more common as these constraints are becoming more and more common.

The choice of a microprocessor or a FPGA as an implementation device is generally based on the requirements of the application. FPGA provides important benefits, such as: reduced dimension of the device, fast execution time, high computational speed, low power consumption, which makes possible further development of portable equipment, and simpler hardware implementation compared to other devices such as DSPs, which require dedicated peripherals and possibly even an operating system, or external memory modules.

The future belongs to those who believe in the beauty of their dreams.

Eleanor Roosevelt (1884 – †1962)

CHAPTER

10

Conclusions and Future Work

THIS chapter seeks to provide an overview of the described work and the contributions this dissertation has generated. Therefore, the hypothesis and objectives introduced in Chapter 1 are analyzed to evaluate to what extent they have been achieved. Some of the results of this research have been disseminated to validate their contribution with the research community. That is, the accomplishment of those objectives is objectively supported by the publications reviewed in this chapter. To conclude with this dissertation, future lines of work and ideas are proposed to continue the presented research line, and some final remarks in the form of discussion are presented.

The rest of the chapter is structured as follows: Section 10.1 summarizes the work done in this dissertation and the conclusion obtained throughout it, Section 10.2 lists the contributions from this work, Section 10.3 validates the hypothesis and the objectives that were set in Chapter 1, and Section 10.4 includes the scientific manuscripts published during the development of this dissertation. To finish with, Section 10.5 introduces the future work, while Section 10.6 draws some final remarks.

10.1. Summary of work and conclusions

As described throughout this dissertation, tremendous technological advances and the advent of fractional calculus have made possible a renewed interest in academia and industry in practical applications based on fractional calculus, making possible the transition from classical models and controllers to those described by differential equations of non-integer order.

The present dissertation is devoted to the investigation of identification and control of dynamical systems based on fractional-order calculus.

The first chapter of this dissertation introduces the work, including the context and motivation, the hypothesis, objectives and contributions, as well as the research methodology followed to achieve them.

Chapter 2 presents an analysis of the State of the Art in those concepts that constitute the theoretical basis of this dissertation. These are classified into (i) fractional-order model identification methods, (ii) fractional-order control methods, in particular, those related to the fractional-order PID algorithm, and (iii) their implementation in various hardware devices, indicating the practical issues with each technology.

Chapter 3 introduces the reader to the basic concepts and algorithms used in the thesis. This chapter includes an introduction to the tools of fractional calculus, the definitions and properties of fractional operators, and tools related to modelling and analysis of dynamic systems.

From the analysis of the State of the Art in Chapter 2, it can be concluded that:

- Over the last decades, the emergence of fractional calculus has made possible a great deal of academic and industrial effort focused on obtaining methods for more accurate modelling and identification of real-world phenomena.
- It is well-known that obtaining a simple-structure fractional-order model for a process has significant relevance and is very useful in practice for the design of both integer-order and fractional-order control systems.
- Industry requires methods for identification of fractional-order models.
- For these identification procedures to have an impact on the process industry, they must be simple to understand by engineers and practitioners and to implement in industrial control hardware devices.

Since the physical interpretation of the step response of a process is straightforward and the integer-order model identification algorithms based on fitting several representative points of the process reaction curve are easy to apply, it may be considered natural to extend such methods to the fractional-order case. For this purpose, Part I of this thesis is devoted to the development of fractional-order model identification procedures based on the process reaction curve, where simplicity in the identification procedures has been emphasized.

Chapter 4 presents an FFOPDT model identification procedure based on fitting three symmetrical points on the process reaction curve.

In this context, it has been verified that the symmetrical method provides an efficient way to obtain the parameters of the fractional-order model, by requiring to select the optimal location of only one of the points ($x_1 = x$), since the central point is $x_2 = 50\%$ and the other extreme point is immediately established by the symmetry requirement ($x_3 = 100 - x$).

The results of the symmetrical method verify that the accuracy of the identified fractional-order model is sensitive to the selection of the symmetrical set of points on the reaction curve, and it has been discussed that a more accurate model is obtained for low x values. New insights into this selection of the set of points have been offered in the context of the proposed symmetrical procedure.

In particular, this identification procedure has been found to give good results in comparison with other well-known methods of integer- and fractional-order identification.

Chapter 5 presents an FFOPDT model identification method that maintains the symmetry of the extreme points ($x_1 = x$, $x_3 = 100–x$), while displacing the location of the central point x_2 on the process reaction curve.

One of the main conclusions of this chapter is to prove that the accuracy of the identified FFOPDT model is sensitive to the location of the set of representative points and that a significant improvement in the accuracy of the identified fractional-order model can be obtained by moving the central point x_2 to another location different from $x_2 = 50\%$, keeping the symmetry of the extreme points $x_1 = x\%$ and $x_3 = (100–x)\%$.

More specifically, the author has found that the accuracy of the identified model exhibits a minimum value for $x_2 > 50\%$ and around 65% is common to several fractional-order dynamics in the considered order range $0.50 \leq \alpha \leq 1.00$. Therefore, by choosing $x_2 = 65\%$ the accuracy of the identified model is significantly improved.

Chapter 6 validates the general identification procedure presented in Chapter 4 by considering symmetrical and asymmetrical sets of points on the process reaction curve. The effect of the location of the three points on the accuracy of the identified fractional order model is also analysed.

More precisely, in the context of this work, the proposed identification method for symmetrical and asymmetrical set of points has been compared with several two- and three-point identification methods for integer-order models, which are based on data collected from the process reaction curve. It has been shown that the proposed method significantly outperforms methods for integer-order models. In some cases, even better results are obtained with the estimated fractional-order model than with the optimal integer-order model.

In addition, some empirical rules of thumb, based on experimentation, have been provided to obtain information on the selection of points for the symmetrical and asymmetrical case, respectively, in the context of the proposed identification method.

Although the step response of the fractional-order model considered can conveniently describe both monotonic and non-monotonic behaviour depending on the fractional order α, the identification procedures presented in Chapters 4, 5 and 6 only refer to processes that have an S-shaped step response, since systems with essentially monotonic step responses are very common in process control.

Thus, the identification procedures presented in Chapters 4, 5, and 6 exhibit the following common characteristics:

1. They are analytical methods, which considerably simplifies their implementation on a hardware device.
2. Simplicity is their main characteristic. For these identification procedures to have a significant impact on industry, they must be simple methods for engineers and practitioners to understand and to apply in industrial equipment.
3. They require a very low computational cost without sacrificing accuracy. There is usually a trade-off between the accuracy of the model and the complexity of the algorithm in terms of its computational effort.
4. They are efficient methods. They allow to determine the fractional-order model with a high accuracy with respect to other well-known identification methods for integer- and fractional-order models.

In the industrial context, large process industries often have hundreds or thousands of control loops. For this reason, simplicity is of primary interest when identifying a process model for control purposes.

In the author's opinion, such identification methods, which emphasize simplicity, will promote their industrial use and help to bridge the gap between theoretical research on fractional models and their practical application in the process industry. This expectation is one of the main motivations for this dissertation.

Chapter 7 presents the conceptualization of a novel hardware control architecture that combines the capability of implementing PC-based control applications with embedded applications on microprocessor- and FPGA-based real-time targets. The main advantages of this hardware architecture over other available alternatives are the following:

1. It is a novel hardware control architecture that uniquely and efficiently exploits the different hardware available in myRIO device enabling their use indistinctly.
2. From the control hardware point of view, it features great flexibility since it can be configured to use the following technologies or control modes: PC-based, microprocessor-based, or FPGA-based control.
3. From the software point of view, it offers simplicity and transparency since the same programming language is used, regardless of the control hardware. Thus, instead of spending time developing user interfaces or debugging code syntax, end users can apply the LabVIEW graphical programming paradigm to focus on implementing their conventional or advanced identification and control algorithms without the added pressure of a complicated programming language for each hardware platform.

4. From a practical training perspective, the engineer has three hardware technologies on the same device for their use, without having to perform an experimental setup for each hardware platform to be used.

In Chapter 8, the proposed hardware architecture is used to validate its applicability and effectiveness for the implementation of fractional-order simple-structure model identification algorithms and tested on a laboratory prototype. Furthermore, insights into the practical issues related to the implementation of the identification algorithm in industrial control hardware are gained.

In the specific scope of this chapter, the implemented identification procedures described in the Part I of this dissertation has been compared with various well-recognized identification procedures for integer- and fractional-order systems that use process data taken from the process reaction curve. It has been obtained that the estimated fractional-order models significantly outperform integer-order models in terms of accuracy. This confirms the well-known benefit obtained when using fractional calculus and justified in the technical literature in terms of more accurate modeling.

In Chapter 9, the proposed hardware control architecture has been used to validate its effectiveness for the implementation of integer- and fractional-order control algorithms on microprocessor- and FPGA-based real-time targets, which constitute part of the proposed hardware architecture, and have been applied to the temperature-based experimental setup under two different configurations.

Therefore, both integer- and fractional-order PI controllers have been implemented in microprocessor- and FPGA-based real-time targets, validating the effectiveness of the proposed hardware architecture for this purpose. In addition, a straightforward procedure for the development of a fractional-order PI controller has been provided and, at the same time, the implementation issues on both real-time platforms have been addressed.

The main advantage of this hardware architecture over other alternatives is that it provides three control technologies in the same hardware equipment, which increases significantly its possibilities for the training with the aforementioned technologies in the development of identification and control algorithms. In addition, all of these three control technologies use the same programming language: LabVIEW. In this way the engineer can concentrate on the implementation of control algorithms instead of being concerned with learning other programming languages for each hardware platform.

10.2. Contributions

As illustrated in previous chapters of this dissertation, the knowledge and findings obtained from this thesis are diverse. As a consequence of those findings, the scientific and technical contributions generated from this dissertation are presented in this section. Those contributions are linked to their respective objectives, described in Section 1.2.

10.2.1. Scientific contributions

- SC1: A survey of current methods for identifying fractional-order models, a review of the different laboratory prototypes used to verify fractional-order identification and control methods, and an analysis of the implementation issues of fractional-order systems on real-time hardware targets.

Chapter 2 presents a State-of-the-Art analysis focusing on identification and control methods based on fractional calculus, as well as on the implementation issues of fractional-order systems in real-time targets.

From this study one can conclude:

a) Industry needs such identification and control procedures, especially when simplicity is emphasized.

b) For such identification and control procedures to have an impact on industry they must be easy to understand and apply.

This analysis accomplishes objective O1 and contributes to the development of objective O2.

- SC2: A fractional-order model identification method based on fitting three symmetrical points on the process reaction curve.

The proposed method, presented in Chapter 4, describes a procedure to identify an FFOPDT model for industrial processes with S-shaped step responses and based on fitting three symmetrical points on the process reaction curve. As discussed above, this symmetrical method provides an efficient and simple way to obtain the model parameters by requiring the selection of the optimal location of only one of the points (x), since the other is immediately established by the symmetry requirement.

This contribution is related to objective O2 and is in line with objective O5 since, being a simple and analytical identification method, its application to real-time targets is straightforward.

- SC3: A method that improves the accuracy of the identified model obtained with the identification procedure for a set of symmetrical points by maintaining the symmetry of the extreme points and moving the central point.

This contribution is also related to objective O2 and seeks to improve the accuracy of the identified model with respect to the method proposed in Chapter 4. It also contributes to the achievement of objectives O3 and O5, since this method will also be implemented on hardware devices and applied to a laboratory prototype.

Chapter 5 discusses an FFOPDT model identification procedure based on the symmetrical location of the two extreme points while moving the central point on the process reaction curve.

- SC4: Validation of the general fractional-order model identification procedure considering both a symmetrical and asymmetrical set of points on the process reaction curve.

Chapter 6 discusses an FFOPDT model identification procedure, which is based on information obtained from three arbitrary points on the process reaction curve. This identification procedure has been verified for both cases, considering three symmetrical and asymmetrical points on the reaction curve.

This contribution is also related to objective O2 and aims to generalize the symmetrical identification method for any arbitrary set of points on the process reaction curve. As in the previous case, it also contributes to the achievement of objectives O3 and O5.

Contributions SC2, SC3 and SC4 propose procedures for the identification of fractional order models following the same approach and maintaining the following features:

1. They are analytical methods, which considerably simplifies their implementation on a hardware device.
2. They are characterized by a low computational effort. There is a trade-off between accuracy and computational effort. Although it is possible to find methods that further improve the accuracy of the estimated fractional-order model, this is accomplished at a cost of more complex algorithms or a higher computational effort.
3. They are simple methods. This feature is mainly due to the fact that identification methods based on fitting several points of the process reaction curve have a simple physical interpretation and are usually easy to implement and apply. This is of significant importance in the industrial context, where easy-to-implement identification methods are required.
4. They are efficient methods. These identification methods give very good results, improving the ones obtained using other well-recognized identification methods for integer- and fractional-order models that also rely on information taken from the process reaction curve, especially when simplicity is emphasized.

- SC5: Conceptualization and implementation of a novel control hardware architecture aimed to the practical implementation of identification and control algorithms for fractional-order systems using the different available hardware technologies.

This contribution has been presented in Chapter 7 and consists of the conceptualization and practical implementation of a control hardware architecture that combines the capability of implementing PC-based control applications with embedded applications on microprocessor- and FPGA-based real-time targets. Therefore, it allows to implement, among others, the fractional order model identification procedures developed in Chapters 4, 5, and 6.

This contribution is in line with Objective O4 and enables the achievement of O5.

- SC6: Verification of the effectiveness and applicability of the proposed control hardware architecture for the practical implementation of fractional-order identification and control algorithms.

Chapters 8 and 9 provide detailed results of implementing different fractional-order identification and control algorithms on real-time hardware targets. In addition, the practical issues related to the implementation of such algorithms on different hardware platforms are studied in detail.

10.2.2. Technical contributions

- TC1: Design and construction of a temperature-based experimental prototype, which has been used to demonstrate the effectiveness and applicability of the control hardware architecture proposed in this dissertation.

Chapter 7 and the first part of Chapter 8 describe in detail the temperature-based laboratory prototype and its main characteristics. More specifically, the temperature process, which involves thermal conduction, exhibits fractional behaviour in the different configurations. Also noteworthy is its non-linear behaviour and the possibility to choose multiple operating points with different dynamic characteristics. All these features make this laboratory prototype suitable for the application of all the aspects related to the modelling and implementation of integer- and fractional-order model identification methods discussed in this thesis.

- TC2: The LabVIEW-based programming developed in this thesis, which includes the implementation of the fractional-order differential and integral operators and enables the hardware control architecture for the implementation of fractional-order system identification and control algorithms using the different hardware technologies available.

Part II of this thesis, comprising Chapters 7 to 9, details the control hardware architecture and the LabVIEW-based applications that have been implemented to operate the laboratory prototype and implement the aforementioned identification and control algorithms.

10.3. Hypothesis and objective validation

At the beginning of the dissertation, in Section 1.2, the following hypothesis was formulated:

Hypothesis: It is possible to conceive and implement a novel architecture, integrating various hardware technologies, that enables a straightforward and simple implementation of newly developed algorithms for identification and control of fractional-order systems, contributing to overcome the implementation issues of such systems on real-time targets and promoting their use at industrial level.

Then, in order to validate it, the following goal was proposed:

Goal: Design and implement a novel control hardware architecture that enables implementation in various real-time hardware technologies of:
(i) New fractional-order model identification procedures, which are characterised by their effectiveness and simplicity,
(ii) Fractional-order control algorithms,
and that contributes to overcoming their implementation issues on such real-time targets, generally used in industry.

To achieve this goal, more specific objectives were defined. Although these objectives have been introduced in the review of the contributions of this dissertation, the following is a more specific description of how each subobjective has been addressed in this dissertation:

- O1: To study the current State of the Art on approaches to fractional calculus-based identification and control methods and their implementation on hardware devices.

Chapter 2 explores the most relevant works related to the three main concepts that articulate this dissertation.

- O2: To develop procedures for the identification of simple-structure fractional-order models from time-domain information taken from the reaction curve, according to an approach that simplifies their implementation on hardware devices.

This objective has been tackled throughout Chapters 4, 5, and 6. More specifically, in Section 4.2, the general identification method based on the reaction curve is proposed. In Section 4.3, the general method is particularized for the symmetrical case. The symmetrical method with arbitrary central point x_2 is proposed in Section 5.3. And finally, Section 6.2 discusses the proposed identification method for both symmetrical and asymmetrical sets of points on the process reaction curve.

- O3: To design and build a laboratory prototype with industrial characteristics, which enables the integration of industrial control hardware providing the appropriate characteristics for the application of fractional-order identification and control algorithms.

This objective has been addressed in Chapters 7 and 8. In particular, Section 7.2 presents in detail the experimental temperature prototype to be used in Chapters 8 and 9. In addition, the static and dynamic characteristics of the temperature-based controlled process for each of the three configurations are shown in Section 8.2.1.

- O4: To design and implement an architecture integrating hardware and software resources that optimally provides access to various hardware real-time targets.

This objective has been discussed in Chapter 7. More specifically, the conceptualization of the control hardware architecture is detailed in Section 7.3.

- O5: To implement procedures for the identification and control of fractional-order systems on hardware real-time targets and to identify an evaluation methodology for such procedures.

This objective has been fully discussed in Chapters 8 and 9. More specifically, Section 8.2.3 describes the identification algorithms that have been implemented on microprocessor-based hardware and Section 8.2.4 details the experimental procedure that has been followed to evaluate the effectiveness and applicability of these procedures using the proposed control hardware architecture. Section 9.2 discusses the hardware implementation aspects of integer- and fractional-order PID control algorithms on microprocessor- and FPGA-based real-time targets. Experimental results are presented in Section 9.3.

Taking into account the points considered above, it can be claimed that all the previous objectives have been accomplished.

As can be seen, Chapters 4, 5, and 6 evaluate the FFOPDT model identification methods by simulation. Although the symmetrical method provides good results compared to other well-established methods in the literature, with the symmetrical method and arbitrary central point and with the asymmetrical method significant improvements can be obtained based on a higher accuracy of the model step response with respect to the process reaction curve.

Chapter 4 defines the approach of the proposed identification methods. In Chapters 5 and 6, modifications to the general method are established to improve the results obtained in Chapter 4 with the symmetrical method. These chapters constitute Part I of this dissertation.

Chapter 7 establishes the material and technological resources required, on the one hand, to verify the identification methods proposed in Part I applied to a real process and using industrial hardware and, on the other hand, enables a hardware architecture that facilitates the practical implementation of fractional-order identification and control algorithms on real-time targets.

Therefore, this chapter presents the conceptualization of a novel hardware control architecture aimed to the practical implementation of fractional-order identification and control algorithms. It also describes in detail the thermal-based experimental prototype that has been designed and built to test the performance of the control hardware architecture proposed in this thesis.

Chapter 8 evaluates the identification methods proposed in Part I of this dissertation, verifying their effectiveness when implemented on industrial hardware and applied to the experimental temperature-based process. This allows testing the performance of the hardware architecture in the field of fractional-order identification.

In addition, Chapter 9 evaluates various integer- and fractional-order PID control algorithms on various hardware platforms and applied to an experimental temperature-based process. An implementation methodology has been established for each platform in the context of the proposed hardware architecture. This allows testing the performance of the control architecture in the field of applied control.

To finish with, through accomplishing these objectives and the main goal, the hypothesis set at the beginning of this dissertation has been validated.

10.4. Relevant publications

Through this dissertation, several scientific manuscripts have been published in order to validate with the research community the advances reflected in this work. The included publications fall into two categories: (i) the ones that are directly related to the specific context of this work and its contributions, and (ii) those complementary works that extend this context. Also included in this section are those supplementary materials that are published and that contribute to the body of knowledge.

Table 10.1 summarises the articles that have been derived from work carried out in this dissertation, classifying them by type (journal, book chapter, or conference) and indicates their current status.

#	Title of the work	Conference/Journal/Book	Status
J1	Influence of the selection of reaction curve's representative points on the accuracy of the identified fractional-order model	**Journal of Mathematics** Special issue "Analytical Methods to Model Nature" **IF: 1.555 (Q1)**	**Sent** (2022/02/15) **Accepted** (2022/29/04) **Published** (2022/06/04)
J2	Proposal of a general identification method for fractional-order processes based on the process reaction curve	**fractal and fractional** Special issue "Application of Fractional Calculus as an Interdisciplinary Modeling Framework" **IF: 3.577 (Q1)**	**Sent** (21/07/2022) **Accepted** (10/09/2022) **Published** (17/09/2022)
J3	A novel control hardware architecture for implementation of fractional-order controllers applied to a temperature prototype	**Mathematics** Special issue "Fractional Dynamical Systems and Its Applications in Science and Engineering" **IF: 2.592 (Q1)**	**Sent** (2022/11/21) **Accepted** (2022/12/21) **Published** (2022/12/28)
J4	Improvement of the accuracy for a fractional-order model identification method with symmetry considerations	**Journal of Mathematics** Special issue "Mathematical Methods for Fractional Differential Equations in Applied Sciences" **IF: 1.555 (Q1)**	**Sent** (2022/11/03) **Under review**
B1	Proposal of a control hardware architecture for implementation of fractional-order controllers	**Springer** Dynamical Systems in Mechatronics and Life Sciences	**Sent** (2021/12/31) **Accepted** (2022/12/01) **In process of publication**
B2	Time-domain identification of a fractional-order model from the process reaction curve	**Elsevier** Computation and Modeling for Fractional Order Systems	**Sent** (2022/09/15) **Under review**
C1	Revisiting the modified Ziegler-Nichols method for fractional PI controllers	2nd Online Conference on Nontinear Dynamics and Complexity October 4-6, 2021	**Accepted** **Presented** (2021/10/4-6)
C2	Proposal of a control hardware architecture for implementation of fractional-order controllers	16th International Conference Dynamical Systems Theory and Application DSTA 2021 December 6-9, 2021	**Accepted** **Presented** (2021/12/6-9)
C3	Effect of the central point on the accuracy of a fractional-order model identification method based on the process reaction curve	1st International Conference on Mathematical Modelling in Mechanics and Engineering ICME 2022 September 8-10, 2022	**Accepted** **Presented** (2022/09/8-10)

Table 10.1. List of research articles submitted as book chapters, to international conferences or to indexed journals.

10.4.1. International JCR Journals

This subsection presents the papers that have been published in relevant indexed journals and their connection to the content of the dissertation. The articles are listed below with a summary.

- J1. Juan J. Gude, Pablo García Bringas. "Influence of the Selection of Reaction Curve's Representative Points on the Accuracy of the Identified Fractional-Order Model", *Journal of Mathematics* 2022, Article ID 7185131, 22 pages. DOI: 10.1155/2022/7185131.

  Journal of Mathematics – JCR Impact Factor (2021): 1.555.
  Q1 in Mathematics (66/333)

Abstract: In this paper, a general procedure for identifying a fractional first-order plus dead-time (FFOPDT) model is presented. This procedure is based on fitting three arbitrary points on the process reaction curve, where process information is obtained from a simple open-loop test. A simplification of the general identification procedure is also considered, where only points symmetrically located on the reaction curve are selected. The proposed symmetrical procedure has been applied to the following sets of representative points: (5-50-95%), (10-50-90%), (15-50-85%), (20-50-80%), (25-50-75%), and (30-50-70%). Analytical expressions of the corresponding FFOPDT model parameters for these sets of symmetrical points have been obtained.
In order to show the effectiveness and applicability of this procedure for the identification of fractional-order models and to get insight into the influence of selection of the set of symmetrical points on the accuracy of the identified model, some numerical examples are proposed. This identification procedure gives good results in comparison with other integer- and fractional-order identification methods. Finally, some conclusions and final remarks are offered in this context.

- J2. Juan J. Gude, Pablo García Bringas. "Proposal of a General Identification Method for Fractional-Order Processes Based on the Process Reaction Curve". *Fractal Fract.* 2022, *6(526)*. DOI: 10.3390/fractalfract6090526.

  Fractal and Fractional – JCR Impact Factor (2021): 3.577.
  Q1 in Mathematics, Interdisciplinary Applications (18/108)

Abstract: This paper aims to present a general identification procedure for fractional first-order plus dead-time (FFOPDT) models. This identification method is general for processes having S-shaped step responses, where process information is collected from an open-loop step-test experiment and has been conducted on fitting three arbitrary points in the process reaction curve. In order to validate this procedure and check its effectiveness for the identification of fractional-order models from the

process reaction curve, analytical expressions of the FFOPDT model parameters have been obtained for both situations: as a function of any three points and three points symmetrically located on the reaction curve, respectively. Some numerical examples are provided to show the simplicity and effectiveness of the proposed procedure. Good results have been obtained in comparison with other well-recognized identification methods, especially when simplicity is emphasized. This identification procedure has also been applied to a thermal-based experimental setup in order to test its applicability and to get insight into the practical issues related to its implementation in a microprocessor-based control hardware. Finally, some comments and reflections about practical issues relating to industrial practice are offered in this context.

- J3. Juan J. Gude, Pablo García Bringas. "A novel control hardware architecture for implementation of fractional-order identification and control algorithms applied to a temperature prototype". *Mathematics*. 2023, *11(1)*, 143. DOI: 10.3390/math11010143.

  Mathematics – JCR Impact Factor (2021): 2.592.
  Q1 in Mathematics (21/333)

Abstract: In this paper, the conceptualization of a control hardware architecture aimed to the implementation of integer- and fractional-order identification and control algorithms is presented. The proposed hardware architecture combines the capability of implementing PC-based control applications with embedded applications on microprocessor- and FPGA-based real-time targets. In this work, the potential advantages of this hardware architecture over other available alterna-tives are discussed from different perspectives. The experimental prototype that has been designed and built to evaluate the control hardware architecture proposed in this work is also described in detail. The thermal-based process taking place in the prototype is characterized for being reconfigurable and exhibiting fractional behaviour, which results in a suitable equipment for the purpose of fractional-order identification and control. In order to demonstrate the applicability and effectiveness of the proposed control hardware architecture, integer- and fractional-order identification and control algorithms implemented in various control technologies have been applied to the temperature-based experimental prototype described before. Detailed discussion about results and identification and control issues are provided. The main contribution of this work is to provide an efficient and practical hardware architecture for implementing fractional-order identification and control algorithms in different control technologies, helping to bridge the gap between real-time hardware solutions and software-based simulations of fractional-order systems and controllers. Finally, some conclusions and concluding remarks are of-fered in the industrial context.

- J4. Juan J. Gude, Pablo García Bringas. "Improving the accuracy of a method for identifying fractional-order models with symmetry considerations", *Journal of Mathematics* (Under review)

  Journal of Mathematics – JCR Impact Factor (2021): 1.555.
  Q1 in Mathematics (66/333)

Abstract: Recently, a general procedure to identify a fractional first-order plus dead-time (FFOPDT) model has been presented. The approach considered is based on fitting three arbitrary points (x_1-x_2-x_3%) on the process reaction curve. In this general identification procedure, a particular simplification has been considered for the case where the representative points that have been selected are symmetrically located on the process reaction curve, x_1 = x%, x_2 = 50%, and x_3 = (100 – x)%. This symmetrical approach is an effective method of estimating the fractional-order model parameters, by only requiring the selection of the optimal location of one of the three points (x) on the process reaction curve, since the others are set immediately by the symmetry requirement.
This paper explores the possibility of moving the central point x_2 on the process reaction curve, while maintaining the symmetry of the extreme points with respect to the centre of the total range. In this work, results with fractional-order models verify that the accuracy of the estimated model is sensitive to the position of the central point within the symmetrical set of points on the process reaction curve and it has been discussed how a more accurate identified model can be determined. The results obtained in this paper have also been applied to a temperature-based prototype to confirm its applicability when implemented on a microprocessor-based control hardware.
Finally, new insights into the selection of the central point x_2 have been offered in the context of the considered FFOPDT model identification procedure based on the process reaction curve and symmetrical sets of points. Some reflections about the industrial practice of this identification procedure are also provided.

Figure 10.1 illustrates the connection between the content of the dissertation and the following indexed publications.

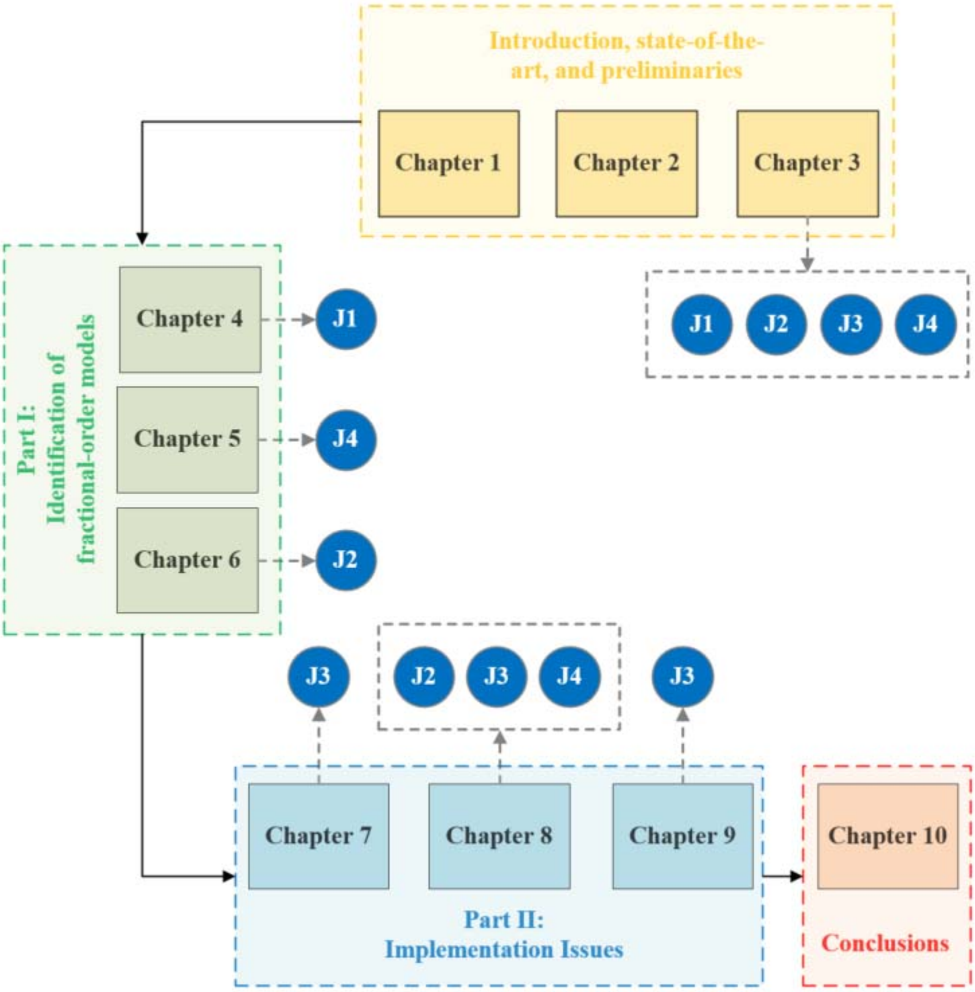

Figure 10.1. Scheme of microprocessor-based closed-loop implementation of temperature control with Controlled Process Configuration #1.

10.4.2. Book chapters

This subsection presents the book chapters that have been accepted and are currently in the process of being published. The book chapters are listed below with a summary.

- B1. Juan J. Gude, Pablo García Bringas. "Proposal of a control hardware architecture for implementation of fractional-order controllers applied to a temperature prototype", Dynamical Systems in Mechatronics and Life Sciences, Springer. 2023.

Abstract: In this paper, a control hardware architecture for the implementation of integer- and fractional-order controllers is proposed. From the hardware point of view, the proposed architecture offers the following control technologies: computer control, real-time microcontroller, and FPGA-based control. From the software point of view, LabVIEW is used as a unique programming language, regardless of the

selected control technology. In order to demonstrate the applicability and effectiveness of the proposed control hardware architecture, the design and experimental validation of fractional-order controllers implemented in several control technologies are applied to a temperature laboratory setup. Finally, some conclusions and final remarks are offered in this context.

- B2. Juan J. Gude, Pablo García Bringas. "Time-domain identification of a fractional-order model from the process reaction curve", Computation and Modeling for Fractional Order Systems, Elsevier. 2023.

Abstract: The technical literature has proven the advantages of using fractional calculus in modeling and control of dynamic systems, primarily from an industrial point of view. The academic and industrial community recognizes that the practical performance of controller design methods is highly dependent on the relevance of the identified models. Several works have shown that fractional-order models provide more accurate modeling of process dynamics than low-order integer transfer functions, such as the first-order plus dead-time (FOPDT) and second-order plus dead-time (SOPDT) models, which are widely used in the industrial context.
A discussion on the use of a fundamental numerical solution method of fractional calculus in identification problems of fractional first order plus dead time (FFOPDT) models is presented in this paper. The identification process is carried out by estimating the parameters of a FFOPDT-type transfer function model, so that the step response of the FFOPDT model can be sufficiently fit to the experimental data of the step response.
In this work, the step response of the FFOPDT model is calculated numerically using the Grunwald-Letnikov (GL) function. Data fitting is performed using particle swarm optimization (PSO) algorithm.
Some illustrative examples are provided to show the simplicity and effectiveness of the proposed procedure for estimating the parameters of the simple-structure fractional-order model. An experimental study is performed to modelling a thermal-based experimental setup in order to evaluate the applicability of the identification procedure and its implementation on an industrial control hardware.
Finally, some comments and reflections about the practical issues relating to the implementation of the identification algorithm in a microprocessor-based hardware are offered in this context.

10.4.3. International conferences

This subsection presents the papers presented at International Conferences. These papers are listed below with a summary.

- C1. Juan J. Gude, Pablo García Bringas. "Revisiting the modified Ziegler-Nichols method for fractional PI controllers", 2nd Online Conference on Nonlinear Dynamics and Complexity, Porto (Portugal), October 4-6, 2021.

Abstract: The Ziegler-Nichols tuning rules have been very influential and have been used extensively in process industry. This paper revisits an extension of the modified Ziegler-Nichols tuning rules for fractional-order PI controllers. The design method consists on minimizing a frequency objective function subject to a constraint on the maximum sensitivity function M_S. In this paper it is also demonstrated that substantially better performance can be obtained using fractional PI instead of PI controllers. An interpretation of these tuning rules as methods where one point of the Nyquist curve is positioned in a desired point is also given. These tuning rules are compared with other tuning rules and shown to give good results, especially when simplicity, performance and robustness are emphasized.

- C2. Juan J. Gude, Pablo García Bringas. "Proposal of a hardware architecture for implementation of fractional-order controllers", 16th International Conference Dynamical Systems Theory and Applications DSTA 2021, Lodz (Poland), December, 6-9, 2021.

Abstract: This paper presents a proposal of a control hardware architecture for the implementation of integer-order (IO) and fractional-order (FO) controllers. In particular, the design and experimental validation of the FO controllers implemented in several control technologies are applied to a temperature laboratory setup in order to demonstrate the effectiveness of the proposed hardware architecture. Some comments relating to industrial practice are offered in this context.

- C3. Juan J. Gude, Pablo García Bringas. "Effect of the central point on the accuracy of a fractional-order model identification method based on the process reaction curve", 1st International Conference on Mathematical Modelling in Mechanics and Engineering ICME 2022, Belgrade (Serbia), September 8-10, 2022.

Extended Abstract: A general procedure for identifying a fractional first-order plus dead-time (FFOPDT) model has been recently presented in [1]. This procedure is based on fitting three arbitrary points $\{x_1\text{-}x_2\text{-}x_3\%\}$ on the process reaction curve, where the process information is obtained from a simple open-loop test. In [2] a simplification of the general identification procedure has also been considered, particularizing for the case where only symmetrically located points $\{x\text{-}50\text{-}(100–x)\%\}$

on the reaction curve are selected. This symmetrical method provides an efficient way to obtain the parameters of the FFOPDT model, by requiring the selection of the optimal location of only one of the points (x), since the other is immediately established by the symmetry requirement.

Analytical expressions of the corresponding FFOPDT model parameters have been obtained for these sets of symmetrical points.

The effectiveness and applicability of this symmetrical procedure for the identification of fractional-order models has been shown and the influence of the selection of the symmetrical set of points on the accuracy of the identified model has been determined from several numerical examples. It has also been shown that this identification procedure gives good results compared to other integer- and fractional-order identification methods.

However, in [2] it has been considered that the central point x_2 is always located in the middle of the output total change ($x_2 = 50\%$). In this paper, the possibility of moving the central point or centroid on the reaction curve is explored, maintaining the symmetry of the extreme points with respect to the selected central point.

The results of this work verify that the accuracy of the identified fractional order model is sensitive to the position of the central point within the set of symmetrical points on the reaction curve and it has been discussed how a more accurate identified model can be obtained. New insights have also been offered on this selection of the central point x_2 in the context of the proposed symmetrical procedure.

Another aspect to note is that the proposed method is analytical, which facilitates its applicability in terms of less computational effort compared to complicated identification algorithms usually based on optimization. In the industrial context, large process industries usually have hundreds or thousands of control loops. For this reason, simplicity is of primary interest when identifying a process model for control purposes.

In the authors' opinion, this type of identification methods, in which simplicity is emphasized, will encourage their industrial use and help to bridge the gap between theoretical research on fractional models and their practical application in the process industry. This expectation is the main motivation for the present study.

References:

[1] Juan J. Gude, Pablo García Bringas. "Proposal of a General Identification Method for Fractional-Order Processes Based on the Process Reaction Curve". *Fractal Fract.* 2022, *6(526)*. DOI: 10.3390/fractalfract6090526.

[2] Juan J. Gude, Pablo García Bringas. "Influence of the Selection of Reaction Curve's Representative Points on the Accuracy of the Identified Fractional-Order Model", *Journal of Mathematics* 2022, Article ID 7185131, 22 pages. DOI: 10.1155/2022/7185131.

10.5. Future work

The following research lines and future work have been identified inspired by the observations and limitations found throughout this dissertation:

- The step response of the FFOPDT model can conveniently describe monotonic or non-monotonic behaviors depending on the fractional order α. It is worth pointing out that the identification method proposed in this paper is restricted to values of the fractional order in the range $0.5 \leq \alpha \leq 1.0$, and as a future work, this method is being extended using the same methodology for processes with underdamped step response, extending the range of the fractional order to $1.0 \leq \alpha \leq 2.0$.

- In this dissertation, analytical fractional-order model identification methods have been implemented on hardware platforms. A future line of research could be to implement on such hardware platforms more complicated identification algorithms, generally based on optimization, that seek a balance between computational effort and simplicity.

- In this work, mainly SISO control problems have been considered. However, real-life industrial control problems often include multiple loops. Therefore, a more sophisticated and generalized implementation approach should be developed for fractiona-order PI/PID control loops. In addition, the automatic tuning procedure for multiple control loops should be properly addressed in this context (Yu 2006).

- The control hardware architecture proposed in this dissertation has been applied only to the temperature-based experimental prototype. However, the hardware architecture could be used in a platform for real-time hardware-in-the-loop control experiments. While such a platform is defined in (Tepljakov 2017), the integration of the proposed hardware architecture into such a hardware-in-the-loop platform would allow verifying and evaluating the performance of any identification and control algorithm implemented on microprocessor- and FPGA-based real-time targets applied to the case of arbitrary complex models of control objects.

10.6. Final remarks

This dissertation aimed to make significant contributions to the research field of identification and control of dynamic systems based on fractional-order calculus, but, especially, to contribute, on the one hand, to the practical implementation of fractional-order system identification and control algorithms on real-time hardware platforms and, on the other hand, to bridge the gap between software-based simulations of fractional systems and controllers and real-time hardware solutions.

In the author's opinion, this type of identification methods, which emphasize simplicity, will promote their industrial use. This expectation is the main motivation for the present study.

It is the firm belief of the author that using generalized fractional models in system theory is a natural step towards more accurate modelling and developing efficient control systems, which the results of this thesis seem to indicate. Therefore, using fractional models and controllers is expected to become part of standard practice in the coming years.

Bibliography

Abel, N.H. *Solution de quelques problémes á l'aide d'intégrales definies.* Christiania, Norway: Grondahl, 1881.

Ahmed, S. "Parameter and delay estimation of fractional order models from step response." *IFAC-PapersOnLine* 48 (2015): 942–947.

Alagoz, B.B., A. Tepljakov, A. Ates, E. Petlenkov, and C. Yeroglu. "Time-domain identification of one noninteger order plus time delay models from step response measurements." *International Journal of Modeling, Simulation, and Scientific Computing* 10 , no. 1 (2019): 1941011.

Alfaro, V.M. "Low-order model identification from the process reaction curve." *Ciencia y Tecnología* 24, no. 2 (2006): 197–216.

Alfaro, V.M., and R. Vilanova. "Control of high-order processes: repeated-pole plus dead-time models' identification." *International Journal of Control*, 2021.

Åström, K. J., and T. Hägglund. *Advanced PID Control.* The Instrumentation, Systems, and Automation Society ISA, 2006.

Åström, K. J., and T. Hägglund. "Revisiting the Ziegler–Nichols step response method for PID control." *Journal of Process Control* 14, no. 6 (2004): 635–650.

Åström, K.J., and T. Hägglund. "Benchmark Systems for PID Control." *IFAC Proceedings Volumes* 33 (2000): 165-166.

Bergman, T.L., A.S. Lavine, F.P. Incropera, and D.P. DeWitt. *Fundamentals of Heat and Mass Transfer.* Wiley. 8th edition, 2017.

Bhaskaran, T., Y.Q. Chen, and D. Xue. "Practical Tuning of Fractional Order Proportional and Integral Controller (I): Tuning Rule Development." *Proceedings of the ASME 2007 International Design Engineering Technical Conferences and Computers and Information in Engineering Conference.* Las Vegas, NV, USA, 2007. 1245–1258.

Birs, I., C. Muresan, I. Nascu, and C. Ionescu. "A Survey of Recent Advances in Fractional Order Control for Time Delay Systems." *IEEE Access* 7 (2019): 30951-30965.

Caponetto, R., G. Dongola, L. Fortuna, and I. Petrás. *Fractional Order Systems: Modeling and Control Applications.* Singapore: World Scientific Publishing Company, 2010.

Charef, A., H.H. Sun, Y.Y. Tsao, and B. Onaral. "Fractal system as represented by singularity function." *IEEE Transactions on Automatic Control* 37, no. 9 (1992): 1465–1470.

Chen, Y.Q. "Ubiquitous Fractional Order Controls?" *IFAC Proceedings Volumes,* 39, no. 11 (2006): 481-492.

Chen, Y.Q., and K.L. Moore. "Discretization schemes for fractional-order differentiators and integrators." *IEEE Transactions on Circuits and Systems I: Fundamental Theory and Applications* 49, no. 3 (2002): 363-367.

Chen, Y.Q., B.M. Vinagre, and I. Podlubny. "Continued Fraction Expansion Approaches to Discretizing Fractional Order Derivatives: an Expository Review." *Nonlinear Dynamics* 38 (2004): 155–170.

Chen, Y.Q., I. Petras, and D. Xue. "Fractional order control - A tutorial." *Proceedings of the American Control Conference.* 2009. 1397-1411.

Chevalier, A, C. Francis, C. Copot, C.M. Ionescu, and R. De Keyser. "Fractional-order PID design: Towards transition from state-of-art to state-of-use." *ISA Transactions*, 2019: 178-186.

Copot, C, C.M. Ionescu, and C.I. Muresan. *Image-Based and Fractional-Order Control for Mechatronic Systems.* Cham, Switzerland: Springer, 2020.

Das, S. *Functional Fractional Calculus for System Identification and Controls.* Berlin, Germany: Springer, 2010.

Das, S., and I. Pan. *Fractional order signal processing: Introductory concepts and applications.* Heidelberg, Germany: Springer, 2012.

Dastjerdi, A.A., B.M. Vinagre, Y.Q. Chen, and S.H. HosseinNia. "Linear fractional order controllers: A survey in the frequency domain." *Annual Reviews in Control* 47 (2019): 51-70.

Dastjerdi, A.A., N Saikumar, and S.H. HosseinNia. "Tuning guidelines for fractional order PID controllers: Rules of thumb." *Mechatronics* 56 (2018): 26-36.

Dzieliński, A., D. Sierociuk, and D. Sarwas. "Some applications of fractional order calculus." *Bull. Polish Acad. Sci. Techn. Sci.* 58, no. 4 (2010): 583–592.

Elwakil, A.S. "Fractional-order circuits and systems: An emerging interdisciplinary research area." *IEEE Circuits and Systems Magazine* 10, no. 4 (2010): 40-50.

Franklin, G.F., J.D. Powell, and A.F. Emami-Naeini. *Feedback control of dynamic systems.* 8th edition. Pearson Education Limited, 2019.

Gabano, J.-D., and T. Poinot. "Fractional modeling applied to non destructive thermal characterization." *IFAC Proceedings Volumes* 44, no. 1 (2011): 13972-13977.

Gabano, J.-D., T. Poinot, and H. Kanoun. "Identification of a thermal system using continuous linear parameter-varying fractional modelling." *IET Control Theory & Applications* 11, no. 7 (2011): 889–899.

Garpinger, O., T. Hägglund, and K.J. Åström. "Performance and robustness trade-offs in PID control." *Journal of Process Control* 24 (2014): 568-577.

Gude, J.J., and E. Kahoraho. "An innovative equipment for practical teaching in process control." *IFAC Proceedings Volumes* 42, no. 24 (2010a): 233-239.

—. "Comparison between Ziegler-Nichols type tuning rules for PI and fractional PI controllers." *Proceedings of the 3rd Seminar for Advanced Industrial Control Applications (SAICA 2009).* Madrid, Spain, 2009a.

—. "Comparison between Ziegler-Nichols type tuning rules for PI and fractional PI controllers-Part 2: The frequency method." *Proceedings of the 3rd Seminar for Advanced Industrial Control Applications (SAICA 2009).* Madrid, Spain, 2009b.

—. "Modified Ziegler-Nichols method for fractional PI controllers." *Proceedings of IEEE 15th Conference on Emerging Technologies & Factory Automation (ETFA 2010).* Bilbao, Spain, 2010b.

—. "Simple tuning rules for fractional PI controllers." *Proceedings of IEEE 14th Conference on Emerging Technologies & Factory Automation (ETFA 2009).* Palma de Mallorca, Spain, 2009c.

Gude, J.J., and P. García Bringas. "Effect of the central point on the accuracy of a fractional-order model identification method based on the process reaction curve." *Proceedings 1st International Conference on Mathematical Modelling in Mechanics and Engineering (ICME 2022).* Belgrade, Serbia, 2022.

—. "Proposal of a control hardware architecture for implementation of fractional-order controllers." *Proceedings 16th International Conference Dynamical Systems Theory and Applications (DSTA 2021).* Lodz, Poland, 2021.

Guevara, E., H. Meneses, O. Arrieta, R. Vilanova, A. Visioli, and F. Padula. "Fractional order model identification: computational optimization." *IEEE 20th Conference on Emerging Technologies & Factory Automation (ETFA 2015).* Luxembourg city, Luxembourg, 2015.

Gupta, M., P. Varshney, and G.S. Visweswaran. "Digital fractional-order differentiator and integrator models based on first-order and higher order operators." *International Journal of Circuit Theory and Applications* 39, no. 5 (2011): 461–474.

Hägglund, T., and K.J. Åström. "Revisiting the Ziegler-Nichols Tuning Rules for PI Control." *Asian J. Control* 4 (2002): 364–380.

Hilfer, R. *Applications of Fractional Calculus in Physics.* Singapore: World Scientific, 2000.

Ho, W.K., C.C. Hang, and L.S. Cao. "Tuning PID controllers based on gain and phase margin specifications." *Automatica* 31 (1995): 497–502.

Huang, H.P., and J.C. Jeng. "Process reaction curve and relay methods identification and PID tuning." In *PID Control: New Identification and Design Methods*, by M.A. Johnson and M.H. Moradi, 297–337. London, UK: Springer-Verlag London Limited, 2005.

Huang, H.P., M.W. Lee, and C.L. Chen. "A System of Procedures for Identification of Simple Models Using Transient Step Response." *Ind. Eng. Chem. Res.* 40 (2001): 1903-1915.

Ionescu, C., A. Lopes, D. Copot, A. Tenreiro Machado, and J.H.T. Bates. "The role of fractional calculus in modeling biological phenomena: a review." *Communications in Nonlinear Science and Numerical Simulation* 51 (2017): 141–159.

Jahanmiri, A.H., and H.R. Fallahi. "New methods for process identification and design of feedback controllers." *Chemical Engineering Research and Design* 75, no. 5 (1997): 519–522.

Kalúz, M., J. García-Zubía, M. Fikar, and Ľ. Čirka. "A Flexible and Configurable Architecture for Automatic Control Remote Laboratories." *IEEE Transactions on Learning Technologies* 8, no. 3 (2015): 299-310.

Koszewnik, A., E. Pawłuszewicz, and M. Ostaszewski. "Experimental Studies of the Fractional PID and TID Controllers for Industrial Process." *International Journal of Control, Automation and Systems* 19 (2021): 1847–1862.

Krishna, B.T. "Studies on fractional order differentiators and integrators: A survey." *Signal Processing*, 2011: 386-426.

Kulczycki, P., J. Korbicz, and J. Kacprzyk. *Fractional dynamical systems: Methods, algorithms and applications.* Cham, Switzerland: Springer Nature, 2022.

Lacroix, S.F. *Traité du calcul Différentiel et du Calcul Intégral. Tome 3.* Paris, France: Courcier, 1819.

Li, H., Y. Luo, and Y.Q. Chen. "A Fractional Order Proportional and Derivative (FOPD) Motion Controller: Tuning Rule and Experiments." *IEEE Transactions on Control Systems Technology* 18 (2010): 516-520.

Li, Z., T. Zhao, and Y.Q. Chen. "A low cost research platform for modeling and control of multi-input multi-output fractional order dynamic systems." *In Proceedings of the International Conference on Fractional Differentiation and Its Applications (ICFDA 2014).* Catania, Italy, 2014.

Liu, T, and F. Gao. *Industrial process identification and control design: Step-test and Relay-experiment-based methods.* Springer-Verlag London Limited, 2012.

Liu, T., Q.G. Wang, and H.P. Huang. "A tutorial review on process identification from step or relay feedback test." *Journal of Process Control* 23, no. 10 (2013): 1597–1623.

Ljung, L. "Identification for control: simple process models." *Proceedings of the 41st IEEE Conference on Decision and Control.* Las Vegas, Nevada, USA, 2002.

—. *System Identification: Theory for the User.* Upper Saddle River, New Jersey: Prentice Hall, 1999.

Luo, Y., Y.Q. Chen, C.Y. Wang, and Y.G. Pi. "Tuning fractional order proportional integral controllers for fractional order systems." *Journal of Process Control* 20 (2010): 823-831.

Lützen, J. *Differentiation of arbitrary order.* New York, USA: Springer, 1990.

Macias, M., and D. Sierociuk. "Fractional order calculus for modeling and fractional PID control of the heating process." *In Proceedings of the 13th International Carpathian Control Conference (ICCC 2012), .* High Tatras, Slovakia, 2012.

Malek, H., Y. Luo, and Y.Q. Chen. "Identification and tuning fractional order proportional integral controllers for time delayed systems with a fractional pole." *Mechatronics* 23 (2013): 746–754.

Maundy, B., A.S. Elwakil, and T.J. Freeborn. "On the practical realization of higher-order filters with fractional stepping." *Signal Processing* 91, no. 3 (2011): 484-491.

Mollenkamp, R.A. *Introduction to Automatic Process Control.* Research Triangle Park, Noth Carolina, USA: Instrument Society of America, 1984.

Monje, C.A., B.M. Vinagre, G.E. Santamaría, and I. Tejado. "Auto-tuning of fractional order PIλDμ·controllers using a PLC." *Proceedings of the IEEE Conference on Emerging Technologies & Factory Automation (ETFA 2009).* Palma de Mallorca, Spain, 2009.

Monje, C.A., B.M. Vinagre, V. Feliu, and Y.Q. Chen. "Tuning and auto-tuning of fractional order controllers for industry applications." *Control Engineering Practice* 16 (2008): 798-812.

Monje, C.A., Y.Q. Chen, B.M. Vinagre, D. Xue, and V. Feliu. *Fractional-order systems and Controls.* London: Springer-Verlag, 2010.

Możaryn, J., J. Petryszyn, and S. Ozana. "PLC based fractional-order PID temperature control in pipeline: Design procedure and experimental evaluation." *Meccanica* 56 (2021): 855–871.

Muresan, C. I., and C.M. Ionescu. "Generalization of the FOPDT Model for Identification and Control Purposes." *Processes* 8, no. 6 (2020): 682-699.

Muresan, C. I., G. Mois, S. Folea, and C. M. Ionescu. "Alternative implementations of a fractional order control algorithm on FPGAs." *International Conference on Reconfigurable Computing and FPGAs (ReConFig).* Cancun, Mexico, 2013. 1-6.

Muresan, C.I., S. Folea, and G. Mois. "Optimal implementation of advanced control methods on FPGA targets." *Proceedings of the 2013 IEEE RIVF International Conference on Computing & Communication Technologies-Research, Innovation, and Vision for Future (RIVF 2013).* Hanoi, Vietnam, 2013.

Muresan, C.I., S. Folea, G. Mois, and E.H. Dulf. “Development and implementation of an FPGA based fractional order controller for a DC motor.” *Mechatronics* 23, no. 7 (2013): 798-804.

Narang, A., S.L. Sirish, and T. Chen. “Continuous-time model identification of fractional-order models with time delays.” *IET Control Theory and Applications* 5, no. 7 (2011): 900-912.

National Instruments,. “NI myRIO-1900 User Guide and Specifications.” 2022. http://www.ni.com/pdf/manuals/376047c.pdf.

O'Dwyer, A. *Handbook of PI and PID controller tuning rules.* Singapore: Imperial College Press, 2009.

Oldham, K., and J. Spanier. *The Fractional Calculus.* Orlando, Florida: Academic Press, 1974.

Oldham, K.B., and J. Spanier. *The Fractional Calculus: Theory and Applications of Differentiation and Integration to Arbitrary Order.* Dover Publications, 2006.

Oprzedkiewicz, K., M. Rosół, and J. Zeglen-Włodarczyk. “The Frequency and real-time Properties of the Microcontroller Implementation of fractional-order PID Controller.” *Electronics* 10, no. 5 (2021).

Ortigueira, M. *Fractional Calculus for Scientists and Engineers.* Dordrecht, Netherlands: Springer, 2011.

Oustaloup, A., F. Levron, B. Mathieu, and F.M. Nanot. “Frequency-band complex noninteger differentiator: characterization and synthesis.” *IEEE Transactions on Circuits and Systems I: Fundamental Theory and Applications* 47, no. 9 (2000): 25–39.

Padula, F., and A. Visioli. *Advances in Robust Fractional Control.* Bücher, Germany: Springer, 2014.

Panagopoulos, H., K.J. Åström, and T. Hägglund. “Design of PID controllers based on constrained optimization.” *IEE Proc. Control Theory Appl.* 149 (2002): 32–40.

Petráš, I. *Fractional-Order Nonlinear Systems: Modeling, Analysis and Simulation.* Berlin, Germany: Springer, 2011a.

—. “Practical aspects of tuning and implementation of fractional-order controllers.” *Proceedings of the ASME Conference.* 2011b. 75-84.

Pillonetto, G., T. Chen, A. Chiuso, G. De Nicolao, and L. Ljung. *Regularized System Identification. Learning Dynamic Models from Data.* Cham, Switzerland: Springer Nature, 2022.

Podlubny, I. *Fractional Differential Equations.* San Diego, USA: Academic Press, 1999a.

Podlubny, I. "Fractional-order systems and PIλDμ-controllers." *IEEE Transactions on Automatic Control* 44, no. 1 (1999b): 208-214.

Podlubny, I., R.L. Magin, and I. Trymorush. "Niels Henrik Abel and the birth of fractional calculus." *Fract. Calc. Appl. Anal. 20(5),* 20, no. 5 (2017): 1068–1075.

Radici, A., Y.Q. Chen, F. Padula, and A. Visioli. "A Laboratory Setup for an Introduction to Fractional Order Systems." *IFAC-Pap.* 52 (2019): 62-67.

Rana, K. P. S., V. Kumar, N. Mittra, and N. Pramanik. "Implementation of fractional order integrator/differentiator on field programmable gate array." *Alexandria Engineering Journal* 52, no. 2 (2016): 1765–1773.

Rangaiah, G.P., and P.R. Krishnaswamy. "Estimating second-order dead time parameters from underdamped process transients." *Chemical Engineering Science* 51 (1996): 1149-1155.

Rangaiah, G.P., and P.R. Krishnaswamy. "Estimating second-order plus dead time model parameters." *Ind. Eng. Chem. Res.* 33 (1994): 1867–1871.

Rojas, J.D., O. Arrieta, and R. Vilanova. *Industrial PID Controller Tuning: With a Multiobjective Framework Using MATLAB.* London, UK: Springer, 2021.

Ross, B. "The developement of fractional calculus 1695–1900." *Historia Mathematica* 4 (1977): 75–89.

Ross, B.E. "Fractional Calculus and Its Applications." *Proceedings of the International Conference held at the Universiy of New Haven.* London, UK: Springer, 1975.

Rossiter, J.A., B. Pasik-Duncan, S. Dormido, L. Vlacic, B. Jones, and R. Murray. "A survey of good practice in control education." *European Journal of Engineering Education , 43(6), pp. . DOI:* 43, no. 6 (2018): 801-823.

Rybarczyk, D. "PLC implementation of fractional PI controller in positioning of electrohydraulic servodrive." *Control Cybern* 45 (2016): 301–316.

Sabatier, J. "Modelling Fractional Behaviours Without Fractional Models." *Frontiers in Control Engineering* 2, no. 716110 (2021).

Sánchez-Peña, R.S., J. Quevedo, and V. Puig. *Identification and Control: The Gap between Theory and Practice*. London, UK: Springer, 2007.

Shah, P., and S. Agashe. "Review of fractional PID controller." *Mechatronics* 38 (2016): 29-41.

Sierociuk, D., A. Dzielinski, G. Sarwas, I. Petras, I. Podlubny, and T. Skovranek. "Modelling heat transfer in heterogeneous media using fractional calculus." *Phil. Trans. R. Soc. A* 371, no. 20120146 (2013,).

Skogestad, S. *Chemical and Energy Process Engineering.* CRC Press. 1st edition, 2009.

Smith, C.L. *Digital Computer Process Control.* Oahu, HI, USA: International Textbook Educational Publishers, 1972.

Tan, K.K., Q.G. Wang, C.C. Hang, and T. Hägglund. *Advances in PID control;.* London, UK: Springer-Verlag London Limited, 1999.

Tavakoli-Kakhki, M., and H. Haeri. "Fractional order model reduction approach based on retention of the dominant dynamics: Application in IMC based tuning of FOPI and FOPID controllers." *ISA Transactions* 50, no. 3 (2011): 432-442.

Tavakoli-Kakhki, M., and M.S. Tavazoei. "Estimation of the order and parameters of a fractional order model from a noisy step response data." *ASME J. Dyn. Sys. Meas. Control* 136, no. 031020 (2014).

Tavakoli-Kakhki, M., M. Haeri, and M.S. Tavazoei. "Simple fractional order model structures and their applications in control system design." *European Journal of Control* 16, no. 6 (2010): 680-694.

Tavakoli-Kakhki, M., M.S. Tavazoei, and A. Mesbahi. "Parameter and order estimation from noisy step response data." *IFAC Proceedings Volumes* 46 (2013): 492–497.

Tenreiro Machado, J.A., A.M. Galhano, A.M. Oliveira, and J.K. Tar. "Approximating fractional derivatives through the generalized mean." *Communications in Nonlinear Science and Numerical Simulation* 14, no. 11 (2009): 3723-3730.

Tenreiro Machado, J.A., et al. "Some Applications of Fractional Calculus in Engineering." *Mathematical Problems in Engineering*, no. 639801 (2010).

Tepljakov, A. *Fractional-order Modeling and Control of Dynamic Systems.* Cham, Switzerland: Springer, 2017.

Tepljakov, A., B.B. Alagoz, C. Yeroglu, E. Gonzalez, S.H. HosseinNia, and E. Petlenkov. "FOPID Controllers and Their Industrial Applications: A Survey of Recent Results." *IFAC-PapersOnLine*, 2018: 25-30.

Tepljakov, A., et al. "Towards industrialization of FOPID controllers: A survey on milestones of fractional-order control and pathways for future developments." *IEEE Access* 9 (2021): 21016-21042.

Thomson, D., and F. Padula. "Introduction to Fractional-Order Control: A Practical Laboratory Approach." *IFAC-Pap.* 55 (2022): 126-131.

Victor, S., R. Malti, H. Garnier, and A. Oustaloup. "Parameter and differentiation order estimation in fractional models." *Automatica* 49 (2013): 926-935.

Vilanova, R., and A. Visioli. *PID Control in the Third Millennium: Lessons Learned and New Approaches.* London, UK: Springer, 2012.

Vinagre, B.M., I. Podlubny, A. Hernández, and V. Feliu. "Some Approximations of fractional order operators used in control theory and applications." *Fractional Calculus and Applied Analysis* 3, no. 3 (2000): 231-248.

Vinagre, B.M., Y.Q. Chen, and I. Petras. "Two direct Tustin discretization methods for fractional-order differentiator/integrator." *Journal of the Franklin Institute: Engineering and applied mathematics* 340 (2003): 349-362.

Visioli, A. *Practical PID control.* London, UK: Springer-Verlag, 2006.

Vitecková, M., A. Vitecek, and L. Smutny. "Simple PI and PID controllers tuning for monotone self-regulation plants." *IFAC Proceedings Volumes* 33, no. 4 (2000): 259–264.

Wang, B., S. Wang, Y. Peng, Y. Pi, and Y. Luo. "Design and High-Order Precision Numerical Implementation of Fractional-Order PI Controller for PMSM Speed System Based on FPGA." *Fractal Fract.* 6, no. 218 (2022).

Xue, D. *Fractional-Order Control Systems: Fundamentals and Numerical Implementations.* Berlin, Germany: De Gruyter, 2017.

Yu, C. *Autotuning of PID Controllers: A Relay Feedback Approach.* London, UK: Springer, 2006.

Yuan, J., Y. Ding, S. Fei, and Y.Q. Chen. "Identification and parameter sensitivity analyses of time-delay with single-fractional-pole systems under actuator rate limit effect." *Mechanical Systems and Signal Processing* 163, no. 108111 (2022).

Žecová, M., and J. Terpák. "Heat conduction modeling by using fractional-order derivatives." *Applied Mathematics and Computation* 257 (2015): 365-373.